

PA 00817

NASA CR-
141871

Antenna and Radome Loss Measurements for MFMR and PMIS

by
K. R. Carver
Project Director

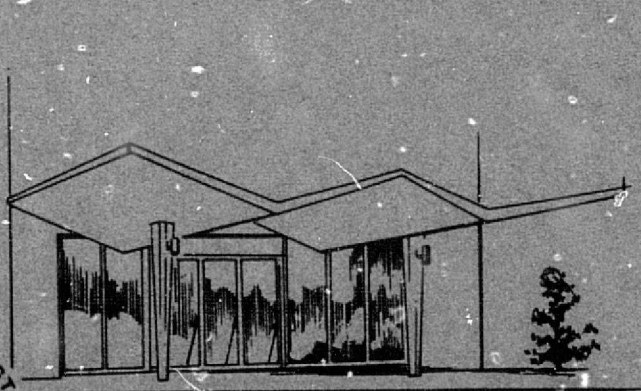
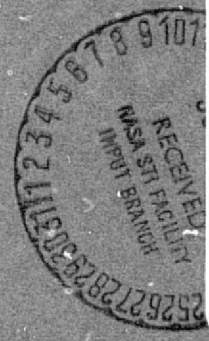
with
Appendix on MFMR/PMIS Computer Programs

by
Wm. K. Cooper
Project Engineer

(NASA-CR-141871) ANTENNA AND RADOME LOSS
MEASUREMENTS FOR MFMR AND PMIS WITH APPENDIX
ON MFMR/PMIS COMPUTER PROGRAMS (New Mexico
State Univ.) 199 p HC \$7.00 CSDL 17B

G3/32
Unclas
27291

N75-26202



Physical Science Laboratory

BOX 3548, LAS CRUCES, NEW MEXICO 88003 (505) 524-2851 TWX 910-983-0541

prepared for
NASA Johnson Space Center
contract No. NAS-9-95451
May, 1975

PA 00817

Antenna and Radome Loss Measurements for MFMR and PMIS

by

K. R. Carver
Project Director

with

Appendix on MFMR/PMIS Computer Programs

by

Wm. K. Cooper
Project Engineer

prepared for
NASA Johnson Space Center
contract No. NAS-9-95451
May, 1975

ACKNOWLEDGMENT

Special thanks are extended to Bill Cooper who took charge of developing the entire software package and spent many sleepless nights bringing a complex concept into a practical reality usable in real-time data reduction. It was this feature that transformed an aluminum bucket into a useful tool for scientific/engineering measurement.

Grateful acknowledgement is made to Morrie Drexler and Cecil Post for coordinating a myriad of mechanical details in the construction of the bucket and associated antenna and radome positioners. Dennis Henry provided yeoman service in managing an unending procession of administrative and economic details, as well as working through a numerical analysis of the Fresnel field interaction between a horn and a surrounding bucket. It was this exercise that led to the final bucket dimensions.

Hank Schubert, Dick Lara, and Arun Pattni deserve special recognition for a truly outstanding job as night operators and for responding wherever help was needed. Lou Snow, Bobby Stout and Bronson Woods also were instrumental in taking care of several details before and during the measurement period.

In the final report preparation, Cecil Post took charge of preparing final versions of all figures and photographs. Mary Lou Kearns provided special assistance in preparing the Appendix. Jane Johnson deserves special thanks for typing the manuscript and enduring many intervening changes by the author.

TABLE OF CONTENTS

	Page
Acknowledgement.	i
List of Illustrations.	v
List of Tables	viii
List of Abbreviations.	ix
 Chapter	
I. SUMMARY.	1
1.0 Introduction.	1
1.1 NMSU/PSL Radiometer Calibration Facility.	1
1.2 Highlights of Test Results.	2
1.3 Recommendations	4
II. ANTENNA LOSS MEASUREMENT TECHNIQUES.	5
2.0 Introduction.	5
2.1 Definitions	6
2.2 Directivity/Gain Technique.	9
2.3 Cryoload Technique.	12
2.4 Bucket Technique.	15
2.4.1 Theory	15
2.4.2 Errors due to bucket emissivity.	18
2.4.3 Bucket shape criteria.	19
2.4.4 Bucket effect on antenna pattern - an X-Band experiment	19
2.4.5 Description of full-scale bucket	19
III. ANTENNA/RADOME DATA REDUCTION TECHNIQUES	31
3.0 Introduction.	31
3.1 Theoretical Foundation for Loss Calculations.	31
3.2 PMIS/MFMR Data Systems.	34

TABLE OF CONTENTS (Continued)

	Page
IV. ESTIMATION OF SKY BRIGHTNESS TEMPERATURES.	48
4.0 Introduction.	48
4.1 Theoretical Background.	48
4.2 Local Topography.	51
4.3 Variation with Zenith Angle	61
4.4 Errors in T_{sky}	63
V. PMIS LOSS MEASUREMENTS	64
5.0 Introduction.	64
5.1 Mechanical Positioning Technique.	64
5.2 Radiometer Receiver Calibration	65
5.3 PMIS Data Flow.	68
5.4 PMIS Antenna and Radome Loss Values	70
5.5 PMIS Error Budget	75
5.5.1 Theoretical Background	75
5.5.2 PMIS antenna loss errors	76
5.5.3 PMIS radome loss errors.	80
5.6 Effect of Errors in L_A , L_R on PMIS User	81
5.6.1 Random errors.	81
5.6.2 Systematic errors.	83
5.6.3 Total uncertainty.	84
VI. MFMR LOSS MEASUREMENTS	85
6.0 Introduction.	85
6.1 Mounting Configuration.	85
6.2 Radiometer Receiver Calibration	86
6.3 MFMR Data Flow.	89
6.4 MFMR antenna and radome loss values (K_u , K_a -Bands.	90
6.5 Interaction mechanisms between the MFMR horns and the aircraft bulkhead	90

TABLE OF CONTENTS (Continued)

	Page
6.5.1 Introduction	90
6.5.2 Near-field-patterns of circular horns	103
6.5.3 Geometry of horn relative to bulkhead	106
6.5.4 Contribution of absorber to brightness temperature	106
6.5.5 Conclusions	112
6.6 MFMR antenna and radome loss values (L-Band)	112
6.7 MFMR Error Budget.	119
 VII. BUCKET PERFORMANCE TESTS.	 122
7.0 Introduction	122
7.1 Effect of Antenna Location Change.	122
7.2 Long-Term Bucket Emissivity Changes.	125
7.2.1 X-Band Measurements	126
7.2.2 L, K _u , K _a -Band Measurements	130
7.3 EMI.	133
 APPENDIX - PMIS & MFMR RADIOMETER PROGRAMS.	 P.1-M3.9
 REFERENCES.	 134

LIST OF ILLUSTRATIONS

FIGURE	Page
2-1 Radiative transfer in an antenna.	8
2-2 Apparent temperature error (ΔT_B) versus antenna loss (L_A)	13
2-3 Cryoload for loss calibrations of small antennas.	14
2-4 Bucket technique for loss measurements.	17
2-5 Scale model bucket for X-Band standard gain horn.	20
2-6 Standard gain horn antenna pattern.	21
2-7 Bucket and antenna geometry	22
2-8 Pre-fabrication and painting bucket parts	24
2-9 Cementing aluminum foil to bucket interior surface.	24
2-10 Bucket assembly underway.	25
2-11 South face of bucket showing braces and rigging to sustain 100 mph wind.	25
2-12 PMIS in position for test - main bucket door open	26
2-13 PMIS in mockup on sling and handling dolly.	26
2-14 MFMR radome in handling sling	27
2-15 Mounting MFMR radome.	28
2-16 Mounting PMIS - note counterweight.	29
2-17 PMIS equipment setup.	30
2-18 MFMR with absorber mounted for test	30
3-1 Radiometer, waveguide and antenna (without and with radome).	33
3-2 Uncorrected brightness temperature versus PCM counts.	36
3-3 PMIS calibration repeatability - vertical polarization.	37
3-4 PMIS calibration repeatability - horizontal polarization.	38
3-5 MFMR calibration history.	39
3-6 Data flow chart	41
3-7 PMIS-1 sample output.	42

LIST OF ILLUSTRATIONS (Continued)

	Page
3-8 MFMR-1 sample output.	43
3-9 PMIS-2 sample output.	44
3-10 MFMR-2 sample output.	45
3-11 PMIS-3 sample output.	46
3-12 MFMR-3 sample output.	47
4-1 Atmospheric radiative transfer model (after Paris, 1971).	50
4-2 Location of NMSU/PSL radiometer calibration facility. .	52
4-3 Radiosonde profiles - Feb. 12, 1973 - 0200 MST.	54
4-4 Calculated sky temperature spectrum versus frequency from radiosonde data.	55
4-5 Zenith sky temperature versus frequency	56
4-6 Scattergram of T_{sky} versus precipitable water	57
4-7 Histogram of zenith sky temperature	59
4-8 Comparison of computed sky temperature versus time. . .	60
4-9 Comparison of computed sky temperature versus angle from zenith	62
5-1 Symbolic diagram of X-Band reference cold load for PMIS receiver calibration	66
5-2 PMIS antenna loss versus beam position.	72
5-3 PMIS radome 1 loss versus beam position	73
5-4 PMIS radome 2 loss versus beam position	74
6-1 MFMR calibration history.	88
6-2 MFMR antenna loss versus pitch angle -- K_u -Band	94
6-3 MFMR antenna loss versus pitch angle -- K-Band.	95
6-4 MFMR antenna loss versus pitch angle -- K_a -Band	96
6-5 MFMR radome 1 loss versus pitch angle -- K_u -Band.	97
6-6 MFMR radome 1 loss versus pitch angle -- K-Band	98

LIST OF ILLUSTRATIONS (Continued)

	Page
6-7 MFMR radome 1 loss versus pitch angle -- K_a -Band	99
6-8 MFMR radome 2 loss versus pitch angle -- K_u -Band	100
6-9 MFMR radome 2 loss versus pitch angle -- K-Band.	101
6-10 MFMR radome 2 loss versus pitch angle -- K_a -Band	102
6-11 Fresnel and far-field patterns for 25 dB circular Taylor distribution.	104
6-12 Fresnel and far-field patterns	105
6-13 On axis power density versus axial distance from horn mouth	107
6-14 Positions relative to bulkhead - MFMR.	108
6-15 Source and apparent brightness temperature versus pitch angle	111
6-16 MFMR antenna loss versus pitch angle -- K_u -Band channel 1.	113
6-17 MFMR AIL antenna loss (roll=0°) versus pitch angle -- L-Band.	114
6-18 MFMR AIL array, uncorrected brightness temperature versus pitch angle -- L-Band	116
6-19 MFMR Aerojet antenna temperature versus pitch angle -- L-Band.	117
6-20 Voltage Standing Wave Ratio versus pitch angle -- antenna in bucket.	118
7-1 MFMR antenna loss versus pitch angle -- K_u -Band Channel 2.	123
7-2 MFMR antenna loss versus pitch angle -- K_a -Band.	124
7-3 Bucket calibration at X-Band	127
7-4 Loss (L) of horn antenna plus attenuator	128
7-5 Absorbing disk located above MFMR antenna assembly . . .	131
7-6 L, K_u , K_a bucket verification tests.	132

LIST OF TABLES

TABLE	Page
4-1. Simulated Tropopause Data.	51
4-2. Systematic Errors in T_{sky}	63
5-1. Number of Independent Loss Measurement Sets.	68
5-2. Loss Value Averaging Technique	69
5-3. PMIS Loss Summary.	71
6-1. MFMR Laboratory Calibration Summary.	87
6-2. MFMR Antenna Loss (L_A)	91
6-3. MFMR Radome #1 Loss (L_R)	92
6-4. MFMR Radome #2 Loss (L_R)	93

LIST OF ABBREVIATIONS

AGC	-	Automatic Gain Control
AIL	-	Airborne Instruments Laboratory
EMI	-	Electromagnetic Interference
JSC	-	Johnson Space Center
LC-36	-	Launch Complex 36
LN ₂	-	Liquid Nitrogen
LRC	-	Langley Research Center
MFMR	-	Multifrequency Microwave Radiometer
NASA	-	National Aeronautics and Space Administration
NMSU	-	New Mexico State University
PCM	-	Pulse Coded Modulation
PMIS	-	Passive Microwave Imaging System
PSL	-	Physical Science Laboratory
RACF	-	Radiometer Antenna Calibration Facility
SMR	-	Small Missile Range
UHF	-	Ultra High Frequency
VHF	-	Very High Frequency
VSWR	-	Voltage Standing Wave Ratio

CHAPTER I

SUMMARY

1.0 INTRODUCTION

The two principal objectives of this report are (1) to describe the NMSU/PSL Radiometer Antenna Calibration Facility (RACF) and (2) to summarize the antenna and radome loss measurements made on the Passive Microwave Imaging System (PMIS) and the Multifrequency Microwave Radiometer (MFMR) during January and February of 1975. This chapter summarizes the major features of the facility, points out highlights of the PMIS/MFMR loss measurements, and makes several recommendations for future measurements.

1.1 NMSU/PSL Radiometer Antenna Calibration Facility

The physical facility used at PSL for the loss calibration of antennas and radomes consists of a large reflecting bucket and an electronic equipment building, both located at A-Mountain, approximately 5 km east of the New Mexico State University. The bucket is at an altitude of 1.46 km above MSL and is an aluminum foil covered wooden truncated inverted pyramid with dimensions as shown in Fig. 2-7. The purpose of the bucket is to block thermal emission from surrounding terrain and from near-horizon atmospheric sources. Thus, the thermal emission incident on the antenna is ideally isothermal and equal to the zenith sky temperature at the frequency of interest.

In addition to the physical plant, an extensive data reduction program has been written for PMIS and MFMR, with separate software components tailored to the PCM output format used in the NASA P-3A earth resources aircraft. This is discussed further in Chapter III and the Appendix.

The bucket is similar to an enclosure at Table Mountain, California used previously by NASA. However, the timely availability of PSL support personnel and a real-time data reduction capability make the RACF more useful as a radiometer test bed.

1.2 Highlights of Test Results

It is shown conclusively in Chapter VI that the bucket technique provides sufficient accuracy and repeatability for the loss values to be used in an aircraft radiometric measurement mission when the radiometer aircraft mockup exhibits sufficient fidelity to the actual aircraft situation. An extensive error analysis for PMIS and MFMR (Secs. 5.5 and 6.7) establishes the following:

1. For PMIS (10.69 GHz) the total uncertainty (sum of random plus systematic errors) in the antenna loss is ± 0.022 and ± 0.039 for the vertical and horizontal channels respectively. The total uncertainty in the radome loss is ± 0.014 and ± 0.039 for the vertical and horizontal channels. This would correspond to a total uncertainty in the measured brightness temperature (in flight) of ± 5.2 K and ± 5.7 K for the vertical and horizontal channels respectively.

2. For MFMR, L-Band (1.4135 GHz), the bulkhead and associated absorber were not sufficiently good replicas of the actual aircraft situation, with the result that the mutual coupling between the AIL array and the radome was so strong that the measured values of the radome loss were virtually meaningless. However, as explained in Sec. 6.6, a constant value of $L_R \approx 1.09$ is a reasonable choice. The antenna loss values were typically $L_A \approx 1.36$ (essentially independent of pitch angle) when the PSL-furnished X-Band absorber was in place on the bulkhead. However, this

material is virtually transparent at L-Band and thus does not simulate the actual aircraft situation where an L-Band absorbing material is used. Thus, in the flight situation, it may be expected that $L_A > 1.36$ for pitch angles near 0° or 180° , since the relatively hot absorber will contribute noise power through the antenna sidelobes. In the absence of accurate near-field in situ patterns for the AIL array, it is difficult to see how the effect of the absorber can be estimated, short of new improved measurements.

3. For MFMR, K_u , K , K_a -Bands (18.0, 22.05 and 37.0 GHz), the antenna loss is less than the radome loss and both losses depend much more on the pitch and roll angles than was the case at L-Band. The antenna loss is slightly higher in Channel 1 than in Channel 2 and generally rises as the pitch angle approaches 180° when the horns are nearest the bulkhead (c.f. Figs. 6-2, 6-3, and 6-4). However, as explained in Sec. 6.5), the exact values of L_A and the slope $dL_A/d\theta_0$ depend critically on the fidelity of the mockup used, the exact shape of the absorber used on the bulkhead, etc.

The radome loss at K_u , K , and K_a -Bands also depends critically on both pitch and roll angles, as shown in Figs. 6-5 - 6-10. The jagged nature of these loss graphs is not due to errors in the measurement (the repeatability was much better than this), but seems to stem from resonant scattering between the horns and radome material or radome resonant thickness effects (especially at K_a -Band).

Thus, it may be stated that the precision of measurement was good, but the accuracy was poor, since the antenna system furnished was an insufficiently good replica of the antenna system used. The MFMR error budget is discussed at considerable length in Sec. 6.7.

1.3 Recommendations

As a result of the measurement program, several major recommendations can be made:

1. Future tests of the MFMR should be made with a much better replica of the aircraft bulkhead, including the same absorber that would be used in flight operations, along with any other significant structural features such as weather radars, etc.
2. Measurements of the input vs. pitch angle at L, K_u , K, and K_a -Bands should be made, with and without the radome.
3. A study of the MFMR pitch and roll positioning repeatability should be made.
4. If the K_u , K, and K_a -Band channels are to be used for skyward viewing, the horns should be located at a roll angle of 180° , rather than 0° . This would obviate the critical dependence on the exact bulkhead geometry.
5. Greater attention should be paid to reducing PCM noise and long-term instability in the PMIS receivers, particularly the horizontal channel.

CHAPTER II

ANTENNA LOSS MEASUREMENT TECHNIQUES

2.0 INTRODUCTION

The temperature calibration of a radiometer system normally proceeds in two parts: (1) the calibration of the connecting waveguide, front end, etc., by use of known reference load temperatures, and (2) the calibration of the antenna and radome loss. The purpose of the NMSU/PSL Radiometer Antenna Calibration Facility is to measure the antenna and radome loss by using a calibrated radiometer receiver and a known source brightness temperature.

This facility differs by comparison to many other past calibration efforts, in that relatively large aircraft and satellite-borne radiometer systems, including automatic positioners and radomes, may be accommodated. Also, the bucket technique employed is easily adaptable to multi-frequency use since radio-sonde support is locally available on a timely and convenient basis. The genesis of this effort was the requirement to periodically calibrate the NASA JSC Passive Microwave Imaging System (PMIS) at 10.69 GHz and the Multifrequency Microwave Radiometer (MFMR) at 1.4, 18, 22.05, and 37 GHz. These systems are complicated by a variety of requirements for beam scanning, polarization switching, multiplexed data handling and subsequent data reduction.

In response to the need for near real-time data reduction, PSL has developed an extensive set of software packages to handle the PCM encoded radiometer and housekeeping data, both for PMIS and MFMR. These make use of a PCM decommutation device and an IBM System 7 computer which transfers the stripped data from the magnetic tape to an IBM System 370 Computer for processing. This will be described in more detail in Chapter 3.

2.1 Definitions

The antenna loss of a receiving antenna is defined as

$$L_A = \frac{P_{\text{capt}}}{P_{\text{del}}} \quad (2-1)$$

where

P_{capt} = power incident on and captured by antenna

P_{del} = power delivered to load

Since the received or captured power includes both incidence and re-radiation effects, it follows that

$$P_{\text{capt}} = P_{\text{del}} + P_J \quad (2-2)$$

where

P_J = power lost as Joule heating

Thus

$$L_A = 1 + \frac{P_J}{P_{\text{del}}} \quad (2-3)$$

so that $1 \leq L_A < \infty$. (2-4)

A radome inserted between an antenna and an incident field will introduce an insertion loss

$$L_R = \frac{P_B}{P_A} \quad (2-5)$$

where

P_A = power received before radome insertion

P_B = power received after radome insertion

It is observed that $P_B > P_A$ if the radome does not interact with the near-field distribution of the antenna, since radome dielectric materials have non-zero a.c. conductivities. Thus,

$$1 \leq L_R < \infty \quad (2-6)$$

Since antennas and radomes are lossy networks, it is clear that they will introduce a small amount of their own noise power, even when no external wave is incident. Generalizing to a two-port network, as in Fig. 2-1, we may solve for the apparent antenna brightness temperature, i.e.

$$T'_B = \underbrace{\left(1 - \frac{1}{L}\right)}_{\text{Emission}} T_A + \underbrace{\frac{T_S}{L}}_{\text{Absorption}} \quad (2-7)$$

where it is assumed that an unpolarized random noise signal of equivalent temperature T_S is incident on an isothermal antenna at thermometric temperature T_A and of loss L . The first term in (2-7) is the component of the apparent brightness temperature due to the self-generated noise in the antenna and the second term is due to the absorption attenuated equivalent temperature, or received noise power. If the incident brightness temperature distribution is $T_{\text{sky}}(\theta, \phi)$ and the antenna gain pattern is $G(\theta, \phi)$, then the second term of (2-7) is

$$\frac{T_S}{L} = \frac{1}{4\pi} \iint_{4\pi} T_{\text{sky}}(\theta, \phi) G(\theta, \phi) d\Omega \quad (2-8)$$

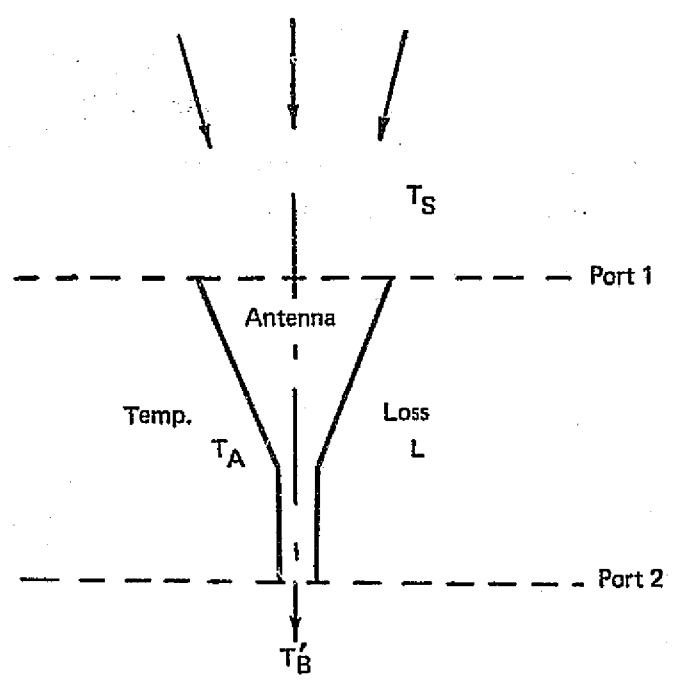


Fig. 2-1. Radiative transfer in an antenna.

2.2 Directivity/Gain Technique

It has been unofficially estimated by NBS that both the gain and directivity of moderate to high gain antennas can be measured, using the near-field sampling technique [Kerns, 1970], to an accuracy of 0.1 dB (at the 3 σ point) throughout the frequency range L to K_a-Band. This is assumed to be the state of the art. We wish to examine the effect of such gain and directivity measurement errors on the radiometer antenna temperature uncertainty.

The power gain of an antenna is related to its directivity by

$$G = \frac{D}{L_A} \quad (2-9)$$

where

- G = power gain (dimensionless)
- D = directivity (dimensionless)
- L_A = antenna loss

We next calculate the effect of systematic and independent errors ΔG , ΔD on the insertion loss error ΔL^* . From (2-9)

$$L_A = \frac{D}{G} \quad (2-10)$$

Differentiating and using the worst case formula,

$$\Delta L_A = \frac{1}{G} \Delta D + \frac{D}{G^2} \Delta G \quad (2-11)$$

* It is assumed that there is zero systematic error.

which can be written as

$$\Delta L_A = \frac{1}{G} (\Delta D + L \Delta G) \quad (2-12)$$

It is next assumed that G and D are independent random variables, normally distributed with zero mean so that $\bar{L} = L_A$. Letting σ_L^2 , σ_G^2 , σ_D^2 be the variances of L, G and D respectively, we can determine σ_L^2 by the familiar quadrature formula, i.e.,

$$\sigma_L^2 = \left[\frac{\partial L_A}{\partial G} \right]^2 \sigma_G^2 + \left[\frac{\partial L_A}{\partial D} \right]^2 \sigma_D^2 \quad (2-13)$$

which yields

$$\sigma_L = \frac{1}{G} \sqrt{\sigma_D^2 + L_A^2 \sigma_G^2} \quad (2-14)$$

Since the errors are normally distributed we can express the 3 σ error as

$$3\sigma_L = \frac{3}{G} \sqrt{\sigma_D^2 + L_A^2 \sigma_G^2} \quad (2-15)$$

The incremental errors σ_L , σ_G , and σ_D can be related to their corresponding decibel errors by

$$\delta L(\text{dB}) = 10 \log (L + 3\sigma_L) - 10 \log L = 10 \log \left(1 + \frac{3\sigma_L}{L} \right) \quad (2-16)$$

If it is assumed that $\delta D(\text{dB}) = \delta G(\text{dB})$, then it can be shown that

$$\delta L(\text{dB}) = 10 \log \left[1 + \sqrt{2} \left(10^{\frac{\delta D}{10}} - 1 \right) \right] \quad (2-17)$$

When $\delta D = \delta G = 0.1$ dB, (9a) yields

$$\delta L = 0.14 \text{ dB} \quad (2-18)$$

For example, when $L_A = 1$ dB, $3\sigma_L = 0.041$.

We next consider the effect of the insertion loss error on the apparent antenna temperature, T_R . The noise temperature T_R at the terminals of an antenna is composed of two parts: (1) the integrated brightness temperature T_S , diminished by the antenna loss and (2) the emissive temperature of the lossy antenna structure itself.

Eqn. (2-7) can be written as

$$T_B = \frac{T_S - T_A}{L_A} + T_A \quad (2-19)$$

Assuming that T_S and T_A are known, the effect of a random error σ_L on T_B is given by

$$\sigma_{T_B} = (T_A - T_S) \frac{\sigma_L}{L_A^2} \quad (2-20)$$

Assuming that the insertion loss uncertainty is entirely caused by the random $\delta G = \delta D = 0.1$ errors (typifying the state of the art), eqns. (2-16), (2-17) and (2-20) can be used to calculate σ_{T_B} . For example, a 1 dB insertion loss ($L_A = 1.259$) corresponds to $\delta L = 0.14$ dB ($3\sigma_L = 0.041$). Assuming $T_S = 10$ K* and $T_A = 300$ K,

$$\sigma_{T_B} = (300 - 10.0) \frac{0.041}{1.259^2} = 7.5 \text{ K} \quad (2-21)$$

For antennas with low insertion loss such as scalar horns, $L_A \approx 1$ and a 0.14 dB insertion loss error would correspond to $L_A = 1 \pm 0.032$.

* This would be a typical figure for the antenna looking at the cold sky.

However, since $L_A \geq 1$, the effective $3\sigma_L = \frac{0.032}{2} = 0.016$, corresponding to $\sigma_{T_B} = 4.6$ K. Using this approach, we obtain the curve of Fig. 2-2 which plots the antenna temperature uncertainty vs. the insertion loss for two assumed values of G, D measurement error.

The preceding results demonstrate that in the calibration procedures where the measured insertion loss is used to deduce the integrated brightness temperature, relatively small errors in insertion loss can cause unacceptably high antenna temperature errors. In particular, when the insertion loss is inferred from the D/G ratio, independent random errors of 0.1 dB in the measurement of D and G correspond to temperature errors of 5 - 9 K for typical values of insertion loss.

Thus, single-frequency direct measurement techniques are not yet sufficiently accurate for the determination of the insertion loss in a microwave radiometric calibration situation. In addition, this method suffers from the disadvantage that an extremely large near-field sampling device would be required for large radome-covered radiometer systems such as PMIS or MFMR, and that to date no such large system has been built.

2.3 Cryoload Technique

A second technique which is usable for smaller antennas such as horns makes use of a LN₂ cooled microwave absorbing hohlraum or cooled blackbody enclosure, as shown in Fig. 2-3. If the horn views an isothermal brightness distribution T_S in a perfectly absorbing (and emitting) medium, then solving for L_A from (2-7).

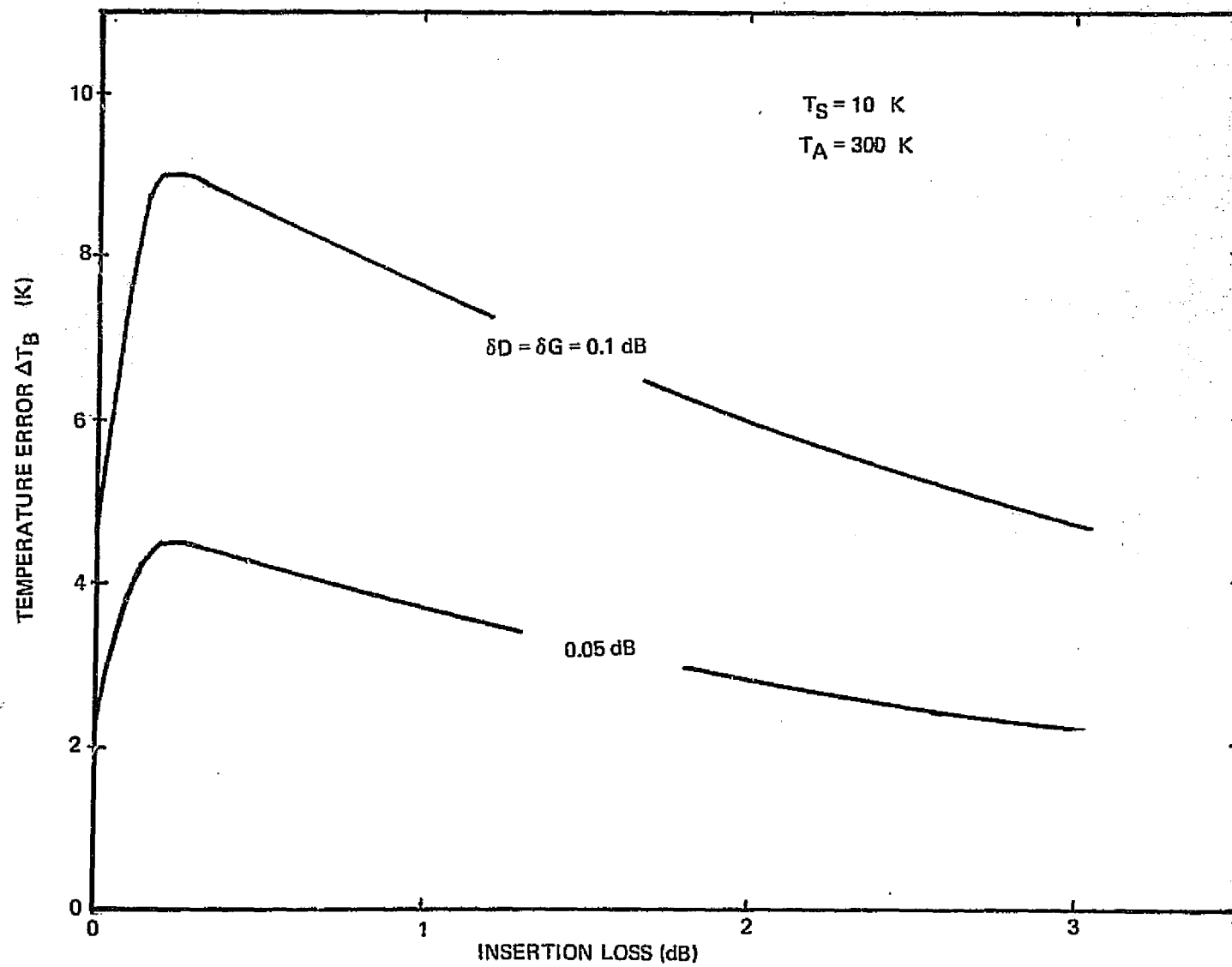


Fig. 2-2. Apparent temperature error (ΔT_B) versus antenna loss (L_A).

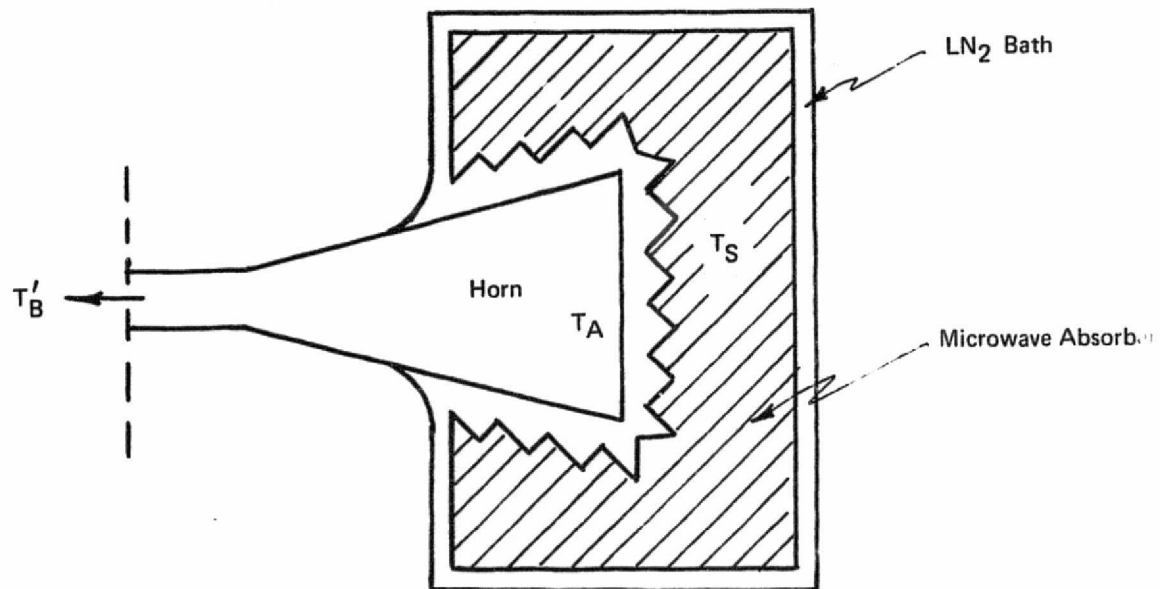


Fig. 2-3. Cryoload for loss calibrations of small antennas.

$$L_A = \frac{T_A - T_S}{T_A - T'_B} \quad (2-22)$$

where

- L_A = antenna loss
 T_A = thermometric temp. of antenna (K)
 (assumed here to be isothermal)
 T_S = brightness temp. of cryoload (K)
 T'_B = uncorrected brightness temperature
 measured by radiometer (K)

Blume and Swift [1972] of NASA LRC have used this technique to calibrate the loss of an S-Band horn and have achieved an absolute accuracy of ± 1 K.

The technique has the advantage of being inexpensive and accurate for relatively small antennas (diameters less than 6'), but as yet no isothermal cryoloads have been developed which are large enough to accommodate such large radiometer antennas/radome systems as PMIS or MFMR where 30 m³ volumes are encountered.

2.4 Bucket Technique

2.4.1 Theory

It is clear from (2-22) that the antenna thermometric temperature (T_A) must differ substantially from the integrated source brightness temperature (T_S) in order for L_A to be measured with acceptable accuracies. The bucket technique achieves this by placing the antenna in a large reflecting enclosure which blocks thermal emission from surrounding terrain, thus allowing the antenna to receive atmospheric noise only. The equivalent sky temperature can be calculated from radiosonde data by calculating the radiative transfer of an assumed 2.7 K cosmic background temperature through a clear atmosphere with both

water and oxygen resonant molecular constituents [Paris, 1971].
This technique is shown in Fig. 2-4.

In general,

$$T_S = \frac{\int \int \int_{4\pi} T_{\text{sky}}(\theta, \phi, f) D(\theta, \phi, f) F(f) d\Omega df}{4\pi \int F(f) df} \quad (2-23)$$

where

- T_S = integrated antenna brightness temp. (K)
- T_{sky} = sky brightness temp. distribution (K)
- F = spectral transfer function of radiometer system (Hz^{-1})
- Δf = bandwidth (Hz)

If the bandwidth is much smaller than the pressure-broadened spectral widths of the H_2O and O_2 emission lines and if the antenna pattern is independent of frequency across the bandwidth, then (2-23) reduces to

$$T_S = \frac{1}{4\pi} \int \int_{4\pi} T_{\text{sky}}(\theta, \phi, f_0) D(\theta, \phi, f_0) d\Omega \quad (2-24)$$

where f_0 is the center frequency. If the sky temperature distribution is essentially constant across the main beam and first few sidelobes of the antenna in the bucket, then (2-24) reduces to

$$T_S = T_{\text{sky}}(f_0) \quad (2-25)$$

which is the form used in all subsequent calculations.

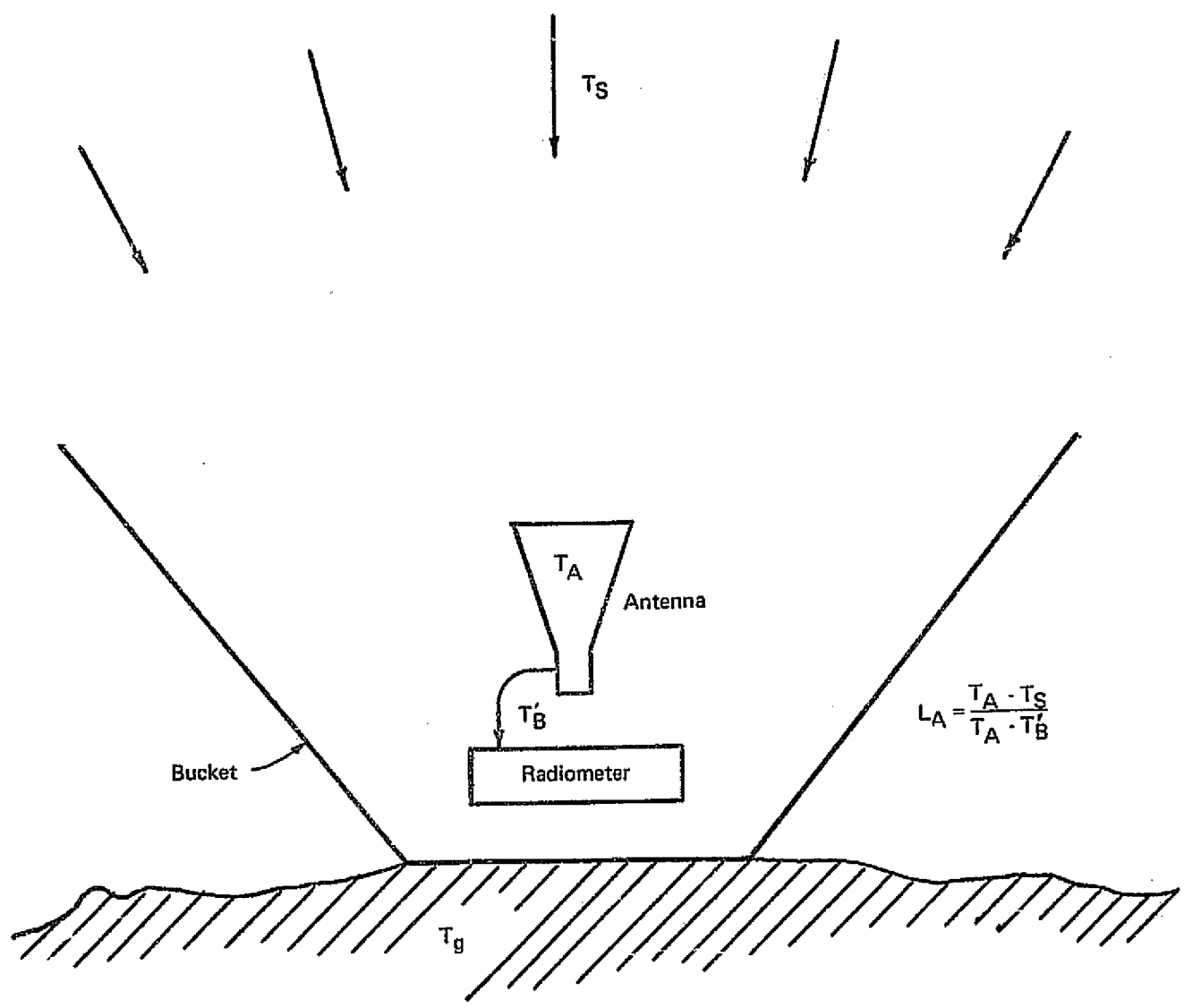


Fig. 2-4. Bucket technique for loss measurements.

ORIGINAL PAGE IS
OF POOR QUALITY

2.4.2 Errors due to Bucket Emissivity

It is apparent that (2-25) implies that the antenna in the bucket is assumed to be surrounded by an isothermal brightness temperature distribution, i.e., the bucket has a net zero emissivity. Also, it is tacitly assumed that the bucket is large enough so that there is no mutual coupling between the test antenna and the bucket. Assuming an emissivity of .001 for aluminum, the bucket brightness temperature would be [Carver,1973]

$$T_{BK} = e T_A = (.001)(290) = .29 \text{ K} \quad (17)$$

Assuming that the main beam views a 10 K sky and a 95% bucket efficiency*, the contribution from the sky plus bucket would be

$$\begin{aligned} T_B &= \eta T_{\text{sky}} + (1 - \eta)(T_{BK} + T_{\text{sky}}) \\ &= T_{\text{sky}} + (1 - \eta) T_{BK} \\ &= 10 + (.05)(.29) \\ &= 10.01 \text{ K} \end{aligned}$$

Thus the error in neglecting the emissive temperature of the bucket walls is only .01 K. Even under severe oxidation conditions in which the emissivity might increase by a factor of 10, the error is still less than 0.2 K.

*The bucket efficiency η is the percent power received by the antenna which is not reflected by the bucket.

2.4.3 Bucket Shape Criteria

How large does the bucket need to be in order to avoid first order mutual coupling effects? The answer to this depends on the near-field distribution of the worst-case antenna(s) being used, i.e., the antenna(s) having the strongest fields near the bucket walls. For the case of PMIS/MFMR, the L-Band array and the X-Band array are electrically closest. These near-field distributions can be estimated using Hansen's [1964] calculated curves for uniform and tapered distribution horns, and setting a criterion that the distance from the antenna to any bucket wall should be large enough so that the near field reflected power is at least 30 dB below the main beam on-axis power at the same distance.

2.4.4 Bucket Effect on Antenna Pattern - An X-Band Experiment

A small model bucket was built using this approach, scaled for use with an X-Band standard gain horn, and with dimensions shown in Fig. 2-5. The power patterns of the horn in free space and inside the bucket are compared in Fig. 2-6 where it is seen that the effect of the bucket is to eliminate sidelobes beyond the bucket shadow boundaries and to introduce a distortion to the free-space pattern. The horn is relatively large in comparison to the bucket so that the perturbation is most likely due to the phase interference of multiply edge-diffracted rays and the unreflected incident rays.

2.4.5 Description of Full Scale Bucket

The full-scale bucket was made much larger than any antenna to be put in it, so that no appreciable perturbations in the lit-zone pattern is expected. Dimensions are given in Fig. 2-7 along with sketches of the antenna positioner and PMIS/MFMR systems.

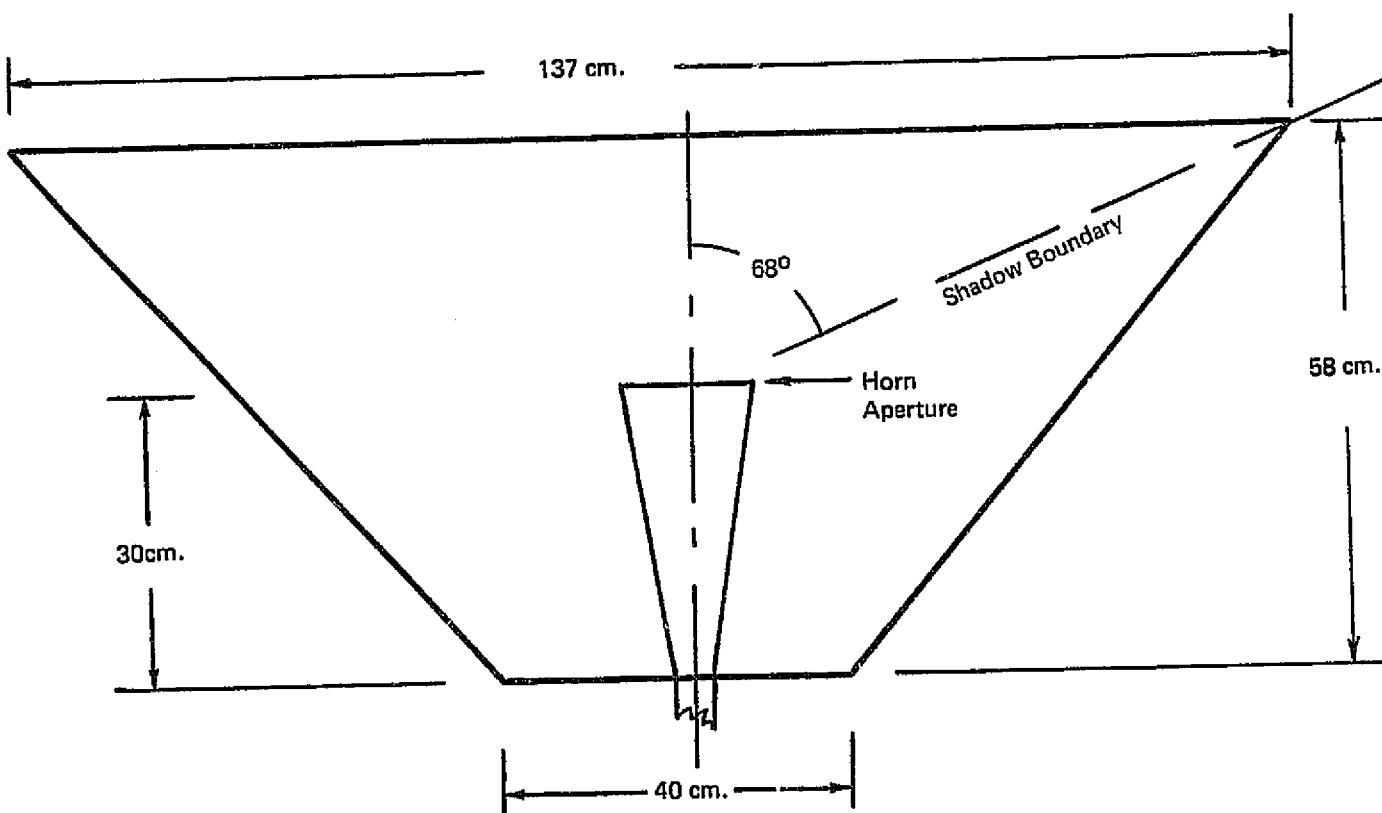


Fig. 2-5. Scale model bucket for X-Band standard gain horn.

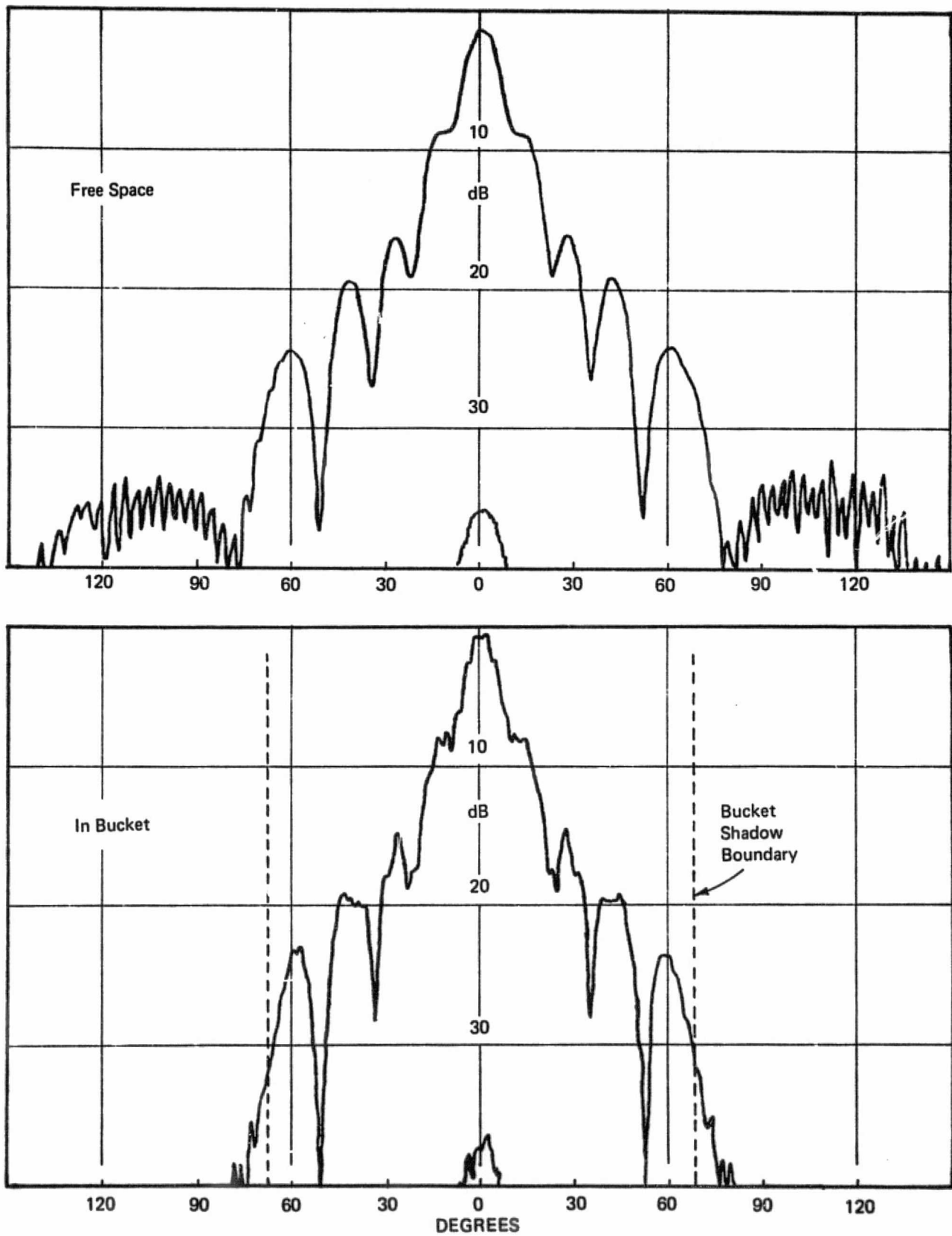
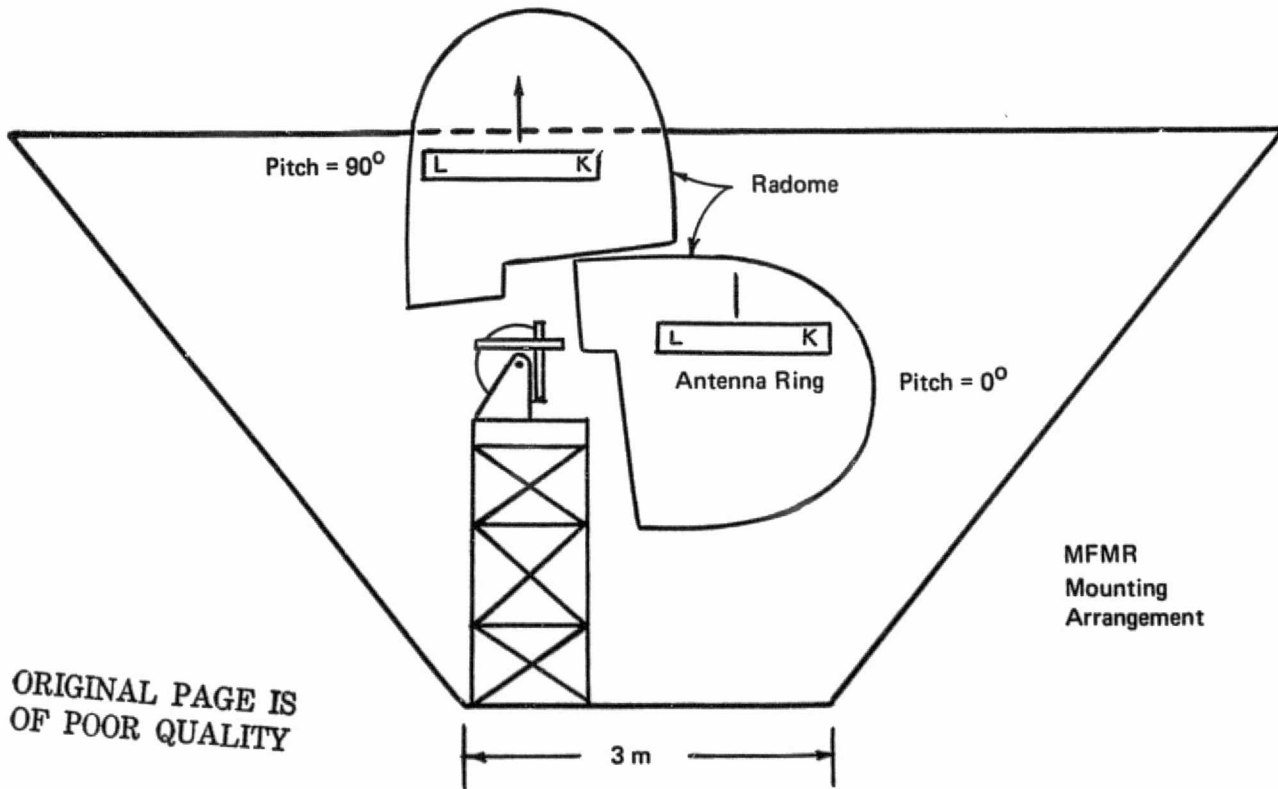
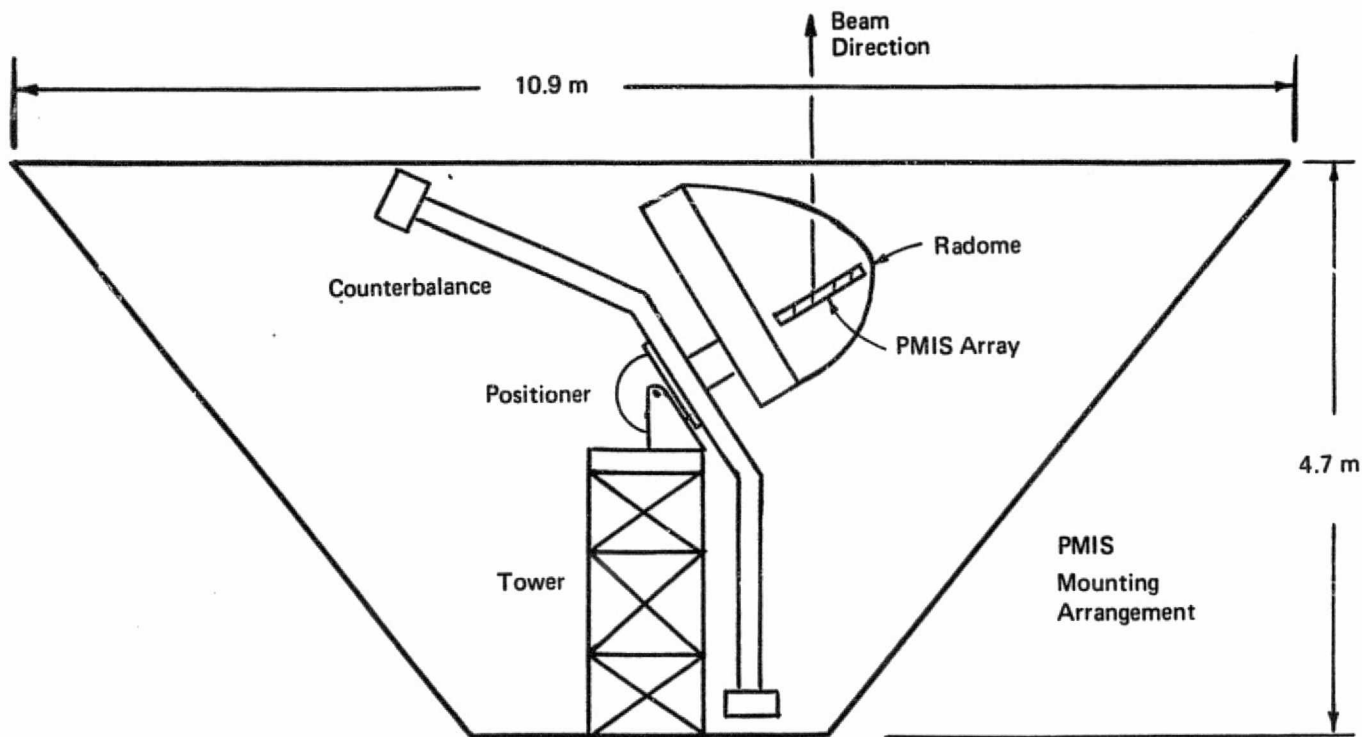


Fig. 2-6. Standard gain horn antenna pattern.



ORIGINAL PAGE IS
OF POOR QUALITY

Fig. 2-7. Bucket and antenna geometry.

The bucket is an aluminum foil covered wooden truncated and inverted pyramid, with a reinforced concrete base pad. It is located about 9 km east of the NMSU campus at an altitude of 1.46 km on "A" Mountain. The photographs of Fig. 2-8 - 2-11 show phases of the bucket construction. Equipment access is through a 3 m x 6 m door, as shown in Fig. 2-12, with special lifting rigs available for the PMIS and MFMR antenna and radome systems, as shown in Figs. 2-13 - 2-16. Personnel access is through a small removable door on the south side. Antenna/radome mockups are mounted on a Scientific-Atlanta az over el positioner affixed to the top of a steel support tower, with center-of-gravity maintained on the tower axis by use of counterbalance assemblies.

Electronic and control equipment is housed in a large temperature controlled concrete block building (see Fig. 2-17) about 15 m south of the bucket with an interconnecting cableway. During operations, a weather station is used to give temperature, relative humidity, pressure, wind speed and wind direction. An all-weather gravel road permits truck transport of equipment to the facility.



Fig. 2-8 Pre-fabrication and Painting Bucket Parts
(12 Nov. 1974)



Fig. 2-9 Cementing Aluminum Foil to
Bucket Interior Surface
(13 Nov. 1974)

ORIGINAL PAGE IS
OF POOR QUALITY

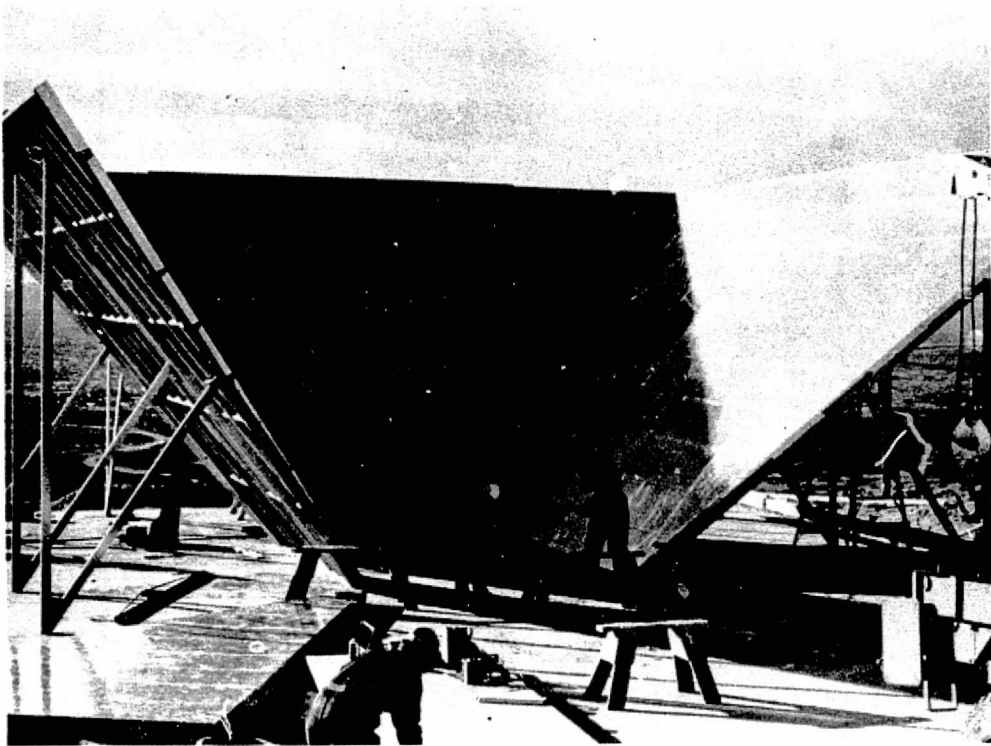


Fig. 2-10 Bucket Assembly Underway
(14 Nov. 1975)

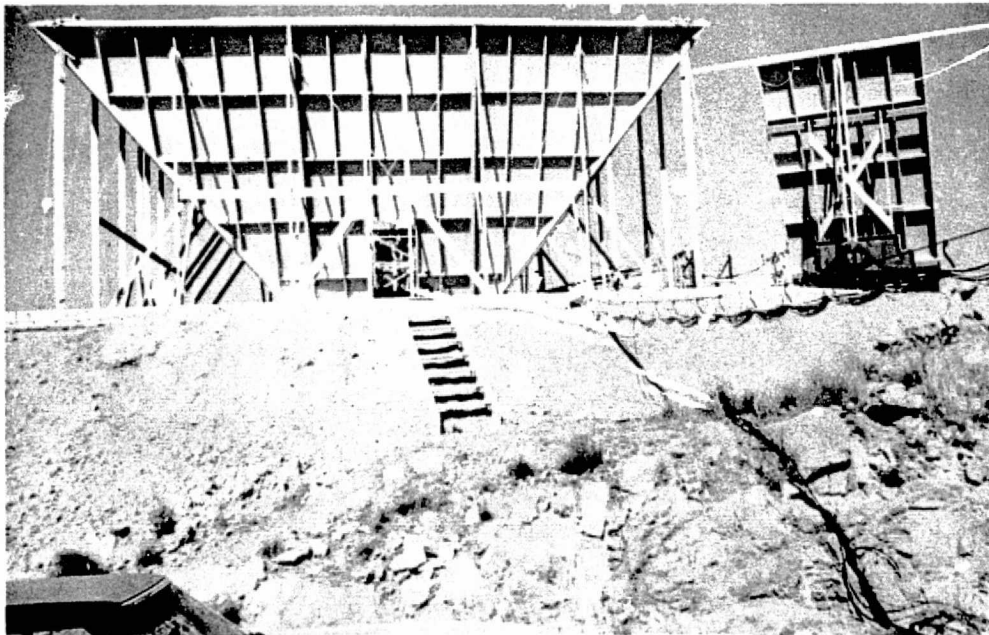


Fig. 2-11 South Face of Bucket Showing Braces
and Rigging to Sustain 100 mph Wind
(Jan. 1975)

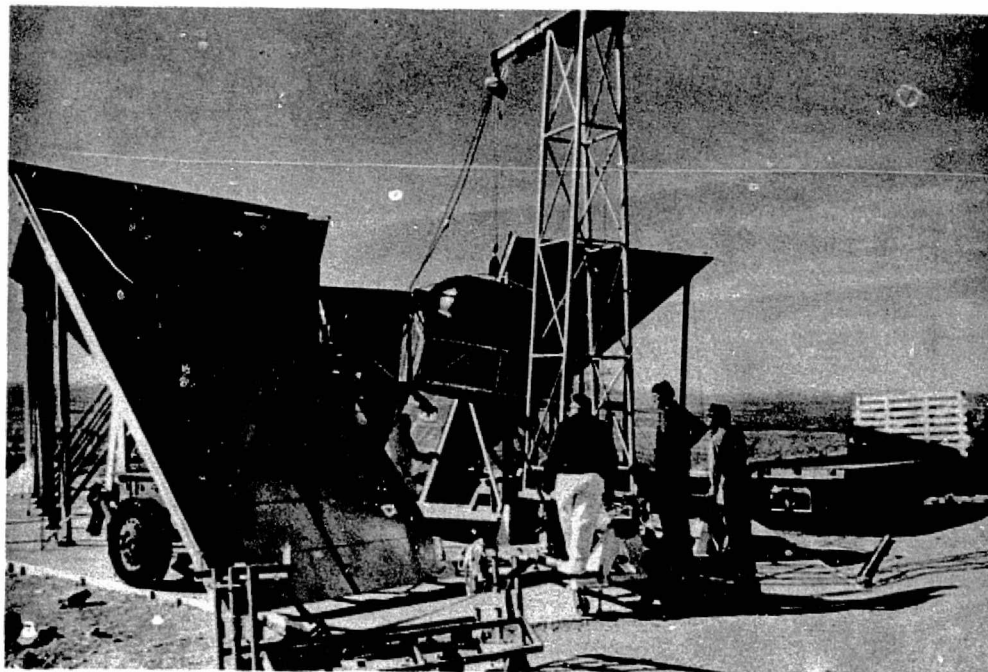


Fig. 2-12 PMIS in Position for Test -
Main Bucket Door Open
(Jan. 1975)

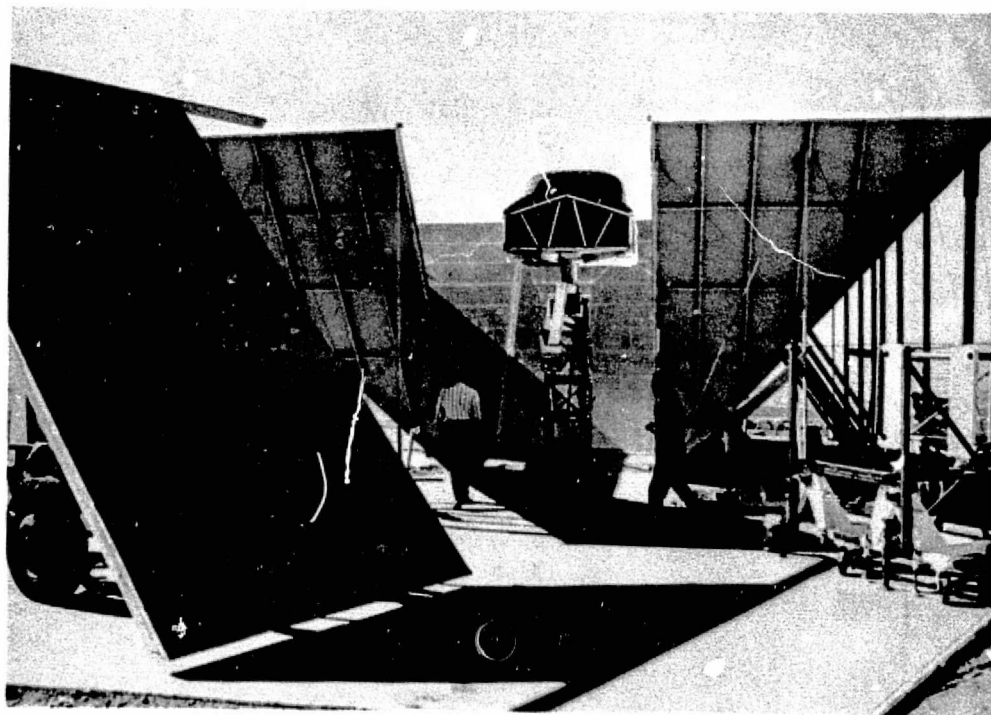


Fig. 2-13 PMIS in Mockup on Sling and Handling Dolly
(6 Feb. 1975)

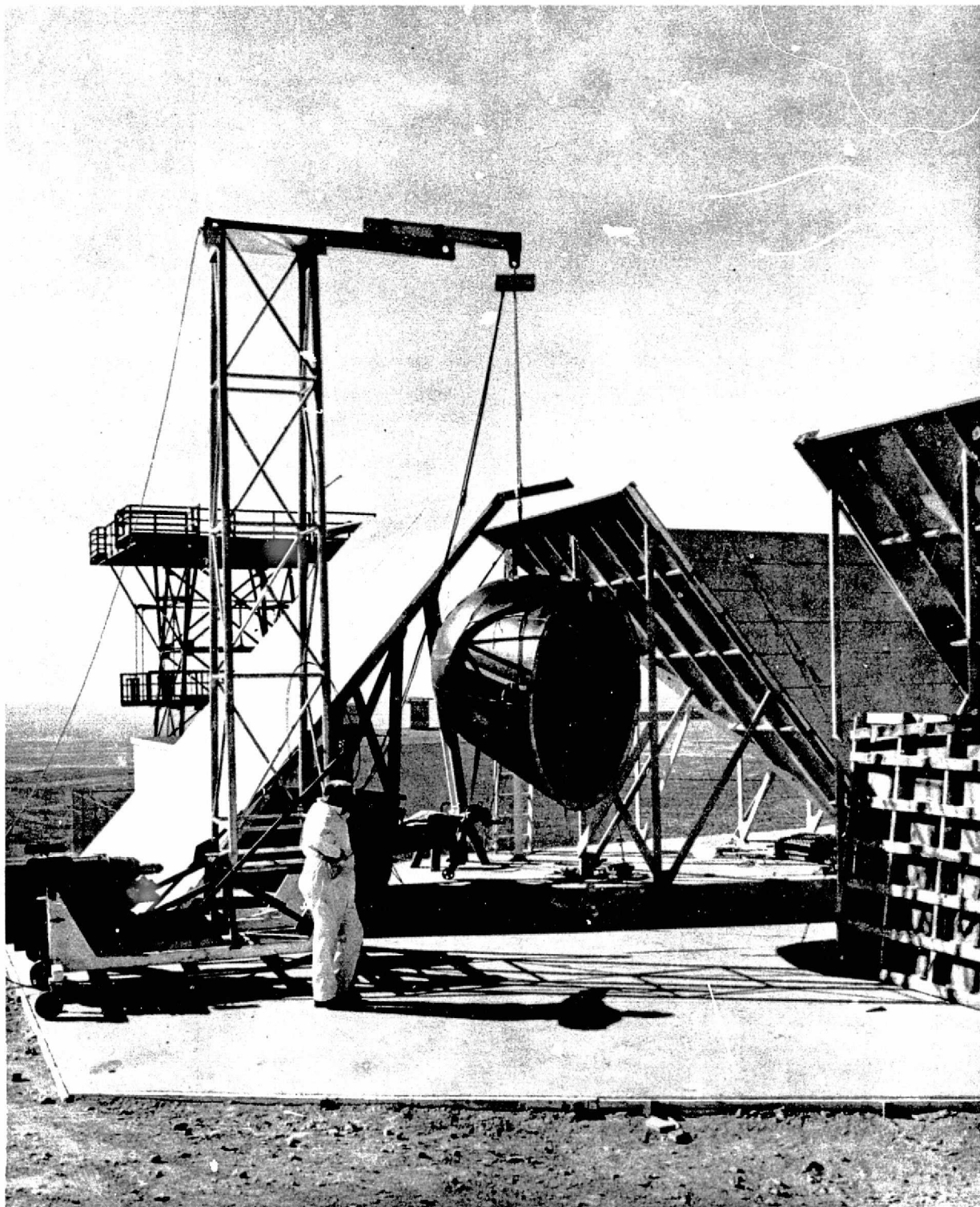


Fig. 2-14 MFMR Radome in Handling Sling
(20 Feb. 1975)

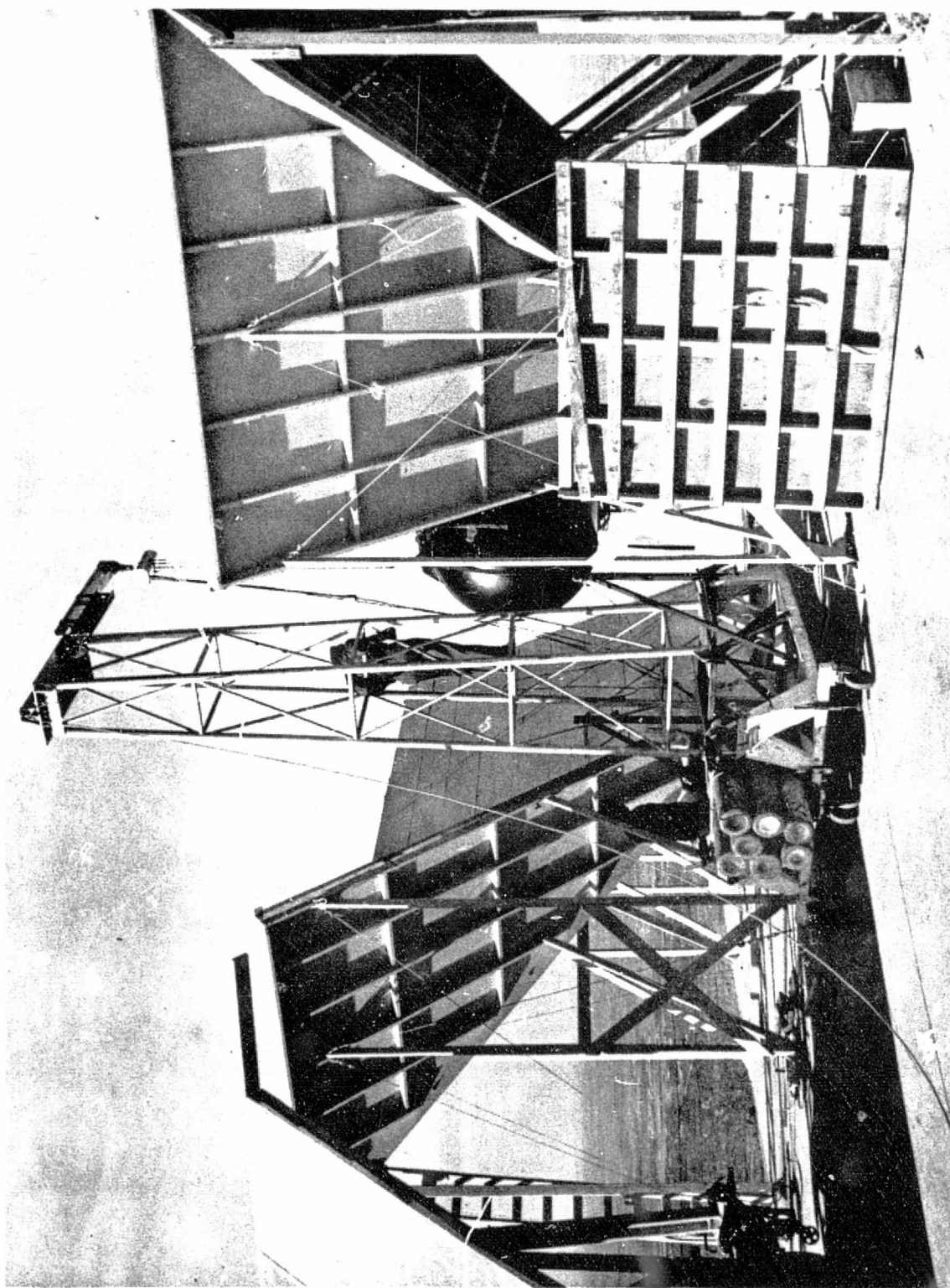


Fig. 2-15 Mounting MFMR Radome
(20 Feb. 1975)

ORIGINAL PAGE IS
OF POOR QUALITY

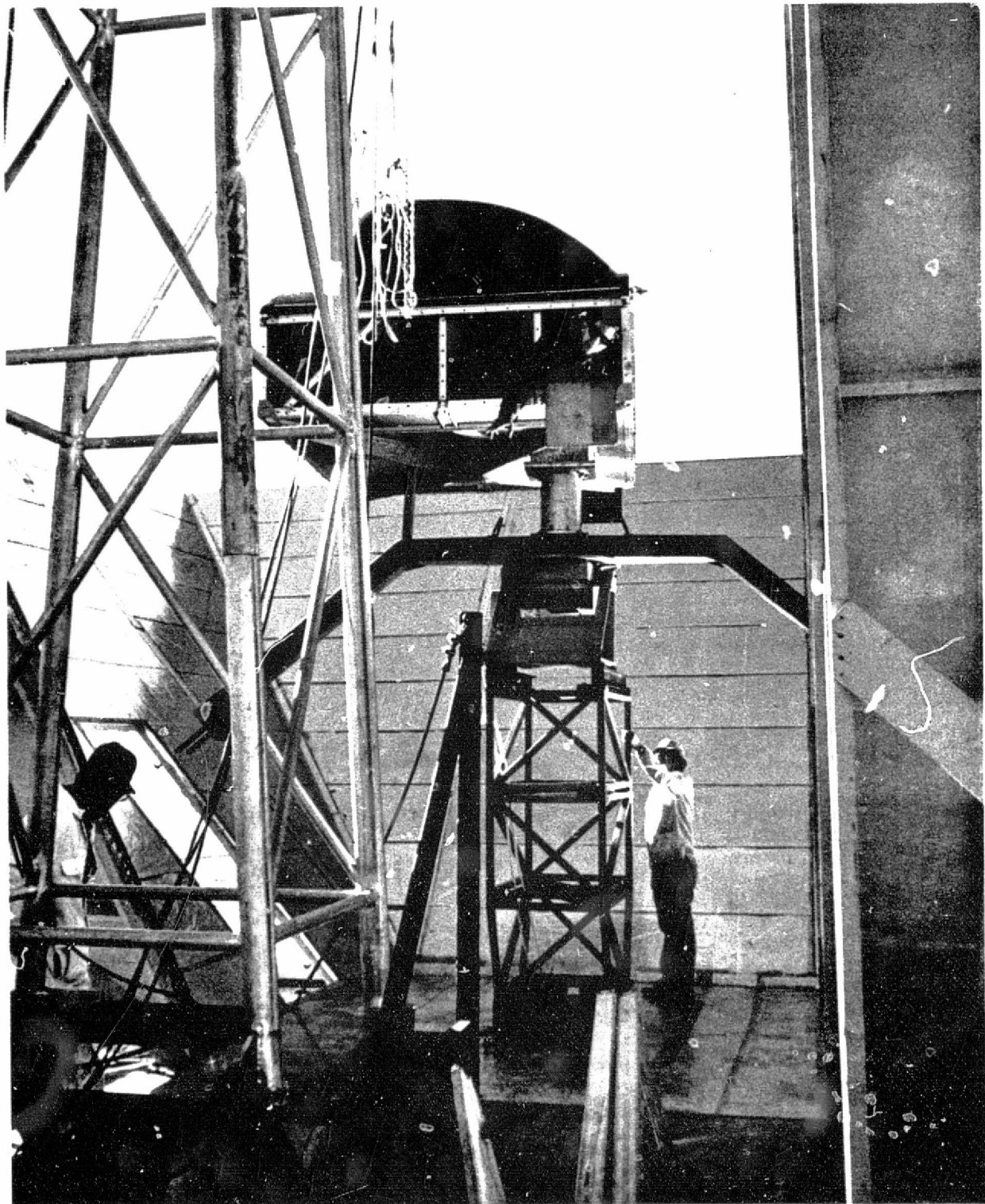


Fig. 2-16 Mounting PMIS - Note Counter Weight
(24 Jan. 1975)

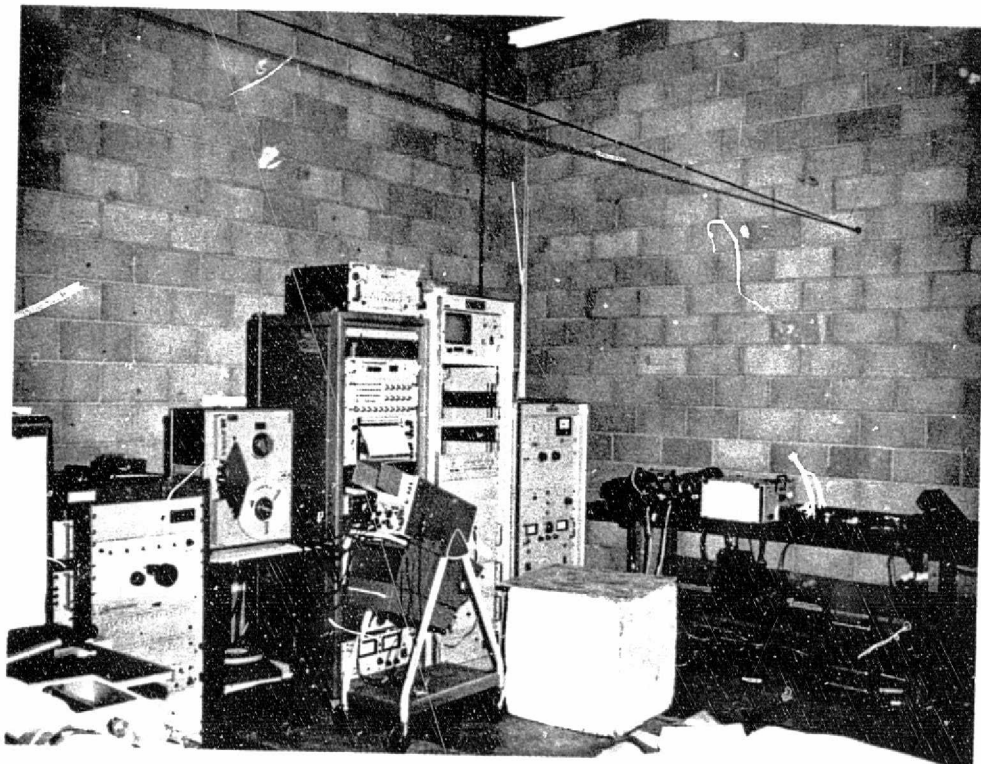


Fig. 2-17 PMIS Equipment Setup
(Dec. 1974)

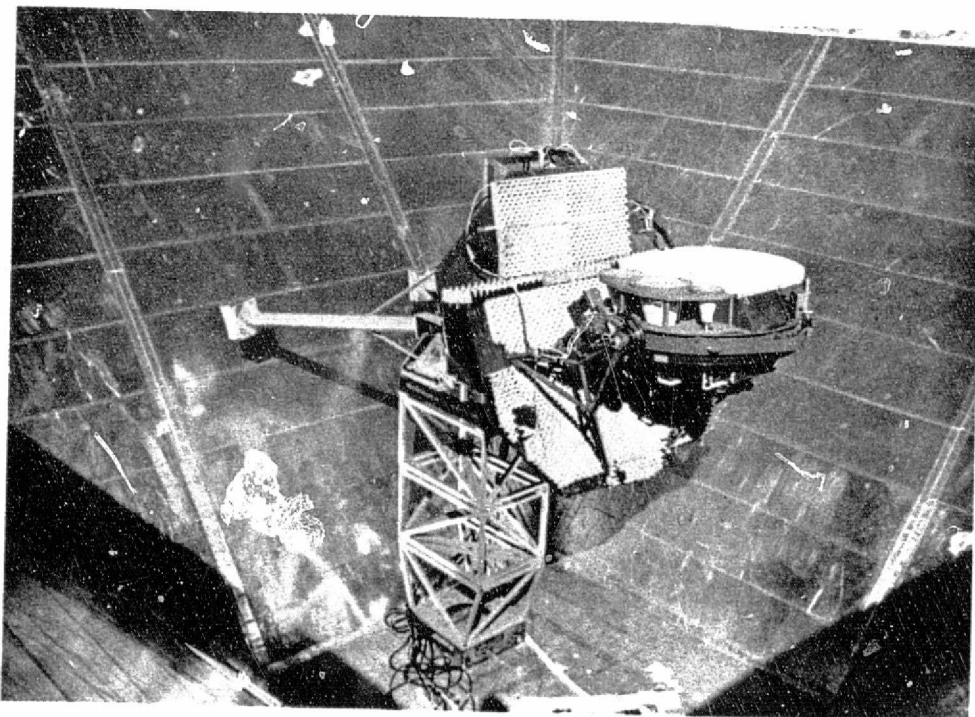


Fig. 2-18 MFMR with Absorber Mounted for Test
(Feb. 1975)

ORIGINAL PAGE IS
OF POOR QUALITY

CHAPTER III

ANTENNA/RADOME DATA REDUCTION TECHNIQUES

3.0 INTRODUCTION

This chapter discusses the theoretical framework for the inference of antenna and radome loss as well as the practical techniques used for the PMIS and MFMR systems.

It is worth repeating that the loss values L_A and L_R are used in establishing the absolute accuracy of an integrated radiometer (antenna plus receiver) and that the need for these values must be established by the user. How accurate must the inferred brightness temperatures be? At present, accuracies of ± 1 K are considered to be very good with receiver sensitivities between 0.1 K and 1.0 K achievable using integration times ranging from 100 - 1000 milliseconds. But can a user establish a need for a ± 1 K accuracy? Will ± 3 K suffice? This is a difficult question, having to do with the adequacy of radiative transfer models, the availability of sufficient ground truth in controlled areas, aircraft/spacecraft platform stability, etc.

It is clear, however, that relative loss values are extremely important. In the case of PMIS, there are 44 beam positions, electronically scanned, and it is necessary to establish the loss value of a given beam position relative to its adjacent beam positions with maximum precision. For MFMR, the variation in loss with pitch angle change is of greater immediate importance than the absolute value of those losses.

3.1 Theoretical Foundation for Loss Calculations

A calibrated radiometer viewing an isothermal source T_S indicates an uncorrected brightness temperature T_B' which is

greater than T_S , due to the added emissive contributions of the intervening waveguide, antenna, and radome. Considering first the radiative transfer when there is no radome (Fig. 3-1a), we have [Kraus, 1966]

$$T'_B = \underbrace{\left(1 - \frac{1}{L_W}\right) T_W}_{\text{emissive contr. from waveguide}} + \frac{1}{L_W} \left\{ \underbrace{\frac{T_S}{L_A}}_{\text{antenna absorption term}} + \underbrace{\left(1 - \frac{1}{L_A}\right) T_A}_{\text{emissive contr. from antenna}} \right\} \quad (3-1)$$

where

T'_B = uncorrected brightness temp. measured by radiometer (K)

T_S = sky brightness temp. (K)

T_A = antenna kinetic temp. (K)

T_W = waveguide kinetic temp. (K)

L_A = antenna loss ($L_A > 1$)

L_W = waveguide loss ($L_W > 1$)

It is assumed that the waveguide loss is known from laboratory measurements. Solving for L_A ,

$$L_A = \frac{T_A - T_S}{T_A + (L_W - 1)T_W - L_W T'_B} \quad (3-2)$$

Turning now to the radome loss L_R (Fig. 3-1b), the radiative transfer equation is

$$T'_B = \left(1 - \frac{1}{L_W}\right) T_W + \frac{1}{L_W} \left\{ \left(1 - \frac{1}{L_A}\right) T_A + \frac{1}{L_A} \left[\left(1 - \frac{1}{L_R}\right) T_R - \frac{T_S}{L_R} \right] \right\} \quad (3-3)$$

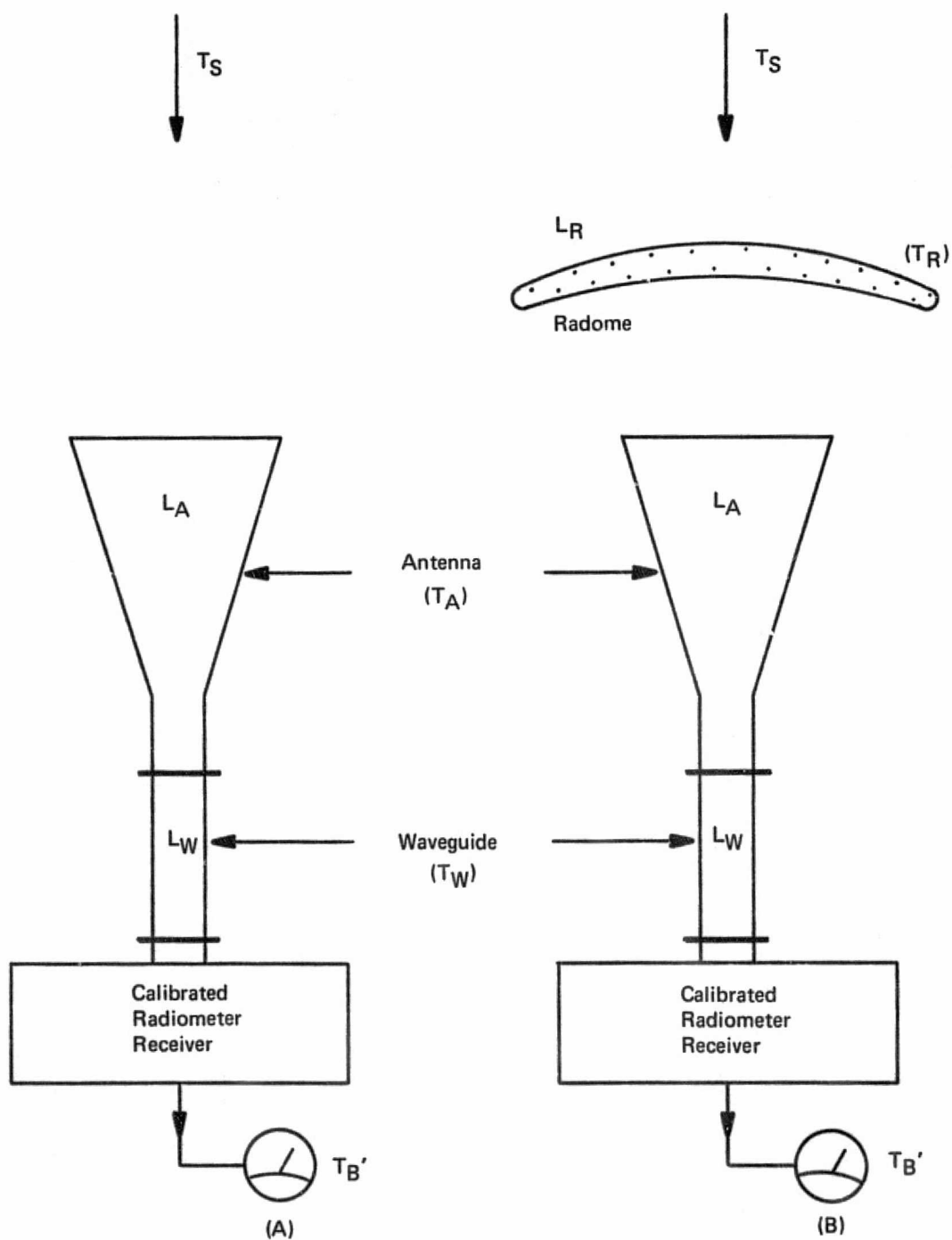


Fig. 3-1. Radiometer, waveguide and antenna (without and with radome).

Solving for L_R ,

$$L_R = \frac{T_R - T_S}{T_R + T_A(L_A - 1) + \frac{T_W L_A (L_W - 1) - L_A L_W T_B}{L_A L_W}} \quad (3-4)$$

The coupled equations (3-2) and (3-4) form the basis for the measurement of the antenna loss and radome loss. It is assumed that the L_A value in (3-4) is the same as that calculated in (3-2), i.e., there is no mutual coupling between radome and antenna.

The thermometric temperatures of the antenna, radome and waveguide structures are read by imbedded thermistors. The sky brightness temperature is calculated by techniques described in Chap. IV and the uncorrected brightness temperature T_B' is that indicated by the calibrated radiometer.

In practice, both random and systematic errors are introduced into (3-2) and (3-4) with concomitant effects on both precision and accuracy. These are discussed in detail in Chaps. V and VI.

3.2 PMIS/MFMR Data Systems

Both PMIS and MFMR are operated on a Lockheed P-3A aircraft, along with other remote sensors such as multi-spectral optical scanners, etc., with all electronic data being recorded on magnetic tape in PCM format. Thus, the output of both PMIS and MFMR is in PCM counts with integration times of 100 ms being typical during flight operations. However, an integration time of 1 minute was used during the loss calibration tests so that an improved sensitivity would be obtained.

The sensitivity of the radiometer is continuously monitored by the use of two internally generated equivalent temperatures known as the calibrate and baseline modes, with corresponding PCM counts C_C and C_B , respectively. Assuming the radiometer is linear, the uncorrected brightness temperature is given by

$$T'_B = T_1 + \Delta T \frac{\bar{C}_A - \bar{C}_B}{\bar{C}_C - \bar{C}_B} \quad (3-5)$$

where

T_1 & ΔT = constants to be determined (K)

\bar{C}_A = one minute average of data counts

\bar{C}_B = one minute average of baseline counts

\bar{C}_C = one minute average of calibrate counts

as shown in Fig. 3-2.

T_1 and ΔT are determined by connecting known noise temperatures to the radiometer input port and by computing the best linear regression fit to the resulting data, or if only a hot and cold load are available, by solving two equations and two unknowns. Figs. 3-3 and 3-4 show the calibration history of T_1 and ΔT for the PMIS vertically and horizontally polarized channels, over the Jan. 20 - Feb. 6, 1975 time period. The horizontal channel shows much more long-term instability than the vertical, which was the basis for recurring difficulties in data reduction. Fig. 3-5 shows a similar history of T_1 and ΔT for MFMR, comparing the initial calibration on Feb. 8, 1975 to the final calibration on Feb. 21, 1975. The K-Band (22.05 GHz) receiver was not working

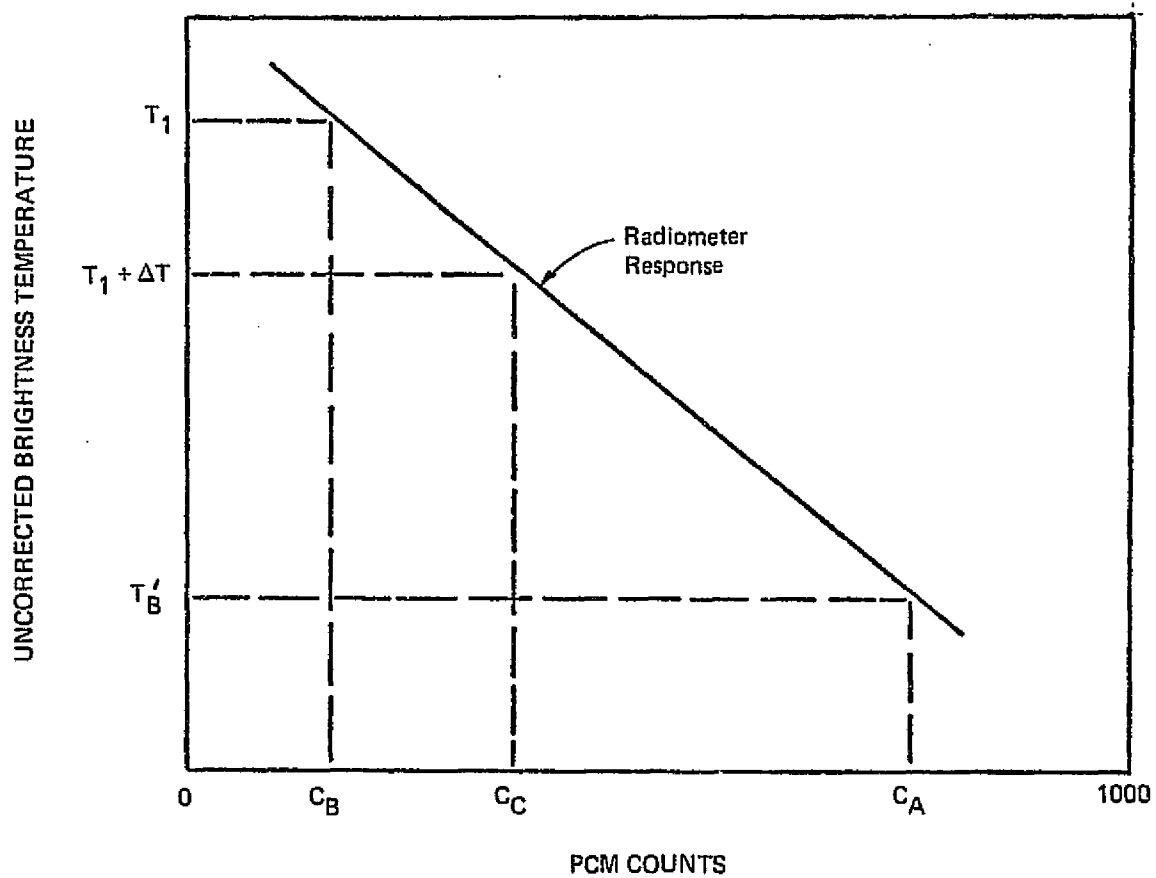


Fig. 3-2. Uncorrected brightness temperature versus PCM counts.

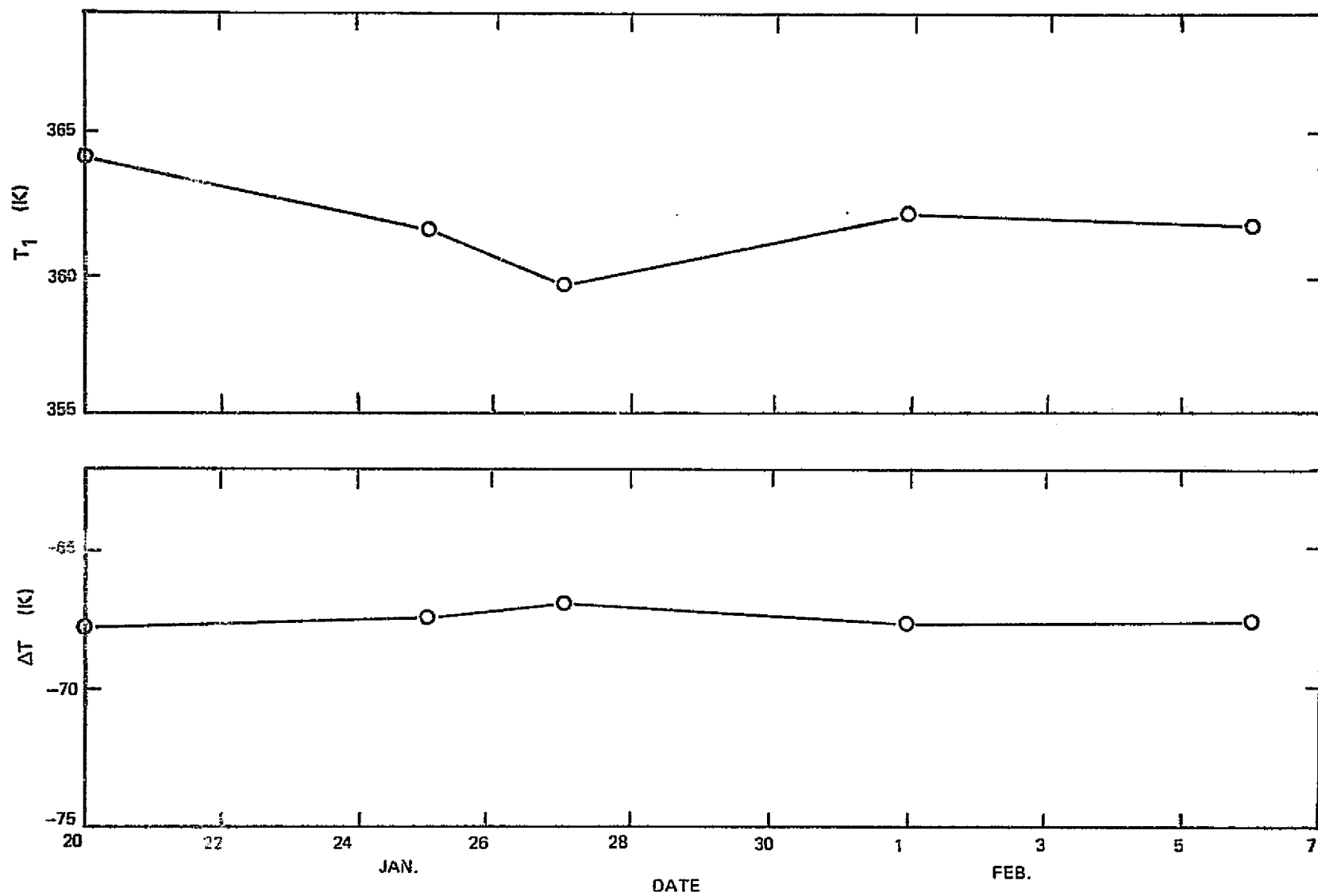


Fig. 3-3. PMIS calibration repeatability - vertical polarization.

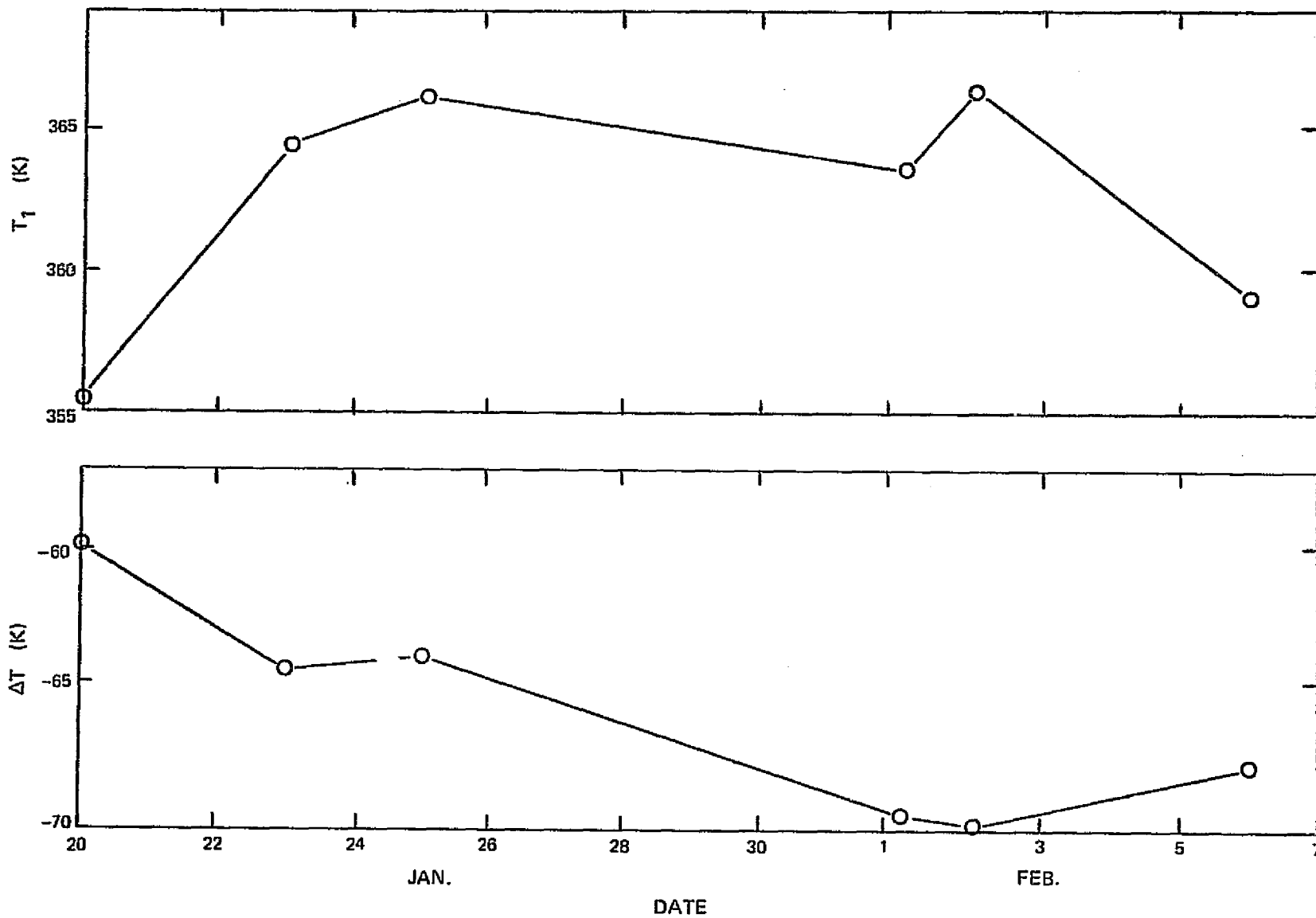


Fig. 3-4. PMIS calibration repeatability - horizontal polarization.

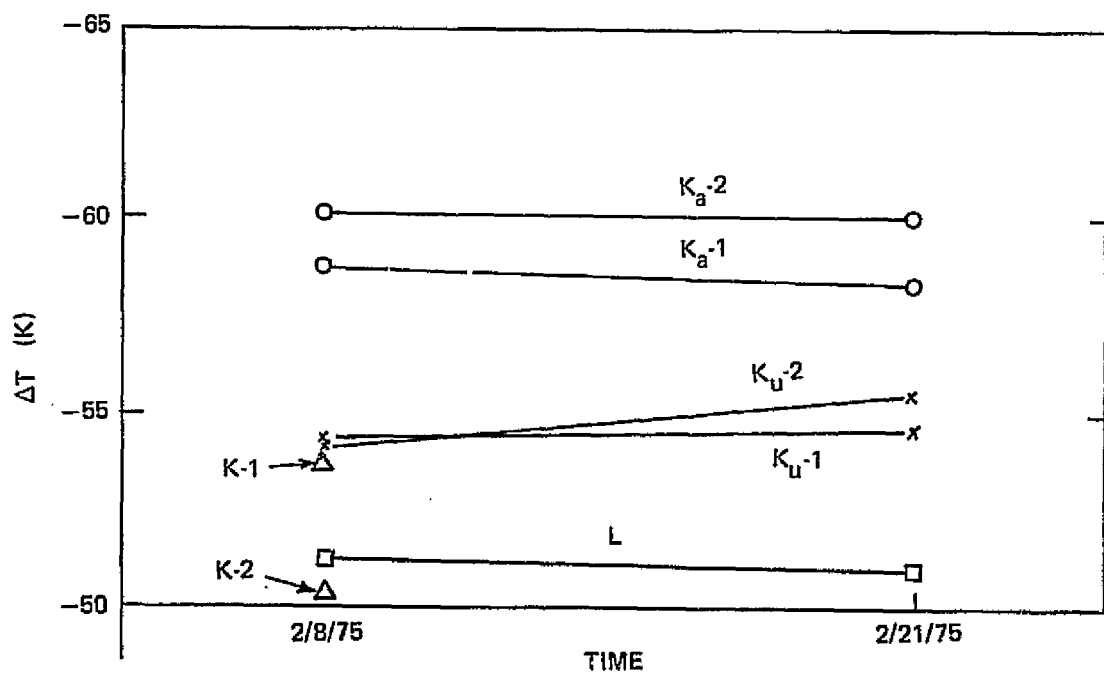
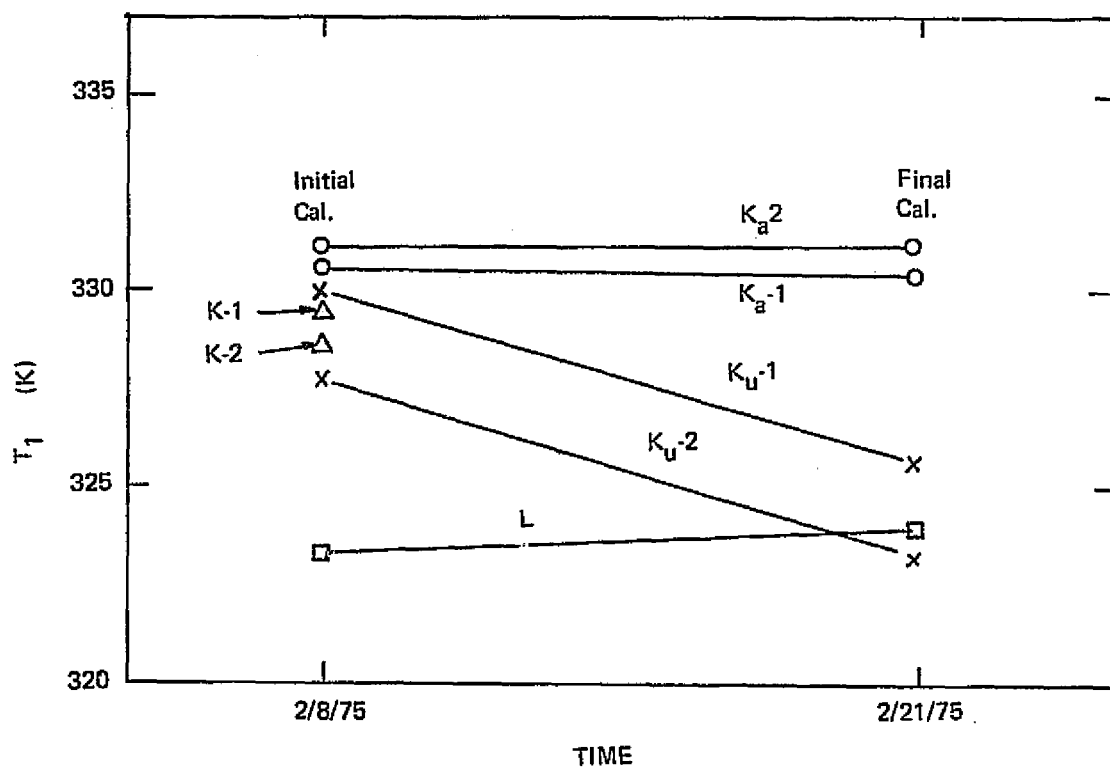


Fig. 3-5. MFMR calibration history.

on Feb. 21, so that only an initial set of values are shown. The apparent downward drift in the T_1 value for K_u -Band was caused by not allowing sufficient warmup time before calibration.

In addition to the PCM counts corresponding to the radiometric data, both PMIS and MFMR software require the monitoring of other housekeeping data, such as antenna, radome and waveguide thermistors, AGC voltages, electronics enclosure temperatures, etc. These data are multiplexed and recorded on magnetic tape for subsequent processing, as shown in Fig. 3-6. Data tapes recorded at the bucket site are brought to the computer facility at the PSL building on campus. Data on the tapes are then decommutated, and transferred to storage addresses within the IBM 370 computer, all of this being under control of the IBM SYSTEM 7 process controller.

Data reduction then proceeds under three phases of software: PMIS/MFMR -1, 2, and 3 as shown in Fig. 3-6. Phase 1 strips and sorts data from the tape, calculates means and standard deviations and prints significant data in counts, as shown in Figs. 3-7, 3-8. Phase 2 converts radiometric housekeeping data into appropriate engineering units, as shown in Figs. 3-9, 3-10. Phase III then calculates loss values and associated standard deviations by using eqns. (3-2) and (3-4), and prints the results as shown in Figs. 3-11, 3-12.

The detailed instructions for the reduction of PMIS and MFMR data tapes are given in the Appendix. The software written for this purpose is extremely complex and powerful. However, it must be complemented by a parallel intervention of the project engineer and programmer in order to monitor the health of the various components of the PMIS/MFMR systems and to properly intermesh the L_A values (eqn. 3-2) into the computation of L_R (eqn. 3-4).

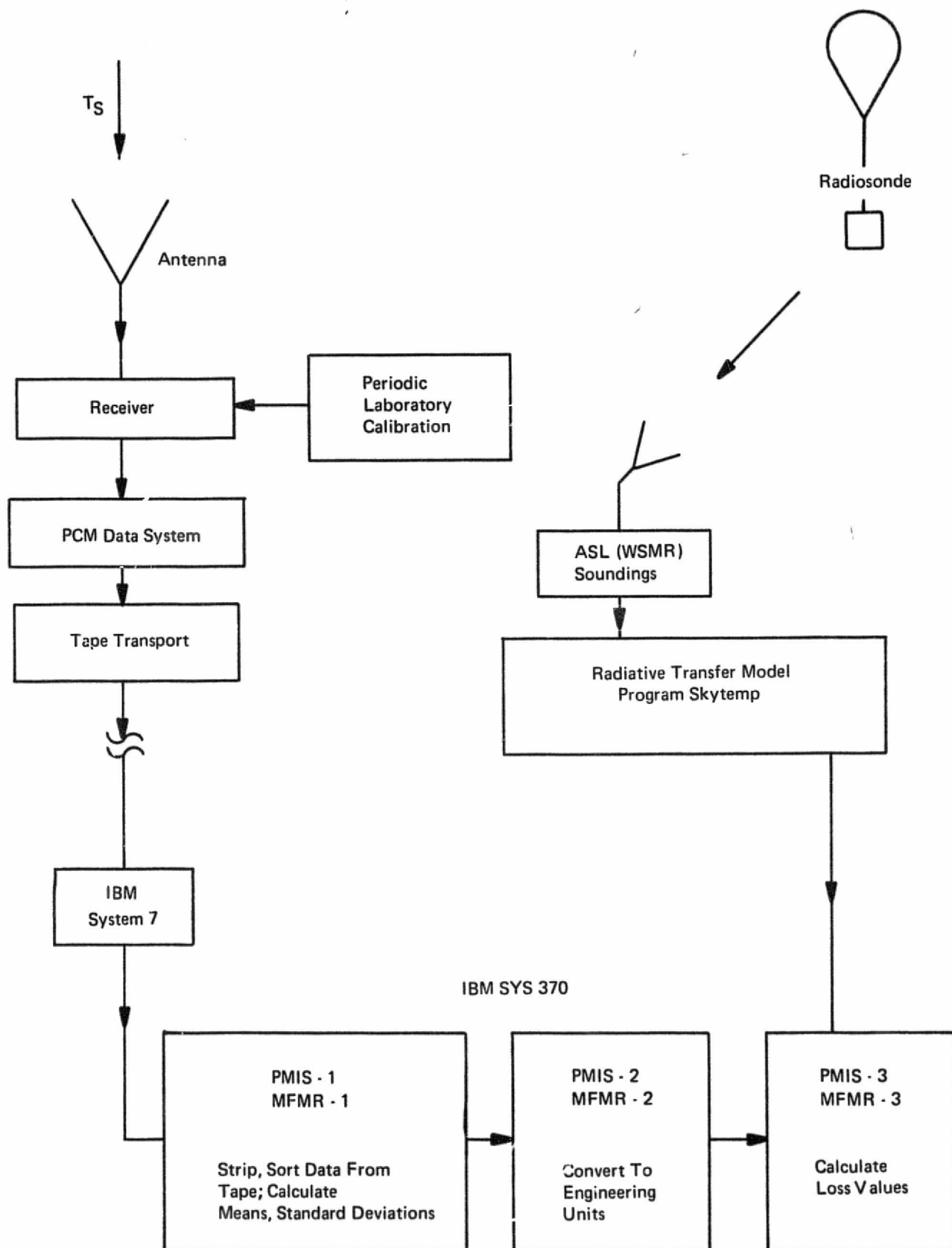


Fig. 3-6. Data flow chart.

NUMBER OF DATA CYCLES = 288 CONTROL CODE = FFFF0000 LOGID = P040
 START TIME = 1 HOURS 37 MINUTES 8.10 SECONDS END TIME = 1 HOURS 38 MINUTES 30.01 SECONDS
 HIGH DISK ADDRESS OF THIS DATA SET = 116649 HIGHEST ADDRESS OF DATA USED = 116499 HIGH ADDRESS AT THE END OF LAST JOB = 116499
 HALF BEAM STEP RATE = 0 FRAME PULSE = 1 SCAN MANUAL = 1
 BEAM POSITION = 22 V/H RATIO = 66 VALID DATA WORD = 605

PCM COUNT	PCM COUNT SQUARED	NUMBER OF FULL CYCLES	CAL COUNT VERTICAL	CAL COUNT HORIZONTAL	CAL COUNT SQUARED VERTICAL POLARIZATION	CAL COUNT SQUARED HORIZONTAL POLARIZATION	NUMBER OF ELEMENTS	BASE LINE COUNT	BASE LINE SQUARED	NUMBER OF ELEMENTS
210236	162108306	273	46257	0	10917019	0	196	5701	200977	162
0	0	0	0	0	0	0	0	996970	53929660	18431

Fig. 3-7 PMIS-1 Sample Output.

ORIGINAL PAGE IS
 OF POOR QUALITY

THE MODE IS JPR
 AVG OF KU-BAND RADIOMETER CH.1 = 876 AVG OF THE SQUARES = 764876
 AVG OF KU-BAND RADIOMETER CH.2 = 873 AVG OF THE SQUARES = 763024
 AVG OF KA-BAND RADIOMETER CH.1 = 793 AVG OF THE SQUARES = 628989
 AVG OF KA-BAND RADIOMETER CH.2 = 789 AVG OF THE SQUARES = 623214
 AVG OF K- BAND RADIOMETER CH.1 = 868 AVG OF THE SQUARES = 754663
 AVG OF K- BAND RADIOMETER CH.2 = 909 AVG OF THE SQUARES = 826376
 AVG OF L- BAND RADIOMETER = 779 AVG OF THE SQUARES = 605675

NUMBER OF DATA CYCLES IN FILE = 222 VALID DATA = 00000245 LOGID = #003
 START TIME = 2 HOURS 45 MINUTES 46.03 SECONDS END TIME = 2 HOURS 46 MINUTES 46.06 SECONDS
 HIGH DISK ADDRESS OF THIS DATA SET = 255399 HIGHEST ADDRESS OF DATA USED = 243249 HIGH ADDRESS AT THE END OF LAST JOB = 252249

Fig. 3-8 MFMR-1 Sample Output.

DISK ADDRESS	RAW COUNT	DESCRIPTION	CHANNEL NUMBER	DISK ADDRESS	ENGINEERING UNITS	FORMAT	IDP OR EDP SUBSCRIPT
508000	325	BEAM POSITION	3- 1-D	508050	22	I	1
508001	66	V/H PATIO	3- 2-D	508051	66	I	2
508002	214052	VERT POLARIZATION	3- 3-D	508052	770.4392 AVG CTS	F	3
508003	0	HORIZ POLARIZATION	3- 4-D	508053	***** AVG CTS	F	4
508004	605	VALID DATA CODE	3- 5-D	508054	0000025D CTS	I	5
508005	165023318	STD VERTICAL	3-27-D	508055	5.7097	F	6
508006	0	STD HORIZONTAL	3-23-D	508056	0.0	F	7
508007	109185	ANTENNA THERMISTOR 1	3-41-A	508057	4.9896 DEG C	F	8
508008	111871	ANTENNA THERMISTOR 2	3-42-A	508058	4.2549 DEG C	F	9
508009	74054	AVE OF 4 ANT TEMPS	3-43-A	508059	16.4990 DEG C	F	10
508010	296721	RADOME THERMISTOR 1	3-44-A	508060	-70.9019 DEG C	F	11
508011	297819	RADOME THERMISTOR 2	3-45-A	508061	-72.3959 DEG C	F	12
508012	298704	AVE OF 4 RADOME TEMPS	3-46-A	508062	-73.6000 DEG C	F	13
508013	295176	BOMB BAY THERMISTOR 1	3-47-A	508063	-68.8000 DEG C	F	14
508014	296364	BOMB BAY THERMISTOR 2	3-48-A	508064	-70.4162 DEG C	F	15
508015	296176	AVE OF 4 BOMB BAY TEMPS	3-49-A	508065	-70.1604 DEG C	F	16
508016	61742	HORIZ WAVE GUIDE TEMP	3-57-A	508066	21.8767 DEG C	F	17
508017	68329	VERT WAVE GUIDE TEMP	3-51-A	508067	19.1333 DEG C	F	18
508018	1331	HORIZ HOT LOAD TEMP	3-52-A	508068	167.3197 DEG C	F	19
508019	262646	VERT HOT LOAD TEMP	3-52-A	508069	130.0541 DEG C	F	20
508020	0	HORIZ WARM LOAD TEMP	3-54-A	508070	89.5239 DEG C	F	21
508021	246989	VERT WARM LOAD TEMP	3-55-A	508071	60.7170 DEG C	F	22
508022	1373	HORIZ PARAMETRIC AMP TEMP	3-56-A	508072	93.4742 DEG C	F	23
508023	55178	VERT PARAMETRIC AMP TEMP	3-57-A	508073	54.9325 DEG C	F	24
508024	1417	HORIZ ENCLOSURE TEMP	3-58-A	508074	93.4406 DEG C	F	25
508025	54869	VERT ENCLOSURE TEMP	3-59-A	508075	55.0974 DEG C	F	26
508026	116840	ELECT ENCLOSURE TEMP	3-60-A	508076	35.3007 DEG C	F	27
508027	294	NO. OF DATA CYCLES				I	28
508028	FFFF0000	CONTROL CODE				Z	29
508029	-672074512	LOG ID		= P040		A	30
508030	95952960	START TIME		= 1 HOURS 37 MINUTES 8.10 SECONDS		I	31
1165756400	96518148	END TIME		= 1 HOURS 38 MINUTES 30.01 SECONDS		I	32

IDP(22) = 46257
 IDP(34) = 10917019
 IDP(35) = 196
 IDP(36) = 6823
 IDP(37) = 239125
 IDP(38) = 195
 IDP(39) = 278
 IDP(40) = 0
 IDP(41) = 0
 IDP(42) = 0
 IDP(43) = 1017820
 IDP(44) = 55061830
 IDP(45) = 18815
 IDP(46) = 0

AVERAGE CALIBRATE COUNT VERT = 236.0051 SIGMA= 0.8197
 AVERAGE CALIBRATE COUNT HORIZ = 0.0 SIGMA= 0.0
 AVERAGE BASE LINE COUNT VERT = 34.9897 SIGMA= 1.4145
 AVERAGE BASE LINE COUNT HORIZ = 54.0962 SIGMA= 0.2961
 UNCORRECTED SKY BRIGHTNESS TEMP VERT = 115.1094
 UNCORRECTED SKY BRIGHTNESS TEMP HORIZ =*****

THE VALUES OF T1 & DELTA T & X USED WERE.
 T1VP = 361.96 K, DTVP = -67.47 K, T1HP = 365.30 K, DTHP = -69.62 K XV = 3.659 XH = *****
 SIGTRV = 2.5058 SIGTBH = *****

ORIGINAL PAGE IS
 OF POOR QUALITY

Fig. 3-9 PMIS-2 Sample Output

LOGID = 4003 VALID DATA CODE = 00000245
 START TIME = 2 HOURS 45 MINUTES 46.03 SECONDS END TIME = 2 HOURS 46 MINUTES 46.06 SECONDS
 RAW TOTAL DATA FOR THIS FILE STARTS AT DISK ADDRESS 242500
 ENGINEERING DATA FOR THIS FILE STARTS AT DISK ADDRESS 242500

RAW COUNT	SENSOR SYSTEM MEMO	CHAN NO	ENGINEERING UNITS
1	876	KU-BAND RADIOMETER CH 1	2A-1-A 8.7664E 02 AVG CTS
2	872	KU-BAND RADIOMETER CH 2	2A-2-A 8.7250F 02 AVG CTS
3	793	KA-BAND RADIOMETER CH 1	2A-13-A 7.9303F 02 AVG CTS
4	789	KA-BAND RADIOMETER CH 2	2A-14-A 7.9945F 02 AVG CTS
5	868	K-BAND RADIOMETER CH 1	2A-25-A 8.6867F 02 AVG CTS
6	909	K-BAND RADIOMETER CH 2	2A-26-A 9.0906F 02 AVG CTS
7	778	L-BAND RADIOMETER	2A-37-A 7.7821E 02 AVG CTS
8	12928	KU-BAND COLD REF. TEMP.	2A-3-A 2.7199E 02 DEG K
9	132880	KU HOT REF. TEMP.	2A-4-A 3.8131F 02 DEG K
10	121525	KU ANTENNA TEMP.	2A-5-A 2.7560F 02 DEG K
11	132098	KU SWITCH TEMP.	2A-6-A 3.2217F 02 DEG K
12	113399	KU CH.1 WAVE GUIDE TEMP.	2A-7-A 2.7962F 02 DEG K
13	116411	KU CH.2 WAVE GUIDE TEMP.	2A-8-A 2.7862F 02 DEG K
14	135028	KU-BAND AGC VOLTAGE	2A-9-A 2.9969F 00 VOLTS
15	129554	KA-BAND COLD REF. TEMP.	2A-15-A 2.7140F 02 DEG K
16	174860	KA HOT REF. TEMP.	2A-16-A 3.8207F 02 DEG K
17	121063	KA ANTENNA TEMP.	2A-17-A 2.7736F 02 DEG K
18	129580	KA SWITCH TEMP.	2A-18-A 3.2357F 02 DEG K
19	118685	KA CH.1 WAVE GUIDE TEMP.	2A-19-A 2.7774F 02 DEG K
20	120089	KA CH.2 WAVE GUIDE TEMP.	2A-20-A 2.7751F 02 DEG K
21	103041	KA-BAND AGC VOLTAGE	2A-21-A 2.3979F 00 VOLTS
22	128480	K-BAND COLD REF. TEMP.	2A-27-A 2.7118E 02 DEG K
23	131339	K HOT REF. TEMP.	2A-28-A 3.8182F 02 DEG K
24	120559	K ANTENNA TEMP.	2A-29-A 2.7744F 02 DEG K
25	121560	K SWITCH TEMP.	2A-30-A 3.2326F 02 DEG K
26	117899	K CH.1 WAVE GUIDE TEMP.	2A-31-A 2.7579F 02 DEG K
27	119094	K CH.2 WAVE GUIDE TEMP.	2A-32-A 2.7579F 02 DEG K
28	127658	K-BAND AGC VOLTAGE	2A-33-A 2.8522F 00 VOLTS
29	135344	L-BAND COLD REF. TEMP.	2A-39-A 2.7083F 02 DEG K
30	125124	L HOT REF. TEMP.	2A-40-A 3.8139F 02 DEG K
31	116456	L ANTENNA TEMP.	2A-41-A 2.7810F 02 DEG K
32	127600	L SWITCH TEMP.	2A-42-A 3.2389F 02 DEG K
33	107214	L WAVE GUIDE TEMP.	2A-42-A 2.7973F 02 DEG K
34	116735	L-BAND AGC VOLTAGE	2A-45-A 2.5909E 00 VOLTS
35	130243	L-BAND FILTER TEMP.	2A-46-A 3.2423E 02 DEG K
36	0	RADOME THERMISTOR NO.1	2A-51-A 2.1800F 02 DEG K
37	0	NO.4	2B-54-A 2.1800F 02 DEG K
38	0	NO.5	2B-55-A 2.1800F 02 DEG K
39	0	NO.6	2B-56-A 2.1800F 02 DEG K
40	0	RADOME THERMISTOR NO.7	2B-57-A 2.1800F 02 DEG K
41	57200	MODE & POLARIZATION SWITCH	2B-1-A 2.6000F 02 CODE
42	25844	ANTENNA ELEVATION ANGLE	2B-60-A 1.5932E 02 AVG DEG
43	748652	SIGMA KU-BAND CH.1	2A-1-A 1.7517E 01 COUNTS
44	762005	SIGMA KU-BAND CH.2	2A-2-A 2.6114E 00 COUNTS
45	628011	SIGMA KA-BAND CH.1	2A-13-A 1.6957E 00 COUNTS
46	623234	SIGMA KA-BAND CH.2	2A-14-A 2.5145E 00 COUNTS
47	754547	SIGMA K-BAND CH.1	2A-25-A 5.3402E 00 COUNTS
48	826405	SIGMA K-BAND CH.2	2A-26-A 2.5567E 00 COUNTS
49	605619	SIGMA L BAND	2A-37-A 3.6288E 00 COUNTS
50	220		
51	581		
52	4003		
53	170661900		
54	171186200		

Fig. 3-10 MFMR-2 Sample Output.

ORIGINAL PAGE IS
 OF POOR QUALITY

LOGID = P040 VALID DATA CODE = 0000024F
 START TIME = 4 HOURS 10 MINUTES 20.19 SECONDS END TIME = 4 HOURS 11 MINUTES 20.09 SECONDS
 PMIS2 DISK ADDRESS = 146500

DISK ADDRESS OF ANTENNA LOSS DATA IS 509050

BEAM POSITION IS 4

RADOME LOSS ()							
	SKY TEMP (K)	ANT LOSS LA	TR (K)	SIGMA TR (K)	RADOME LOSS LR	SIGMA LR	RADOME LOSS (DR)
VERT	5.00	1.68	134.0129	8.5660	1.1129	-0.0801	0.4645
HORZ	5.00	0.00	292.0999	0.0	-2.4222	0.0	0.0000

Fig. 3-11 PMIS-3 Sample Output.

LOGID = M003 VALID DATA CODE = 00000245
 START TIME = 2 HOURS 45 MINUTES 46.03 SECONDS END TIME = 2 HOURS 46 MINUTES 46.06 SECONDS

ANTENNA LOSS						
	SKY TEMP (K)	TR (K)	SIGMA TR (K)	ANT. LOSS LA	SIGMA LA	ANT. LOSS (DB)
KU-1	6.17	37.65	5.8100	1.1132	0.0272	0.4655
KU-2	6.17	39.05	5.8049	1.1069	0.0272	0.4412
KA-1	10.91	59.93	4.9572	1.1210	0.0256	0.4962
KA-2	10.91	58.47	5.1687	1.1144	0.0263	0.4703
K-1	12.16	45.48	5.7641	1.0836	0.0269	0.3498
K-2	13.16	43.27	5.5761	1.0777	0.0257	0.3251
L	4.29	99.46	5.2219	1.2661	0.0380	1.3548

Fig. 3-12 MFMR-3 Sample Output.

CHAPTER IV

ESTIMATION OF SKY BRIGHTNESS TEMPERATURES

4.0 INTRODUCTION

Eqn. (2-23) and its special case (2-25) form the basis for estimating the isothermal brightness temperature seen by the antenna. The purpose of the bucket is to equate this temperature to the sky brightness temperature at zenith.

The calculation of this temperature using the spherical shell model of Paris [1971] depends on the availability of contemporary radiosonde data at the bucket site in clear sky conditions, and it assumes negligible random fluctuations (within-the-hour). In practice, however, logistic considerations make it difficult to obtain soundings at the exact desired time and/or place. These and other factors can introduce systematic errors in T_{sky} which become greatest at the water resonance frequency of 22.235 GHz.

This chapter discusses the general technique and pitfalls involved in this approach.

4.1 Theoretical Background

The low-level noise power emanating from the atmosphere in the microwave spectrum results primarily from absorption and re-radiation by water and oxygen molecular constituents with an extremely weak cosmic background ($T_{\text{cosmic}} = 2.7 \text{ K}$), believed by many cosmologists to be due to radiation from the remnants of a diffuse expanding primordial fireball. Superimposed on this are occasional localized radio objects such as the sun, the galactic center and various point sources. Almost all of these, however, have flux densities which decrease rapidly with increasing

frequency and may be safely ignored at X-Band and above. At 1.4 GHz it is possible to detect solar radiation with only moderate gain antennas, so that mid-day calibration measurements should be avoided at L-Band.

For PMIS and MFMR, the task of primary concern is the modelling of radiative transfer within the atmosphere. The model constructed by Paris [1971] uses concentric spherical shells to describe the radiative transfer, as shown in Fig. 4-1. The equation of radiative transfer through one shell (shown in inset) is

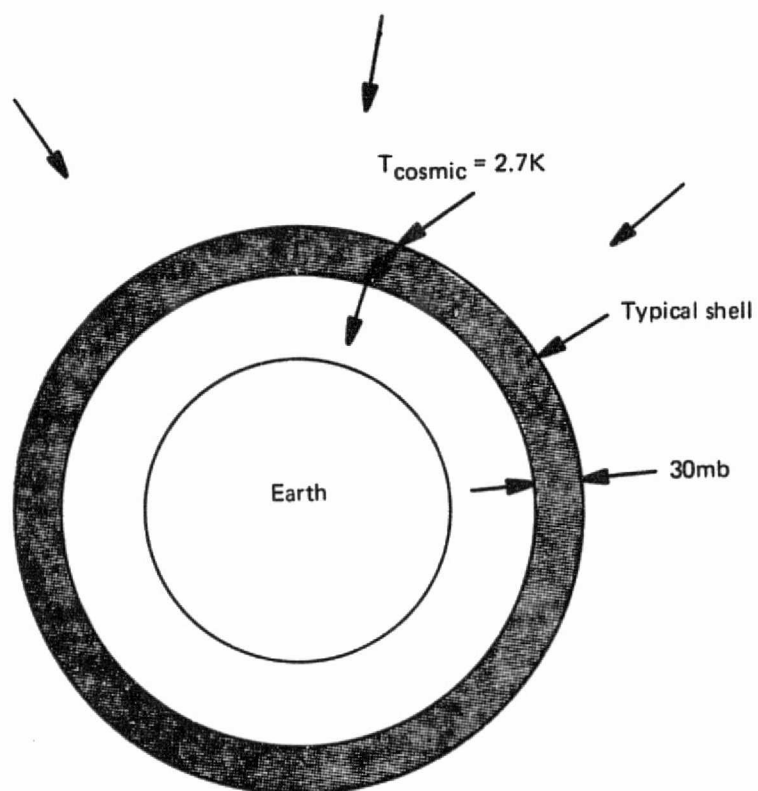
$$T_{B\Delta Z} = T_{Bo} e^{-\alpha \Delta Z \sec \theta} + T(1 - e^{-\alpha \Delta Z \sec \theta}) \quad (4-1)$$

where

- T_{Bo} = incident brightness temperature (K)
- T = mean thermodynamic temperature (K)
- $T_{B\Delta Z}$ = transmitted brightness temperature (K)
- α = volume absorption coefficient (m^{-1})
- ΔZ = thickness of shell (m)
- θ = angle from zenith (rad)

By summing over a sufficient number of shells (with thickness equal to or less than 30 mb pressure), the total incident brightness temperature can be computed for any station altitude or pressure.

The volume absorption coefficient α is due to absorption by both water and oxygen and is modified to include pressure broadening effects using the model of Van Vleck and Weisskopf [1945]. The necessary input data for (4-1) are taken from radiosonde profiles of air temperature (T), pressure (p) and relative humidity (R.H), which are then converted to more useful forms.



ORIGINAL PAGE IS
OF POOR QUALITY

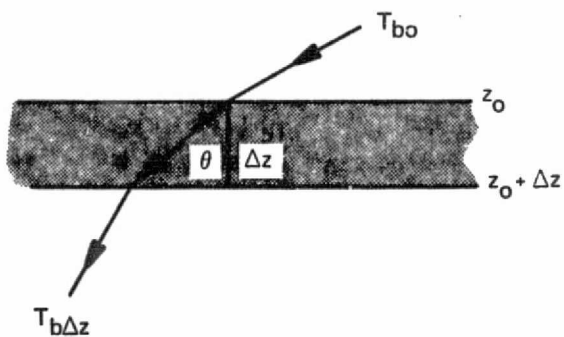


Fig. 4-1. Atmospheric radiative transfer model (after Paris, 1971).

It is necessary to include sounding data to 10 mb in order to accurately assess the sky temperature at 22 GHz where total precipitable water is of great importance.

Unfortunately, however, many soundings are terminated at 300 mb so that it is necessary to simulate profiles above this level. This simulated tropopause effect is shown in Table 4-1.

Simulated Tropopause Data		
Pressure (mb)	Air Temp. (°C)	Dew Pt. Temp. (°C)
200	-60.0	-70.0
100	-65.0	-75.0
50	-62.0	-72.0
10	-52.0	-62.0

It has been found through computer simulation that these numbers are not critical, even at 22 GHz, but that some reasonable simulation must be made.

4.2 Local Topography

The radiometer calibration facility is located approximately 7 km east of the NMSU campus in Las Cruces, and is at an altitude of 4816' (1.468 km), as shown in Fig. 4-2. Most of the regular soundings (daily, at 0200 MST) are taken at White Sands Missile Range WSD site, although other soundings are taken occasionally at the SMR, LC-36 and Airport sites shown. Between the WSD site and the A-Mtn. bucket site is the Organ Mountain range with some peaks rising to 9000' (2.743 km).

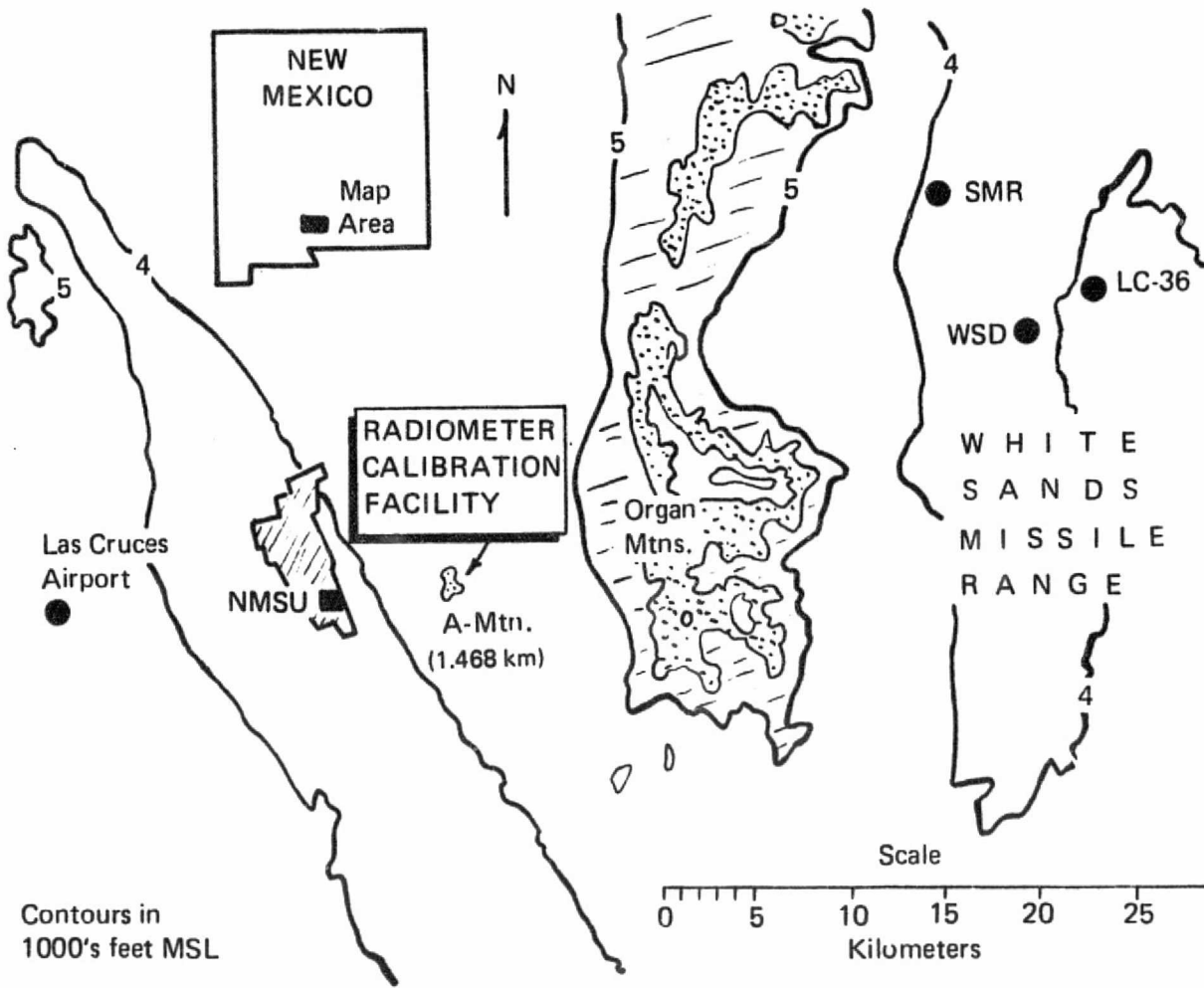


Fig. 4-2. Location of NMSU/PSL radiometer calibration facility.

Can the regular soundings at WSD be used to adequately estimate the sky temperature at the bucket site? The answer is a qualified yes, with the proviso that clear sky conditions be prevailing, that the WSD sounding be within 3 hours of the measurement, and that the wind be predominantly westerly. This technique has evolved as the result of systematic study of the correlation between sounding data in the area, and of the correlation between total precipitable water (W_p) and the sky temperature T_{sky} . For example, Fig. 4-3 compares contemporary soundings at A-Mtn. and WSMR at 0200 MST on Feb. 12, 1975, and shows a higher temperature and slightly higher humidity on the WSMR side of the mountains. The effect of this difference on the T_{sky} spectrum is shown in Fig. 4-4, where the sensitivity to total precipitable water at K-Band becomes immediately apparent.

These data are referenced to an average A-Mtn. surface pressure of 850 mb. The effect of smaller pressures (higher altitudes) is shown in Fig. 4-5 in the T_{sky} spectrum. As the pressure broadening decreases, water and oxygen line shapes become more distinct, and the 2.7 K asymptotic value is approached at lower frequencies.

The correlation between the zenith sky temperature and total precipitable water (W_p) is shown in Fig. 4-6 for 18, 22 and 37 GHz. The total precipitable water is found by integrating from the atmospheric top (10 mb) to the station pressure of 850 mb, using sounding data and standard meteorological expressions. At 18 and 37 GHz the computed zenith sky temperature is closely correlated to the indicated linear fits with slopes of 0.28° and 0.38° per mm respectively. At 22 GHz the slope of $2^\circ/\text{mm}$ is much steeper and the correlation is not as good, with one point departing 2.5 K from the standard curve. The points shown on this scattergram were computed from sounding data in the winter time period

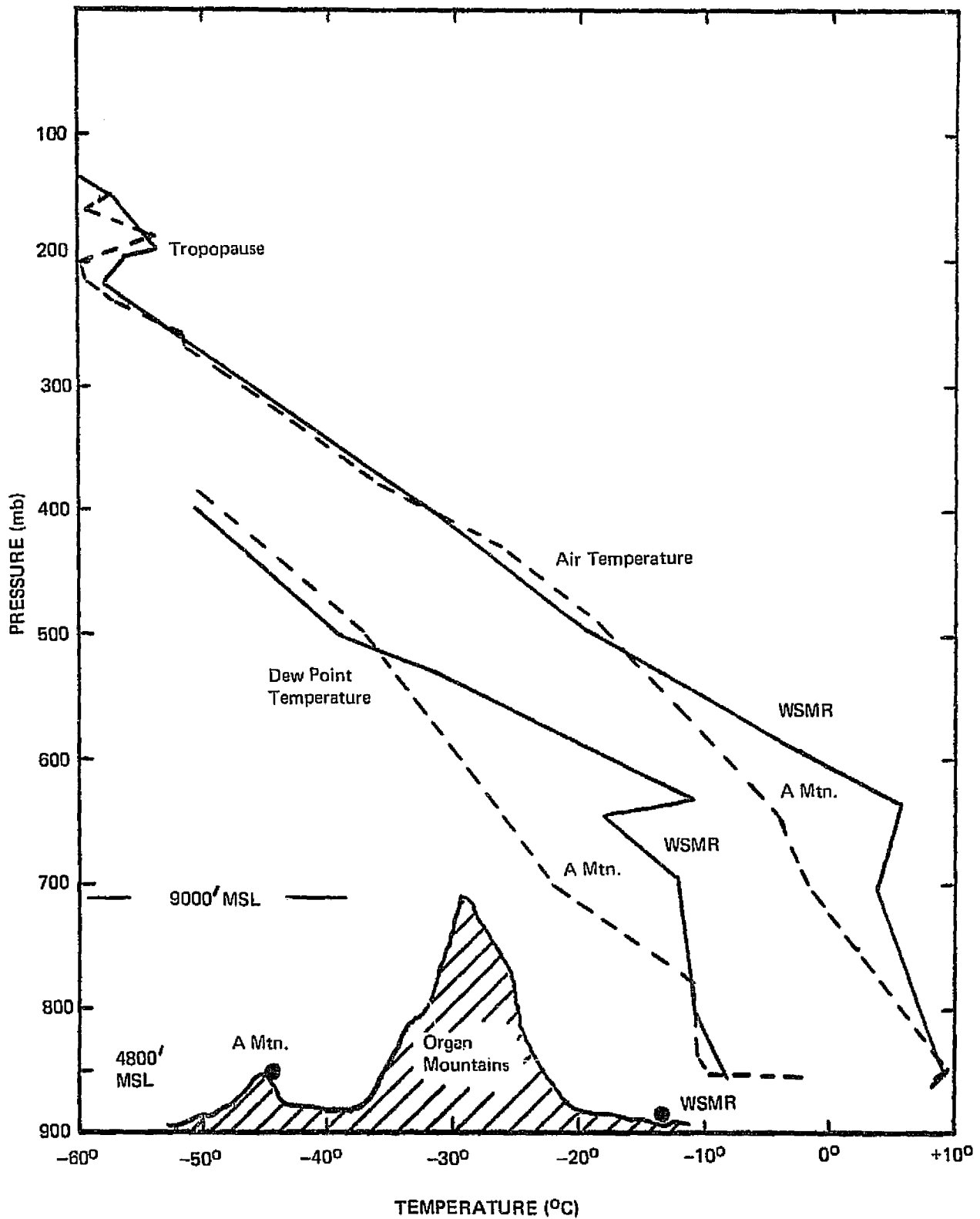


Fig. 4-3. Radiosonde profiles - Feb. 12, 1973 - 0200 MST.

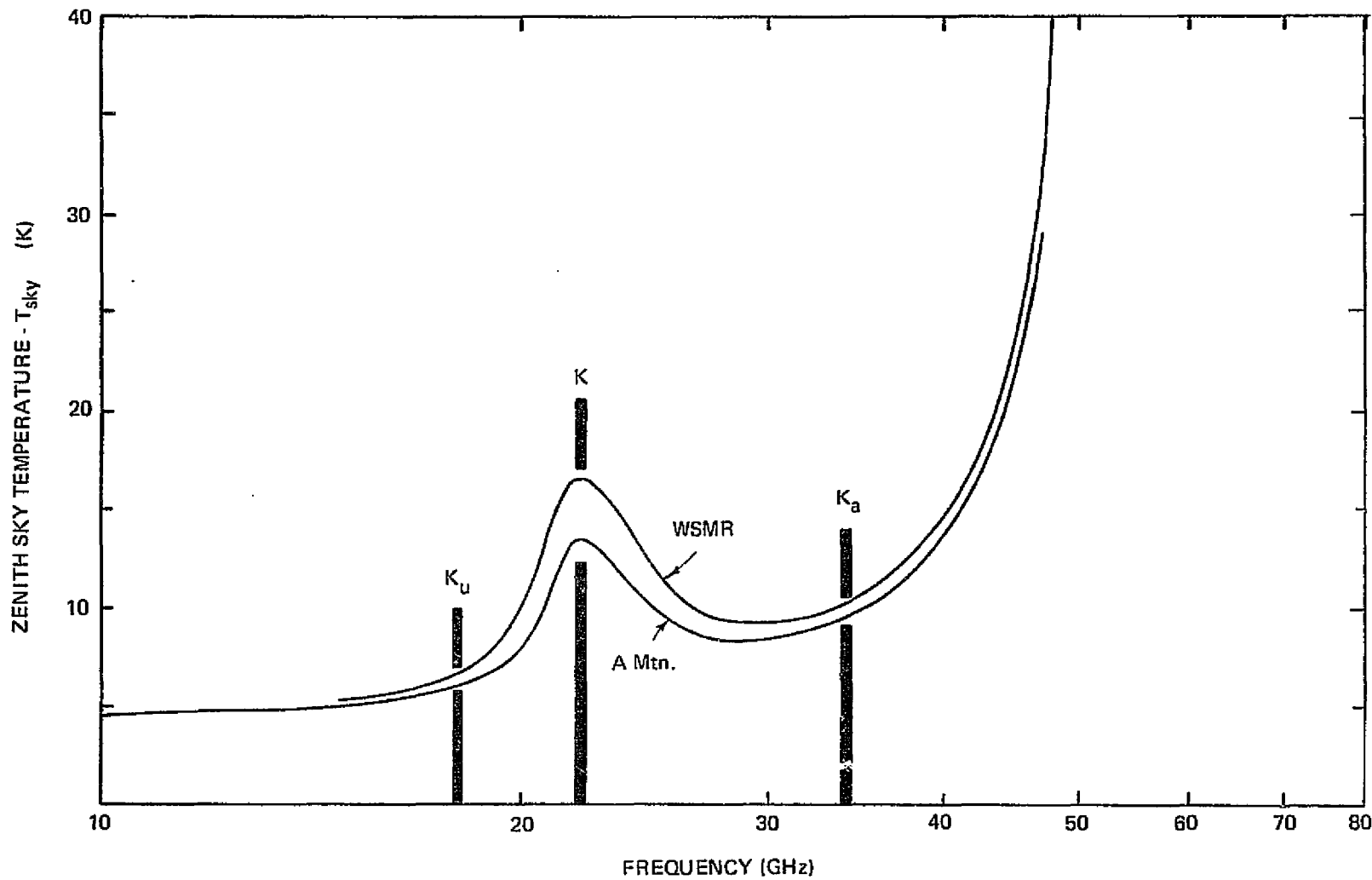


Fig. 4-4. Calculated sky temperature spectrum versus frequency from radiosonde data.

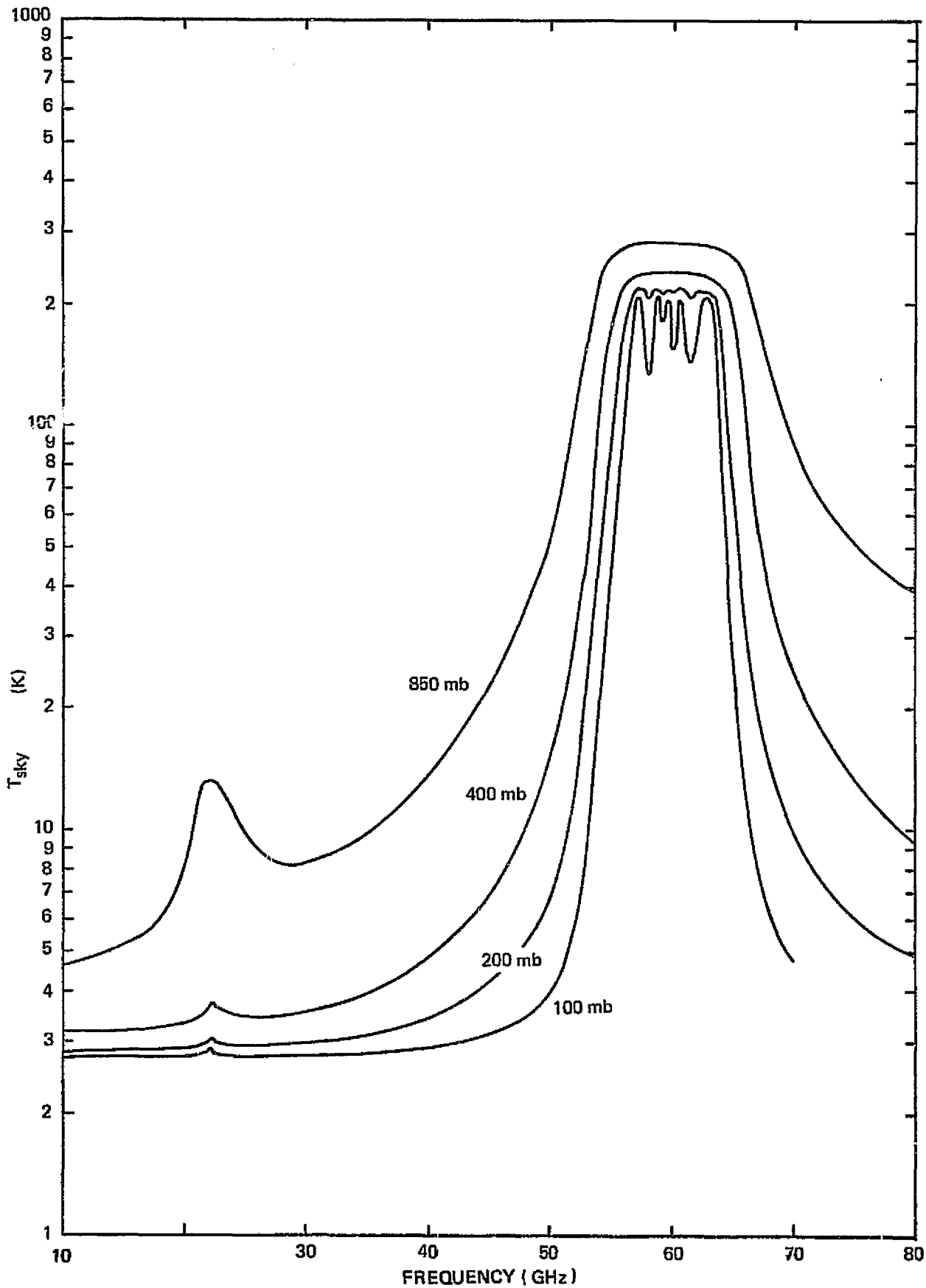


Fig. 4-5. Zenith sky temperature versus frequency.

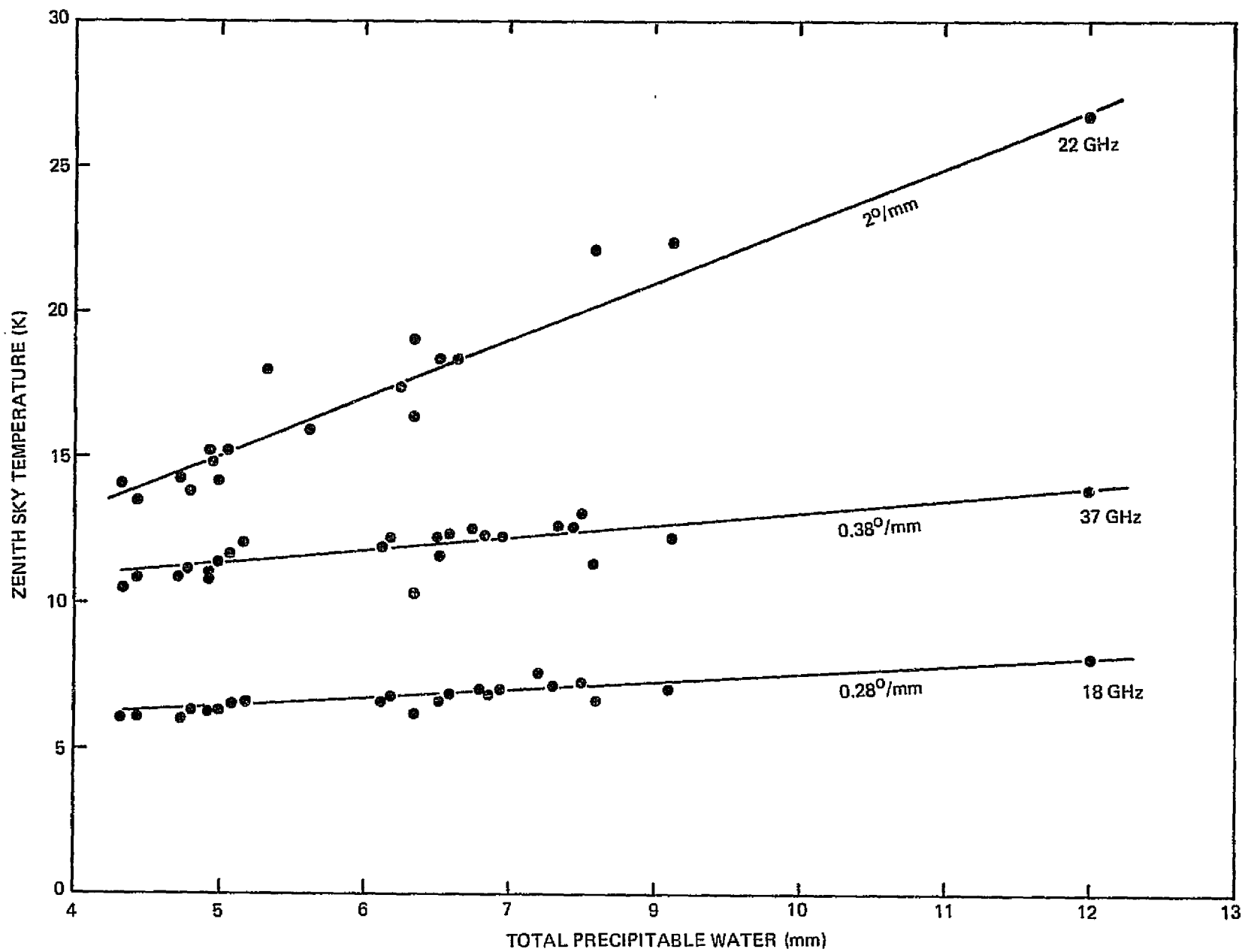


Fig. 4-6. Scattergram of T_{sky} versus precipitable water.

Nov. 1, 1974 to Feb. 20, 1975. A histogram showing the distribution of 22.05 GHz temperatures is shown in Fig. 4-7 and indicates the most recurrent temperatures to be in the 14-17 K range [Carver, Cooper and Paris, 1975].

Even under clear sky conditions, the zenith sky temperature can vary widely over a period of several days, as shown in Fig. 4-8, which compares A-Mtn. temperatures to WSMR (WSD) values in the Feb. 12-14, 1975 time period. Excursions over 10 K are evident at 22 GHz (WSD) in a little less than two hours.

Since 22 GHz is the most difficult frequency from the standpoint of prediction, a key question is whether the zenith sky temperature can be estimated with sufficient accuracy using only total precipitable water (W_p) as a basis. Fogarty [1975] has very recently reported on the correlation between 22.2 GHz measured zenith temperatures and surface dew point temperatures over the Oct. 1972 - Nov. 1974 time period for a Brazilian coastal zone site 850m above MSL. He observed large seasonal, daily and even hourly variations in the zenith attenuation with typical clear sky values of 0.64 dB in the winter and 1.70 dB in the summer, corresponding to 40 K - 88 K temperature variations respectively. He concludes that, contrary to previous recommendations [Sullivan, 1971], the prediction of zenith sky temperature by surface dew point temperature or total precipitable water is much less accurate than by use of the "tipping" method, wherein the sky temperature is observed at various angles and calculated by slope techniques. The difficulty with Fogarty's assertion is that no explanations are offered to explain how he calculates total precipitable water, although it is apparent that it is not the total integrated W_p used in the Paris approach.

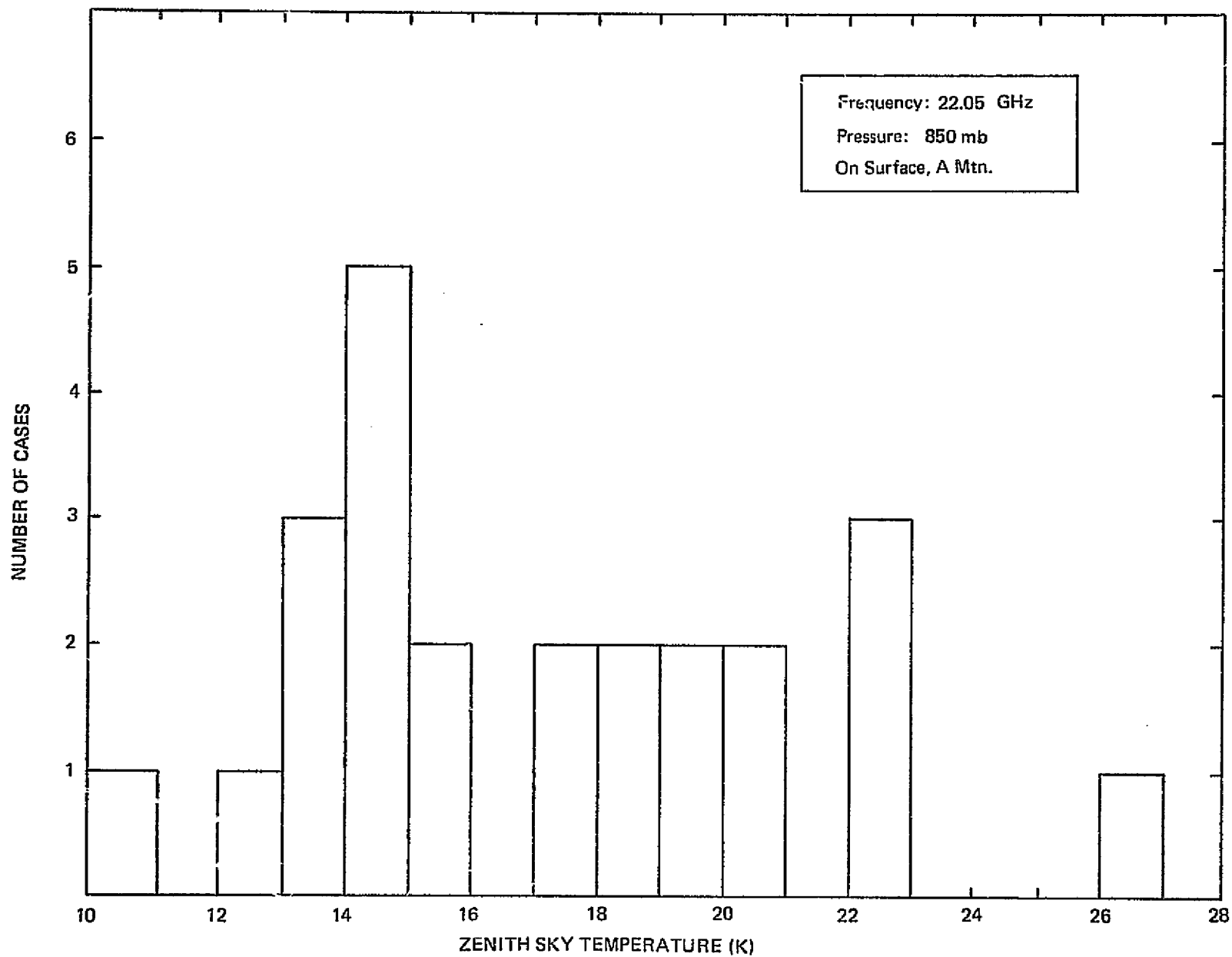


Fig. 4-7. Histogram of zenith sky temperature.

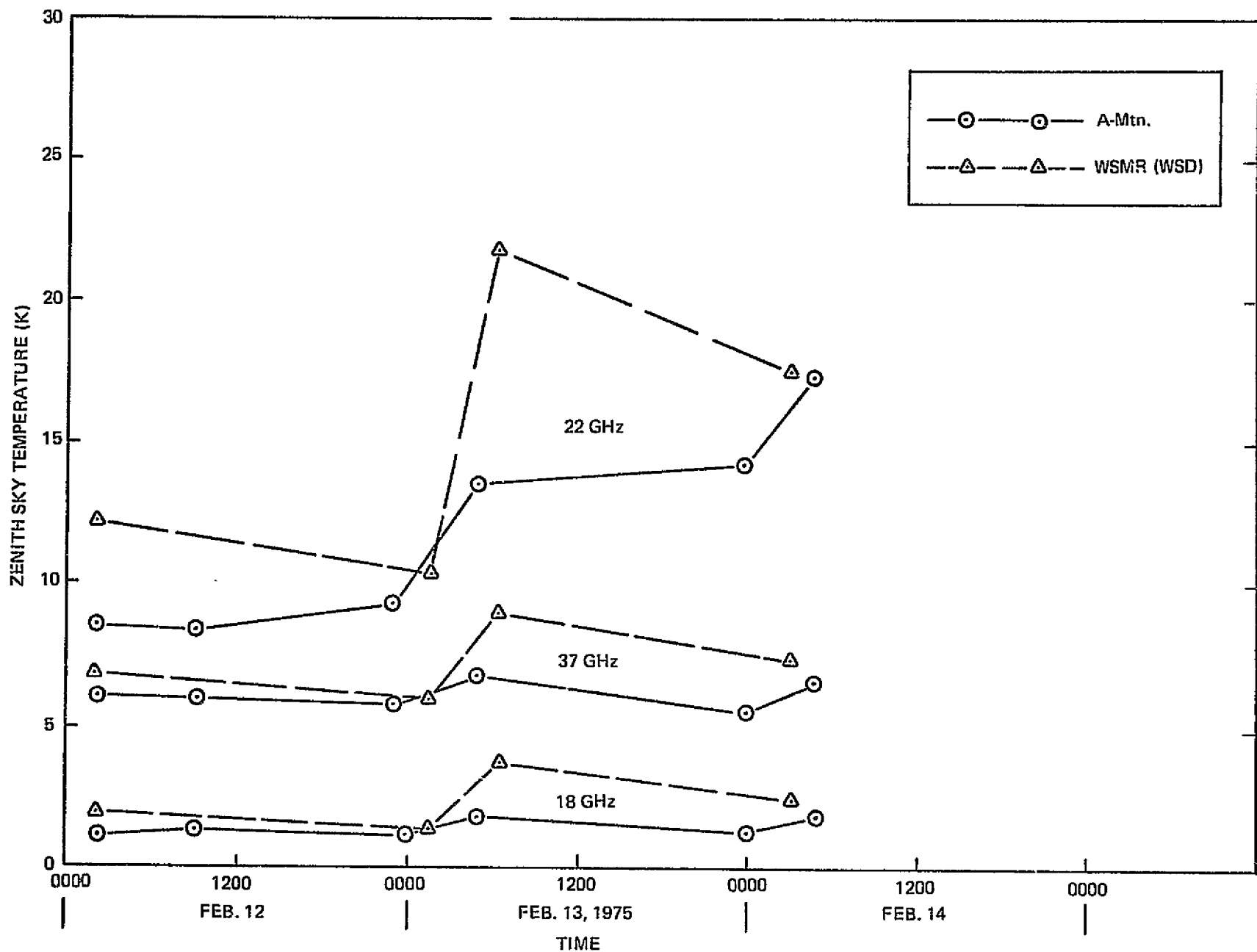


Fig. 4-8. Comparison of computed sky temperature versus time.

It is believed that the proper use of radiosonde profiles with an adequate radiative transfer model leads to an acceptable correlation between the zenith sky brightness temperature and W_p , as indicated in Fig. 4-6. Clearly, a direct calculation of T_{sky} using the SKYTEMP program written by Paris with timely sounding data from A-Mtn offers the most accurate means of estimation. However, on-site soundings are relatively expensive and logistically difficult so that it is desirable to use the regular 0200 WSD soundings where possible.

By comparing the integrated W_p values from several coordinated soundings from Las Cruces Airport, Small Missile Range, and Launch Complex - 36, it has been found that for clear sky conditions and prevailing westerly winds, the W_p value is about 1/2 mm higher on the east side of the Organ Mountains (see Fig. 4-2), so that from Fig. 4-6, T_{sky} should be higher on the west side of the mountains. This is confirmed in Fig. 4-8 where A-Mtn. and WSD temperatures are compared, with the brightness temperatures on the A-Mtn. side being consistently cooler.

4.3 Variation with Zenith Angle

Fig. 4-9 shows the variation in the computed T_{sky} values at 18, 37, and 22.05 GHz with angle from zenith. Both A-Mtn. and WSD curves (Feb. 12, 1975; 0200 MST) are shown. The greatest slopes are found at 22 GHz, although the variation is negligible over the 5° beamwidth of the scalar horn used. Thus the assumption that $T_s = T_{sky}(0^\circ)$, as in eqn. 2-25, is a good one when a reflecting bucket enclosure is used to block emissive radiation from surrounding terrain.

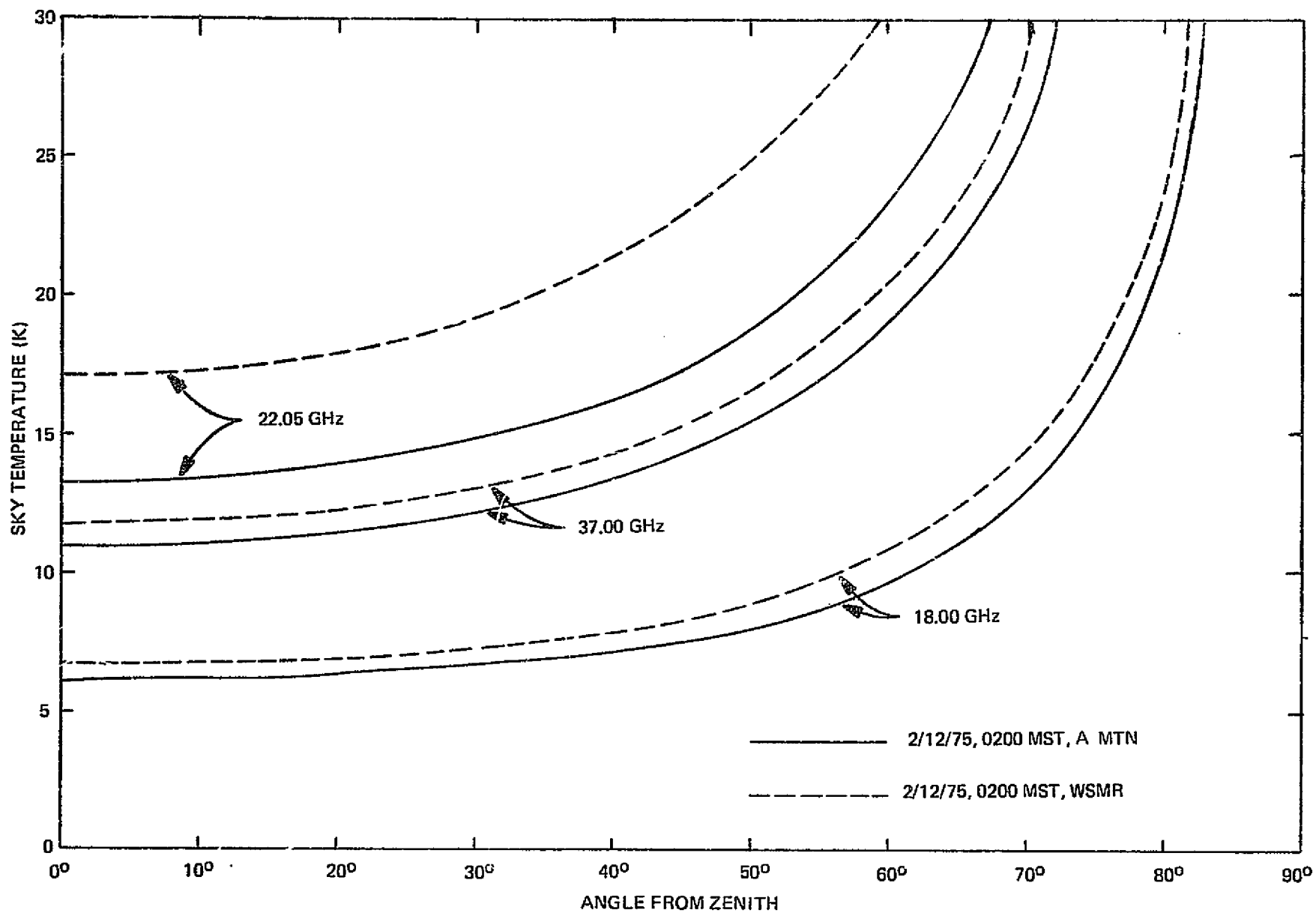


Fig. 4-9. Comparison of computed sky temperature versus angle from zenith.

4.4 Errors in T_{sky}

An extensive analysis of systematic errors in T_{sky} using radiosonde data has been prepared by Paris (1975] especially for the PMIS/MFMR measurement program. His analysis assumes that the sounding is contemporary with the radiometric measurement and is taken at the A-Mtn. site and that random errors can be ignored. These error values are repeated in Table 4-2.

Frequency (GHz)	ΔT_{sky} (K)
1.4135	0.27
10.69	0.40
18.00	0.82
22.05	3.04
37.00	1.84

CHAPTER V

PMIS LOSS MEASUREMENTS

5.0 INTRODUCTION

The PMIS radiometer operates at 10.69 GHz as a dual-polarized imaging sensor using a planar phased array of crossed slots. The beam is scanned through 44 discrete positions on a conical surface and has a typical beamwidth of 2° corresponding to a gain of 35 dBi. Horizontally and vertically polarized components of incident radiation are processed by separate radiometers with beam switching and data initial data processing under control of a dedicated computer. In flight, integration times are variable and controlled by a feedback network. A radome covers the array when it is used on the P-3A aircraft.

In the calibration testing phase, the radiometer's intrinsic integration time was fixed (~ 120 ms) with an effective integration time of 1 minute being provided by computer processing of data tapes. The objective of the test was to provide antenna loss (L_A) values for all 44 beam positions for both vertical and horizontal channels, and radome loss (L_R) values for both radomes supplied, at each of the 44 positions. This totals to 264 separate loss measurements. Tests were run at night, normally from midnight to dawn, so that the regular 0200 MST radiosonde sounding from WSD could be used to calculate the sky brightness temperature.

5.1 Mechanical Positioning Technique

The PMIS array and associated radiometers were mounted in a plywood bomb-bay mockup which was in turn affixed to an

azimuth-over-elevation antenna positioner, as shown in Fig. 2-16. The positioner was set (according to a table in the operator logbook) so that electronic beam steering was compensated, giving a beam always pointed toward the zenith.

A counterbalance assembly was used so that the center of gravity was nearly on the elevation axis. Angular setting errors of the positioner are negligible.

5.2 Radiometer Receiver Calibration

Both horizontal and vertical radiometer receivers were laboratory calibrated by the use of an X-Band waveguide variable temperature cold load, as shown in Fig. 5-1. A matched waveguide load is immersed in a cryobath whose temperature can be varied from approximately 50 K - 250 K. This source of thermal noise causes an equivalent noise temperature T_f to appear at the A-A' waveguide flange connected to the radiometer receiver. Thermistors (one is shown) are used to monitor temperatures along the waveguide. Corrections are made for waveguide absorption and internal emission, as well as mismatch corrections, in arriving at the A-A' flange temperature.

This reference load has not to date been calibrated by NBS and it would be desirable to have this done. However, it is instructive to consider possible sources of error in order to arrive at a total systematic uncertainty in the flange temperature. These errors result primarily from inaccuracies in the cryobath temperature ($\pm .2$ K), and flange mismatch (misalignment) errors ($\pm .5$ K) with the resulting estimate of a ± 1 K overall systematic error.

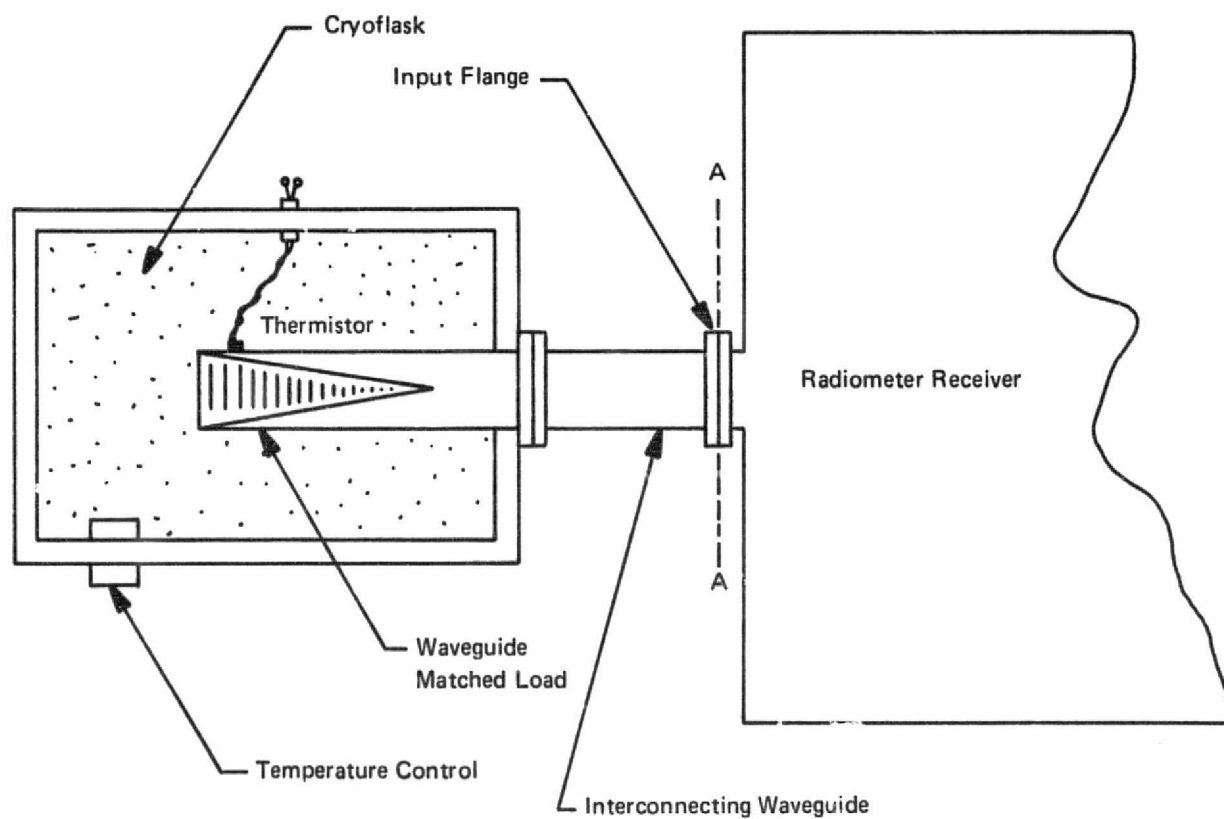


Fig. 5-1. Symbolic diagram of X-Band reference cold load for PMIS receiver calibration.

In practice, the apparent flange temperature T_f (equated to T'_B) in 25 K steps from 100 K to 200 K, which is the normal operating range of the receiver. As the cryoflask mixing is changed, short-term local temperature gradients develop around the matched load so that T_f requires several minutes (typically 10 min.) to stabilize after making a 25 K change. An equation of the form

$$T_{fi} = T'_{Bi} = T_1 + (\Delta T)X_i \quad (5-1)$$

where

$$X_i = \frac{\bar{C}_A - \bar{C}_B}{\bar{C}_C - \bar{C}_B} \quad (5-2)$$

is used to solve for the calibration constants T_1 and ΔT by using standard regression techniques to find the best straight line fit to (5-1). T_{fi} assumes approximate values 100 K, 125 K, 150 K, 175 K and 200 K, and is read from the (827) address of the Varian computer.

The T_1 and ΔT "constants" varied slightly, due to receiver post-detection instabilities, as shown in Figs. 3-3 and 3-4. The horizontal receiver showed about 3 times the drift of the vertical receiver and generally provided a continuum of difficulties. A further source of difficulty in receiver calibration was a high level of PCM noise, which was corrected only near the end of the measurement program.

On Jan. 27, the horizontal receiver failed completely, so that all subsequent data from both horizontally and vertically polarized channels were taken using the vertical receiver front-end.

5.3 PMIS Data Flow

Each of the 264 loss values were measured independently several times so that a reduction in the uncertainty was made possible by averaging. The number of independent measurement sets is shown in Table 5-1.

<u>Table 5-1</u>		
<u>Number of Independent Loss Measurement Sets</u>		
<u>Loss</u>	<u>Polarization</u>	<u>Number of Sets (N_S)</u>
Antenna	Vert.	7
	Horiz.	7
Radome #1	Vert.	3
	Horiz.	4
Radome #2	Vert.	3
	Horiz.	4

The mean loss value for each set was then computed according to

$$\overline{L^M} = \frac{1}{N_S} \sum_{i=1}^{N_S} L_i^M \quad (5-3)$$

where the superscript refers to the beam position number and N_S is the number of sets. The standard deviation of the set was computed according to

$$\sigma^M = \left\{ \frac{1}{N_S - 1} \sum_{i=1}^{N_S} (L_i^M - \overline{L^M})^2 \right\}^{1/2} \quad (5-4)$$

Then

$$L^4 = \frac{\frac{1.557}{.04} + \frac{1.554}{.04} + \frac{1.572}{.05}}{\frac{1}{.04} + \frac{1}{.04} + \frac{1}{.05}} = 1.560$$

This smoothing process essentially borrows statistical information from neighboring beams and is equivalent to convolution of average loss values L^M with a three-beam weighted pulse function.

5.4 PMIS Antenna and Radome Loss Values

The final loss values, as derived by this technique, are tabulated in Table 5-3 and illustrated graphically in Figs. 5-2, 5-3 and 5-4.

ORIGINAL PAGE IS
OF POOR QUALITY

Table 5-3

PMIS Loss Summary

Beam Position	Antenna Loss		Radome 1 Loss		Radome 2 Loss	
	Vert.	Horiz.	Vert.	Horiz.	Vert.	Horiz.
1	1.672	1.555	1.083	1.130	1.064	1.125
2	1.677	1.557	1.083	1.134	1.063	1.127
3	1.679	1.558	1.083	1.136	1.060	1.129
4	1.679	1.560	1.082	1.137	1.059	1.131
5	1.682	1.572	1.080	1.138	1.057	1.133
6	1.685	1.585	1.079	1.138	1.056	1.134
7	1.681	1.585	1.077	1.139	1.055	1.135
8	1.677	1.586	1.077	1.139	1.055	1.135
9	1.669	1.589	1.076	1.139	1.055	1.134
10	1.667	1.595	1.074	1.139	1.054	1.134
11	1.664	1.604	1.072	1.139	1.053	1.132
12	1.666	1.614	1.069	1.139	1.052	1.130
13	1.664	1.634	1.067	1.138	1.051	1.128
14	1.661	1.641	1.066	1.138	1.050	1.127
15	1.657	1.642	1.066	1.138	1.050	1.125
16	1.655	1.638	1.066	1.137	1.050	1.125
17	1.650	1.642	1.066	1.137	1.049	1.124
18	1.646	1.649	1.066	1.136	1.048	1.124
19	1.646	1.646	1.067	1.134	1.048	1.123
20	1.645	1.640	1.067	1.132	1.048	1.122
21	1.644	1.638	1.068	1.130	1.048	1.121
22	1.641	1.637	1.070	1.126	1.048	1.120
23	1.639	1.645	1.071	1.123	1.048	1.118
24	1.639	1.641	1.071	1.119	1.049	1.116
25	1.643	1.656	1.072	1.116	1.048	1.114
26	1.644	1.655	1.071	1.112	1.048	1.111
27	1.646	1.659	1.071	1.109	1.047	1.108
28	1.649	1.661	1.069	1.106	1.047	1.106
29	1.658	1.660	1.068	1.104	1.046	1.105
30	1.662	1.662	1.066	1.105	1.046	1.106
31	1.664	1.651	1.065	1.110	1.046	1.108
32	1.665	1.635	1.065	1.119	1.046	1.111
33	1.667	1.624	1.066	1.125	1.047	1.113
34	1.672	1.615	1.067	1.129	1.048	1.115
35	1.675	1.604	1.068	1.131	1.049	1.117
36	1.679	1.594	1.071	1.132	1.050	1.118
37	1.684	1.592	1.073	1.134	1.052	1.119
38	1.680	1.585	1.075	1.135	1.054	1.120
39	1.684	1.579	1.078	1.136	1.056	1.121
40	1.688	1.570	1.080	1.136	1.057	1.121
41	1.686	1.562	1.080	1.135	1.058	1.122
42	1.681	1.552	1.079	1.133	1.059	1.122
43	1.681	1.552	1.076	1.126	1.059	1.122
44	1.681	1.547	1.075	1.116	1.059	1.122

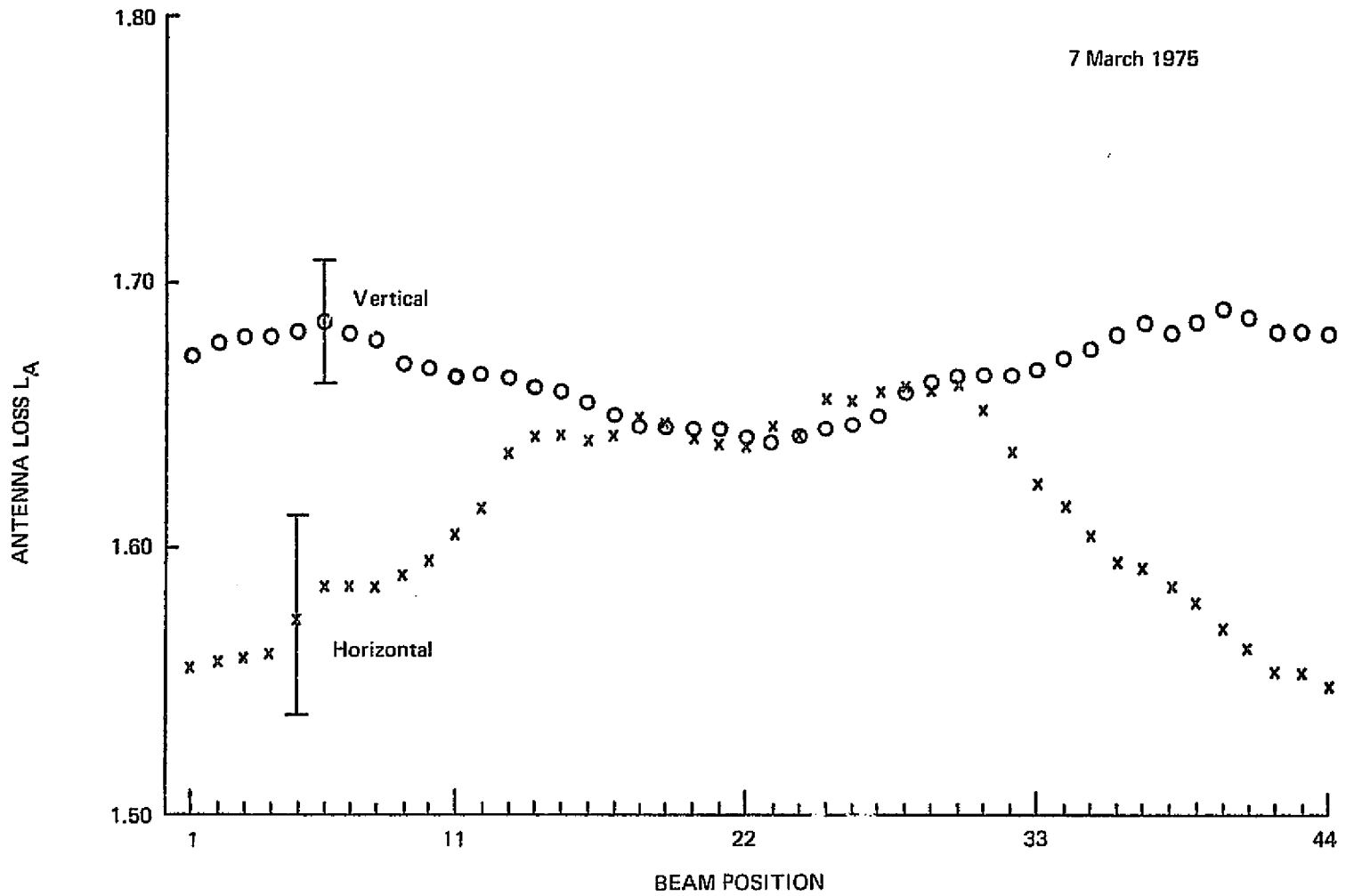


Fig. 5-2. PMIS antenna loss versus beam position.

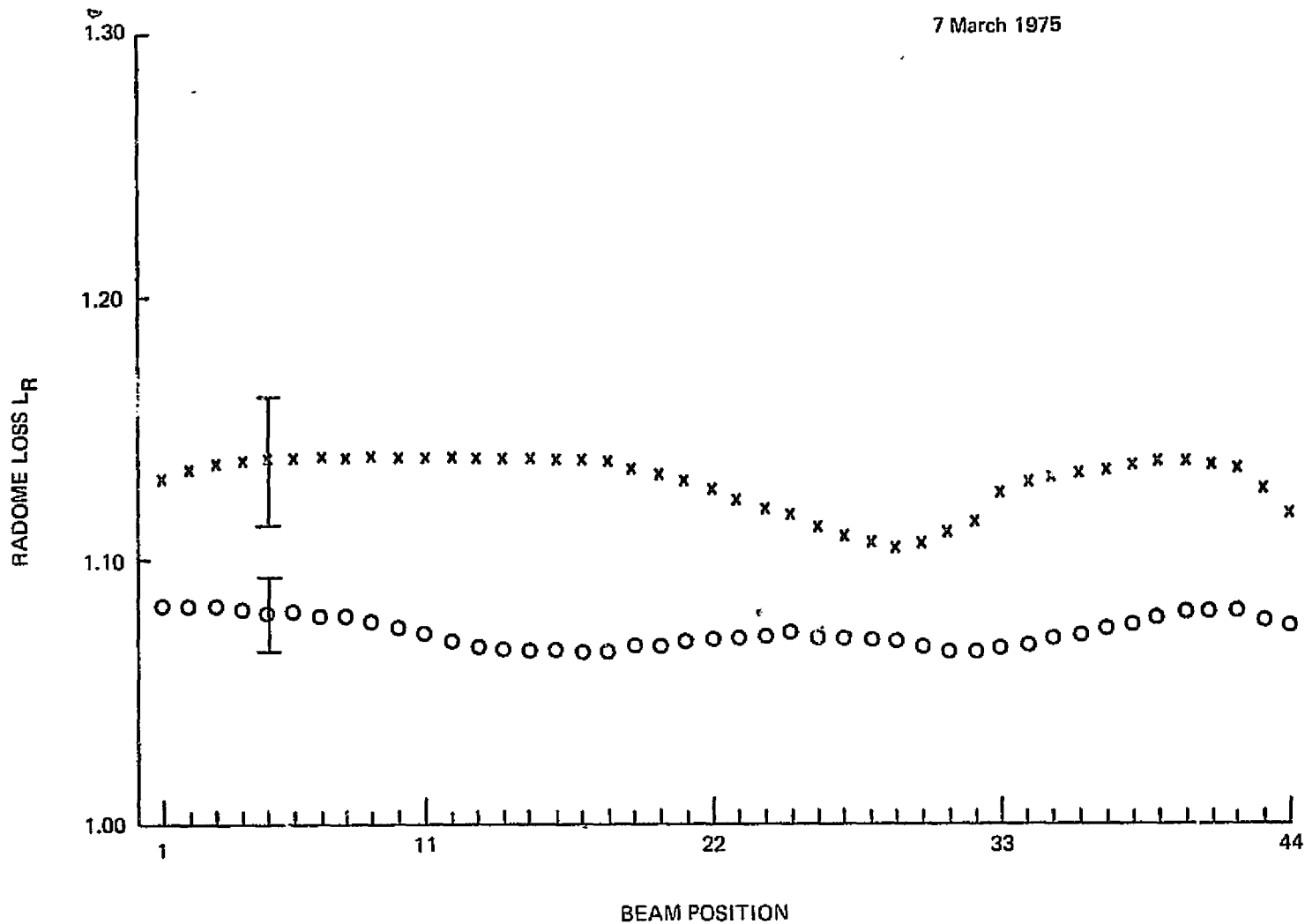


Fig. 5-3. PMIS radome 1 loss versus beam position.

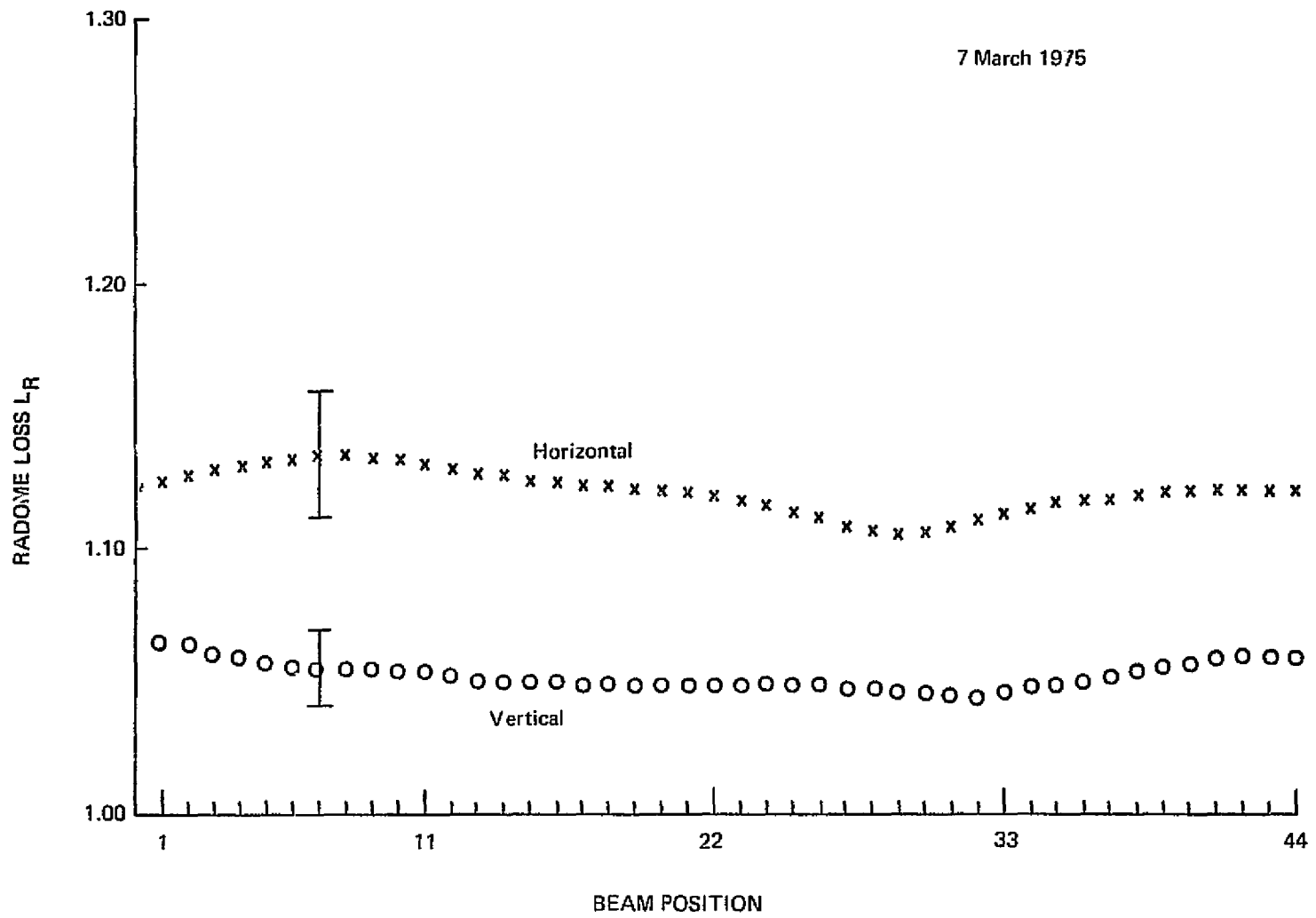


Fig. 5-4. PMIS radome 2 loss versus beam position.

5.5 FMIS Error Budget

5.5.1 Theoretical Background

In experimental measurements, errors may be divided into three classes:

1. Blunders

These errors are due to human mistakes, and all measurement programs suffer from them. Incorrect reading of meters, computer card punching mistakes, careless mating of waveguide flanges, etc., typify these blunders. In most cases, these errors will eventually be discovered and corrected.

2. Systematic Errors

Systematic errors relate to the accuracy of a measurement and stem from incorrectly calibrated instruments, human meter reading error (e.g., meter parallax), or such environmental conditions as strong magnetic fields interacting with meter movements. Systematic errors will thus cause a measured value to be consistently high or low from the absolute value. Instrument calibration and the careful use of these instruments as recommended by the manufacturer will minimize these errors.

If a quantity is deduced from its relationship $f = f(X_1, X_2, X_3, \dots, X_n)$ on n independently measured quantities $(X_1, X_2, X_3, \dots, X_n)$, then the worst case systematic error (accuracy) in f is

$$\Delta f = \sum_{i=1}^n \left| \frac{\partial f}{\partial X_i} \right| \Delta X_i \quad (5-6)$$

where ΔX_i is the accuracy of the measured quantity X_i .

3. Random Errors

Random errors control the precision of a measurement or the number of significant figures that may be quoted. Such errors are noise-related and may stem from short-term gaussian noise or shot noise or they may be caused by the relatively long-term gain instability of an amplifier. If the variances σ_i^2 of the quantities X_i (see above) are known, then the variance of the quantity f is given by the quadrature relationship

$$\sigma_f^2 = \sum_{i=1}^n \left(\frac{\partial f}{\partial X_i} \right)^2 \sigma_i^2 \quad (5-7)$$

5.5.2 PMIS Antenna Loss Errors

For PMIS, the waveguide and antenna are considered as a unit so that (3-2) reduces to

$$L_A = \frac{T_A - T_S}{T_A - T'_B} \quad (5-8)$$

1. Random Error

It can be shown that the random fluctuations in the antenna temperature (σ_{T_A}) and in the sky temperature (σ_{T_S}) at X-Band are two to three orders of magnitude smaller than the fluctuations in the uncorrected brightness temperature. Thus, from (5-7),

$$\sigma_{L_A} = \frac{\partial L_A}{\partial T'_B} \sigma_{T'_B} = \frac{T_A - T_S}{(T_A - T'_B)^2} \sigma_{T'_B} \quad (5-9)$$

The uncorrected brightness temperature is computed by

$$T'_B = T_1 + (\Delta T)X \quad \text{where } X = \frac{\bar{C}_A - \bar{C}_B}{\bar{C}_C - \bar{C}_B} \quad (5-10)$$

where T_1 and ΔT are constants established by laboratory calibration and X is the PCM count ratio. Thus,

$$\sigma_{T_B} = [\sigma_{T_1}^2 + X^2 \sigma_{\Delta T}^2 + (\Delta T)^2 \sigma_X^2]^{1/2} \quad (5-11)$$

The noise process responsible for σ_X is short-term (within-the-minute fluctuations) and originates from the receiver front-end, from antenna phase shifters and from the residual PCM transients. It has been found that with a one-minute integration time,

$$(\Delta T) \sigma_X = \begin{cases} 0.07 \text{ K} & \text{(vertical)} \\ 0.22 \text{ K} & \text{(horizontal)} \end{cases} \quad \text{(typically)} \quad (5-12)$$

Fluctuations in T_1 and ΔT originate from medium-term (within-the-week) gain instability as influenced by the synchronous demodulator in the receiver rear end. Repeated laboratory calibrations during the PMIS loss measurement period at A-Mountain established that

$$\sigma_{T_1} = \begin{cases} 1.60 \text{ K} & \text{(vertical)} \\ 3.00 \text{ K} & \text{(horizontal)} \end{cases} \quad (5-13)$$

$$\sigma_{\Delta T} = \begin{cases} 0.29 \text{ K} & \text{(vertical)} \\ 1.05 \text{ K} & \text{(horizontal)} \end{cases} \quad (5-14)$$

as being typical. Using $X = 3.50$ (a maximum) and substituting 5-12, 5-13 and 5-14 into 5-11,

$$\sigma_{T_B} = \begin{cases} 1.90 \text{ K} & \text{(vertical)} \\ 4.70 \text{ K} & \text{(horizontal)} \end{cases} \quad (5-15)$$

Under typical conditions,

$$\begin{aligned}
 T_A &= 288 \text{ K} \\
 T_S &= 5 \text{ K} \\
 T'_B &= 120 \text{ K} \\
 L_A &= 1.684
 \end{aligned}
 \tag{5-16}$$

Substituting 5-15 and 5-16 into 5-9,

$$\sigma_{L_A} = \begin{cases} 0.019 & \text{(vertical)} \\ 0.047 & \text{(horizontal)} \end{cases}
 \tag{5-17}$$

The three-point convolution process used to borrow statistical information from neighboring beam positions decreases the noise on L_A by 58%, giving a final random error

$ \overline{\sigma}_{L_A} = \begin{cases} 0.010 & \text{(vertical)} \\ 0.027 & \text{(horizontal)} \end{cases} \tag{total random error} $	(5-18)
--	--------

2. Systematic Error

The major source of systematic, or calibration error is the inaccuracy of the laboratory standard X-Band cooled load. Other errors, considerably smaller, include the accuracy of the sky temperature and of the antenna kinetic temperature.

The worst case systematic error may be calculated by

$$\Delta L_A = \frac{1}{T_A - T_S} \Delta T_S + \frac{T'_B - T_S}{(T_A - T'_B)^2} \Delta T_A + \frac{T_A - T_S}{(T_A - T'_B)^2} \Delta T'_B
 \tag{5-19}$$

It is estimated that:

$$\Delta T_A = \pm 0.2 \text{ K} \quad (\text{limited by accuracy of thermistors})$$

$$\Delta T_S = \pm 0.4 \text{ K} \quad (\text{limited by accuracy of knowledge in H}_2\text{O vapor volume absorption coefficient in accuracy of radiosonde instruments - see Section 4.4.})$$

$$\Delta T'_B = \pm 1.0 \text{ K} \quad (\text{See Section 5-2})$$

Substituting 5-16 and 5-20 into 5-19,

$$\Delta L_A = \pm (0.0014 \quad + \quad 0.0008 \quad + \quad 0.0100) \quad (5-21)$$

sky temp. error	ant. temp. error	ref. cold load error
--------------------	---------------------	-------------------------

or

$$\Delta L_A = \pm 0.012 \quad (\text{total systematic error for vert. and horiz.})$$

3. Total Uncertainty

The total uncertainty is found by adding the random and systematic error, i.e.

$$\epsilon_{LA} = \pm (\sigma_{LA} + |\Delta_{LA}|) \quad (5-22)$$

or

$\epsilon_{LA} = \begin{cases} + 0.022 & (\text{vertical}) \\ + 0.039 & (\text{horizontal}) \end{cases}$	(5-23)
--	--------

5.5.3 PMIS Radome Loss Errors

Since the waveguide loss is subsumed within the antenna loss for PMIS, (3-4) reduces to

$$L_R = \frac{T_R - T_S}{T_R + T_A(L_A - 1) - L_A T'_B} \quad (5-24)$$

1. Random Error

It can be demonstrated that random fluctuations in the brightness temperature have a negligible effect on (5-24) in comparison to the contribution from the noise on L_A as computed from (5-18). Also, random fluctuations in the sky temperature and the radome temperature have a negligible effect on L_R . Thus, carrying out the indicated operations of (5-7), using (5-24),

$$\sigma_{L_R} = \frac{T_R - T_S}{(T_A - T'_B)L_A} \sigma_{L_A} \quad (5-25)$$

which, under typical conditions, reduces to

$$\sigma_{L_R} = 0.6 \sigma_{L_A} \quad (5-26)$$

2. Systematic Error

It may likewise be shown that the systematic error in L_R is, under typical conditions, given by

$$\Delta L_R = 0.6 \Delta L_A \quad (5-27)$$

3. Total Uncertainty

It follows from (5-26) and (5-27) that the total uncertainty in the radome loss is

$$\epsilon_{L_R} = 0.6 \epsilon_{L_A} \quad (5-28)$$

which, using (5-23), yields

$$\epsilon_{L_R} = \begin{array}{l} \pm 0.014 \quad (\text{vertical}) \\ \pm 0.039 \quad (\text{horizontal}) \end{array} \quad (5-29)$$

5.6 Effect of Errors in L_A , L_R on PMIS User

What is the significance of these errors in the measured values from the viewpoint of the PMIS data user? In flight, the antenna may be viewing a ground target or possibly a sky target; furthermore, it is covered by a radome so that (5-24) holds, except that T_S now represents the target (or scene) brightness temperature, and it is T_S that the user wishes to measure. Solving for T_S from (5-24),

$$T_S = L_A L_R T'_B - L_R (L_A - 1) T_A - (L_R - 1) T_R \quad (5-30)$$

5.6.1 Random Errors

Even though there were random errors in the measured values of L_A and L_R , the values themselves do not fluctuate. Thus, we may say that we know these values only to a certain precision. However, there is an appreciable random noise-caused error in T'_B (more commonly known as the receiver sensitivity), typically 1 K over a short period of time. Long-term receiver instability may cause this value to become much higher over a period of

hours. Fluctuations in T_A and T_R are negligible. Applying (5-7) to (5-30), the variance in the source brightness temperature is

$$\begin{aligned} \sigma_{T_S}^2 = & [L_R(T_A - T'_B)]^2 \sigma_{L_A}^2 + [L_A T'_B - (L_A - 1)T_A - T_R]^2 \sigma_{L_R}^2 \\ & + (L_A L_R)^2 \sigma_{T_B}^2 \end{aligned} \quad (5-31)$$

Assuming a source brightness temperature of 200 K, antenna and radome temperatures of 288 K and 293 K respectively and antenna and radome losses of 1.684 and 1.100, the uncorrected brightness temperature T'_B would be 241 K. The corresponding variances are

$$\begin{aligned} \sigma_{L_A}^2 &= \begin{cases} (0.010)^2 & \text{vertical} \\ (0.027)^2 & \text{horizontal} \end{cases} \\ \sigma_{T_B}^2 &= \begin{cases} (1)^2 & \text{vertical} \\ (1)^2 & \text{horizontal} \end{cases} \\ \sigma_{L_R}^2 &= \begin{cases} (0.006)^2 & \text{vertical} \\ (0.016)^2 & \text{horizontal} \end{cases} \end{aligned} \quad (5-32)$$

Substituting these figures into (5-31),

$$\begin{aligned} \sigma_{T_S}^2 &= \begin{matrix} \left\{ \begin{array}{lll} 0.94 & + 0.25 & + 3.43 \\ 1.95 & + 1.81 & + 3.43 \end{array} \right. & \begin{matrix} \text{(vertical)} \\ \text{(horizontal)} \end{matrix} \end{matrix} \quad (5-33) \\ &\quad \underbrace{\hspace{1.5cm}} \quad \underbrace{\hspace{1.5cm}} \quad \underbrace{\hspace{1.5cm}} \\ &\quad \text{antenna} \quad \text{radome} \quad \text{receiver} \\ &\quad \text{loss} \quad \text{loss} \quad \text{noise} \\ &\quad \text{imprecision} \quad \text{imprecision} \end{aligned}$$

or

$$\sigma_{T_S} = \begin{cases} 2.2 \text{ K} & \text{(vertical)} \\ 2.7 \text{ K} & \text{(horizontal)} \end{cases} \quad (5-34)$$

These values specify the precision with which a measured source brightness temperature may be quoted. They are larger than the receiver noise related system sensitivity because of the imprecision of the loss numbers. If the statistical fluctuations in T_S are assumed to be normally distributed, then there is a probability of 68% that the measured value of T_S will be within $\pm \sigma$ of the mean. If the random error in L_A and L_R were reduced to zero, then $\sigma_{T_S} = 1.9$ K which is then the tangential sensitivity of the radiometer system.

5.6.2 Systematic Errors

The systematic error, or accuracy, associated with T_S is computed by using (5-6) and (5-30) in a worst case sense, yielding

$$\Delta T_S = |L_R(T_A - T'_B)|\Delta L_A + |L_A(-T_A + T'_B) + (T_A - T_R)|\Delta L_R + L_A L_R \Delta T'_B \quad (5-35)$$

The accuracies involved are

$$\begin{aligned} \Delta L_A &= \pm 0.012 \\ \Delta L_R &= \pm 0.007 \\ \Delta T'_B &= \pm 1 \text{ K} \end{aligned} \quad (5-36)$$

so that, using the same constants as before,

$$\Delta T_S = \pm \left[\underbrace{0.62}_{\substack{\text{antenna} \\ \text{loss} \\ \text{inaccuracy}}} + \underbrace{0.59}_{\substack{\text{radome} \\ \text{loss} \\ \text{inaccuracy}}} + \underbrace{1.85}_{\substack{\text{receiver} \\ \text{calibration} \\ \text{inaccuracy}}} \right] \quad (5-37)$$

or

$$\Delta T_S = \pm 3 \text{ K} \quad (5-39)$$

This means that the measured source brightness mean temperature T_S is within ± 3 K of the true value.

5.6.3 Total Uncertainty

The total uncertainty in T_S is found by adding the random and systematic errors, i.e.,

$$\epsilon_{T_S} = \pm (|\Delta T_S| + \sigma_{TS}) \quad (5-40)$$

or

$$\epsilon_{T_S} = \pm \begin{cases} 5.2 \text{ K} & \text{(vertical)} \\ 5.7 \text{ K} & \text{(horizontal)} \end{cases} \quad (5-41)$$

CHAPTER VI

MFMR LOSS MEASUREMENTS

6.0 INTRODUCTION

The MFMR operates at L-Band (1.4135 GHz), K_u -Band (18.0 GHz), K-Band (22.05 GHz) and K_a -Band (37.0 GHz) with fixed beam antennas so that radiometric profiles in the flight direction are provided. The L-Band antenna is a linearly polarized stripline array, manufactured by AIL, with a 16° beamwidth and a beam efficiency of 95%. In order to obtain both vertically and horizontally components of incident radiation at L-Band, the entire antenna assembly is mechanically rotated through a roll angle of 90° . The K, K_u , and K_a -Band antennas are dual-polarized scalar horns, with simultaneous vertical and horizontal outputs to two radiometer channels for each band. 3 dB beamwidths are 4.0° at K_u , 4.3° at K and 4.5° at K_a -Bands. The seven channels all use Hach [1968] radiometers with 100 ms integration times (in flight) and bandwidths of 27, 200, 200 and 500 MHz at L, K_u , K and K_a -Bands respectively. Radiometric outputs and housekeeping data are all PCM encoded in a similar format to that used by PMIS.

All antennas and radiometers are mounted on a positioning ring so that both roll (0° or 90°) or pitch (0° to 180°) motions are mechanically controlled.

6.1 Mounting Configuration

Fig. 2-18 shows the MFMR on the antenna positioner and tower inside the bucket. During the measurement sequence, the antenna positioner was set to compensate for MFMR pitch motions so that the beam was always pointing toward zenith. However, this caused

the position of the antennas relative to the bucket walls to change considerably, as shown in Fig. 2-7, with the antennas being very close to the top of the bucket when the pitch was 90°. It will be shown later that this displacement had no measurable effect on the loss values.

In flight, microwave absorber is placed on the aircraft bulkhead for two principal reasons: (1) the L-Band array is so close to the bulkhead for a pitch of 0° that mutual coupling between antenna and radome via bulkhead reflections must be eliminated, and (2) when the K_u , K and K_a -Band horns are pointing skyward and viewing a cold and constant sky, considerable radiometric variations may occur in flight due to the backlobes viewing a variable terrain brightness temperature, unless this effect is artificially removed by causing the sidelobes and backlobes to view a relatively hot absorbing bulkhead. The absorber used is Emerson and Cuming flat Eccosorb, tuned for use at L-Band.

In testing at A-Mtn, however, the Eccosorb was not furnished and PSL used its own available absorber, the pyramidal material seen in Fig. 2-18. Unfortunately, this absorber is designed for use at X-Band and above and is essentially transparent at L-Band. The result is that all L-Band tests were with a non-absorbing bulkhead and thus did not simulate flight conditions. This situation will be discussed in detail in Sec. 6.5.4.

6.2 Radiometer Receiver Calibration

Each of the seven radiometer receivers was calibrated by the use of laboratory standard hot loads and cold loads. From (5-1), letting $T'_{Bi} = (T_h, T_c)$ and solving 2 simultaneous eqns. for the 2 unknown calibration constants.

$$T_1 = \frac{T_c X_h - T_h X_c}{X_h - X_c} \quad (6-1)$$

$$\Delta T = \frac{T_h - T_c}{X_h - X_c} \quad (6-2)$$

where X refers to the count ratio (see eqn. 5-2) and the subscripts h and c refer to hot and cold.

During the testing phase, laboratory calibrations were done twice: (1) at the beginning of the MFMR tests on Feb. 8, 1975 and (2) at the end of the MFMR tests on Feb. 21, 1975. Table 6-1 and Fig. 6-1 compare these constants over this period of time. No final calibration at K-Band was possible since the receiver failed during the intervening time.

Table 6-1

MFMR Laboratory Calibration Summary

Band	Initial Cal. (2-8-75)		Final Cal. (2-21-75)	
	T ₁ (K)	ΔT (K)	T ₁ (K)	ΔT (K)
K _u -1	329.87	-54.24	325.51*	-54.48*
K _u -2	327.65	-54.22	323.11*	-55.39*
K _a -1	330.57	-58.73	330.25	-58.17
K _a -2	331.14	-60.02	331.05	-59.89
K-1	329.64	-56.67	**	**
K-2	328.61	-50.20	**	**
L	323.33	-51.15	323.84	-50.93

NOTES:

* Final K_u-Band calibration may be slightly inaccurate since there was insufficient equipment warmup time.

** K-Band receiver was not operating at the time of final calibration.

52

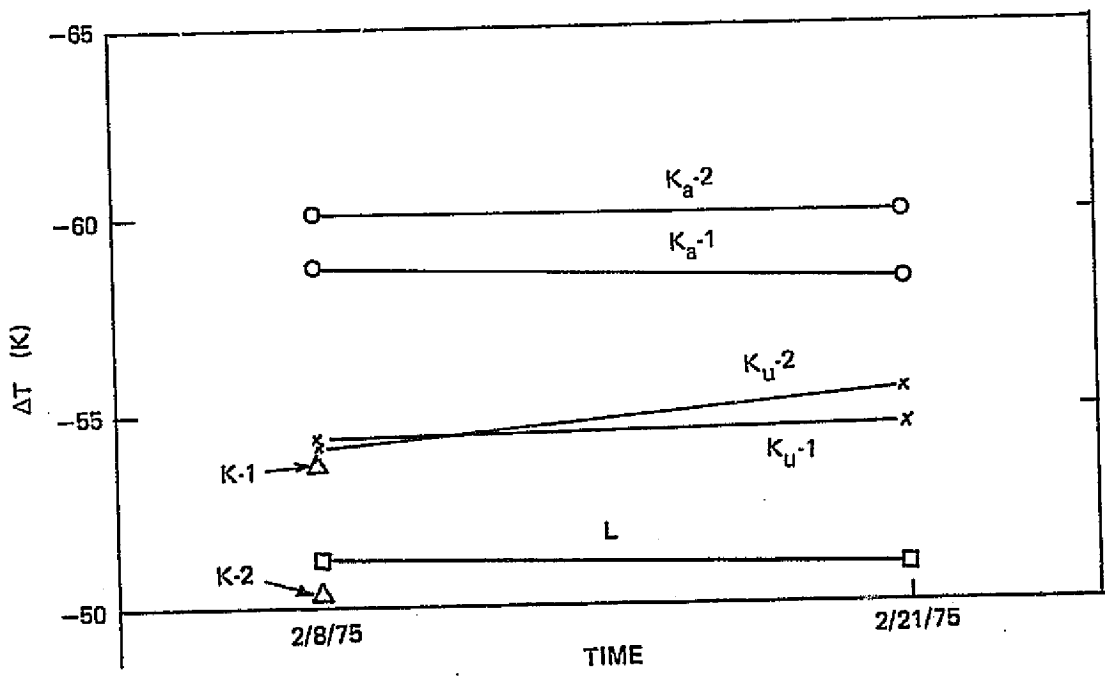
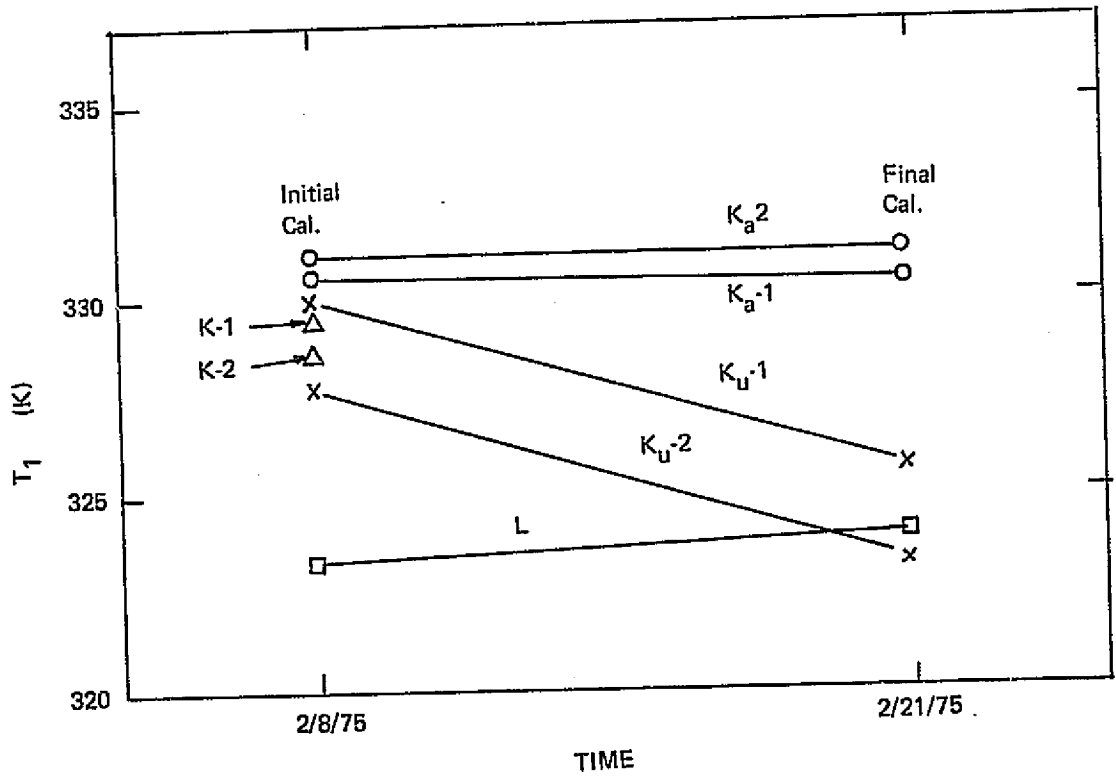


Fig. 6-1. MFMR calibration history.

6.3 MFMR Data Flow

Loss values were measured at roll angles of 0° and 90° for the following pitch angles: 0° , 5° , 10° , 15° , 20° , 25° , 30° , 35° , 40° , 45° , 50° , 60° , 70° , 80° , 90° , 100° , 110° , 120° , 130° , 140° , 150° , 160° , 165° , 170° , 175° and 180° . In flight, a 0° pitch angle has all antenna beams directed toward nadir, with the L-Band array nearest the bulkhead and the horns nearest the radome nose. A 180° pitch angle corresponds to the zenith direction, with the horns nearest the bulkhead and the L-Band array nearest the nose.

This arrangement thus requires 364 antenna loss measurements plus 364 more for each of the two radomes supplied, giving a total of 1092 measurements required. Most of these loss values were measured independently twice (and subsequently averaged), so that roughly 2000 measured values were processed.

Due to an unforeseen interaction between the L-Band antenna and the radome, the radome loss values measured at that frequency are not valid, although an approximate value of $L_R \approx 1.09$ (independent of pitch angle) can be used. This is discussed in detail in Sec. 6.6.

Antenna and radome loss values were calculated by the use of eqns. (3-2) and (3-4), with the sky brightness temperature (T_g) estimated using the algorithm discussed in Chap. 4. The uncorrected brightness temperature T_B' measured for each beam position was a 1-minute average. The 100 ms. integration time rms noise level (std. deviation) was monitored for each channel and a threshold, receiver sensitivity level of 6 K was established. This corresponds to a sensitivity of 0.25 K when referred to a 1-minute integration time. T_B' values noisier than this were discarded.

6.4 MFMR Antenna and Radome Loss Values (K_u , K, K_a -Bands)

The 980 final loss values, as derived by this technique, are tabulated in Tables 6-2, 6-3 and 6-4. The antenna loss values are plotted vs. pitch angle in Figs. 6-2, 6-3 and 6-4. Corresponding radome loss values for both radomes are plotted in Figs. 6-5 - 6-10.

All of these loss measurements were made with PSL-furnished absorber in place on the bulkhead. The rise in L_A as the pitch angle approaches 180° (for a roll of 0°) is due to an increasing contribution to the apparent source brightness distribution T_s as the horns come closer to the hot absorbing material. For a roll of 90° , this distance change with pitch angle is much less so that the effect is less pronounced. Radome losses are generally higher near 0° or 180° for a roll of 0° and are occasionally quite high from 170° - 180° since the antennas are looking straight up and into the radome fairing-bulkhead interface, with the resulting likelihood of strong mutual coupling.

It should be emphasized that the jagged nature of the loss graphs for L_R is not due to errors in the measurement method, since these values were easily repeatable from one measurement set to the next under identical circumstances. Rather, this behavior stems from either resonant scattering between the horns and radome or resonant thickness effects (especially at K_a -Band) of the radome material.

6.5 Interaction Mechanisms between the MFMR Horns and the Aircraft Bulkhead

6.5.1 Introduction

As mentioned previously, it was observed that the antenna

Table 6-2

MFMR
ANTENNA LOSS (L_A)

PITCH	ROLL = 0°							ROLL = 90°						
	L	K_u-1	K_u-2	K-1	K-2	K_a-1	K_a-2	L	K_u-1	K_u-2	K-1	K-2	K_a-1	K_a-2
0°	1.365	1.123	1.119	1.096	1.082	1.124	1.111	1.369	1.136	1.140	1.105	1.098	1.129	1.114
5°	1.366	1.122	1.119	1.092*	1.080*	1.123	1.110	1.365	1.135	1.141	1.104*	1.098*	1.128	1.113
10°	1.365	1.122	1.118	1.086	1.078	1.123	1.111	1.363	1.136	1.139	1.103	1.098	1.129	1.113
15°	1.364	1.122	1.118	1.085*	1.077*	1.121	1.109	1.362	1.136	1.141	1.103*	1.098*	1.129	1.114
20°	1.363	1.122	1.117	1.083	1.077	1.122	1.109	1.362	1.136	1.142	1.102	1.098	1.129	1.113
25°	1.363	1.122	1.117	1.083*	1.078*	1.122	1.109	1.363	1.137	1.142	1.102*	1.097*	1.130	1.115
30°	1.361	1.122	1.117	1.083	1.078	1.122	1.110	1.362	1.138	1.143	1.102	1.096	1.130	1.115
35°	1.361	1.123	1.118	1.087*	1.081*	1.122	1.110	1.363	1.140	1.144	1.100*	1.095*	1.130	1.115
40°	1.362	1.123	1.118	1.089*	1.082*	1.121	1.109	1.363	1.141	1.144	1.099*	1.094*	1.131	1.116
45°	1.361	1.125	1.119	1.089*	1.084*	1.122	1.109	1.364	1.141	1.144	1.098*	1.093*	1.131	1.117
50°	1.362	1.127	1.121	1.091*	1.086*	1.122	1.110	1.363	1.143	1.146	1.097*	1.092*	1.132	1.117
60°	1.360	1.135	1.129	1.094*	1.089*	1.125	1.113	1.365	1.145	1.146	1.096*	1.090*	1.133	1.120
70°	1.360	1.142	1.134	1.098*	1.092*	1.127	1.115	1.365	1.147	1.148	1.094*	1.089*	1.135	1.121
80°	1.361	1.150	1.143	1.101*	1.096*	1.131	1.119	1.367	1.146	1.148	1.092*	1.088*	1.136	1.122
90°	1.360	1.159	1.153	1.103	1.097	1.133	1.121	1.367	1.146	1.148	1.090	1.087	.137	1.123
100°	1.360	1.168	1.162	1.108*	1.102*	1.137	1.127	1.369	1.145	1.147	1.089*	1.085*	.137	1.124
110°	1.360	1.175	1.168	1.111*	1.105*	1.141	1.130	1.367	1.142	1.145	1.088*	1.084*	1.139	1.125
120°	1.360	1.185	1.175	1.114*	1.109*	1.144	1.133	1.362	1.138	1.143	1.087*	1.082*	1.138	1.124
130°	1.360	1.192	1.181	1.118*	1.111*	1.146	1.136	1.365	1.135	1.141	1.085*	1.080*	1.140	1.126
140°	1.360	1.197	1.187	1.121*	1.115*	1.149	1.139	1.362	1.133	1.139	1.083*	1.079*	1.141	1.126
150°	1.361	1.201	1.193	1.124	1.116	1.151	1.141	1.365	1.131	1.138	1.081	1.077	1.141	1.127
160°	1.362	1.204	1.198	1.132	1.124	1.156	1.147	1.365	1.131	1.139	1.082	1.076	1.147	1.131
165°	1.362	1.206	1.201	1.133*	1.125*	1.160	1.150	1.366	1.133	1.141	1.083*	1.078*	1.151	1.135
170°	1.363	1.211	1.204	1.135*	1.126	1.164	1.154	1.367	1.134	1.143	1.084	1.080	1.156	1.140
175°	1.365	1.216	1.208	1.136	1.127	1.167	1.156	1.372	1.136	1.144	1.085	1.079	1.159	1.144
180°	1.366	1.228	1.219	-----	-----	1.173	1.160	1.376	1.138	1.147	-----	-----	1.163	1.148

*Interpolated Data

ORIGINAL PAGE IS
OF POOR QUALITY

Table 6-3

MFMR
RADOME 1 LOSS (L_R)

PITCH	ROLL = 0°							ROLL = 90°					
	L	K_u-1	K_u-2	K-1	K-2	K_a-1	K_a-2	L	K_u-1	K_u-2	K-1	K-2	K_a-1
0°		1.458	1.300	1.221	1.217	1.548	1.521	1.172	1.161	1.370	1.293	1.539	1.574
5°		1.403	1.276	1.204	1.198	1.535	1.512	1.170	1.160	1.245	1.212	1.568	1.591
10°		1.364	1.252	1.205	1.190	1.538	1.531	1.169	1.160	1.244	1.213	1.561	1.578
15°		1.350	1.242	1.191	1.176	1.543	1.549	1.171	1.159	1.248	1.223	1.559	1.555
20°		1.325	1.234	1.198	1.183	1.522	1.536	1.173	1.161	1.246	1.220	1.566	1.545
25°		1.298	1.223	1.226	1.209	1.495	1.504	1.173	1.162	1.221	1.199	1.566	1.536
30°		1.274	1.216	1.232	1.212	1.503	1.527	1.180	1.165	1.216	1.193	1.566	1.530
35°		1.246	1.208	1.205	1.185	1.513	1.542	1.192	1.170	1.207	1.187	1.539	1.512
40°		1.240	1.206	1.201*	1.182*	1.486	1.512	1.198	1.176	1.202*	1.183*	1.489	1.463
45°		1.230	1.194	1.198*	1.178*	1.477	1.506	1.212	1.184	1.197*	1.178*	1.483	1.458
50°		1.222	1.186	1.194*	1.175*	1.472	1.496	1.205	1.181	1.192*	1.174*	1.474	1.450
60°		1.214	1.177	1.191*	1.171*	1.502	1.518	1.192	1.174	1.186*	1.169*	1.494	1.481
70°		1.214	1.193	1.187*	1.168*	1.450	1.466	1.195	1.186	1.181*	1.165*	1.463	1.440
80°		1.217	1.209	1.184*	1.164*	1.478	1.487	1.206	1.204	1.176*	1.160*	1.468	1.454
90°		1.215	1.207	1.180	1.161	1.454	1.461	1.189	1.175	1.171	1.156	1.449	1.436
100°		1.211	1.204	1.189*	1.170*	1.426	1.429	1.193	1.177	1.178*	1.161*	1.435	1.425
110°		1.206	1.199	1.196*	1.179*	1.412	1.414	1.207	1.188	1.184*	1.166*	1.420	1.413
120°		1.202	1.194	1.205*	1.189*	1.338	1.340	1.195	1.176	1.191*	1.171*	1.338	1.342
130°		1.208	1.198	1.214*	1.198*	1.354	1.359	1.171	1.160	1.198*	1.175*	1.331	1.332
140°		1.214	1.205	1.223*	1.207*	1.357	1.360	1.163	1.156	1.204*	1.180*	1.345	1.343
150°		1.207	1.205	1.234	1.216	1.362	1.359	1.165	1.156	1.211	1.185	1.367	1.364
160°		1.292	1.278	1.342	1.325	1.440	1.460	1.177	1.163	1.271	1.244	1.401	1.386
165°		1.378	1.359	1.420	1.419	1.486	1.534	1.190	1.172	1.383	1.346	1.409	1.381
170°		1.379	1.388	1.446	1.419	1.552	1.582	1.195	1.175	1.417	1.376	1.445	1.404
175°		1.412	1.416	1.620	1.595	1.683	1.770	1.252	1.209	1.528	1.463	1.791	1.698
180°		1.366	1.323	-----	-----	1.838	1.922	6.880	6.605	-----	-----	9.473	10.551

*Interpolated Data

NOTE: L-Band data missing because of mutual interaction effects between radome and antenna.

Table 6-4

MFMR
RADOME 2 LOSS (L_p)

PITCH	ROLL = 0°							ROLL = 90°						
	L	K_u-1	K_u-2	K-1	K-2	K_a-1	K_a-2	L	K_u-1	K_u-2	K-1	K-2	K_a-1	K_a-2
0°		1.536	1.357	1.241	1.228	1.520	1.454		1.220	1.196	1.287	1.224	1.480	1.537
5°		1.475	1.329	1.228	1.216	1.577	1.517		1.214	1.193	1.217	1.188	1.463	1.509
10°		1.426	1.290	1.231	1.208	1.601	1.560		1.207	1.187	1.228	1.198	1.478	1.511
15°		1.408	1.280	1.230	1.207	1.595	1.575		1.194	1.182	1.239	1.213	1.495	1.513
20°		1.394	1.278	1.232	1.208	1.571	1.560		1.185	1.177	1.237	1.211	1.494	1.495
25°		1.367	1.263	1.219	1.199	1.544	1.545		1.180	1.178	1.237	1.211	1.487	1.478
30°		1.339	1.250	1.212	1.194	1.547	1.559		1.180	1.176	1.236	1.210	1.486	1.469
35°		1.301	1.237	1.210	1.191	1.531	1.543		1.185	1.180	1.229	1.206	1.486	1.467
40°		1.291	1.239	1.214	1.198	1.569	1.571		1.191*	1.185*	1.223*	1.202*	1.481*	1.463*
45°		1.278	1.229	1.189	1.174	1.515	1.519		1.197*	1.190*	1.218*	1.199*	1.476*	1.460*
50°		1.229	1.194	1.153	1.138	1.482	1.487		1.203*	1.195*	1.212*	1.195*	1.471*	1.456*
60°		1.229	1.214	1.157	1.142	1.459	1.461		1.208*	1.200*	1.206*	1.192*	1.465*	1.452*
70°		1.235	1.225	1.162	1.146	1.512	1.504		1.214*	1.205*	1.200*	1.188*	1.460*	1.448*
80°		1.239	1.231	1.171	1.156	1.463	1.460		1.220*	1.210*	1.195*	1.185*	1.455*	1.445*
90°		1.248	1.240	1.205	1.192	1.457	1.452		1.226	1.215	1.189	1.181	1.450	1.441
100°		1.250	1.243	1.205	1.199	1.479	1.468		1.223*	1.212*	1.193*	1.182*	1.450*	1.440*
110°		1.249	1.245	1.199	1.183	1.508	1.523		1.220*	1.209*	1.195*	1.183*	1.450*	1.439*
120°		1.253	1.246	1.211	1.190	1.522	1.527		1.217*	1.206*	1.199*	1.184*	1.451*	1.438*
130°		1.265	1.256	1.219	1.195	1.516	1.518		1.214*	1.202*	1.202*	1.184*	1.451*	1.437*
140°		1.237	1.230	1.186	1.173	1.425	1.447		1.211*	1.199*	1.206*	1.185*	1.452*	1.436*
150°		1.232	1.235	1.197	1.189	1.402	1.419		1.208	1.196	1.212	1.186	1.452	1.435
160°		1.280	1.279	1.306	1.299	1.492	1.546		1.222	1.202	1.243	1.220	1.436	1.397
165°		1.345	1.358	1.432	1.435	1.451	1.490		1.228	1.205	1.287	1.254	1.393	1.366
170°		1.377	1.404	1.504	1.511	1.427	1.489		1.238	1.209	1.294	1.263	1.468	1.403
175°		1.418	1.469	1.749	1.766	1.577	1.664		1.282	1.254	1.411	1.346	1.885	1.720
180°		1.359	1.422	1.713	1.738	1.690	1.774		1.319	1.290	1.313	1.261	1.924	1.879

*Interpolated Data

NOTE: L-Band data missing because of mutual interaction effects between radome and antenna.

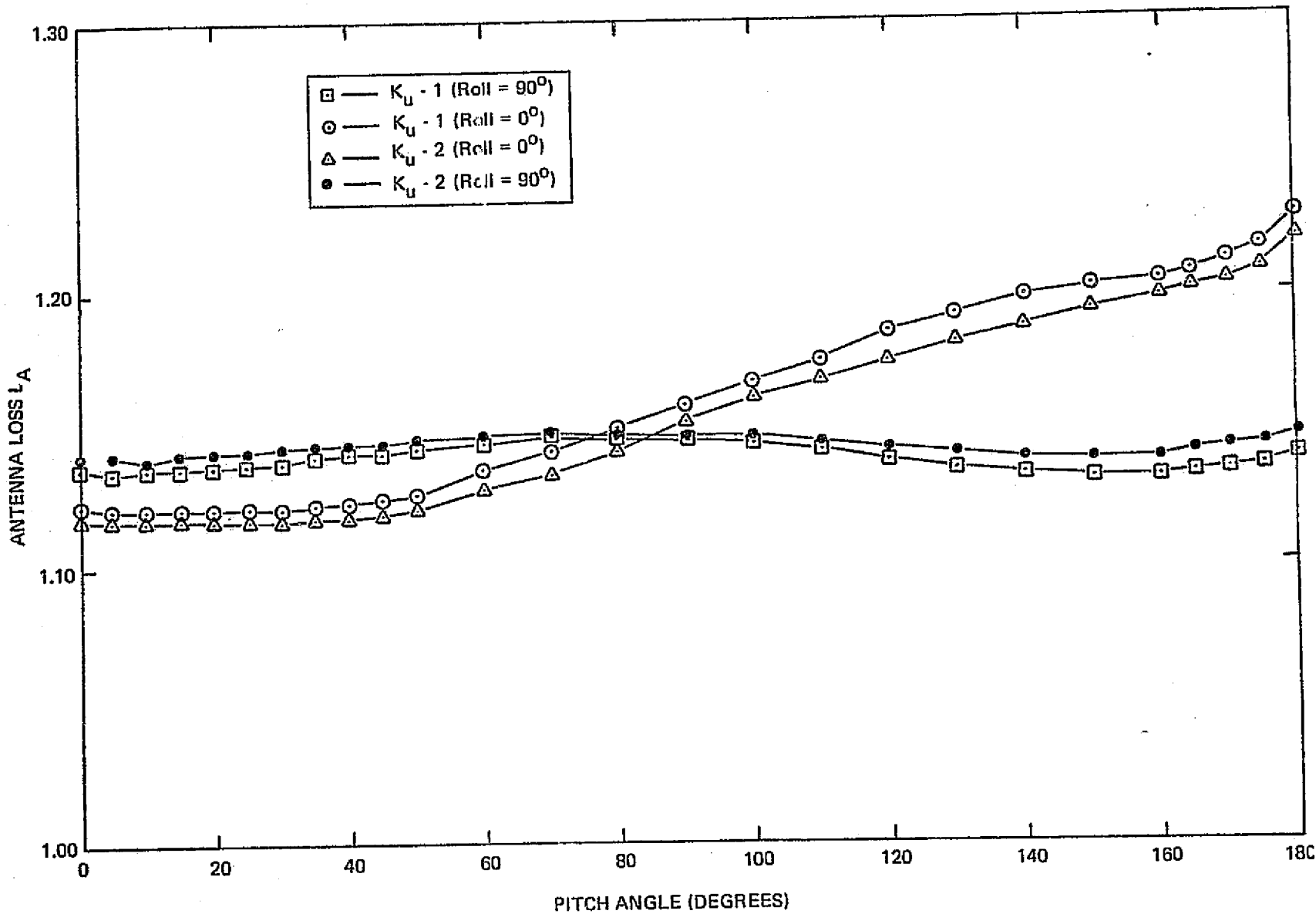


Fig. 6-2. MFMR antenna loss versus pitch angle -- K_u -Band.

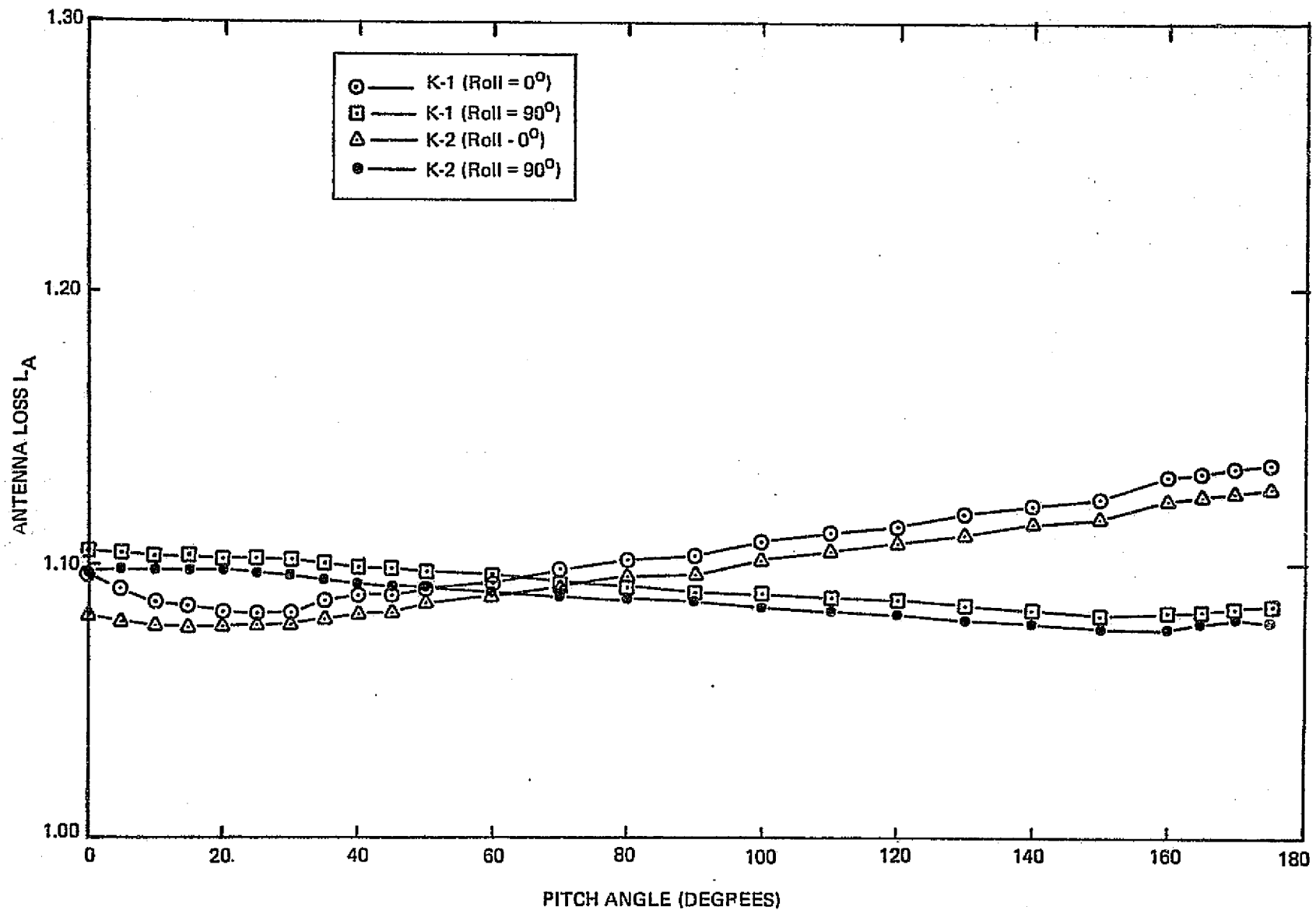


Fig. 6-3. MFMR antenna loss versus pitch angle -- K-Band.

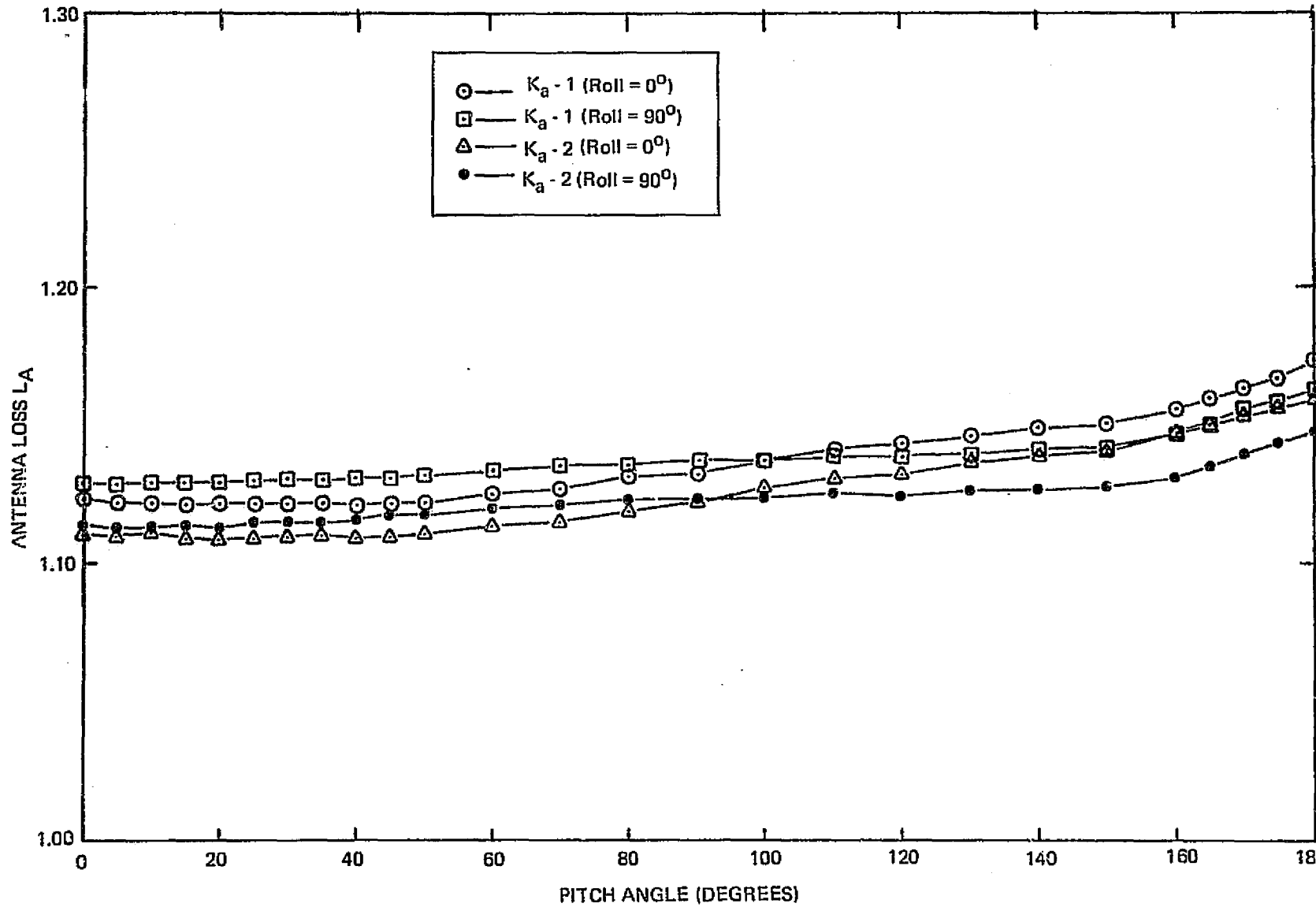


Fig. 6-4. MFMR antenna loss versus pitch angle -- K_a -Band.

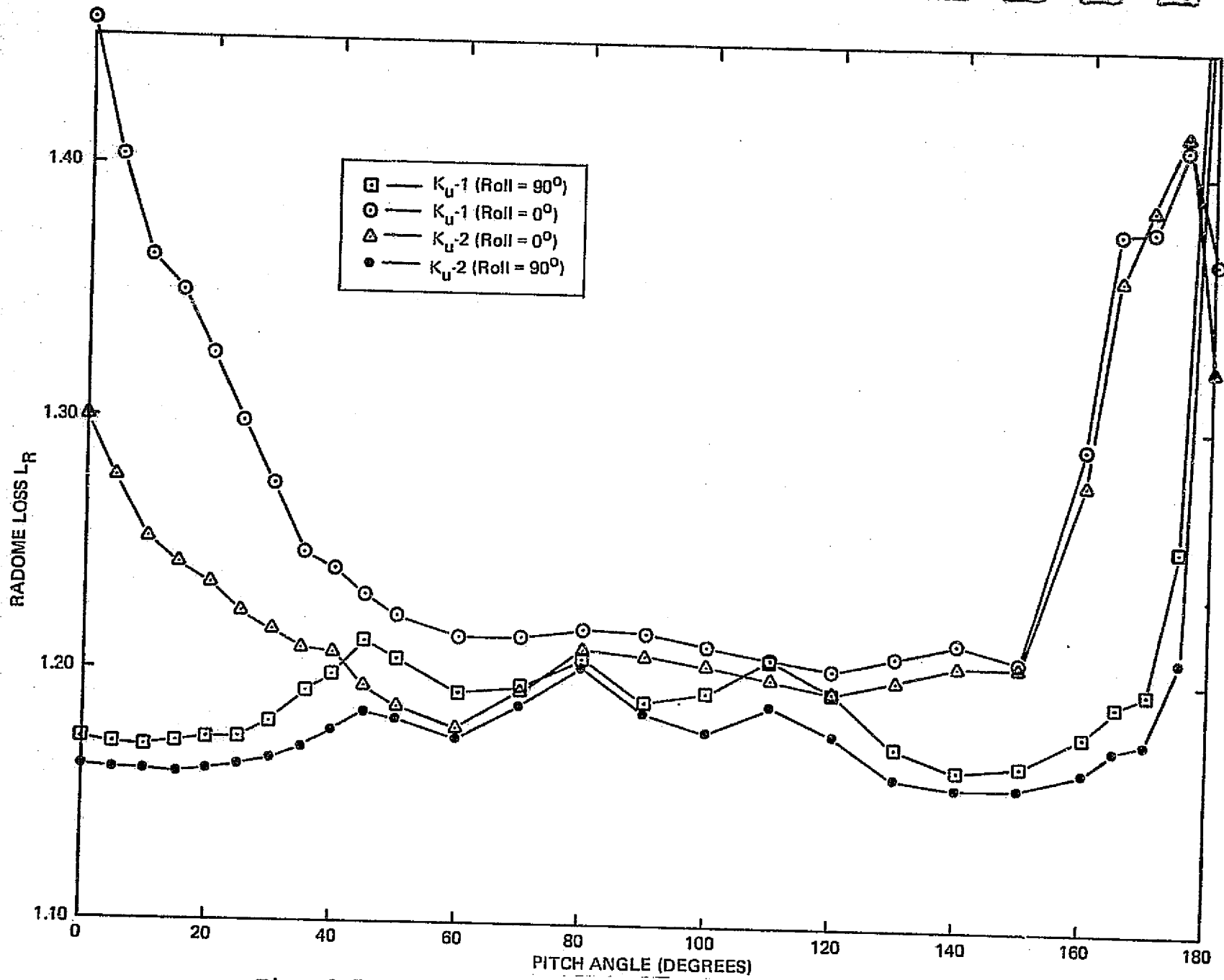


Fig. 6-5. MFMR radome 1 loss versus pitch angle -- K_u -Band.

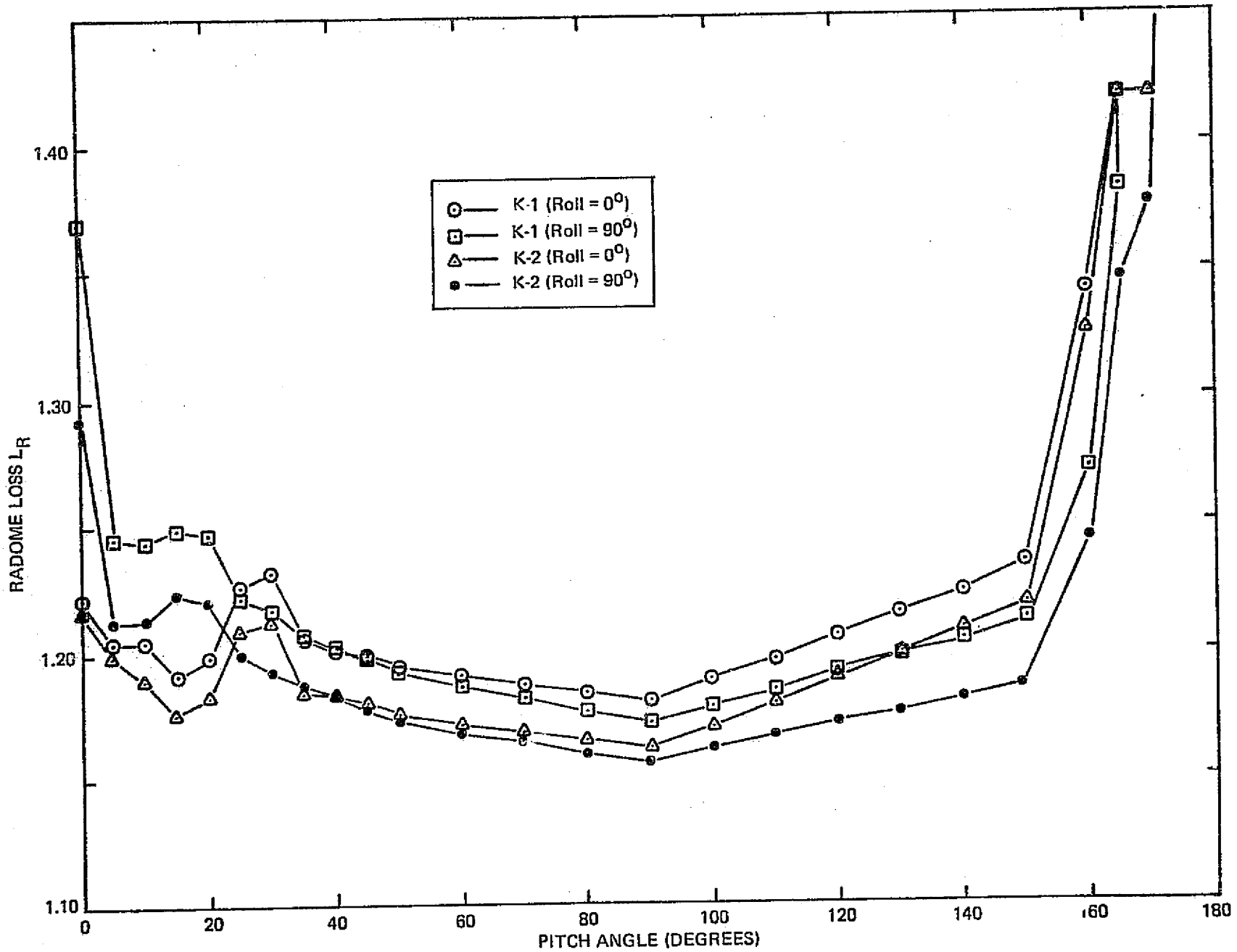


Fig. 6-6. MFM radome 1 loss versus pitch angle -- K-Band.

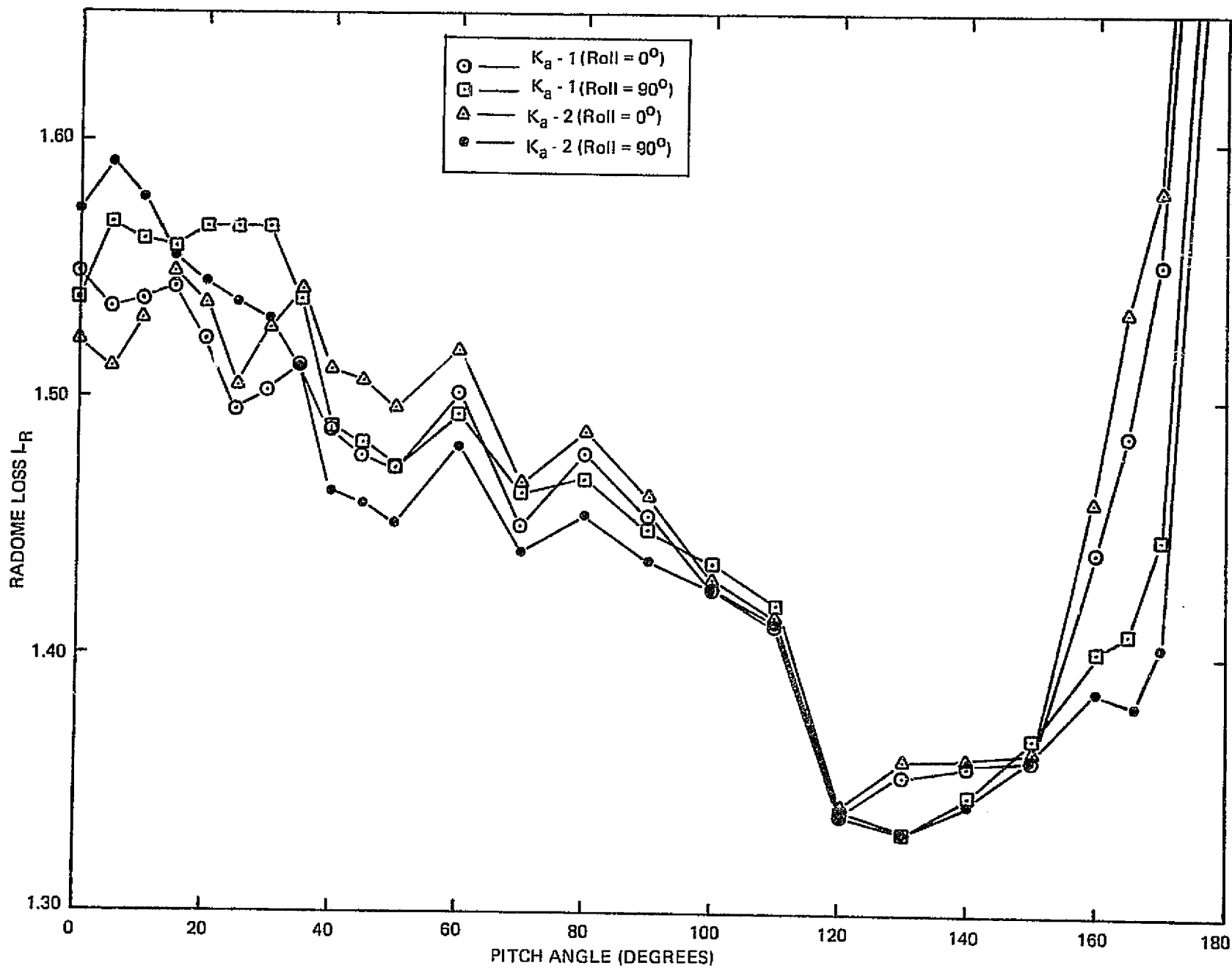


Fig. 6-7. MFMR radome 1 loss versus pitch angle -- K_a -Band.

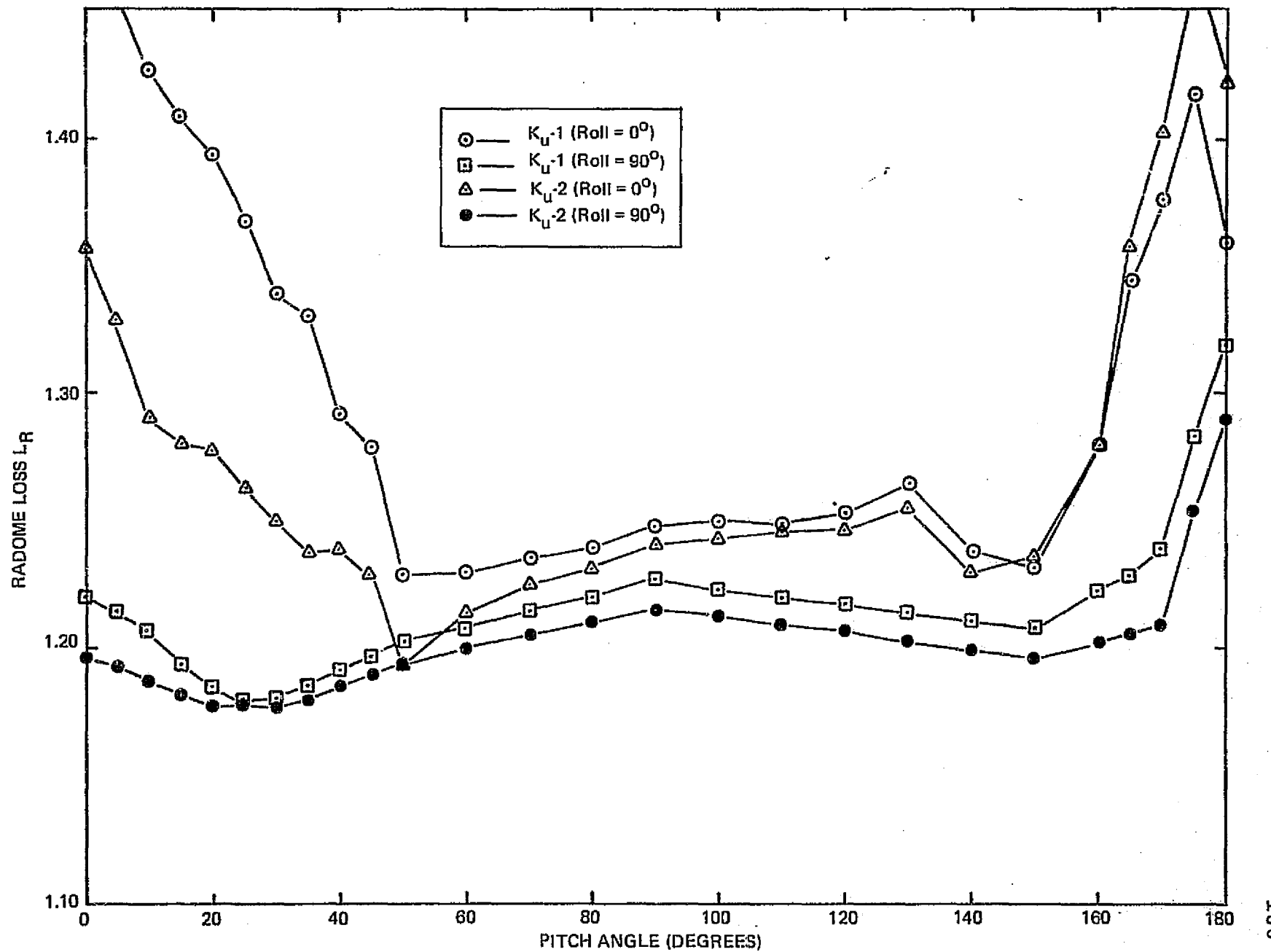


Fig. 6-8. MFMR radome 2 loss versus pitch angle -- K_u -Band.

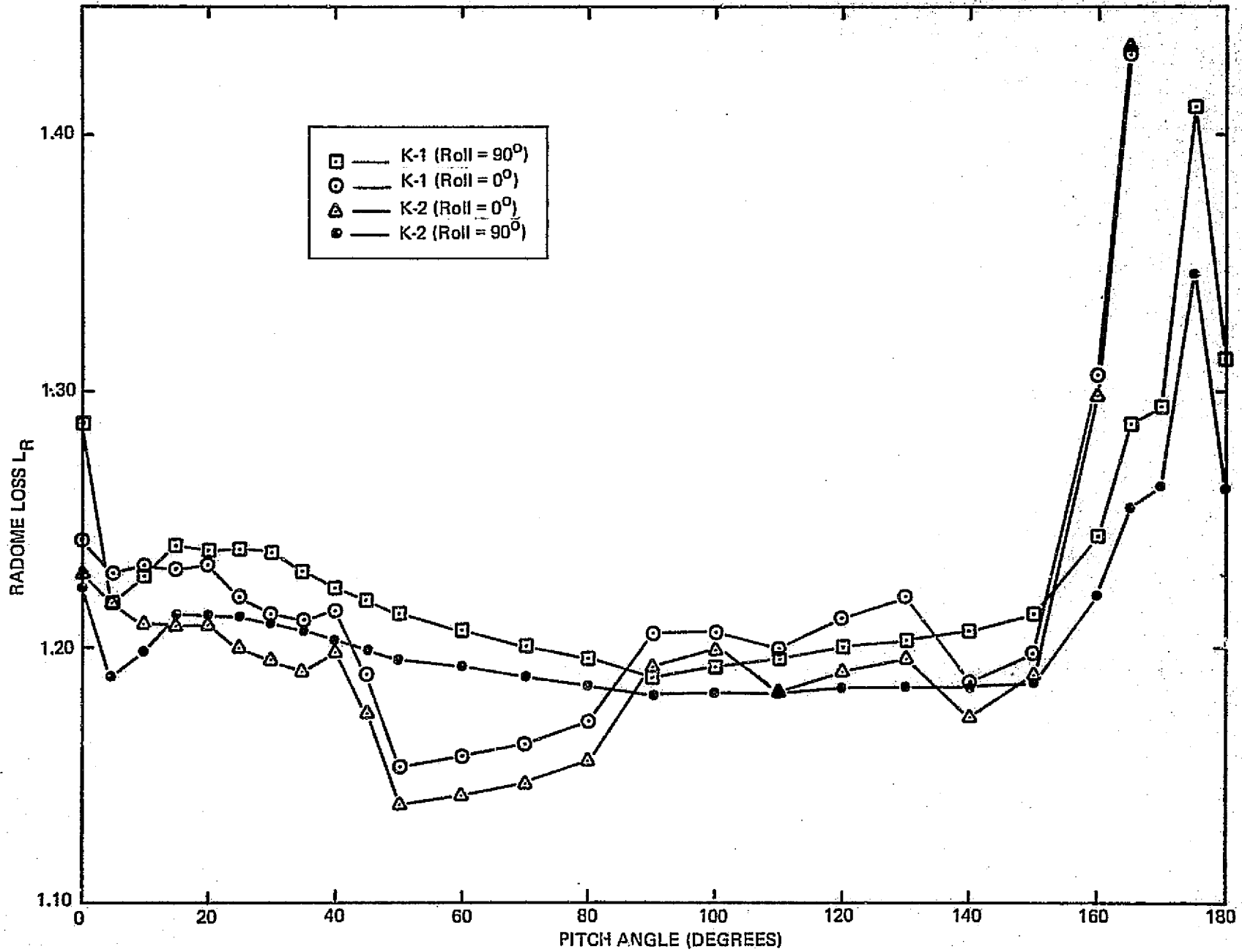


Fig. 6-9. MFMR radome 2 loss versus pitch angle -- K-Band.

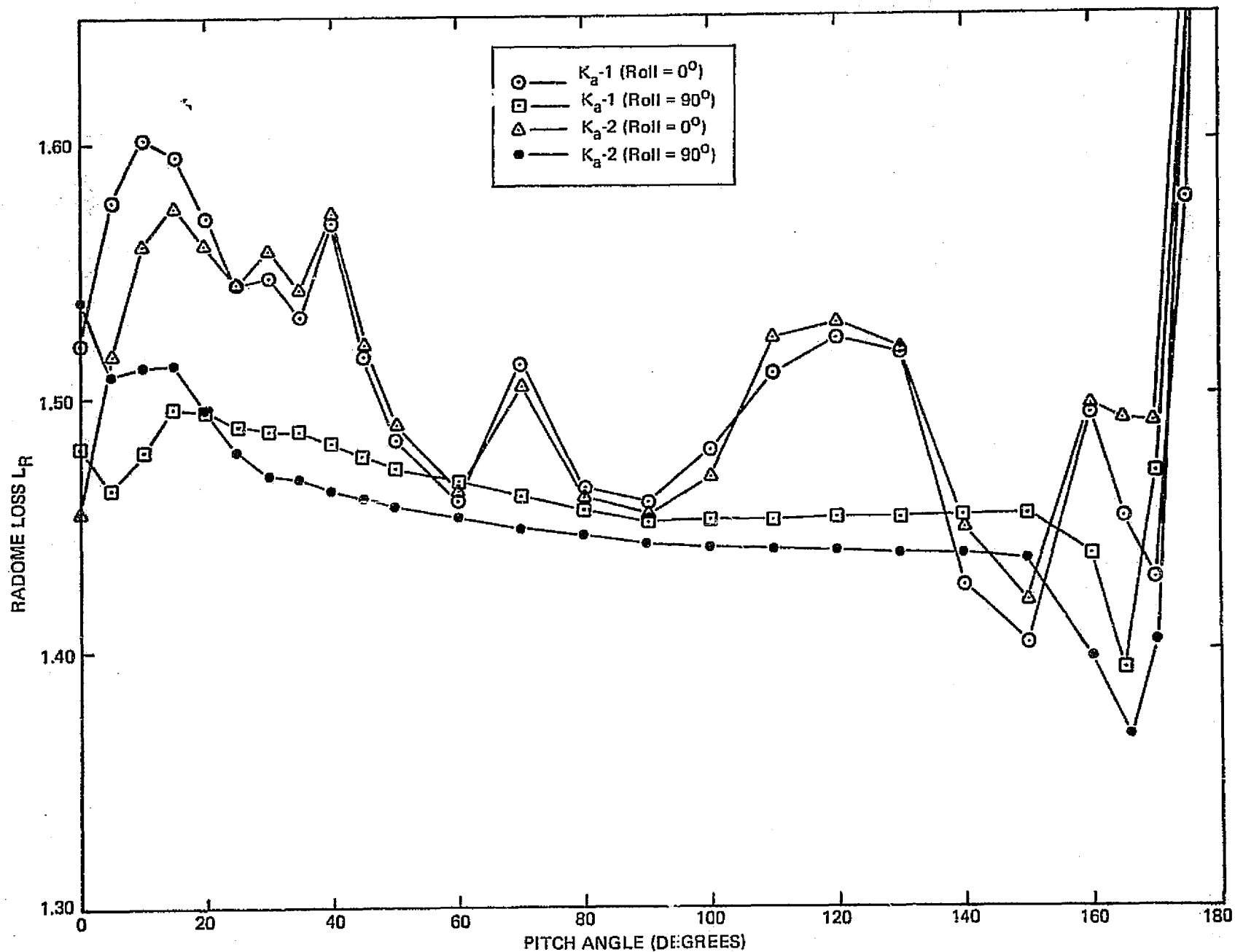


Fig. 6-10. MFMR radome 2 loss versus pitch angle -- K_a -Band.

loss L_A at K_u -Band (and to a lesser extent, at K and K_a -Bands) rose monotonically with pitch angle increasing beyond 60° (when the roll was 0°) when the absorber was in place on the mockup bulkhead of the aircraft. When the absorber was removed, the antenna loss was essentially independent of pitch angle both at K_u and K_a -bands (no measurement at K-Band were made without absorber). It is the intention of Sec. 6.5 to show a mechanism of interaction between the bulkhead and the horn and to suggest further measurements which could improve the accuracy of the loss numbers applied to use in the operational situation on the P-3 aircraft. Comments are restricted mostly to the K_u -Band horn, but the approach can be generalized.

6.5.2 Near-field Patterns of Circular Horns

Assuming the scalar K_u -Band horn has 25 dB sidelobes, the circular Taylor distributions for near-field given by Hansen [1964] for a 10 wavelength diameter aperture can be used by rescaling to the diameter of the K_u -Band horn (36 cm). Fig. 15 (p. 29) of Hansen lists several field patterns for a 10λ diameter horn in free space. Let R be the distance to field point from the horn phase center (taken to be in the center of the mouth of the horn). Hansen defines $\Delta = \frac{R}{2D^2/\lambda}$ and plots field patterns for $\Delta = 0.0375$, 0.05 , 0.075 , 0.125 , 0.25 and ∞ . We are interested in the smallest two of these. Fig. 6-11 is a general plot of the power pattern (dB) for $\Delta = 0.0375$ ($R = 58$ cm.), 0.05 (79 cm.) and ∞ (far-field) with the abscissa $X = ka \sin \theta = \frac{\pi D}{\lambda} \sin \theta = 10\pi \sin \theta$. Since the K_u -Band horn has a diameter of 21.7λ at 18 GHz, Fig. 6-11 can be rescaled to this diameter, producing the graph of Fig. 6-12. According to Hansen, a typical circular Taylor design would require a monotonic aperture distribution with the power density at the edge of the horn down about 8 dB from its value on axis. This produces the aperture distribution curve at a radius of 18 cm shown in Fig. 6-12.

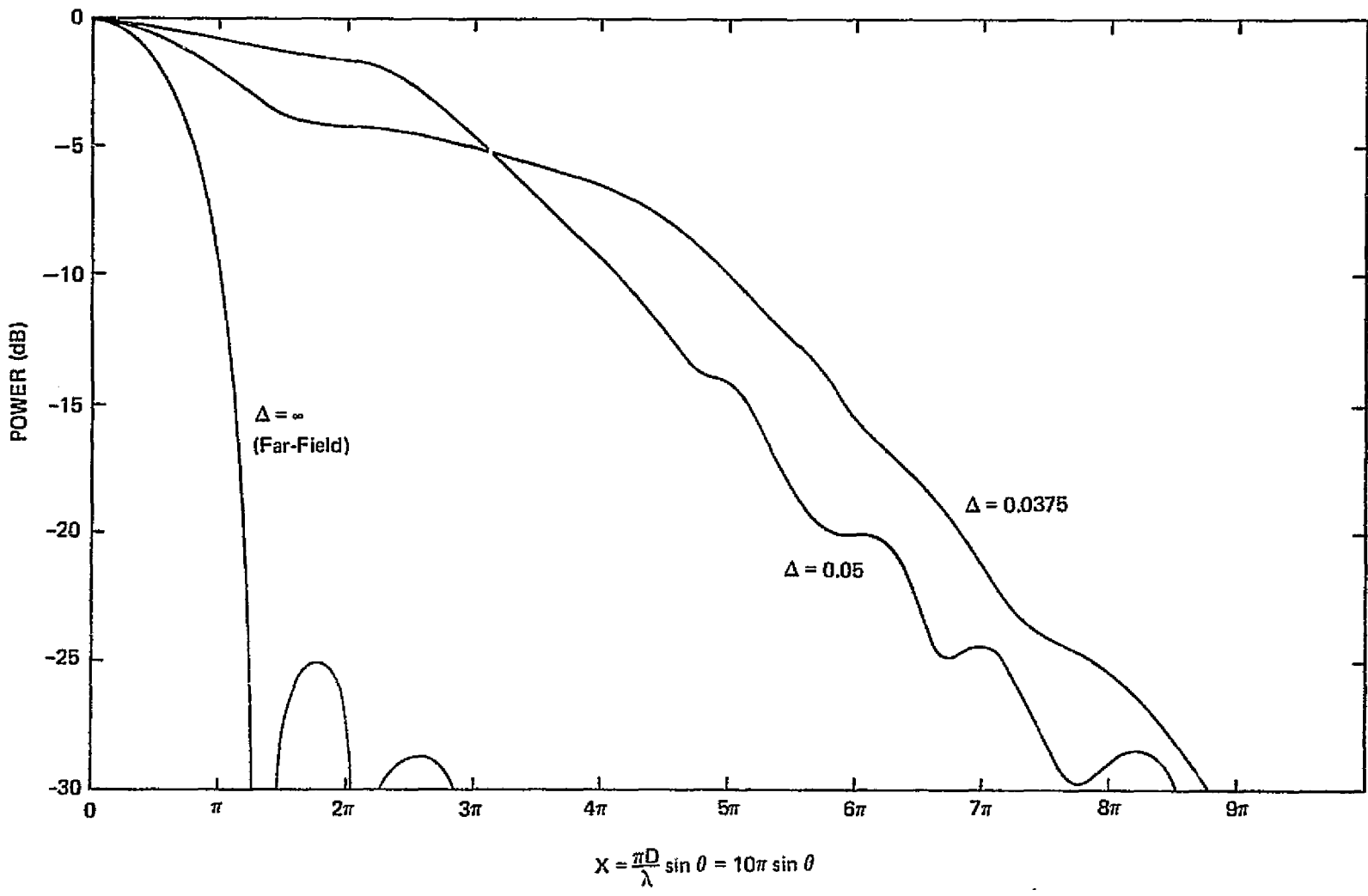


Fig. 6-11. Fresnel and far-field patterns for 25 dB circular Taylor distribution.

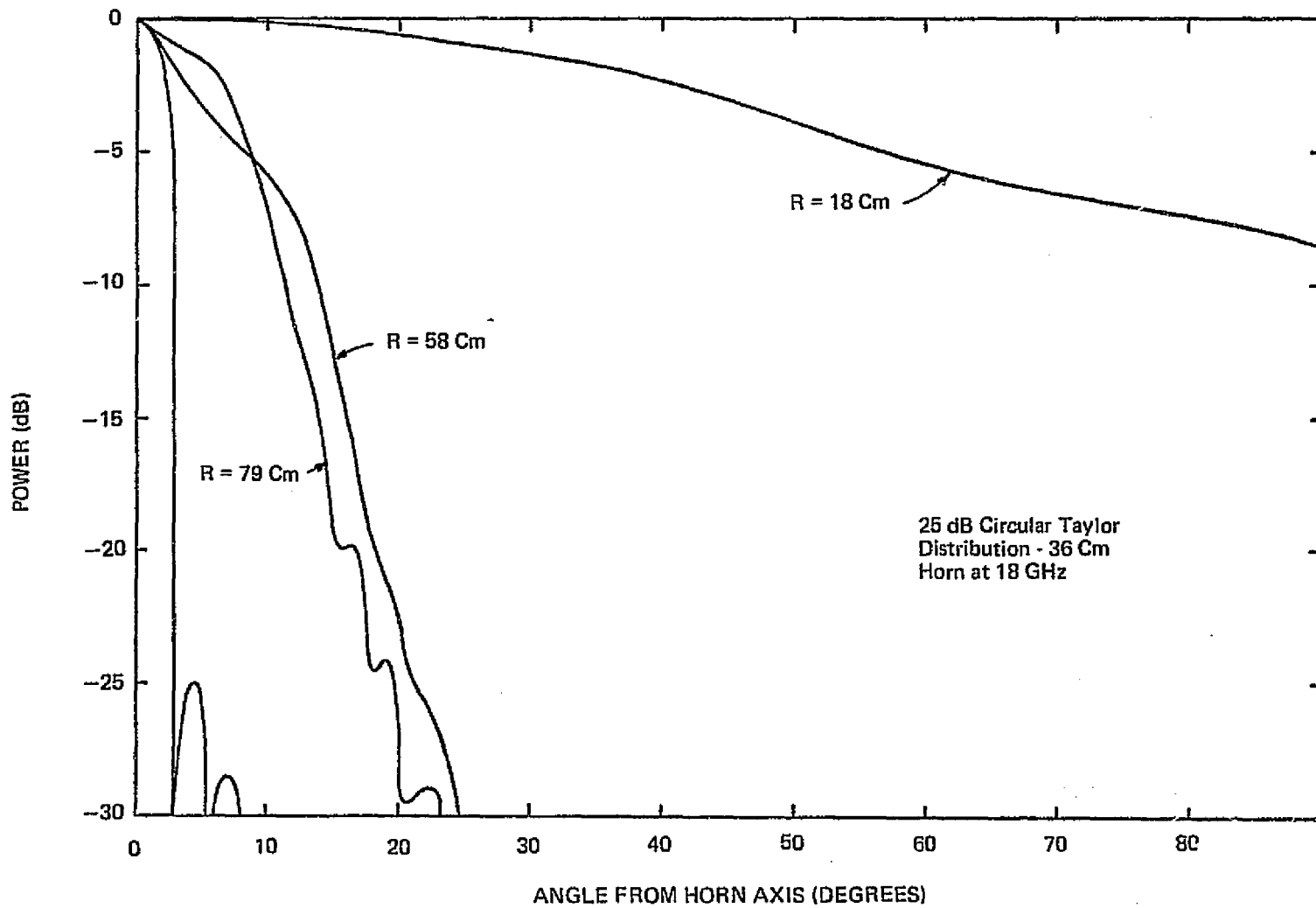


Fig. 6-12. Fresnel and far-field patterns.

The on-axis power density oscillates with distance from the phase center, assumed here to be at or very near the horn mouth. Fig. 6-13 is extrapolated from Hansen's data and plots the on-axis power in dB vs. distance. The variation out to about 200 cm is ± 1 dB and can be seen to fluctuate most rapidly out to 50 cm from the horn. Beyond about 175 cm, the $1/R^2$ far-field behavior begins to predominate.

6.5.3 Geometry of Horn Relative to Bulkhead

Fig. 6-14 shows the geometrical relationship of the horn relative to the absorber-covered bulkhead, for pitch angles of 180° (when horn is looking at zenith) and at 100° (slightly up from the aircraft flight vector). The distance from the horn phase center varies from about 38 cm (closest approach at $\theta = 180^\circ$) to about 81 cm (farthest approach at $\theta = 70^\circ$) so that the near field pattern evaluated at the distance to the absorber must be a function of angle from horn axis as well as radius. To a first approximation, all near field patterns have the same on-axis gain level, and can therefore be normalized to 0 dB.

6.5.4 Contribution of Absorber to Brightness Temperature

The near-field curves of Fig. 6-12 make two assumptions:

- 1) The horn is in free space
- 2) Edge diffracted rays are negligible

In reality, however, the horn is near a number of metallic surfaces, some of them very close. Furthermore, the approximate -8 dB edge taper introduces the possibility of strong near-field interaction between the horn and the mounting ring, L-Band antenna and receiver enclosures. It has been shown in a series of papers by Peters, et. al. [1966, 1975] that a Fourier transformation of an aperture distribution which is assumed to be zero outside the

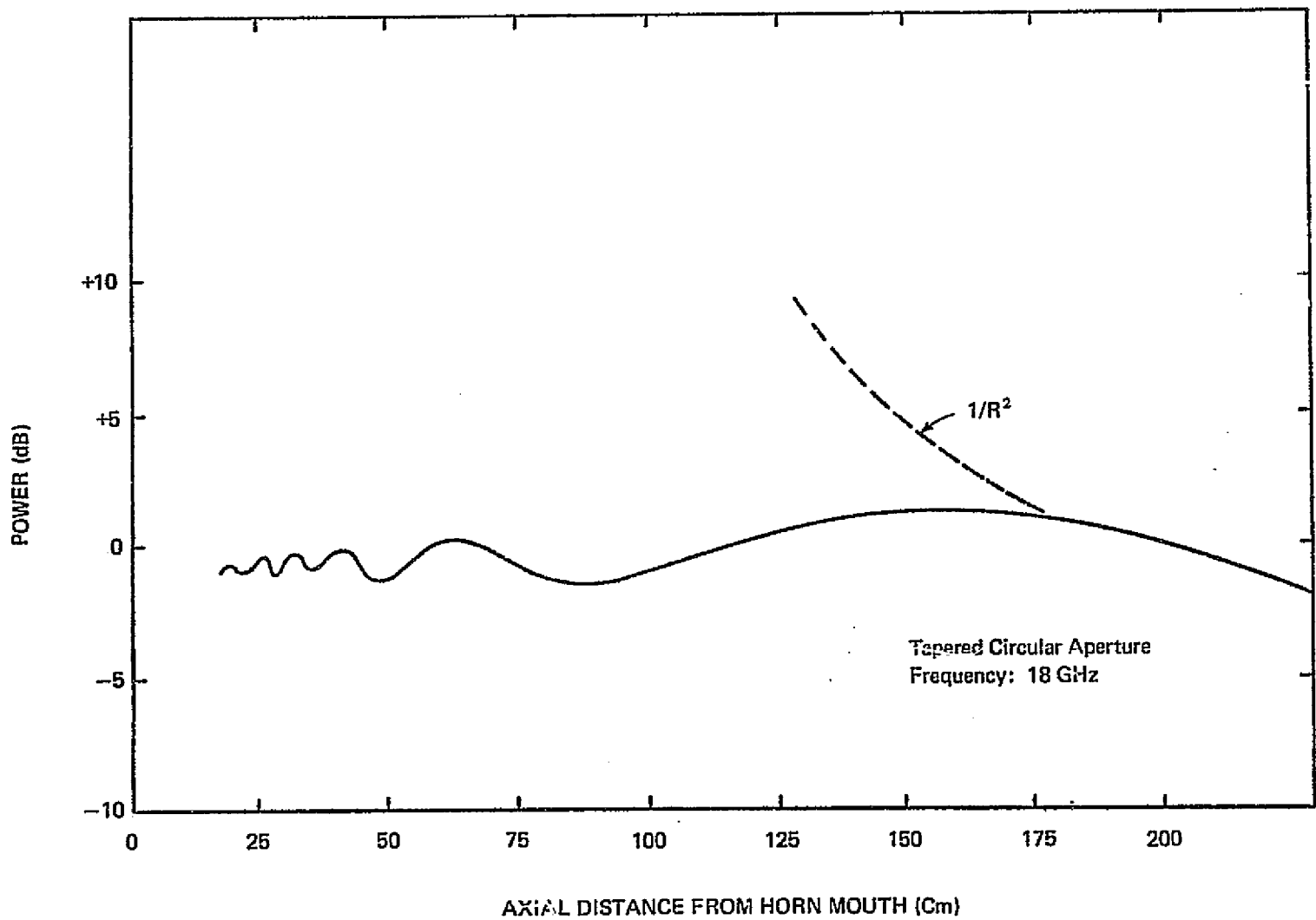


Fig. 6-13. On axis power density versus axial distance from horn mouth.

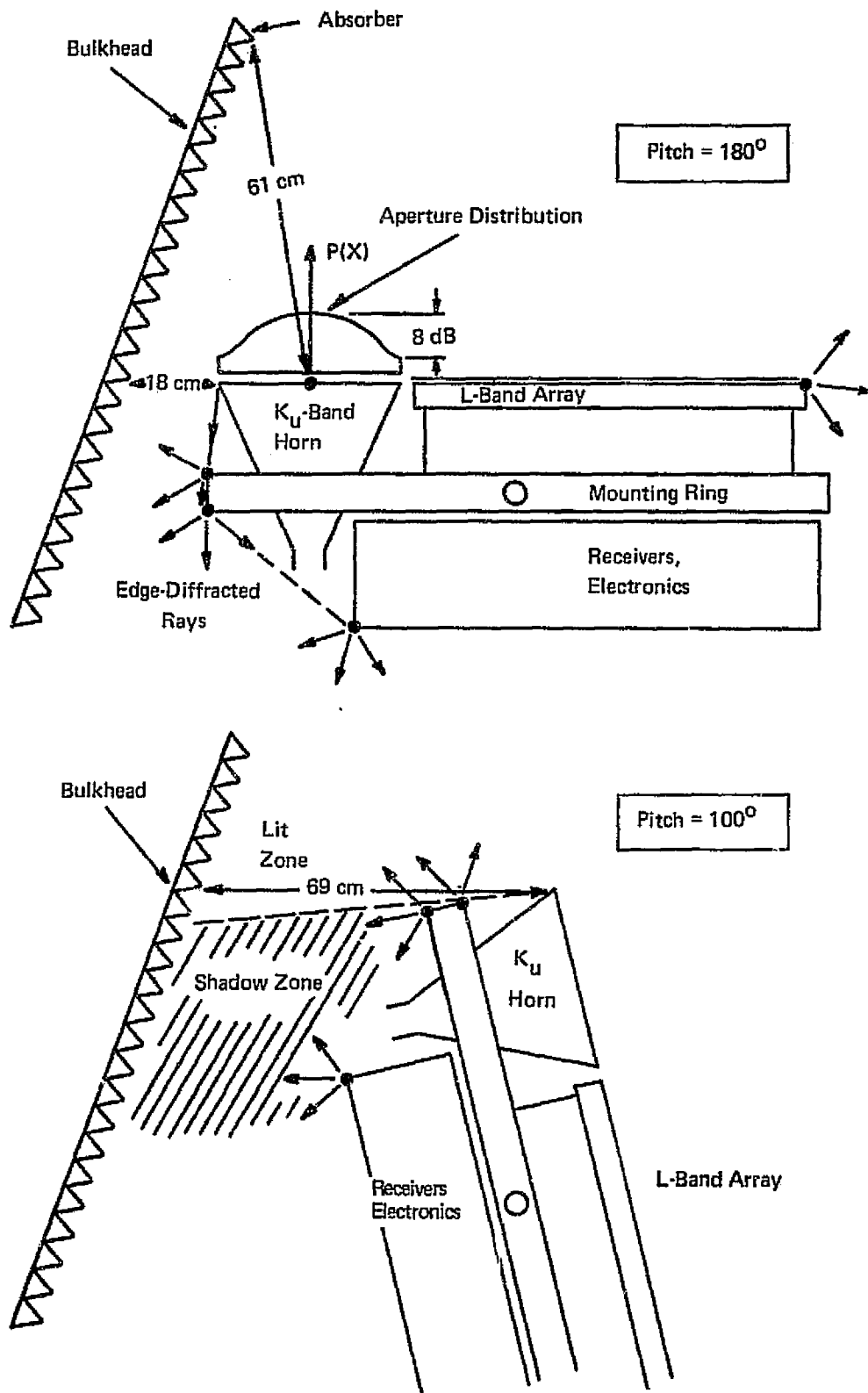


Fig. 6-14. Positions relative to bulkhead - MFMR.

aperture of a horn (i.e., neglecting induced line sources at the horn edges) is satisfactory to predict the far-field shape of the main beam and the first few sidelobes, but fails to predict the level and structure of the far sidelobes and backlobes, either in the E-plane or in the H-plane. Typically, aperture integration methods which neglect the geometrically-diffracted rays from the edge give good agreement with measured results out to about 5 or 6 times the HPBW, when in the far field.

Thus, in the near-field, a similar behavior can be expected so that the patterns of Fig. 6-12 may be considerably broader below about -20 dB, than shown. In addition, the in situ patterns may exhibit considerable asymmetry.

Can this near-field perturbed behavior, including edge diffracted rays, contribute to an increased antenna brightness temperature resulting from the 290 K absorbing wall? The answer is yes, and that it can be explained in terms of a broadened near-zone pattern behavior. The antenna brightness temperature is given by

$$T_A = \frac{1}{4\pi} \iint_{4\pi} T_B(\theta, \phi) G(\theta, \phi) d\Omega \quad (6-3)$$

where T_B is the source brightness temperature distribution (consisting of both the sky temperature and absorber temperature), G is the antenna gain pattern, and $d\Omega = \sin \theta d\theta d\phi$ in a spherical coordinate system. This formula does not explicitly consider the distance from the antenna to the radiating surface. Normally, in the far-field, $G(\theta, \phi)$ is independent of distance R from the antenna. However, in the near-field, the gain is a strong function of distance, i.e.

$$G = G[\theta, \phi, R(\theta, \phi)] \quad (6-4)$$

as shown in Figs. 6-11 and 6-12. A rough approximation to the K_u -Band Brightness distribution (in the bucket) is shown in Fig. 6-15. Also shown are the far-field and estimated near-field patterns of the K_u -Band horns, when the horn axis is at a pitch angle of 100° and a roll of 0° . In this situation, the phase center of the horn is approximately 71 cm from the nearest approach of the absorber. Edge diffraction from the horn and interaction with the adjacent K_a and K-Band horns and the L-Band array may appreciably broaden and distort the near-field patterns from those shown in Fig. 6-12, leading to the dashed pattern (estimated) shown in Fig. 6-15 (top).

Denoting the pitch angle of the horn axis as θ_0 , eqn. (1) may be rewritten more explicitly as

$$T_A(\theta_0) = \frac{1}{4\pi} \iint_{4\pi} T_B(\theta', \phi') G(\theta_0 - \theta', \phi_0 - \phi) \sin \theta' d\theta' d\phi' \quad (6-5)$$

where the roll position is ϕ_0 ($\phi_0 = 0^\circ, 90^\circ$) and (θ', ϕ') are the (pitch, roll) angles measured from the main beam position. This is recognized as the familiar convolution integral, and leads to an antenna temperature profile of the form shown in Fig. 6-15 (bottom). No scale units are placed on the ordinate since the function $G(\theta_0 - \theta', \phi_0 - \phi)$ is not known exactly enough to carry out the integration in (6-5). However, the gradual rise of the antenna temperature from 90° to 180° is due to the increasing contribution from the relatively hot absorber as θ_0 is increased.

If the shape of the absorbing surface or its distance to the horn $R(\theta_0, \phi_0)$ is changed by only a few cm, the near-field pattern of the horn can change appreciably so that the slope

$\frac{dT_A}{d\theta_0}$ in the near-zenith region (Fig. 6-15) may likewise change.

Thus it is of considerable importance that the mockup aircraft bulkhead be as faithful a replica of the actual aircraft bulkhead

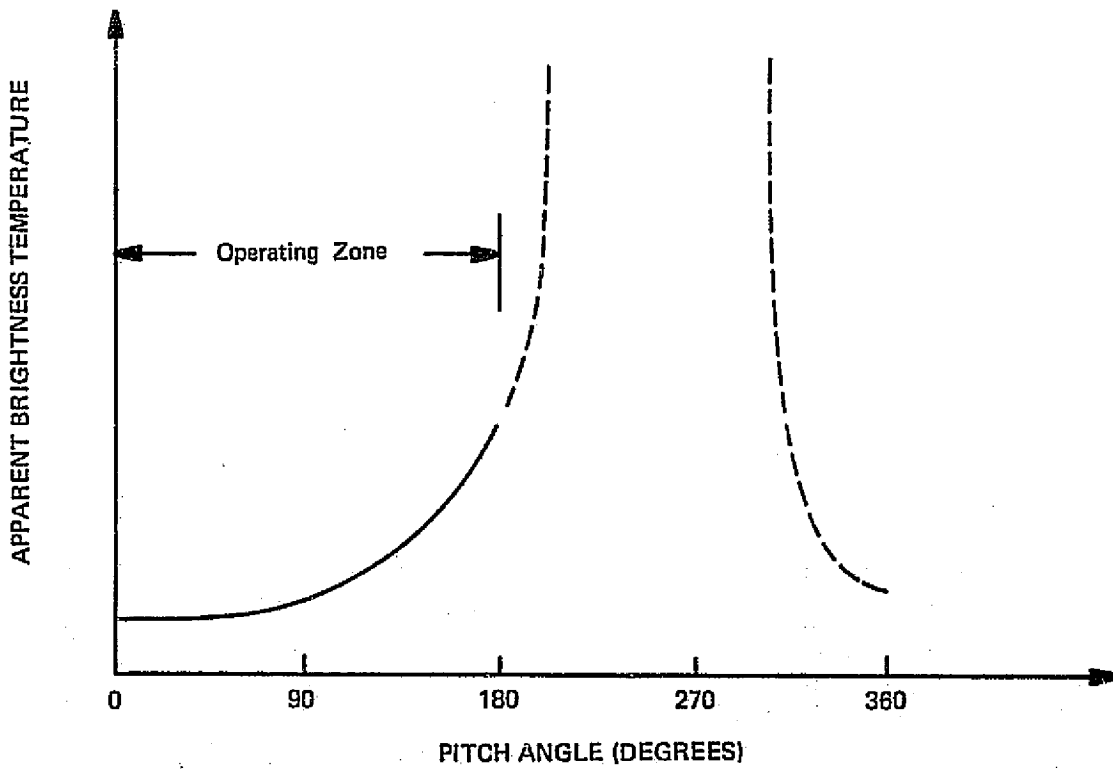
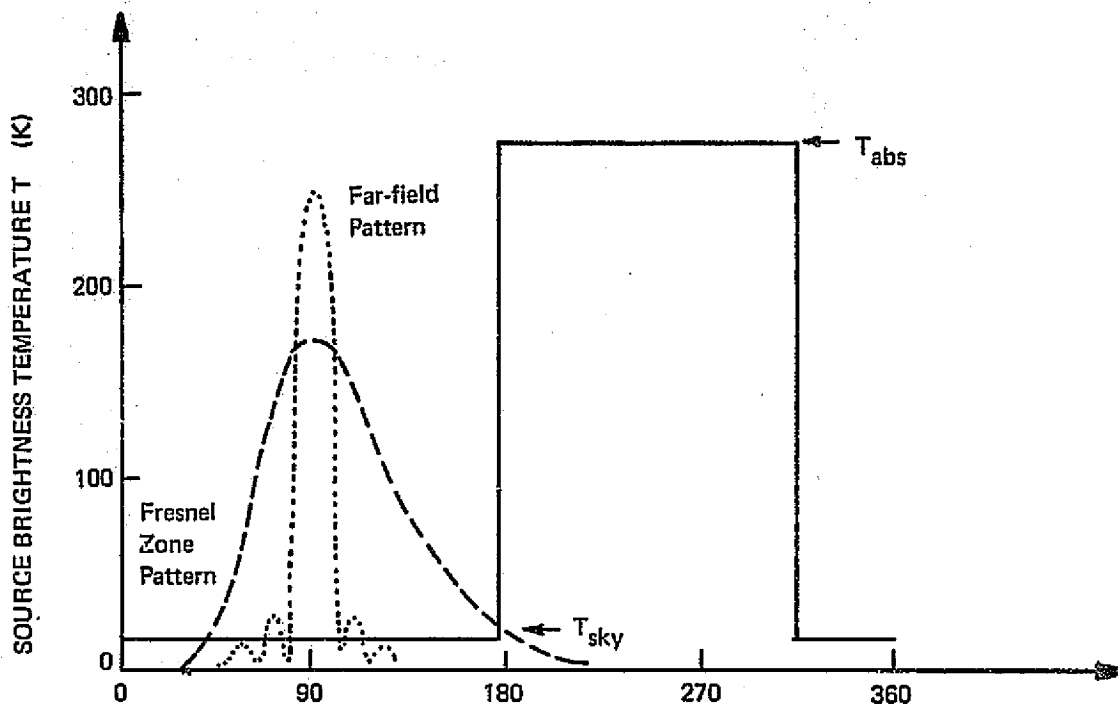


Fig. 6-15. Source and apparent brightness temperature versus pitch angle.

as possible, especially when the "calibrated" antenna is to be used for near-zenith observation.

When the absorber is removed, however, this critical relationship no longer exists and the antenna loss becomes nearly independent of pitch angle, as shown in Fig. 6-16 for Channel 1 at K_u -Band. Similar behavior was observed at K_a -Band; no data without absorber was available at K-Band since the receiver failed during that measurement sequence.

6.5.5 Conclusions

When the absorber is used on the aircraft bulkhead, the MFMR K_u , K and K-Band loss values (both antenna and radome) measured at A-Mountain in February, 1975 are of questionable validity since the mockup and absorber used differ from the operational configuration. The complex nature of the interaction between the horn antennas, the sky temperature and the absorber temperature make it almost insuperably difficult to calculate the slope of the antenna loss $\frac{dL_A}{d\theta_0}$ and therefore the values of radome loss. Future measurements should be taken with a much better bulkhead replica and should use the same absorber type and shape used in flight.

6.6 MFMR Antenna and Radome Loss Values (L-Band)

Table 6-1 lists the antenna loss values for the AIL L-Band antenna and shows that the loss (-1.34 dB) is essentially independent of pitch or roll so long as there is no radome present or L-Band absorber on the bulkhead.

The fact that the X-Band absorber has no effect at L-Band is illustrated in Fig. 6-17 for L_A measured values, both with and without absorber.

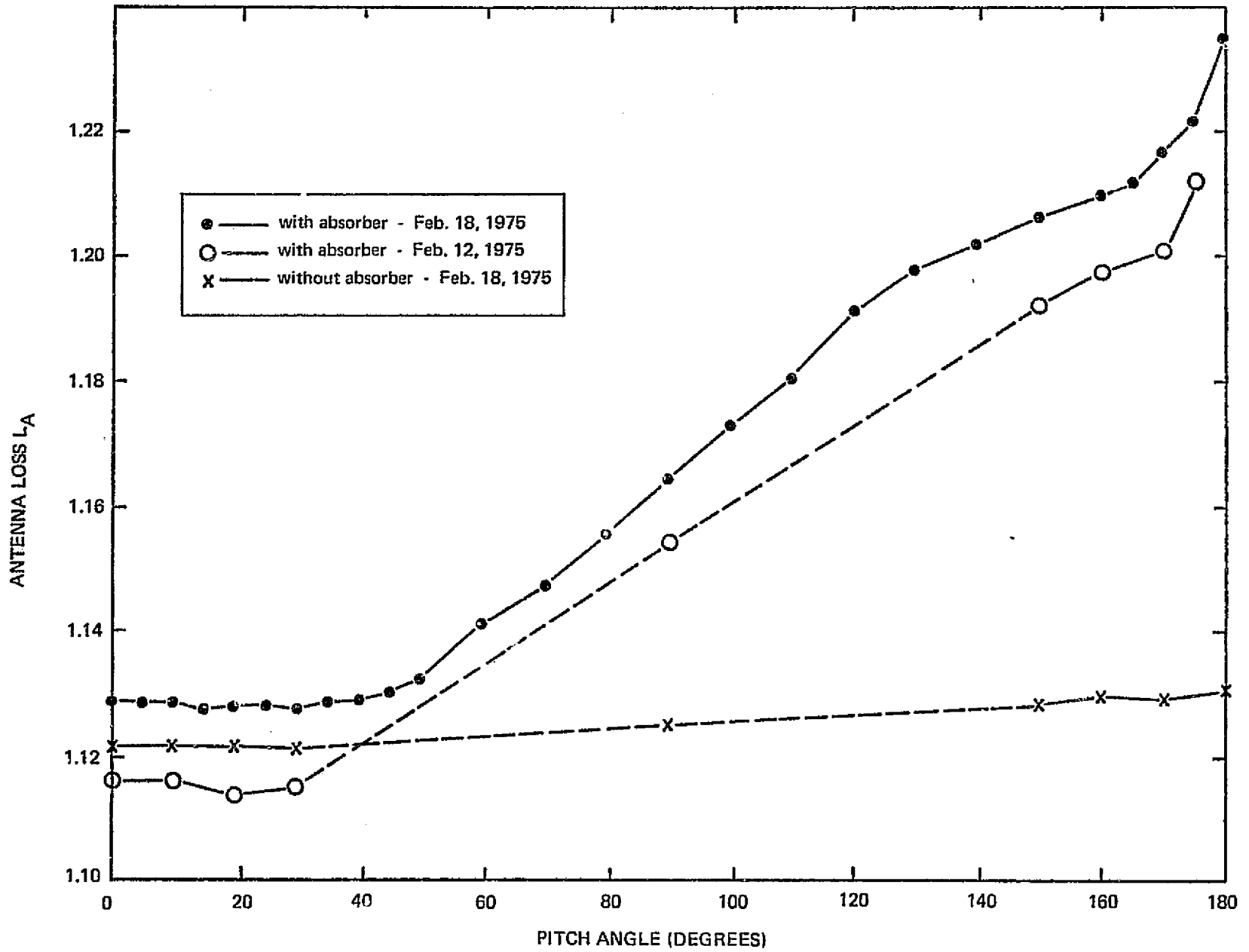


Fig. 6-16. MFMR antenna loss versus pitch angle -- K_u -Band channel 1.

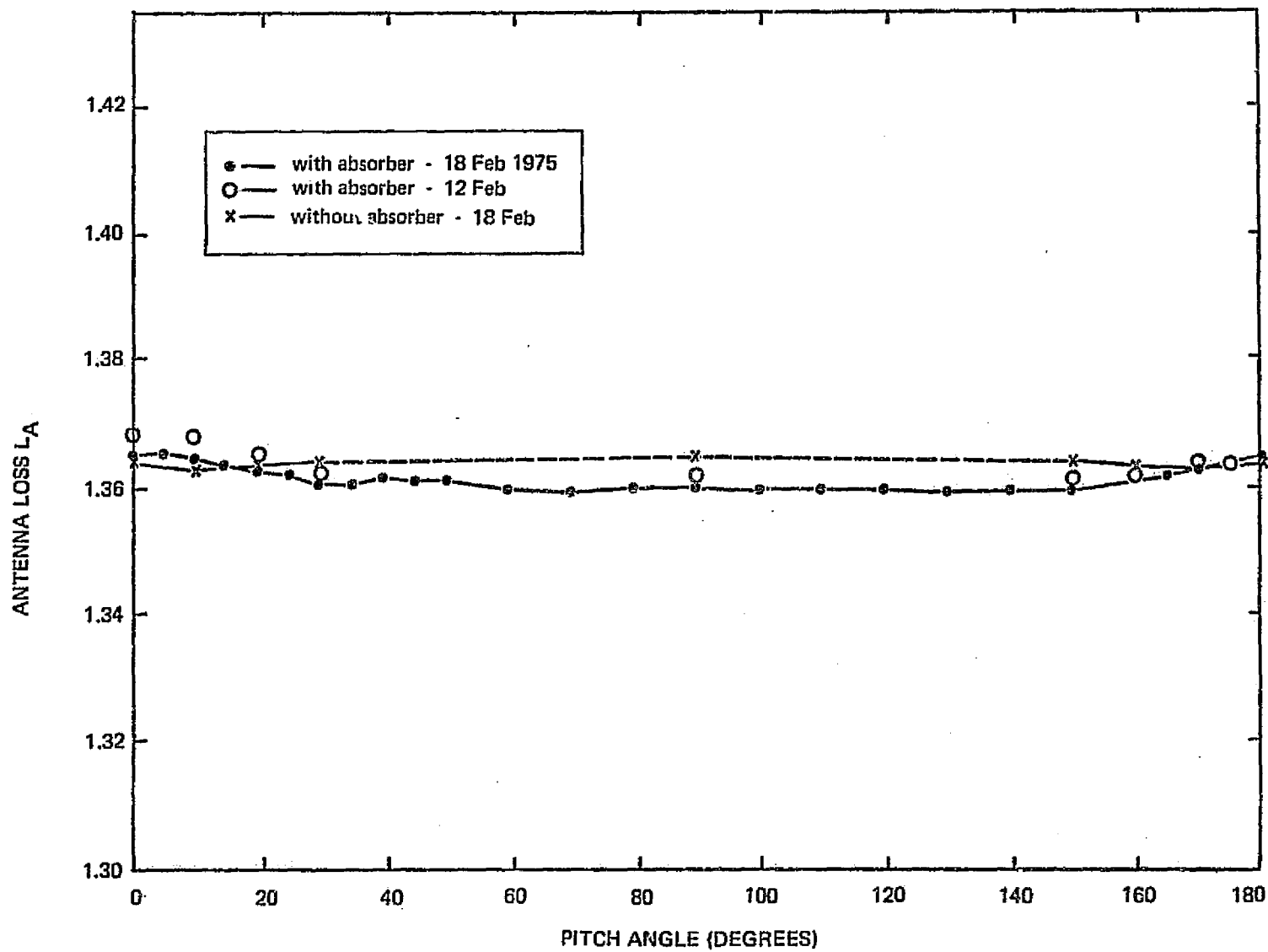


Fig. 6-17. MFMRL antenna loss (roll=0°) versus pitch angle -- L-Band.

It was found that this non-absorbing bulkhead produced a strong interaction between the L-Band antenna and the radome because of multiple internal reflections off the bulkhead. This effect is clearly evident in Fig. 6-18 where the uncorrected brightness temperature is plotted vs. pitch angle, both for radome (#2) on and off. When T'_B (radome on) exceeds T'_B (radome off), the radome loss is greater than unity, but otherwise ($0^\circ \leq \theta_o < 5^\circ$; $90^\circ \leq \theta_o < 165^\circ$) the radome loss would appear to be less than unity, an absurd result. Moreover, it is clear that the radome loss at L-Band should be essentially independent of pitch angle θ_o . The same effect is observed for the Aerojet L-Band array, as shown in Fig. 6-19, although the radome on temperature is consistently higher than the radome off temperature. This unstable behavior is again caused by internal scatter by the radome and is further evidenced in Fig. 6-20 where the VSWR of the Aerojet L-Band array is compared for both radome on and radome off. The peak mismatch at $\theta_o = 5^\circ$ agrees with the peak in T'_B at $\theta_o = 5^\circ$ in Fig. 6-19.

A partial correction of T'_B due to the mismatch loss can be made even though it is not sufficient to describe the more general effect of redistributed antenna currents on the array. Thus, the radome loss would be estimated by

$$L_R = \frac{T_{\text{on}}}{T_{\text{off}}} \left[\frac{1 - |\Gamma_{\text{on}}|^2}{1 - |\Gamma_{\text{off}}|^2} \right] \quad (6-6)$$

where T_{on} and T_{off} refer to the curves of Fig. 6-19 and the bracketed quantity is the mismatch loss correction. $|\Gamma|$ is the magnitude of the voltage reflection coefficient and is related to the VSWR curves of Fig. 6-20 by

$$|\Gamma| = \frac{\text{VSWR} - 1}{\text{VSWR} + 1} \quad (6-7)$$

After L_R is computed for all pitch angles θ_o and averaged, a value

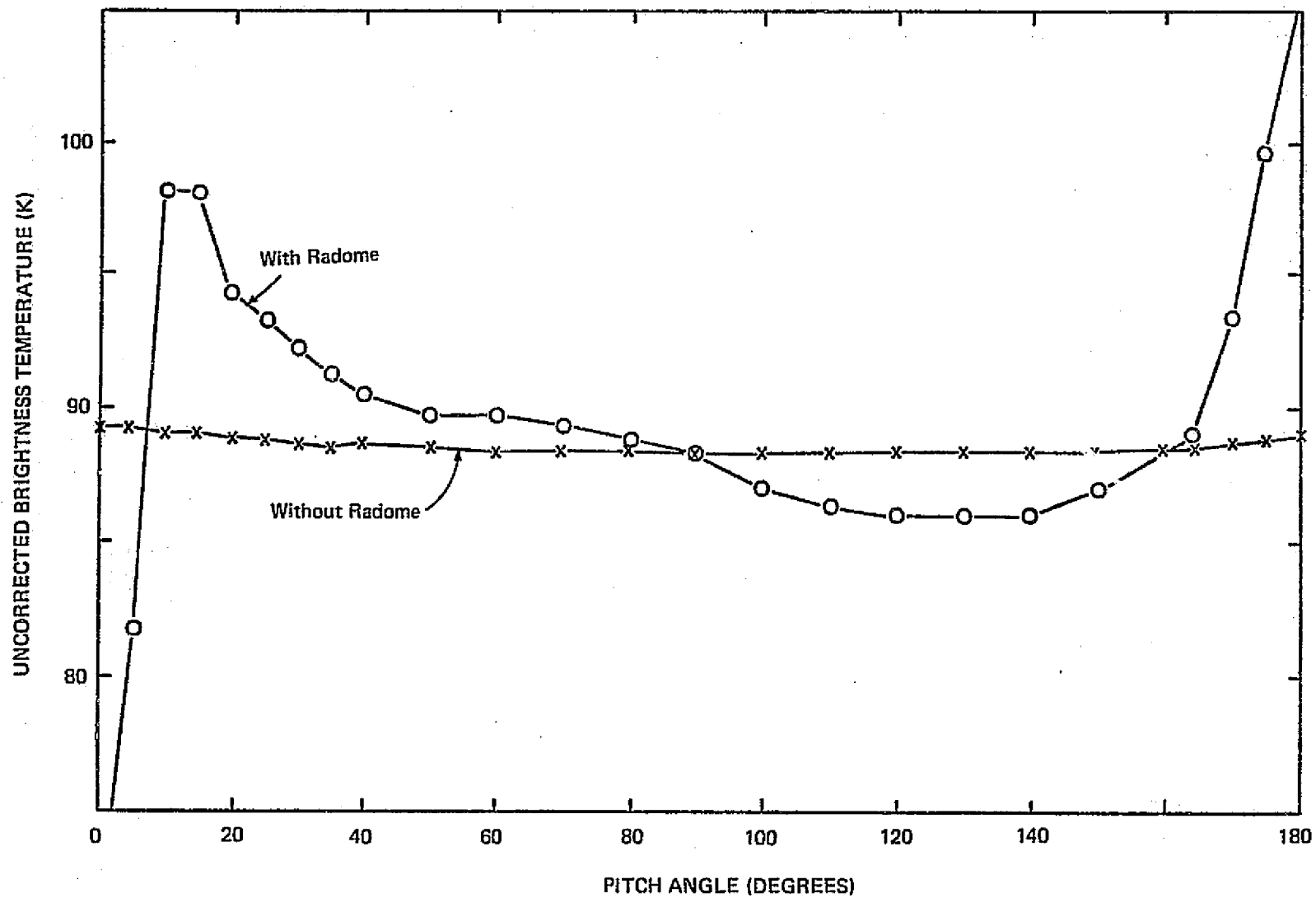


Fig. 6-18. MFMR AIL array, uncorrected brightness temperature versus pitch angle -- L-Band.

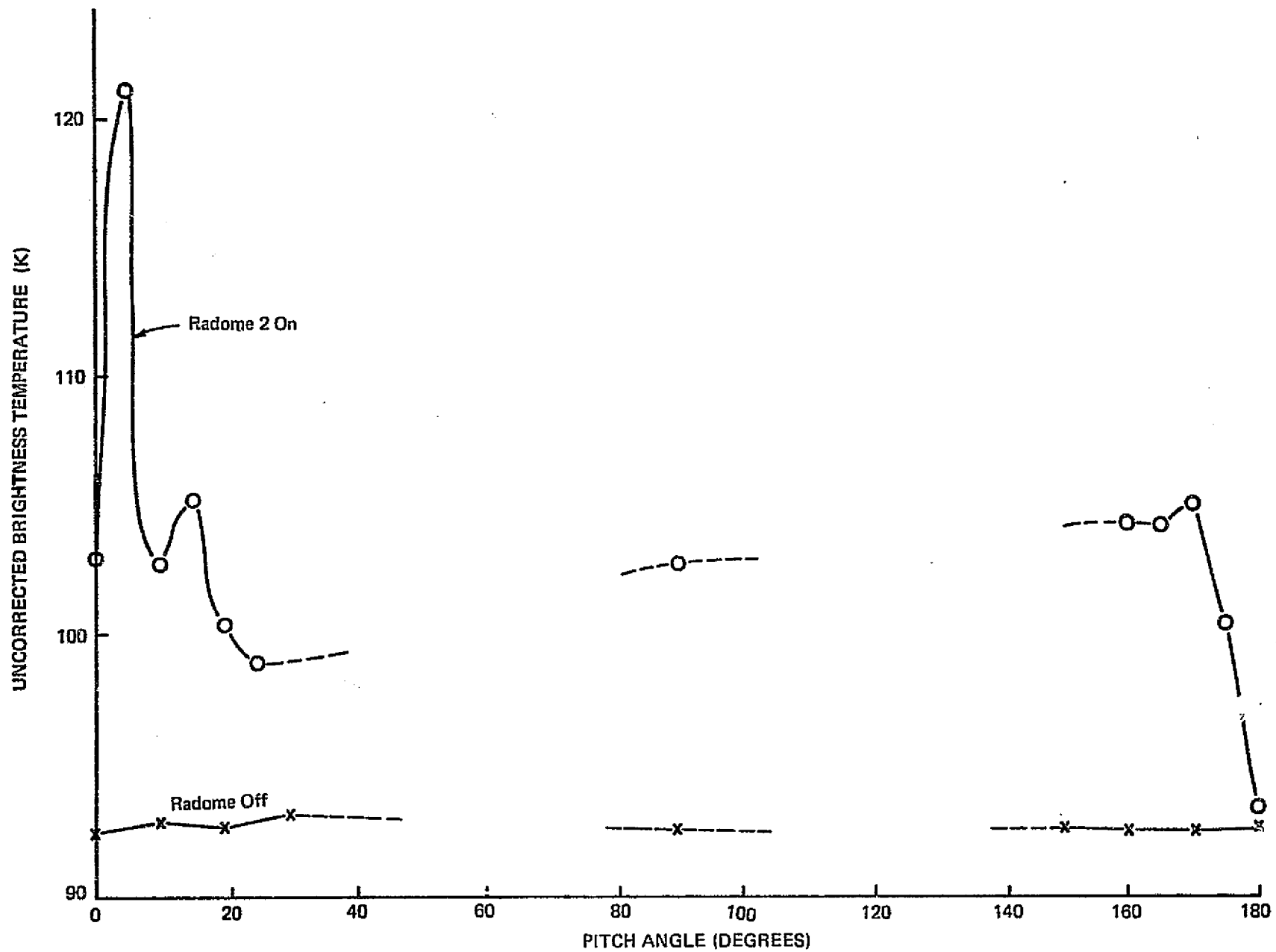


Fig. 6-19. MFMR Aerojet antenna temperature versus pitch angle -- L-Band.

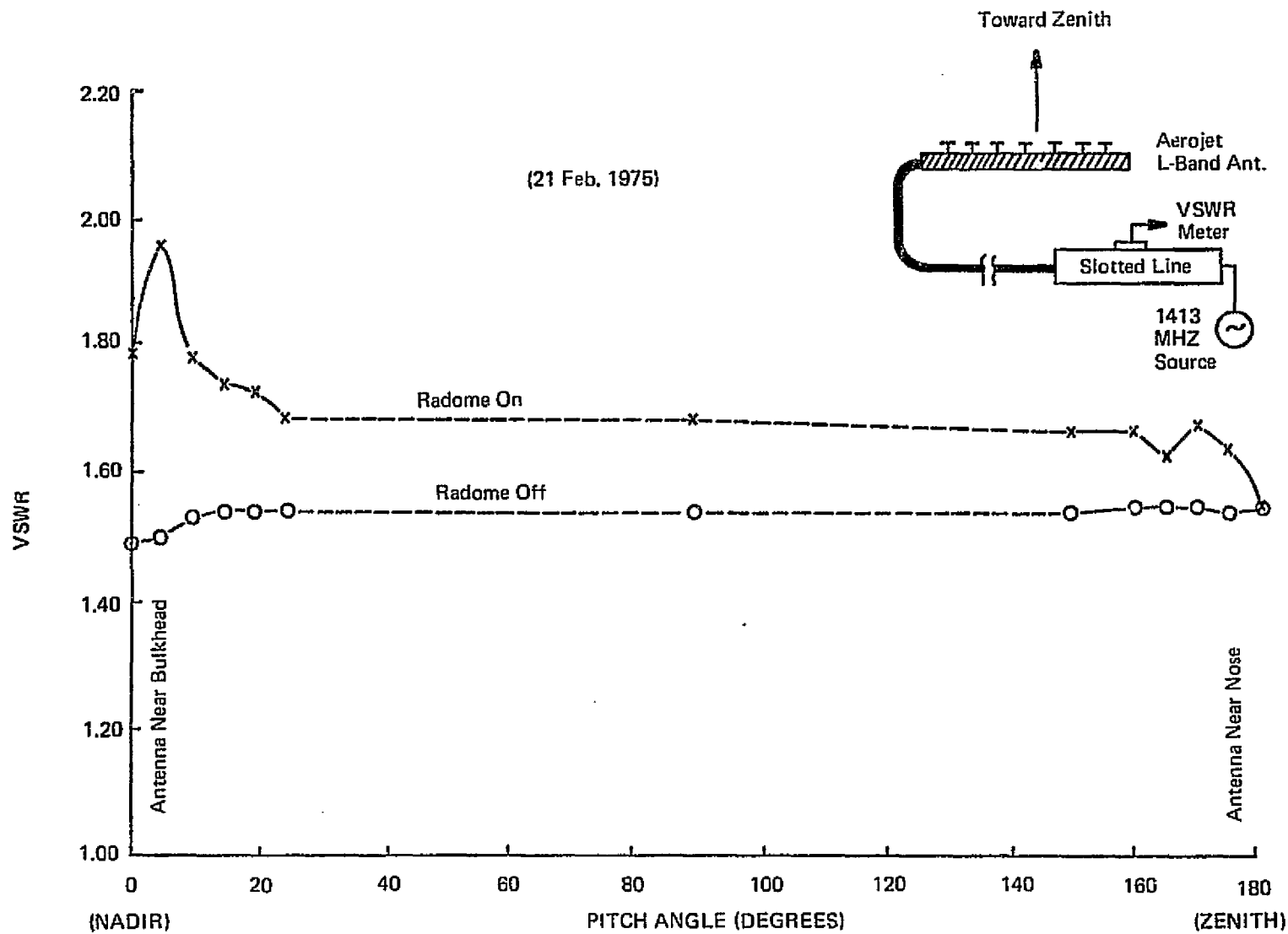


Fig. 6-20. Voltage Standing Wave Ratio versus pitch angle -- antenna in bucket.

$$L_R = 1.09 \text{ (0.38 dB)} \quad (6-8)$$

is obtained. It is suggested that this figure be used until new loss measurements (with a good L-Band absorber) become available.

Since L-Band Eccosorb is being used in flight and must certainly contribute to the apparent source temperature, it is clear that this loss component was excluded from these measurements and that the L_A values in Table 6-1 for L-Band are too low. Furthermore, L_A (with absorber in place) would become even higher as $\theta_0 \rightarrow 0^\circ$ and the near-zone antenna pattern begins to intercept the absorber.

6.7 MFMR Error Budget

The general theory follows that used for PMIS, as discussed in Sec. 5.5.1.

1. Random Error

It can be shown that the standard deviations of the antenna and radome losses are given by

$$\sigma_{L_A} = \frac{(T_A - T_S)L_W}{[T_A + T_W(L_W - 1) - L_W T_B']^2} \sigma_{T_B} \quad (6-9)$$

and

$$\sigma_{L_R} = \frac{(T_R - T_S)L_A}{[T_R + T_A(L_A - 1) + T_W L_A(L_W - 1) - L_A L_W T_B']^2} \sigma_{T_B} \quad (6-10)$$

Under typical circumstances at K_u , K, and K-Bands, $T_S = 13$ K, $T_A = 288$ K, $T_R = 290$ K, $T_B' = 42$ K, $\sigma_{T_B} = 0.25$ K, $L_W = 1.05$, $L_A = 1.065$ and $L_R = 1.30$. Using these values in (6-9) and (6-10),

$$\sigma_{L_A} \approx \sigma_{L_R} \approx 0.001 \quad (6-11)$$

2. Systematic Error

Systematic errors in the antenna loss arise primarily from inaccuracies in (1) the apparent sky temperature, ΔT_S and (2) the receiver calibration, $\Delta T_B'$. Systematic errors in the radome loss arise from not only ΔT_S and $\Delta T_B'$ but in addition, any systematic error ΔL_A in the antenna loss. The worst case systematic errors may be calculated from

$$\Delta L_A = \frac{L_A}{T_A - T_S} \Delta T_S + \frac{L_A L_W}{D_A} \Delta T_B' \quad (6-12)$$

and

$$\Delta L_R = \frac{1}{D_R} \left\{ \Delta T_S + L_R L_A L_W \Delta T_B' + L_R D_A \Delta L_A \right\} \quad (6-13)$$

where

$$D_A = T_A + T_W(L_W - 1) - L_W T_B' \quad (6-14)$$

$$D_R = T_R + T_A(L_A - 1) + T_W L_A(L_W - 1) - L_A L_W T_B' \quad (6-15)$$

Using the assumed constants in 6.7.1-1,

$$\Delta L_A = 0.004 \Delta T_S + 0.004 \Delta T_B' \quad (6-16)$$

and

$$\Delta L_R = 0.004 \Delta T_S + 0.005 \Delta T_B' + \Delta L_A \quad (6-17)$$

The accuracy of the receiver calibration, ΔT_B^i , is related to the calibration of the reference hot and cold loads and again it is assumed that

$$\Delta T_B^i = \pm 1 \text{ K} \quad (6-18)$$

The accuracy of the apparent sky temperature, ΔT_S , depends not only on the adequacy of the Paris model for estimating the sky noise component, but also it depends very critically on the fidelity of the aircraft bulkhead mockup and its absorber geometry. Table 4-2 lists the systematic error in the sky noise component. However, there is apparently no way of estimating the systematic error due to the poor replication of the aircraft bulkhead environment in the mockup furnished. This becomes particularly critical at the pitch angles ($0^\circ - 20^\circ$, $160^\circ - 180^\circ$) where good loss data is most needed. It is easily conceivable that a total systematic error $\Delta T_S = \pm 10 \text{ K}$ could be encountered in such a circumstance, thus yielding

$$\Delta L_A = \pm 0.04 \quad (6-19)$$

$$\Delta L_R = \pm 0.09 \quad (6-20)$$

as a possible systematic error.

This situation clearly leads to unacceptably high accuracy errors in the brightness temperature and can be improved only after a better replica of the aircraft bulkhead has been furnished.

CHAPTER VII

BUCKET PERFORMANCE TESTS

7.0 INTRODUCTION

Several questions arise when evaluating the performance of the bucket and this chapter discusses the most obvious of these, e.g.

1. Does antenna location change within the bucket affect the observed brightness temperature?
2. How does one know that the effective emissivity of the bucket doesn't change over a period of many months or years?
3. Does electromagnetic interference (EMI) affect operation in the bucket?

7.1 Effect of Antenna Location Change

It can be quite naturally suspected that the bucket, being a partially closed metal box, might have resonances associated with it. Clearly, as shown in Fig. 2-6, if the bucket is too small there are observable effects on even the "lit zone" portion of the antenna pattern.

There is, however, clear evidence at L, K_u and K_a -Bands that location change within the bucket has a negligible effect. Figs. 7-1 and 7-2 compare the antenna loss vs. pitch angle at K_u -2 and K_a -1-Bands, with and without absorber on the bulkhead. Two conclusions are immediate: (1) the rise in L_A with increasing θ_o (with absorber) is due to an increased noise contribution from the absorber (see also Sec. 6.5) and (2) when there is no absorber

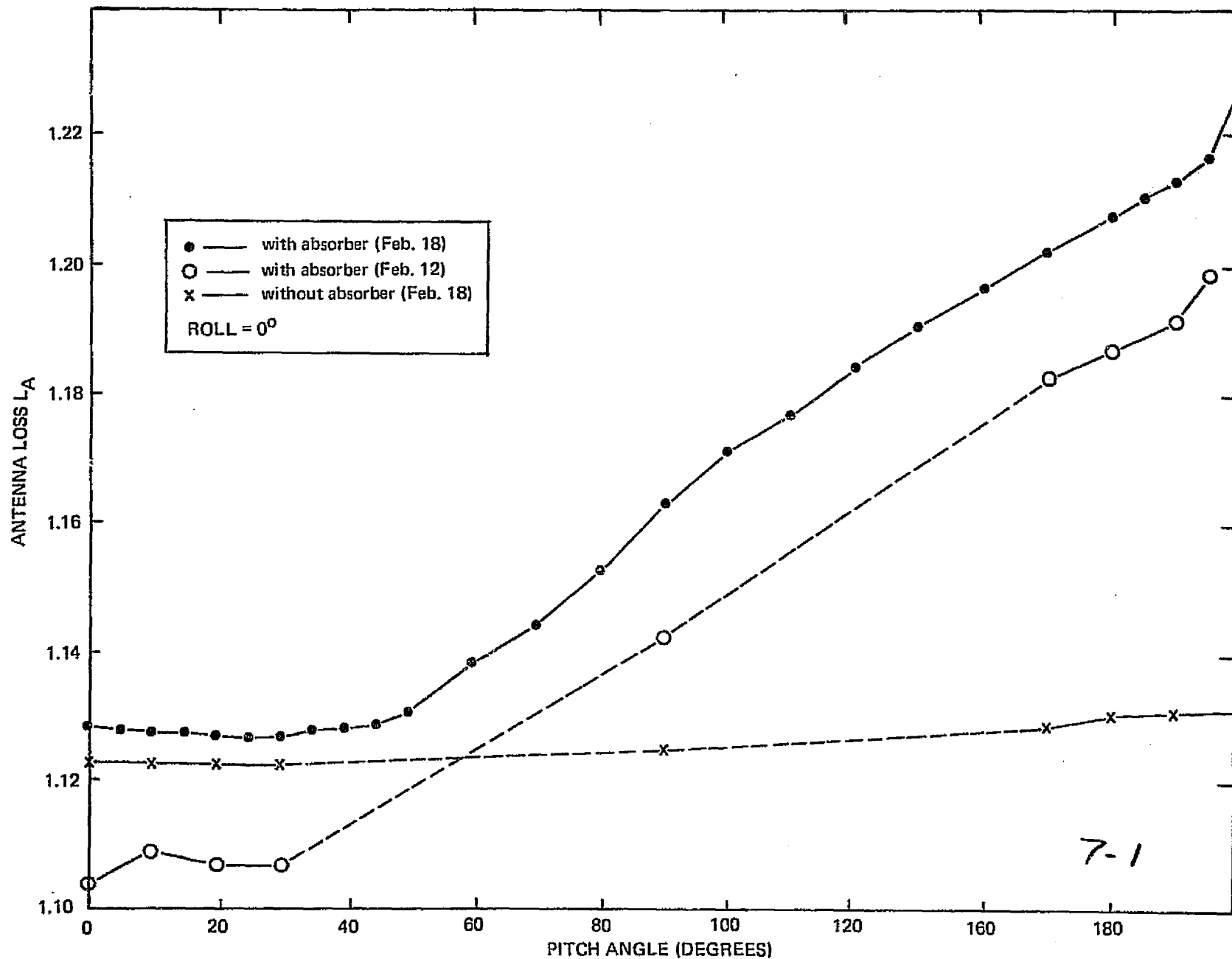


Fig. 7-1. MFMR antenna loss versus pitch angle -- K_u -Band Channel 2.

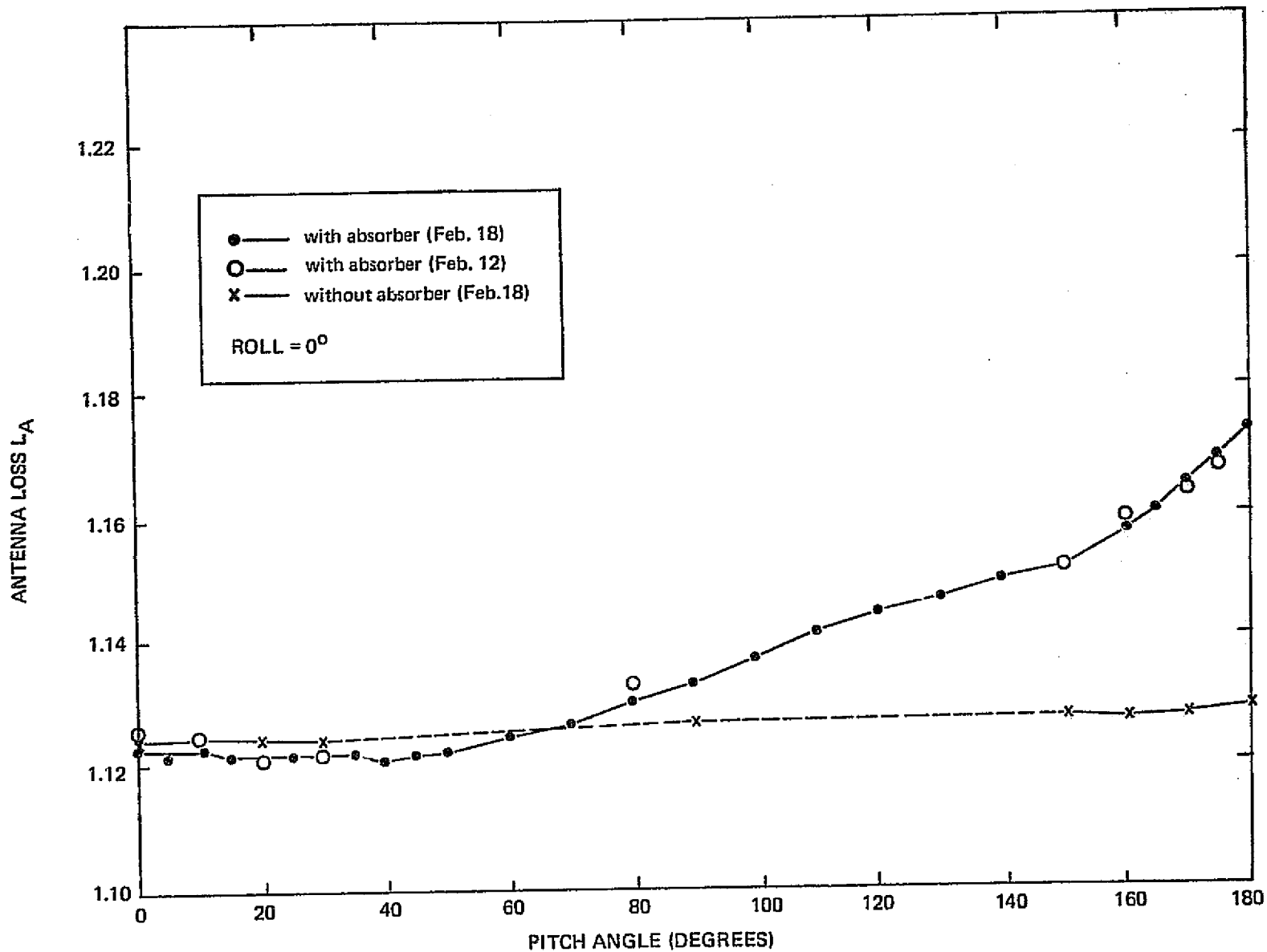


Fig. 7-2. MFMR antenna loss versus pitch angle --- K_a-Band.

on the bulkhead, the flat loss curve indicates that raising the horns from a mid-bucket position (at $\theta_0=0^\circ$ or 180° as in Fig. 2-7) to a position very high in the bucket has a negligible effect.

In early May, 1975 a similar experiment was conducted at L-Band using the S-194 radiometer receiver and a standard gain horn. The horn was connected to the receiver through about 6 m of flexible coaxial cable so that it could be easily positioned at various locations within the bucket. The tests were conducted in mid-afternoon so that the sun was radiometrically visible by pointing the horn toward the southwest corner of the bucket. Thus, some of the variation in T_B' was due to the sun intercepting various portions of the antenna pattern.

Even under these adverse conditions, however, a movement of the horn from near the bucket floor to near the top produced only a 1.7 K change. Pointing the horn directly toward the north wall of the bucket produced only a 3.9 K change.

It may be concluded that if the radiometer has a reasonably low sidelobe level (say, below -25 dB), there is virtually no dependence of the observed brightness temperature on antenna location within the bucket.

7.2 Long-Term Bucket Emissivity Changes

It has been pointed out in Sec. 2.4.2 that from a theoretical viewpoint even the most pessimistic of changes in the bucket emissivity or shape would not be observable by any modern radiometer.

Nonetheless, certain baseline performance checks have been made at X, K_u , and K_a -Bands to produce an eventual verification that the bucket characteristics are stable over a period of months or years. The idea behind the verification check is that

if a calibrated radiometer in the bucket views a known source temperature T_s , then any change in the apparent loss L_A would be due to a change in the emissivity or shape of the bucket.

7.2.1 X-Band Measurements

At X-Band, the sky temperature is typically 5 K and can be calculated (using radiosonde data) to an accuracy of ± 0.4 K. To ensure that the antenna characteristics would not change, an X-Band standard gain horn (Scientific-Atlanta Model 21-8.4) was used and was mounted on the centerline of the bucket with the horn mouth 3/96 m above the floor, as shown in Fig. 7-3. The E-plane was oriented east-west.

In order to bring the antenna brightness temperature within the normal operating range of the radiometer, an HP-Model X382 precision attenuator was inserted between the horn and the radiometer (the PMIS vertical channel was used). The attenuator was set at 1.0, 1.2, 1.4 and 1.6 dB (four 1-minute averages each) and the corresponding values of T'_B noted (74.15, 82.78, 89.67, and 97.87 K respectively). The sky temperature T_s was 4.9 K on the night of measurement (2-6-75), so that for the 1 dB setting,

$$L_A = \frac{T_A - T_s}{T_A - T'_B} = \frac{296 - 4.9}{296 - 74} = 1.312 \text{ (1.18 dB)} \quad (7-1)$$

which leaves 0.18 dB as the antenna loss of the X-Band horn. Continuing in this fashion, the graph of Fig. 7-4 is obtained, in which the uncorrected brightness temperature T'_B is plotted vs. the total loss in dB. The measured points give a slope of 4.0 K/0.1 dB and the calculated slope (obtained by adding 0.18 dB to the attenuator setting and using $T_{\text{sky}} = 4.9$ K) gives 4.8 K/0.1 dB. The difference in slope may be attributed to using the calibration constants T_1 , ΔT outside of their 100 K - 200 K intended range.

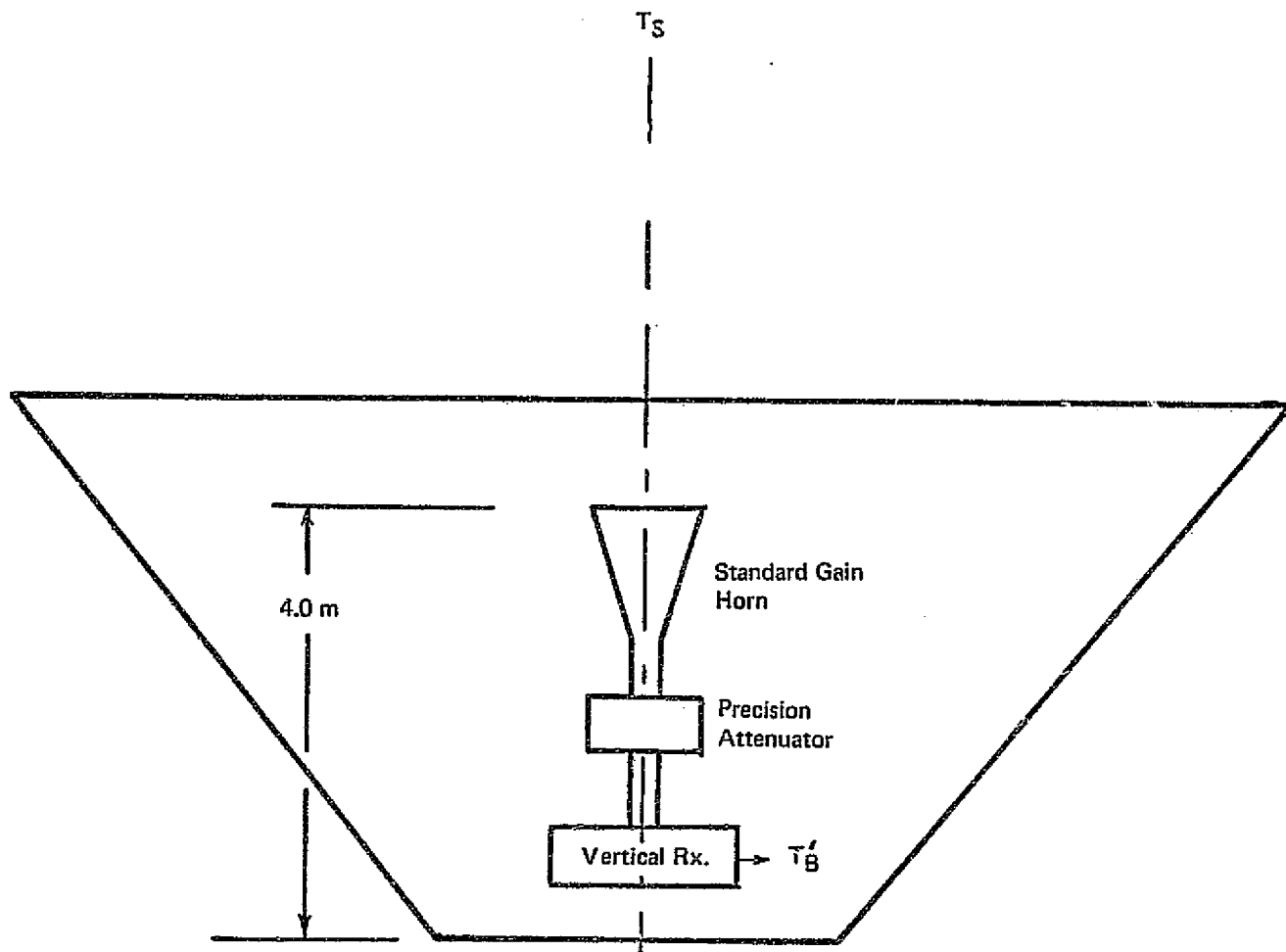


Fig. 7-3. Bucket calibration at X-Band.

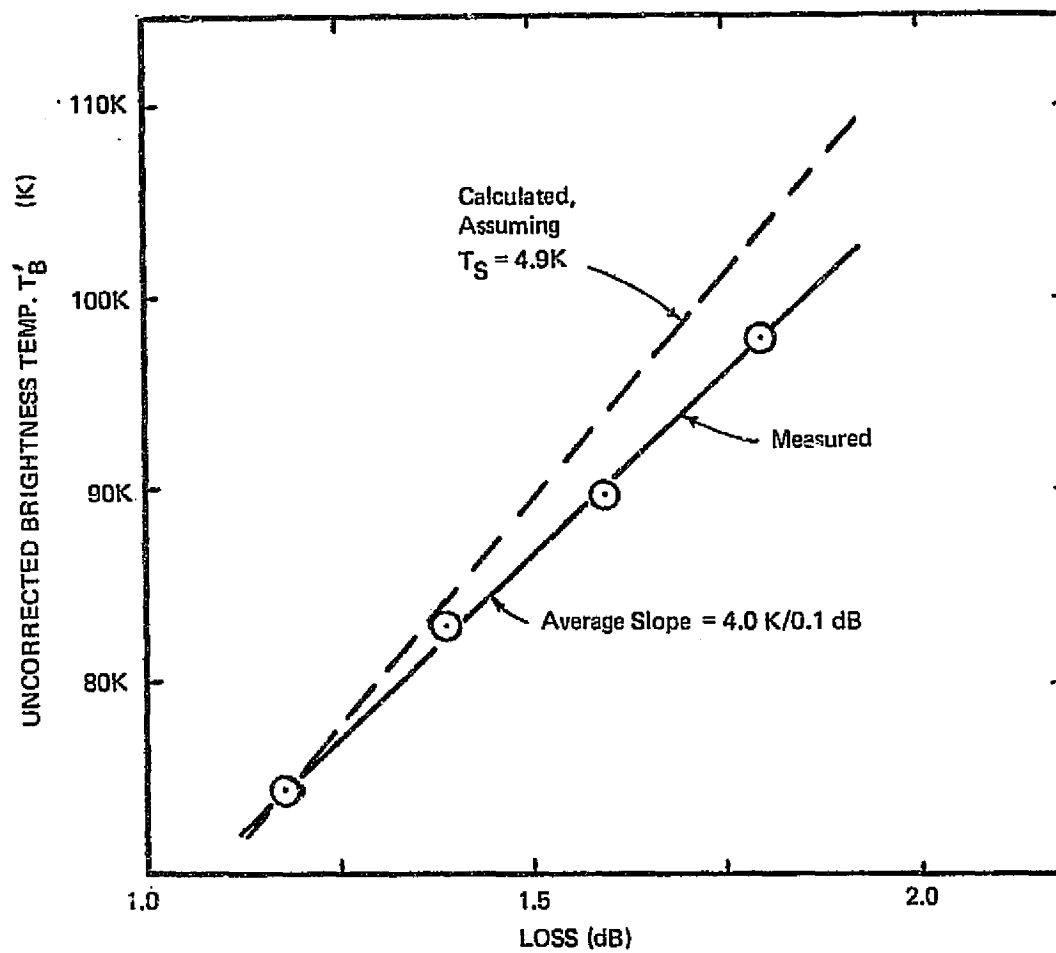


Fig. 7-4. Loss (L) of horn antenna plus attenuator.

If the emissivity of the bucket were to degrade, then $T_s = k T_{sky}$ where $k (>1)$ is the degradation factor. The uncorrected brightness temperature is then given (from 2-7) by

$$T'_B = T_A + \frac{kT_{sky} - T_A}{L_A} \quad (7-2)$$

where all quantities except k are now known. It is straightforward to show that a change of L_A (by attenuation setting) from 1.5 dB to 1.6 dB causes a change in $\Delta T'_B$ given by

$$\Delta T'_B = \frac{T_A - kT_{sky}}{L_A^2} (.033) \quad (7-3)$$

where L_A is the median value, $L_A = 1.429$. Therefore,

$$\Delta T'_B \quad (7-4)$$

For example, when $T_A = 296$ K (thermistor reading) and $T_{sky} = 4.9$ K, and assuming $k = 1$,

$$\Delta T'_B = 4.7 \text{ K}/0.1 \text{ dB} \quad (7-5)$$

If, due to bucket corrosion, deformations, etc. k were to double, then $\Delta T'_B = 4.6 \text{ K}/0.1 \text{ dB}$. Extending this to a 1.0 dB change in L_A , a 1 K difference in slope would be observed.

Clearly, a change in bucket emissivity is indistinguishable from a systematic error in T_{sky} . Therefore, it is imperative in constructing a history of the bucket performance that T_{sky} be accurately assessed from sounding data.

7.2.2 L, K_u, K_a-Band Measurements

Similar bucket performance tests were conducted at L, K_u and K_a-Bands except that a 183 cm diameter microwave absorbing disk was suspended 6 m above the MFMR antenna assembly as shown in Fig. 7-5. The purpose of the disk was to present a known hot brightness temperature which subtended most of the antenna beam solid angle [Kraus and Carver, 1974] and thereby reduce the systematic error in the apparent sky brightness temperature. The disk was held rigidly in place by a quadrupod arrangement of four aluminum spars and the absorber temperature was averaged from the readings of eight thermistors embedded at various locations across the disk.

Five one-minute averages were recorded for each of the five channels, with a pitch angle of 180° in all cases. The roll angle was set to 0°, then to 180° and then back to 0°, with the results as shown in Fig. 7-6. The sky temperatures (2-18-75) at L, K_u and K_a-Bands were 4.3 K, 6.3 K and 11.1 K respectively. The average disk temperature was 288.5 K. It is clear that the high T_B' values indicate that the main beam of each antenna was viewing primarily the disk and that errors in T_{sky} would be of negligible importance in determining the repeatability of the experiment.

However, the lack of repeatability of the T_B' in the two measurements for a roll of 0° indicates that the mechanical repositioning accuracy of the antennas was poor. The roll angle settings were carried out using hand positioning of the ring (by LEC/HASD personnel) and the lack of repeatability may have been due to personnel fatigue and consequent carelessness or it may have been an inherent problem in the MFMR positioning system. Until this problem is corrected, it is not reasonable to expect that these results can be repeated.

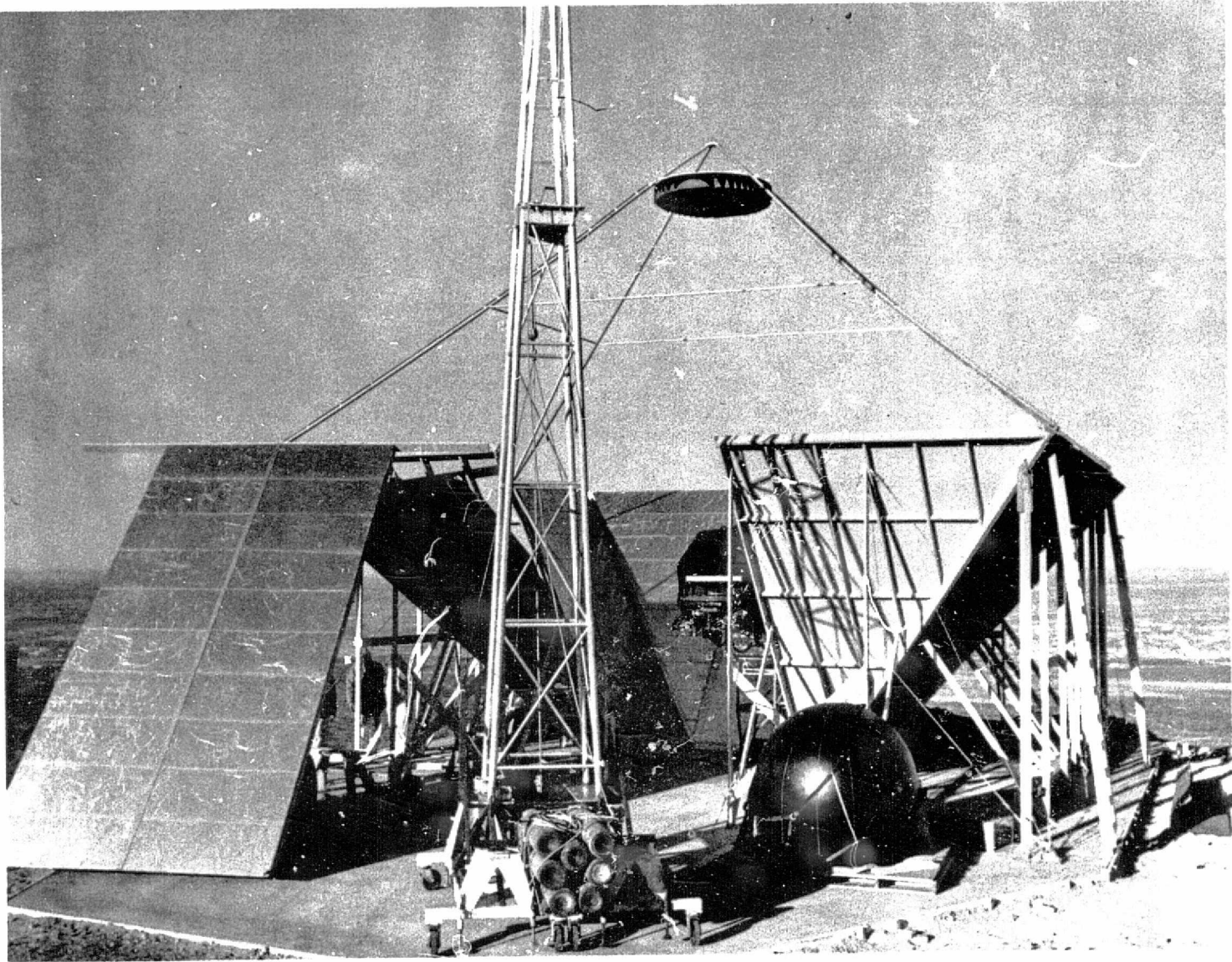
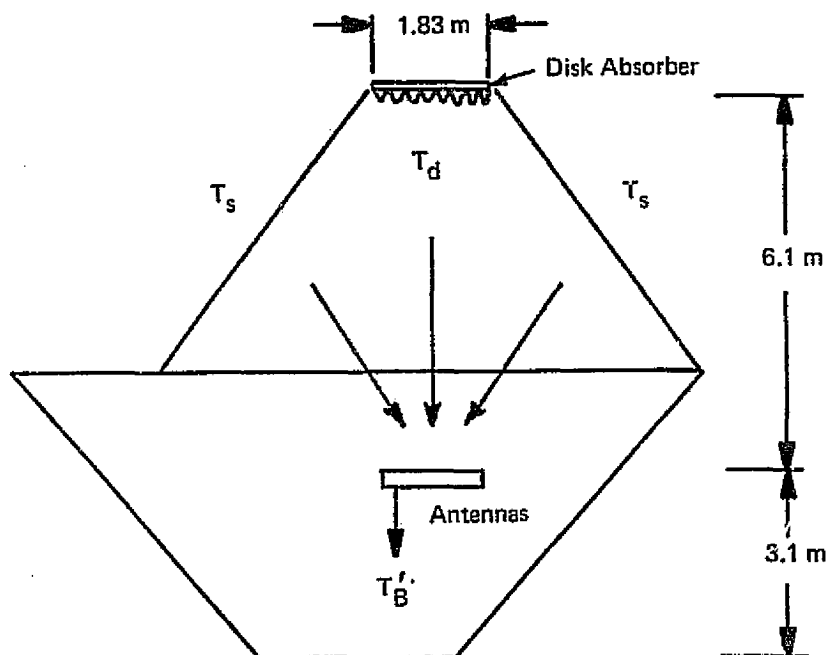


Fig. 7-5. Absorbing disk located above MFMR antenna assembly.

ORIGINAL PAGE IS
OF POOR QUALITY



UNCORRECTED BRIGHTNESS TEMP., T'_B			
FREQUENCY	PITCH = 180°, ROLL = 0°		PITCH = 180°, ROLL = 90°
	NO. 1	NO. 2	
K_u - CH. 1	174.9K	168.8K	221.9K
K_u - CH. 2	176.6K	170.2K	223.3K
K_a - CH. 1	191.1K	184.9K	197.9K
K_a - CH. 2	193.8K	187.2K	197.9K
L	188.1K	187.4K	181.9K

Fig. 7-6. L , K_u , K_a bucket verification tests.

7.3 EMI

Systematic spectrum surveillance tests were conducted throughout the VHF-UHF bands to identify and record interfering RF signals that could possibly be detected by the radiometer IF circuitry. These tests made use of the HP 8550 series spectrum analyzer with various Yagi and log periodic antennas. The antennas were placed in and near the bucket and were pointed in different directions.

The only interfering signal that seemed to be correlated with the radiometer output was a 150 MHz sporadically actuated carrier from a state police repeater tower located approximately 600 m northeast of the bucket. This signal level occasionally exceeded an input power level of -20 dBm when a moderately directive three-element Yagi was pointed directly toward the repeater tower.

No power line interference or ignition noise was observable at the radiometer output.

APPENDIX

PMIS & MFMR RADIOMETER PROGRAMS

INTRODUCTION

Two separate sets of program procedures are given here: one for the PMIS series of programs, and one for the MFMR series of programs. Although some repetition is entailed, the procedures for both series are written as separate modules, designed to be used independently of each other without cross-referencing.

To facilitate use of the procedures, a reference index is provided for each series of programs. The pagination style is a key to the series of programs (PMIS or MFMR), the program within the series (PMIS 1, PMIS 2, SKYTEMP program used with PMIS data, etc.). For example: P1.1 denotes page 1 of the PMIS 1 program procedures; PS.1 is page 1 of the SKYTEMP program as used in the PMIS series; and, P3.1 is page 1 of PMIS 3 program procedures. In like fashion, the prefix "M" indicates a page of the MFMR procedures writeup.

PMIS PROGRAMS - REFERENCE INDEX

Page No.'s

GENERAL

P.1 - P.5

- A. To load and execute System-7 PCM Program P.1
- B. Instructions of A., above, for newcomer to System-7 P.1a
- C. Telemetry Playback console - sketch and power settings. P.2
- D. Comments on System-7 Program. P.3
- E. Example: printout from control typewriter, PMIS data run. P.4
- F. Notes on control typewriter printout
 - 1. Explanation of terms. P.5
 - 2. "Overflow". P.4,5
 - 3. "Valid-Data-Flag Drop". P.4,5

PMIS 1 PROGRAM

P1.1 - P1.3

- A. Card setup for running PMIS 1 on computer P1.1
- B. Discussion of PMIS 1 card setup
 - 1. Phase 1 (PMIS 1). P1.2
 - 2. Phase 2 (PMIS 2). P1.2
 - 3. Phase 3 (Job-Step Disk-Dump). P1.2
- C. Optional Control Cards - PMIS 1 (1st phase)
 - 1. UPSI card P1.2
 - 2. Disk Address card (as used in PMIS 1) P1.3
- D. Optional Control Cards - PMIS 2 (2nd phase)
 - 1. // EXEC EMO3B card; T1 and ΔT card. P1.3

PMIS 2 PROGRAM

P2.1 - P2.7

- A. PMIS 2 Program as 2nd phase of a PMIS 1 job setup
 - 1. "PMIS 2 Card" output by PMIS 2, input to PMIS 3 P2.1
 - 2. Job-Step Disk-Dump. P2.2
- B. PMIS 2 Program as single-phase, separate job
 - 1. PMIS 2: separate job or 2nd phase treatment. P2.3
 - 2. Control cards: when optional, when mandatory P2.3
- C. Card setup for running PMIS 2 (separate job) on computer. P2.4
- D. Control cards
 - 1. T1 and ΔT card. P2.5
 - 2. Disk Address card (as used in PMIS 2) P2.5
- E. Notes on conversion to engineering units in PMIS 2 Program
 - 1. Housekeeping data P2.6
 - 2. Uncorrected sky brightness temperature, T'_B P2.6
 - 3. Standard deviation of uncorrected sky brightness temperature, σ_T P2.6,7

PMIS PROGRAMS - REFERENCE INDEX, cont'd

Page No.'s

SKYTEMP PROGRAM

PS.1 - PS.3

- A. Input data cards for SKYTEMP program
 - 1. Header card, description and format PS.1
 - 2. Pressure, temperature, dew point (PTD) cards - format . . PS.1
- B. Card setup for running SKYTEMP on computer. PS.2
- C. "SKYTEMP Card" output by SKYTEMP, input to PMIS 3 PS.3

PMIS 3 PROGRAM

P3.1 - P3.7

- A. Antenna loss factor, radome loss factor; computational equations P3.1
- B. Standard deviations: antenna loss, radome loss. P3.2
- C. Card setup for running PMIS 3 "Radome Is Off" on computer . . P3.3
- D. Discussion: card setup for "Radome Is Off" job deck
 - 1. Stacking data decks P3.4
- E. Control cards for "Radome Is Off" job deck
 - 1. "Radome Is Off" card. P3.4
 - 2. "PMIS 2 Card" P3.4
 - 3. "SKYTEMP Cards" P3.5
- F. Card setup for running PMIS 3 "Radome Is On" job on computer. P3.6
- G. Discussion: card setup for "Radome Is On" job deck
 - 1. Stacking data decks P3.7
- H. Control cards: "Radome Is On" card P3.7

PROGRAM PROCEDURE TO REDUCE PMIS DATA TAPES

PRIOR TO LOADING THE SYSTEM-7 PCM PROGRAM:

PERFORM CHECKOUT OF ALL PCM HARDWARE AND TAPE(S).

TO LOAD AND EXECUTE THE SYSTEM-7 PROGRAM, PROCEED AS FOLLOWS:

- (1) RUN U-ZERO TAPE (LOAD UNIT ADDRESS = X'0000')
- (2) LOAD IPL PROGRAM FROM DISK (LOAD UNIT ADDRESS = X'0002')

*** IPOO A ENTER CONTROL STATEMENT

- (3) CYCLE HOST ATTACH SWITCH TO (ENABLE AND IPL) AND
THEN TO (ENABLE);

IT MUST REMAIN ON (ENABLE) FOR REMAINDER OF PROGRAM EXECUTION.

- (4) SET DISK PROGRAM "DATA SET NAME" BY FOLLOWING R(REFER) STATEMENT:

R JOBLIB,F2,,PCMUSER

- (5) L(OAD) PCM PROGRAM INTO CORE BY FOLLOWING L(OAD) STATEMENT:

L PCM01B

THE SYSTEM-7 IS NOW PREPARED TO ACCEPT LINKUP WITH THE SYSTEM-370 AND WILL REMAIN IN A WAIT STATE UNTIL PMIS1 PROGRAM IS EXECUTED BY THE SYSTEM-370.

PROGRAM PROCEDURE TO REDUCE PMIS DATA TAPES

Notes: "PMIS" is the name of the program and of the radiometer being tested; procedures are given in large type, while explanatory comments are given in smaller type enclosed by hand-drawn brackets, thus: [for benefit of one who is unfamiliar with the System-7].

PRIOR TO LOADING THE SYSTEM-7 PCM PROGRAM:

PERFORM CHECKOUT OF ALL PCM HARDWARE AND TAPE(S).

TO LOAD AND EXECUTE THE SYSTEM-7 PROGRAM, PROCEED AS FOLLOWS:

(1) RUN U-ZERO TAPE (LOAD UNIT ADDRESS = X'0000')

[U-ZERO, the tape to IPL the computer, is a small, blue punch tape kept right by the computer; put Address switches on 0000 (Addresses are control switches on front of computer; there are 4 Address switches, thus each Address switch is set on 0, as indicated by the four zeros in step (1), above.)]

(2) LOAD IPL PROGRAM FROM DISK (LOAD UNIT ADDRESS = X'0002')

[IPL denotes "Initial Program Load". Leave the first 3 Address switches on zero, move the right hand Address switch to setting of 2.]

*** IPOO A ENTER CONTROL STATEMENT

[The above is a statement that the computer sends back to you after you have done step (2).]

(3) CYCLE HOST ATTACH SWITCH TO (ENABLE AND IPL) AND THEN TO (ENABLE) WHERE IT MUST REMAIN FOR THE REMAINDER OF PROGRAM EXECUTION.

[The Host attach switch is another control switch on the front of the computer; switch it to "Off" (that's down), then up to "Enable and IPL" and back to center position, which is "Enable"; it must stay on "Enable" all the time you're transferring data from Sys.-7 to Sys.-370 - this is done in order to establish a linkage with the System-370.]

(4) SET DISK PROGRAM "DATA SET NAME" BY FOLLOWING R(REFER) STATEMENT:

[step (4) tells you to type an "R", that is, "Reference Statement", on the control typewriter. The statement to be typed, is as follows, below (be sure to leave a space between the "R" and the "J"):]

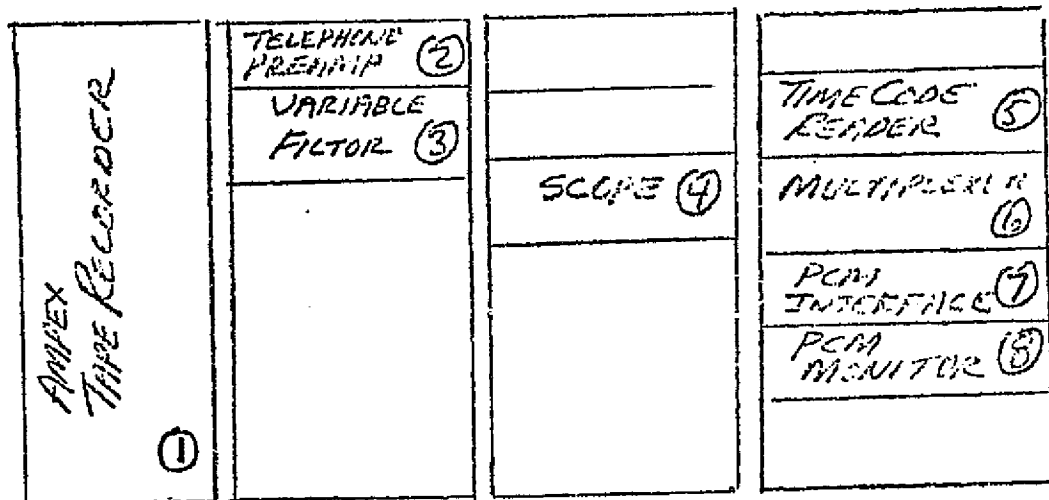
R JOBLIB,F2,,PCMUSER

(5) L(OAD) PCM PROGRAM INTO CORE BY FOLLOWING L(OAD) STATEMENT:

[after typing the statement of step (4)'s instruction, execute step (5) by typing the following statement, below. Leave a space between "L" and "P".]

L PCM01B

THE SYSTEM-7 IS NOW PREPARED TO ACCEPT LINKUP WITH THE SYSTEM-370 AND WILL REMAIN IN A WAIT STATE UNTIL PMIS PROGRAM IS EXECUTED BY THE SYSTEM-370.



Telemetry Playback Console

BIT SYNCHRONIZER ⑨

ORIGINAL PAGE IS
OF POOR QUALITY

① LOAD & RUN

② TURN ON

③ TURN ON [SETTING @ H PASS 250
L PASS 2300]

④ TURN ON [TIMING LEVEL MONITOR
SET 3.5 U/P MAX
3.0 U/P NORM
2.5 U/P MIN]

⑤ TURN ON. [SET RQD TIMES
SYNC ERROR ENABLE COMES
ON BIT SYNC TIMES

⑥ PWR ON 16-BIT [2]

⑦ PWR ON

⑧ PWR ON WORD 159

⑨ PWR ON

BW = .1

Center Deviation Meter

* PRESS TO RESET

COMMENTS ON SYSTEM-7 PROGRAM

STMT	SOURCE STATEMENT	DOS ASM/7	(360A-TX-011) VIM2	12/10/74
2 *	PCMO10 PROGRAM SPECIFICATIONS:			00000030
3 *	PURPOSE; INPUT (MFMR) OR (PMIS) DATA INTO A 648 WORD BUFFERS			00000040
4 *	(A OR B), DETERMINE TYPE (MFMR) OR (PMIS), CHECK FOR			00000050
5 *	PROPER SEQUENCE OF (TIME-WORD-3-FLAG) AND (FID) FORMS,			00000060
6 *	TRANSFER TOGGLED BUFFER AT (TIME-WORD-3) IF (VALID DATA)			00000070
7 *	FLAG IS PRESENT, AND SIGNAL (END-OF-FILE) WHEN			00000080
8 *	(VALID-DATA-FLAG) DROPS.			00000090
9 *				00000100
10 *				00000110
11 *	BUFFER FORMAT;			00000120
12 *				00000130
13 *	HEADER (8-WORDS) DISP (0000) CODE WORD (0000) DATA			00000140
14 *			(FFFF) EOF	00000150
15 *			(EEEE) EOJ	00000160
16 *			BLANK	00000170
17 *		(0002)	LOGID 2-CHARS (EBCDIC)	00000180
18 *		(0003)	LOGID 2-CHARS (EBCDIC)	00000190
19 *		(0004)	TIME-WORD1	00000200
20 *		(0005)	TIME-WORD2	00000210
21 *		(0006)	TIME-WORD3 (QUEUE XFR)	00000220
22 *		(0007)	BLANK	00000230
23 *				00000240
24 *	FRAME NUMBER (1)	(0008)	SYNC1	00000250
25 *		(0009)	SYNC2	00000260
26 *	DATA11 (30 WORDS)	(0010)	DATA	00000270
27 *			THRU	00000280
28 *		(0039)	DATA	00000290
29 *				00000300
30 *	FID1	(0040)	DID1 (FID CHK, SET TYPE)	00000310
31 *				00000320
32 *	DATA12 (127 WORDS)	(0041)	DATA	00000330
33 *			THRU	00000340
34 *		(0167)	DATA	00000350
35 *				00000360
36 *	FRAME NUMBER (2)	(0168) THRU (0169)	SYNC (TIME CHK)	00000370

EXAMPLE OF PRINTOUT FROM CONTROL TYPEWRITER - PMIS DATA RUN

The following System-7 messages will be executed by the System-7 when the System-370/System-7 linkup occurs, as indicated by the statement "S370 is ready to accept data". Responses typed by the operator on the control typewriter are indicated by enclosure in a box.

*** IPOO A ENTER CONTROL STATEMENT

R JOBLIB,F2,,PCMUSER

L PCMO1B

S370 IS READY TO ACCEPT DATA

ENTER OPTIONS BY TYPEWRITER (REQUEST):

REQ (LOG) TO ENTER LOG-ID WORD THEN (OSC) OR (RUN).

REQ (OSC) TO RUN SIMULATED PCM DATA.

REQ (RUN) TO RUN PCM DATA.

REQ (EOF) MARK FILE AND IGNORE DATA. THIS IS NORMALLY AUTOMATIC BY VALID-DATA-FLAG DROP.

REQ (EOJ) TO SIGNAL TERMINATE JOB.

NOTE--NEW FILES MAY BE OPENED BY (LOG)/(OSC) OR (RUN) REQUESTS AFTER AN (EOF) REQUEST.

OR1: LOG

ENTER 4-DIGIT (HEX) LOGBOOK(ID) WORD

P019

REQUEST (OSC) OR (RUN) TO PREP FOR PCM DATA

OK1: RUN

ENTER PCM DATA

EOF PROCEDURES EXECUTED

EOF PROCEDURES EXECUTED

EOF PROCEDURES EXECUTED

EOF PROCEDURES EXECUTED

EOF PROCEDURES EXECUTED

EOF PROCEDURES EXECUTED

EOF PROCEDURES EXECUTED

EOF PROCEDURES EXECUTED

EOF PROCEDURES EXECUTED

EOF PROCEDURES EXECUTED

EOF PROCEDURES EXECUTED

EOF PROCEDURES EXECUTED

EOF PROCEDURES EXECUTED

EOF PROCEDURES EXECUTED

← overflow occurred { see following page, "Notes on Control Typewriter Printout - PMIS Data Run"

OR1: RUN

ENTER PCM DATA

EOF PROCEDURES EXECUTED

EOF PROCEDURES EXECUTED

OR1: EOJ

S7/S370 LINK TERMINATED

← job was started again at selected place on tape

← end of last tape; end of job was requested

NOTES ON CONTROL TYPEWRITER PRINTOUT - PMIS DATA RUN

Explanation of Terms

LOG ID = name of the tape (4-digit word). The first digit must be either "P" or "M" in order for the computer to recognize data as being either PMIS or MFMR data.

OSC = running oscillator to de-bug tape.

PCM = pulse code modulation.

VDC = Test Id. number (name of file). The Test Id. is the "valid data" code, or word.

EOF = end of file.

EOJ = end of job.

Overflow

When overflow occurs, as it did during the processing of PMIS tape P019 (indicated by arrow on "Example of Printout from Control Typewriter - PMIS Data Run" on the previous page), determination of where to re-start the job is made by: counting EOF's; and, by checking the time on the time code reader and the time code on the log. The tape is then backed up to the selected point, and the job is started again.

Although whole files are not lost prior to overflow (all files are lost afterward), it is possible to lose 25 data cycles, spread throughout the files, out of the job. There are 640 words per data cycle.

When data overflows: a bell rings; EOF messages cease to print out; and, the control typewriter skips lines where the messages would have been.

Valid-Data-Flag Drop

The twenty-second word of each PCM data cycle is the "valid data word" (VDC). The high-order bit of this word is the "Valid-Data-Flag". The valid-data-flag is one (1) during each file and is zero (0) between files.

The System-7 program monitors the valid-data-flag and executes an end-of-file procedure each time the valid-data-flag drops, i.e., goes from 1 to 0. The PMIS 1 and MFMR 1 programs also monitor the value of the entire valid-data-word; in case the System-7 fails to execute an end-of-file procedure any time the VDC changes, the PMIS 1 and MFMR 1 programs will do so.

PMIS 1 PROGRAM CARD SETUP

The PMIS 1 program is executed by running the following setup on the System-370:

			18.
18	DUMP (Job Step - Disk Disk) (optional)		17
17	17 EXEC EM03H (Job Step - Disk-Dump)		16
16	361.96 -67.47 365.57 -64.07 "T1 & ΔT card"		15
15	EXEC EM03B (PMIS 2 program - optional in PMIS 1)		13
14			12
13			10.
12	EXEC EM03A (PMIS 1)		9.
11	DEPT 10000011 (optional)		8.
10	EXTENT SYS001, DRZ001, 1, 0, 03000, 01800		7
9	UNIT NAME '1111111' 1, 75, 001		6
8	ASST SYS001, W 935		5
7	PAID MOUNT DRZ001 ON 935		4
6	ASST SYS002, W 901		3
5	ASST SYS001, W 906		2
4	UNIT PMIS1 COOPER, 4100, P, 14305, PMIS1		1.

LOG NO. _____ JOB NAME PMIS 1 D FUND 14305 W.O. PMIS 1

REQUESTOR Cooper TEL 383 CC 4100 BEGIN _____

DATE _____ TIME _____ APPROX RUN TIME _____ END _____

TAPE DR.	TAPE NAME & DATE CREATED	W	TAPE LOC.	DISK	VOLSER NO.
280				335	DRZ001
281					
282					
283					

PUNCH _____ 2701 SEL _____ REAL ALLOCATION _____

FORMS 1 2 4
SPECIAL _____
CARRIAGE TAPE _____

COMMENTS
*System-7 Transfer
Run In Foreground 4*

ORIGINAL PAGE IS
OF POOR QUALITY

PMIS 1 PROGRAM CARD SETUP & PROGRAM OPTIONS

PMIS 1 Program Card Setup

1. Phase 1

The example of a "PMIS 1 Program Card Setup" given on the previous page actually includes three separate programs, PMIS 1, PMIS 2, and Job-Step Disk-Dump, all executed by the PMIS 1 program setup. When the three programs are thus used, PMIS 1, PMIS 2, and Job-Step Disk-Dump are the first, second, and third phases, respectively, of a single job.

By removing the PMIS 2 cards numbered 12, 13, and 14, PMIS 1 can be run as a separate job.

2. Phase 2

PMIS 2 may also be run singly, by choice. However, if certain values must be changed in PMIS 2 data run previously, there is no option; PMIS 2 must be executed as a separate job (see PMIS 2 writeup and card setup).

3. Job-Step Disk-Dump

When PMIS 2 (or PMIS 1, if PMIS 2 was not included in the job setup) has processed all of the data on the disk, control is turned over to Job-Step Disk-Dump (cards #15 and #16). Job-Step Disk-Dump prints all of the data cycles that were dumped into the disk by PMIS 1.

This job step also computes the amount of run time for the entire program and prints this time on the SYSLOG and on the printer, thus must be included in all foreground PMIS and MFMR programs. Disk Dump dumps the disk only if it is enabled by following the // EXEC EMO3H card (#15) with the dump card (#16). If no dump is desired, follow the // EXEC EMO3H with the /* card (#17).

Optional Control Cards - PMIS 1 (First Phase)

1. Card No. 8, the UPSI card, is optional. It contains a string of eight binary digits.

The binary value of the seven low-order bits of this string is the number of data cycles which will be dumped onto the disk each time a new Test Id. is established, i.e., the number of data cycles dumped per file. Note: the last data cycle of each file (Test) is not under the control of the // UPSI card and is always placed (dumped) on the disk.

The high-order bit is a flag to determine whether or not the diagnostic is to be printed from PMIS 1 (Phase 1 of the example, "PMIS 1 Program Card Setup"). If the high-order UPSI bit is 1, the full printout is obtained; if the high-order bit is zero, or if there is no UPSI card, Phase 1 printout is suppressed.

PMIS 1 PROGRAM CARD SETUP & PROGRAM OPTIONS

Optional Control Cards - PMIS (First Phase), continued

2. Card 10, "Disk Address" card, must be used with great caution. Its misuse can destroy all data on the disk, since it updates, i.e., changes the disk directory. On the card shown in the PMIS 1 program setup, each word has the value "99", which is the starting address. This initializes the disk and causes it to start loading data at the beginning of the disk file.

Format of Disk Address Card (when used in PMIS 1): 3I10.

- a. First word, HIGH ϕ N: the highest disk address that PMIS 1 or MFMR 1 has operated on up to a given instant;
- b. Second word, HIGH ϕ FF: the highest disk address that PMIS 2 or MFMR 2 has operated on up to the same given instant;
- c. Third word, J ϕ BEND: the highest disk address that the last PMIS 1 or MFMR 1 job has operated on up to the time it was terminated.

Note: the disk control is set up such that both PMIS 1 and PMIS 2 can operate simultaneously in different partitions of the computer. And, if PMIS 1 is in process of executing while PMIS 2 is also in the process of executing, then PMIS 2 has to know exactly where PMIS 1 is. Three variables are transmitted through the disk so that these two programs can communicate with one another; these variables are HIGH ϕ N, HIGH ϕ FF, and J ϕ BEND.

Optional Control Cards - PMIS 2 (Second Phase)

3. Cards numbered 12 and 13, the "// EXEC EMO3B" and the "T1 and Δ T" cards, respectively, are optional in the PMIS 1 program. Inclusion of these cards causes the PMIS 2 program to be executed in the PMIS 1 program (see example of PMIS 1 program card setup). However, the T1 and Δ T card is optional, and it can be included only if the values of T1 and Δ T are known prior to execution of the job. If omitted, the values used will be those that were used the last time the PMIS 2 program was executed.

Format of T1 and Δ T Data Card: 4F10.4. Words are: T1 vertical; Δ T vertical; T1 horizontal; and, Δ T horizontal, respectively.

If it should later become necessary to change the values of T1 and Δ T in data that were run previously, this is done by re-running PMIS 2 as a single phase (see PMIS 2 writeup).

ORIGINAL PAGE IS
OF POOR QUALITY

PMIS 2 PROGRAM

When the EOJ instruction is issued at the System-7 terminal, the linkage between the System-370 and the System-7 is terminated, and program PMIS 1 (the first phase of the job) ends and turns control over to the second phase (PMIS 2 program).

PMIS 2 retrieves the raw data placed on disk DRZ001 by PMIS 1 and computes the engineering units; it then places these results on the disk, prints them out, and punches a card for each file (Test). These cards are referred to as "PMIS 2 cards" (see example).

The "PMIS 2 card" will be used in the PMIS 3 program (see example of PMIS 3 program card setup).

Data Address (disk address of 1st word of file)	Beam Position	Valid Data Word (Test Id)	Log Id (A format)	Start Time	Stop Time	Uncorrected Sky Brightness Temp Vert (K)	Uncorrected Sky Brightness Temp Horiz (K)
362350	22	530	P001	19 52 40. Hr Min Sec	19 53 39. Hr Min Sec	0.29530472 03	0.19171297 03
00000000	00000000	0000	00	0000000000	0000000000	00000 0000 00	00 00 00000000 00000000
1 2 3 4 5 6 7 8 9 10 11 12 13 14 15 16 17 18 19 20 21 22 23 24 25 26 27 28 29 30 31 32 33 34 35 36 37 38 39 40 41 42 43 44 45 46 47 48 49 50 51 52 53 54 55 56 57 58 59 60 61 62 63 64 65 66 67 68 69 70 71 72 73 74 75 76 77 78 79 80	1 2 3 4 5 6 7 8 9 10 11 12 13 14 15 16 17 18 19 20 21 22 23 24 25 26 27 28 29 30 31 32 33 34 35 36 37 38 39 40 41 42 43 44 45 46 47 48 49 50 51 52 53 54 55 56 57 58 59 60 61 62 63 64 65 66 67 68 69 70 71 72 73 74 75 76 77 78 79 80	1 2 3 4 5 6 7 8 9 10 11 12 13 14 15 16 17 18 19 20 21 22 23 24 25 26 27 28 29 30 31 32 33 34 35 36 37 38 39 40 41 42 43 44 45 46 47 48 49 50 51 52 53 54 55 56 57 58 59 60 61 62 63 64 65 66 67 68 69 70 71 72 73 74 75 76 77 78 79 80	1 2 3 4 5 6 7 8 9 10 11 12 13 14 15 16 17 18 19 20 21 22 23 24 25 26 27 28 29 30 31 32 33 34 35 36 37 38 39 40 41 42 43 44 45 46 47 48 49 50 51 52 53 54 55 56 57 58 59 60 61 62 63 64 65 66 67 68 69 70 71 72 73 74 75 76 77 78 79 80	1 2 3 4 5 6 7 8 9 10 11 12 13 14 15 16 17 18 19 20 21 22 23 24 25 26 27 28 29 30 31 32 33 34 35 36 37 38 39 40 41 42 43 44 45 46 47 48 49 50 51 52 53 54 55 56 57 58 59 60 61 62 63 64 65 66 67 68 69 70 71 72 73 74 75 76 77 78 79 80	1 2 3 4 5 6 7 8 9 10 11 12 13 14 15 16 17 18 19 20 21 22 23 24 25 26 27 28 29 30 31 32 33 34 35 36 37 38 39 40 41 42 43 44 45 46 47 48 49 50 51 52 53 54 55 56 57 58 59 60 61 62 63 64 65 66 67 68 69 70 71 72 73 74 75 76 77 78 79 80	1 2 3 4 5 6 7 8 9 10 11 12 13 14 15 16 17 18 19 20 21 22 23 24 25 26 27 28 29 30 31 32 33 34 35 36 37 38 39 40 41 42 43 44 45 46 47 48 49 50 51 52 53 54 55 56 57 58 59 60 61 62 63 64 65 66 67 68 69 70 71 72 73 74 75 76 77 78 79 80	1 2 3 4 5 6 7 8 9 10 11 12 13 14 15 16 17 18 19 20 21 22 23 24 25 26 27 28 29 30 31 32 33 34 35 36 37 38 39 40 41 42 43 44 45 46 47 48 49 50 51 52 53 54 55 56 57 58 59 60 61 62 63 64 65 66 67 68 69 70 71 72 73 74 75 76 77 78 79 80
2222	222222	2222222222222222	2222222222222222	2222222222222222	2222222222222222	2222222222222222	2 22222222222222
33 33	3333333333333333	3333333333333333	3333333333333333	333333 3 3 33 333	323333 31 333333333333	33333333	33333333
4444	4444444444444444	4444444444444444	4444444444444444	4444444444444444	4444444444444444	4444444444444444	4444444444444444
5555	5555555555555555	5555555555555555	5555555555555555	5555555555555555	5555555555555555	5555555555555555	5555555555555555
6666	6666666666666666	6666666666666666	6666666666666666	6666666666666666	6666666666666666	6666666666666666	6666666666666666
7777	7777777777777777	7777777777777777	7777777777777777	7777777777777777	7777777777777777	7777777777777777	7777777777777777
8888	8888888888888888	8888888888888888	8888888888888888	8888888888888888	8888888888888888	8888888888888888	8888888888888888
9999	9999999999999999	9999999999999999	9999999999999999	9999999999999999	9999999999999999	9999999999999999	9999999999999999

"PMIS 2 CARD" OUTPUT BY PMIS 2 PROGRAM

Note: the Log Id., above, is the name of the tape. The first digit must be either "P" or "M" in order for the computer to recognize data as being either PMIS or MFMR data. The Valid Data Word (or Valid Data Code, VDC) is the Test Id. number (name of file).

PMIS 2 PROGRAM

When PMIS 2 has processed all of the data on the disk, control is turned over to Job-Step Disk-Dump. This is the last job step of the three-phase job illustrated by the PMIS 1 Program Card Setup. Job-Step Disk-Dump prints all of the data cycles that were dumped into the disk by PMIS 1.

Note: the last data cycle of each file (Test) is not under the control of the // UPSI card and is always placed on the disk.

Job-Step Disk-Dump is described in "PMIS 1 Program Card Setup & Program Options" under "PMIS 1 Program Card Setup".

PMIS 2 PROGRAM - USAGE AS SINGLE-PHASE JOB

Whenever it becomes necessary to re-run PMIS 2 program at a later time with new values of T1 and ΔT , PMIS 2 must be executed as a single-phase job.

The PMIS 2 program card setup may include or omit optional control cards as follows:

1. as Phase 2 of a three-phase job setup. For optional inclusion in this setup, as shown in "PMIS 1 Program Card Setup":
 - a. T1 and ΔT card (if such values are known prior to program execution).

2. as a separate, single-phase job to obtain PMIS 2 data not previously run (where the Test, or file, has been processed by PMIS 1, and PMIS 2 program was not included in the job setup). Optional inclusion in this setup, as shown in "PMIS 2 Program Card Setup":
 - a. T1 and ΔT Card;
 - b. Disk Address Card, 2I10 format

3. as a separate, single-phase job to change existing PMIS 2 data by re-running it with new values of T1 and ΔT . Inclusion in this setup, as shown in "PMIS 2 Program Card Setup", is not optional. It is:
 - a. mandatory that the T1 and ΔT card, with new, changed values of T1 and ΔT , be included in setup;
 - b. mandatory that the Disk Address card, 2I10 format, be included in the setup.

PMIS 2 PROGRAM CARD SETUP

The PMIS 2 program is executed as a separate, single-phase job by running the following setup on the System-370:

```

99          99          "Disk Address Card" - 2110 format
1. Mandatory in PMIS 2 as single-phase program re-run with new values of T1 & AT.
2. Optional in PMIS 2 single-phase program except in above re-runs.
361.96      -67.47      365.57      -64.07      "T1 and AT Card"
1. Mandatory in PMIS 2 as single-phase program re-run with new values of T1 & AT.
2. Optional except in re-runs, as above.
EXEC EM03B
I I I I I
EXTENT SYS001, DR2001, 1, 0, 03000, 00800
DIRL FNAME, TTTTTT
ASSGN SYS001, 000000
PAUSE TQUANT DR2001 ON 335
JOB PMIS2 COOPER, 4100, P, 14305, FMIS2
    
```

LOG NO. _____ JOB NAME PMIS 2 D FUND 14305 W.O. PMIS 2

REQUESTOR W. Cooper TEL 383 CC 4100 BEGIN _____

DATE _____ TIME _____ APPROX RUN TIME _____ END _____

TAPE DR.	TAPE NAME & DATE CREATED	W	TAPE LOC.	DISK	VOLSER NO.
280				335	DR2001
281					
282					
283					

PUNCH _____ 2701 SEL. _____ REAL ALLOCATION _____

FORMS 1 2 4
 SPECIAL _____
 CARRIAGE TAPE _____

COMMENTS

950 Rev. 8-74

PMIS 2 PROGRAM - SETUP FOR SEPARATE, SINGLE-PHASE JOB

ORIGINAL PAGE IS
 OF POOR QUALITY

PMIS 2 PROGRAM - USAGE AS SINGLE-PHASE JOB

PMIS 2 Card Setup. Control Cards

When the PMIS 2 program must be re-run with values of T1 and ΔT that are different from those used previously on a particular set of files (Tests):

- a. the PMIS 2 program must be executed as a separate job;
- b. a T1 and ΔT card punched with the new values of T1 and ΔT must be included in the card setup; and,
- c. a Disk Address card punched in the 2I10 format must be included in the card setup.

1. T1 and ΔT Card

Card Format: 4F10.4.

Words are: T1 vertical; ΔT vertical; T1 horizontal; and, ΔT horizontal, respectively.

2. Disk Address Card

The disk address card is used to tell the program what values of HIGHOFF and JOBEND to use for this run. Unlike the Disk Address card used in PMIS 1, the 2I10 format card used in PMIS 2 overrides the disk directory instead of updating it.

Format (when used in PMIS 2 program): 2I10. Words: HIGHOFF; and, JOBEND, respectively.

- a. The first word, HIGHOFF, is -1+ the disk address of the first file to be recomputed. HIGHOFF is the highest address which PMIS 2 or MFMR 2 has operated on up to that time.
- b. The second word, JOBEND, is 149+ the disk address of the last file to be recomputed. JOBEND is the highest disk address PMIS 1 or MFMR 1 has operated on at the time the last job was ended.

Note: if PMIS 2 encounters MFMR data, such data are bypassed. Disk directory usage and the usage of HIGHON and HIGHOFF values proceed as if these data had been used.

NOTES ON CONVERSION TO ENGINEERING UNITS IN THE PMIS 2 PROGRAM

HOUSEKEEPING DATA

PMIS 2 converts the housekeeping data to engineering units by means of a table-look-up subroutine that performs linear interpolation between the closest two points. These tables are derived from tables A, B, C, D, E, and F for PMIS Temperature Calibration as per TMI353, Appendix K, pages 1-4.

UNCORRECTED SKY BRIGHTNESS TEMPERATURE, T'_B

The uncorrected sky brightness temperature is computed according to the formula:

$$T'_B = T_1 + \Delta T \frac{\bar{C}_A - \bar{C}_B}{\bar{C}_C - \bar{C}_B} ,$$

where:

T_1 and ΔT are the Y intercept and slope provided on the $T_1, \Delta T$ card;

\bar{C}_A is the average value of the counts when the radiometer is in the operate mode;

\bar{C}_B is the average of the base line counts; and,

\bar{C}_C is the average of the calibrate counts.

STANDARD DEVIATION OF THE UNCORRECTED SKY BRIGHTNESS TEMPERATURE, σ_T

The standard deviation of the uncorrected sky brightness temperature is computed according to the formula:

$$\sigma_T = \frac{|\Delta T|}{(\bar{C}_C - \bar{C}_B)^2} \sqrt{(\bar{C}_C - \bar{C}_B)^2 \sigma_A^2 + (\bar{C}_A - \bar{C}_C)^2 \sigma_B^2 + (\bar{C}_A - \bar{C}_B)^2 \sigma_C^2} ,$$

where:

σ_A = standard deviation of data counts;

σ_B = standard deviation of baseline counts; and,

σ_C = standard deviation of calibrate counts.

NOTES ON CONVERSION TO ENGINEERING UNITS IN THE PMIS 2 PROGRAM

cont'd

STANDARD DEVIATION OF THE UNCORRECTED SKY BRIGHTNESS TEMPERATURE, σ_T

A standard deviation of zero in any of the data is an indicator of hardware trouble. Therefore, if σ_A , σ_B , or σ_C is zero, σ_T is flagged by changing its sign. A negative value of σ_T is thus an indicator of bad data; and, since this sign propagates through all subsequent calculations of antenna loss and radome loss, it automatically flags these calculations also.

SKYTEMP PROGRAM CARD SETUP

Any number of these data sets may be stacked with one /* card separating data sets. Note that two consecutive /* cards terminates the program.

In order to run program SKYTEMP, execute the following statements on the System-370:

- /* End of Job (EOJ)
- /* End of all files in this job. (EOF)

```

      8.5      -11.3      -99.0
      *          *          *
Intervening PTD cards
      850.0      4.5      -8.4
10.69E09
Header card, Rnd Data Set
04 FEB. 1969 0900 MSTP040
Last PTD data card (1st Data Set) P040
  Rnd Data Set
  Rnd Data Set
First PTD card (1st Data Set) P040
  
```

```

      81.0      -52.9      -99.0
      800.0      -49.5      -99.0
      809.0      -48.2      -99.0
Intervening PTD data cards
      824.0      -22.9      -19.9
      825.0      8.0      -8.0
      850.0      9.0      -7.0
Second PTD card (1st Data Set) P040
First PTD card (1st Data Set) P040
10.69E09
Header Card, 1st Data Set
04 FEB. 1969 0200 MSTP040
  
```

```

/* EXEC EM036
   JOB SKYTEMP COOPER.4100.F.143051 SKYTEMP
  
```

LOG NO. _____ JOB NAME SKYTEMP @D FUND 14305 W.O. SKYTEMP

REQUESTOR Cooper TEL 383 CC 4100 BEGIN _____

DATE _____ TIME _____ APPROX RUN TIME _____ END _____

TAPE DR.	TAPE NAME & DATE CREATED	W	TAPE LOC.	DISK	VOLSER NO.
280					
281					
282					
283					

PUNCH _____ 2701 SEL. _____ REAL ALLOCATION _____

FORMS 1 2 4 _____ COMMENTS _____

SPECIAL _____

CARRIAGE TAPE _____

ORIGINAL PAGE IS
OF POOR QUALITY

PMIS 3

ANTENNA LOSS FACTOR - RADOME LOSS FACTOR

PMIS 3 is the program that computes the antenna loss factors and the radome loss factor.

Antenna loss is computed according to the formula:

$$L_{ant} = \frac{T_{ant} - T'_B}{T_{ant} - T_{sky}}$$

$$\text{where } T_{ant} = \frac{T_8 + T_9 + 4 T_{10}}{6} + 273.1 \text{ } ^\circ\text{K,}$$

the average of the six antenna thermistor readings.

T'_B is the uncorrected sky brightness temperature from PMIS 2 calculations.

T_{sky} is the sky temperature from SKYTEMP.

Radome loss is computed according to the formula:

$$L_R = \frac{T'_{BR} - T_{ant} (1 - L_{ant}) - T_R L_{ant}}{T_{skyR} L_{ant} - T_R L_{ant}},$$

where:

T'_{BR} is the uncorrected sky brightness temperature from PMIS 2 taken with the radome on;

T_{ant} is as above with radome on; and,

L_{ant} is the value computed above with the radome off.

T_{skyR} is the sky temperature from SKYTEMP at the time of the T'_{BR} measurement.

T_R is the average of six radome temperatures.

$$T_R = \frac{T_{11} + T_{12} + 4 T_{13}}{6} + 273.1 \text{ } ^\circ\text{K}$$

PMIS 3
STANDARD DEVIATIONS - ANTENNA LOSS, RADOME LOSS

The standard deviation of the antenna loss is computed according to the formula:

$$\sigma_{LA} = - \frac{L_A \sigma'_T}{T'_{BR} - T_A} ,$$

where σ'_T is the standard deviation of T'_{BR} .

The standard deviation of the radome loss is computed according to the formula:

$$\sigma_{LR} = \frac{L_R L_A \sigma'_T}{T'_{BR} L_A - T_A (L_A - 1) - T_R} ,$$

where T_R is the kinetic temperature of the radome.

PMIS 3 PROGRAM - "RADOME IS OFF" CARD SETUP

A PMIS 3 "Radome Is Off" job is run by executing the following program on the System-370:

```

* EOJ (end of job) 19.
* EOF (end of all files) 18.

145750 44 586 P040 3 1 4 3 59. 0.1313641E 03 0.2937297E 03 14.
PMIS 2 card - 9rd Data Set

RADOME IS OFF 15.
CC C C CC

145600 1 585 P040 4 1 16. 4 2 15. 0.1335681E 03 0.2937297E 03 13.
PMIS 2 card - 2nd Data Set

RADOME IS OFF 12.
CC C C CC

5.30 04 FEB. 0530 MSTP040 10.4999E 09 0.0 Second SKYTEMP 10.
      0000 card - 0530 hrs.

6.45 04 FEB. 0630 MSTP040 10.4999E 09 0.0 First SKYTEMP 9.
      0000 card - 0630 hrs.

145450 22 584 P040 3 59 51. 4 0 36. 0.1291763E 03 0.2937297E 03 8.
PMIS 2 Card

RADOME IS OFF 7.
CC C C CC

// EXEC FMO35 6.
// EXTENT SY5001, DR2001, 1, 0, 03000, 00200 5.
// DLBL FNAME, '1111111' '1, 761001' 4.
// ASSIGN SY5001, X'335' 3.
// PAUSE MOUNT DR2001 ON 335 2.
// JOB PMIS3 COOPER, 4100, P, 143051, PMIS3 1.
    
```

LOG NO. _____ JOB NAME PMIS 3 $\text{\textcircled{D}}$ FUND 14305 W.O. PMIS 3

REQUESTOR Cooper TEL 383 CC 4100 BEGIN _____

DATE _____ TIME _____ APPROX RUN TIME _____ END _____

TAPE DR.	TAPE NAME & DATE CREATED	W	TAPE LOC.	DISK	VOLSER NO.
280				335	DR2001
281					
282					
283					

PUNCH _____ 2701 SEL. _____ REAL ALLOCATION _____

FORMS 1 2 4
SPECIAL _____
CARRIAGE TAPE _____

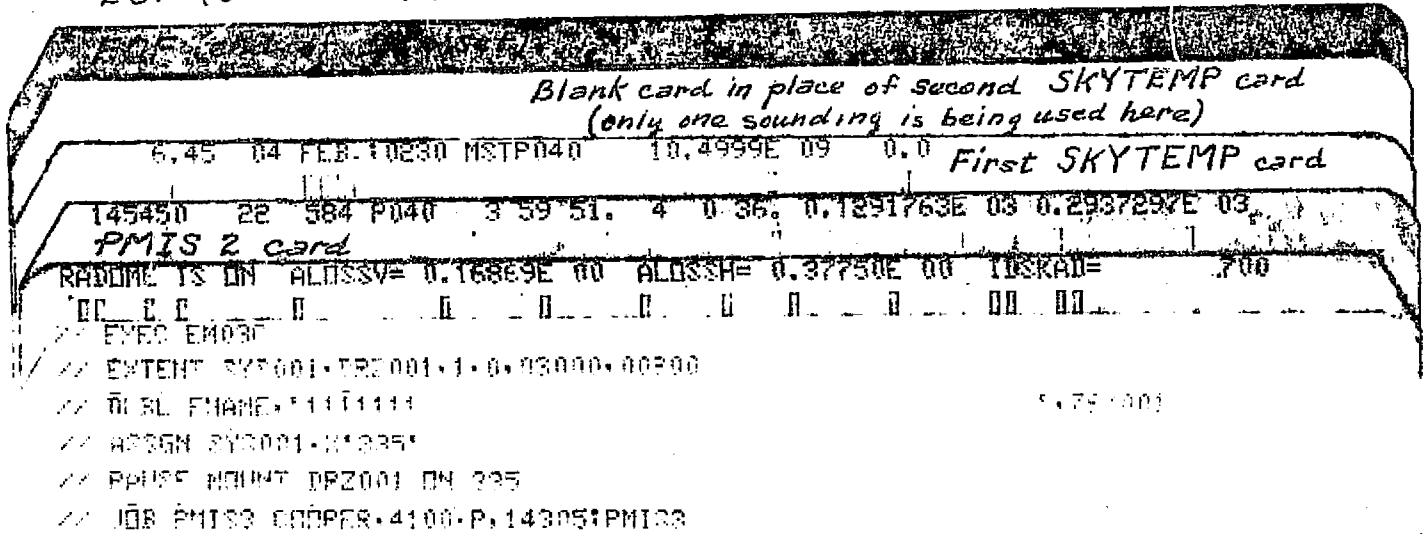
COMMENTS

PMIS 3 PROGRAM - "RADOME IS ON" CARD SETUP

Any number of these data sets may be stacked with one /* card separating data sets.

To execute PMIS 3 when the "Radome Is On", run the following program:

- * EOI (end of job)
- * EOF (end of file(s))



LOG NO. _____ JOB NAME PMIS 3 @D FUND 14305 W.O. PMIS 3

REQUESTOR W. Cooper TEL 383 CC 4100 BEGIN _____

DATE _____ TIME _____ APPROX RUN TIME _____ END _____

TAPE DR.	TAPE NAME & DATE CREATED	W	TAPE LOC.	DISK	VOLSER NO.
280				335	DRZ001
281					
282					
283					

PUNCH _____ 2701 SEL _____ REAL ALLOCATION _____

FORMS 1 2 4
 SPECIAL _____
 CARRIAGE TAPE _____

COMMENTS _____

ORIGINAL PAGE IS
 OF POOR QUALITY

MFMR PROGRAMS - REFERENCE INDEX

Page No.'s

GENERAL

M.1 - M.5

- A. To load and execute System-7 PCM Program. M.1
- B. Instructions of A., above, for newcomer to System-7 M.1a
- C. Telemetry Playback Console - sketch and power settings. M.2
- D. Comments on System-7 Program. M.3
- E. Example: printout from control typewriter, MFMR data run M.4
- F. Notes on control typewriter printout
 - 1. Explanation of terms. M.5
 - 2. "Overflow". M.4,5
 - 3. "Valid-Data Flag-Drop". M.4,5

MFMR 1 PROGRAM

M1.1 - M1.3

- A. Card setup for running MFMR 1 on computer M1.1
- B. Discussion of MFMR 1 card setup
 - 1. Phase 1 (MFMR 1). M1.2
 - 2. Phase 2 (MFMR 2). M1.2
 - 3. Phase 3 (Job-Step Disk-Dump). M1.2
- C. Optional Control Cards - MFMR 1 (1st phase)
 - 1. UPSI card M1.2
 - 2. Disk address card (as used in MFMR 1) M1.3
- D. Optional Control Cards - MFMR 2 (2nd phase)
 - 1. // EXEC EMO3E card, /* card M1.3

MFMR 2 PROGRAM

M2.1 - M2.4

- A. MFMR 2 Program as 2nd phase of a MFMR 1 job setup
 - 1. "MFMR 2 Card" output by MFMR 2, input to MFMR 3 M2.1
 - 2. Job-Step Disk-Dump. M2.2
- B. MFMR 2 Program as single-phase, separate job
 - 1. MFMR 2: separate job or 2nd phase treatment... M2.3
 - 2. Disk address card: when used, when omitted M2.3
 - 3. Disk address card (as used in MFMR 2): purpose, format. M2.3
- C. Card setup for running MFMR 2 (separate job) on computer. M2.4

SKYTMFMR PROGRAM

MS.1 - MS.3

- A. Input data cards for SKYTMFMR program
 - 1. Header card, description and format MS.1
 - 2. Pressure, temperature, dew point (PTD) cards - format MS.1
- B. Card setup for running SKYTMFMR on computer MS.2
- C. "SKYTEMP Cards" output by SKYTMFMR, input to MFMR 3 MS.3

MFMR PROGRAMS - REFERENCE INDEX, cont'd

	<u>Page No.'s</u>
<u>MFMR 3 PROGRAM</u>	<u>M3.1 - M3.9</u>
A. Uncorrected sky brightness temperature, T'_B	M3.1
B. Standard deviation of uncorrected sky brightness temperature, σ_{TB}	M3.1
C. Antenna loss.	M3.2
D. Standard deviation of antenna loss.	M3.2
E. Radome loss	M3.2
F. Standard deviation of radome loss	M3.2
G. Card setup for running MFMR 3 "Radome Is Off" job on computer	M3.3
H. Discussion: card setup for "Radome Is Off" job deck 1. Stacking data decks	M3.4
I. Control cards for "Radome Is Off" job deck 1. "Radome Is Off" card.	M3.4
2. "MFMR 2 Cards": OPR, CAL, and BASE.	M3.4
3. T1 card	M3.5
4. ΔT card	M3.6
5. "SKYTEMP Cards"	M3.7
J. Card setup for running MFMR 3 "Radome Is On" job on computer	M3.8
K. Discussion: card setup for "Radome Is On" job deck 1. Stacking data decks	M3.9
L. Control Cards: "Radome Is On" card	M3.9

PROGRAM PROCEDURE TO REDUCE MFMR DATA TAPES

PRIOR TO LOADING THE SYSTEM-7 PCM PROGRAM:

PERFORM CHECKOUT OF ALL PCM HARDWARE AND TAPE(S).

TO LOAD AND EXECUTE THE SYSTEM-7 PROGRAM, PROCEED AS FOLLOWS:

(1) RUN U-ZERO TAPE (LOAD UNIT ADDRESS = X'0000')

(2) LOAD IPL PROGRAM FROM DISK (LOAD UNIT ADDRESS = X'0002')

*** IPOO A ENTER CONTROL STATEMENT

(3) CYCLE HOST ATTACH SWITCH TO (ENABLE AND IPL) AND
THEN TO (ENABLE);

IT MUST REMAIN ON (ENABLE) FOR REMAINDER OF PROGRAM EXECUTION.

(4) SET DISK PROGRAM "DATA SET NAME" BY FOLLOWING R(EFER)

STATEMENT:

R JOBLIB,F2,,PCMUSER

(5) L(OAD) PCM PROGRAM INTO CORE BY FOLLOWING L(OAD) STATEMENT:

L PCMO1B

THE SYSTEM-7 IS NOW PREPARED TO ACCEPT LINKUP WITH THE SYSTEM-370
AND WILL REMAIN IN A WAIT STATE UNTIL MFMR 1 PROGRAM IS EXECUTED
BY THE SYSTEM-370.

PROGRAM PROCEDURE TO REDUCE MFMR DATA TAPES

Notes: "MFMR" is the name of the program and of the radiometer being tested; procedures are given in large type, while explanatory comments are given in smaller type enclosed by hand-drawn brackets, thus: [for benefit of one who is unfamiliar with the System-7].

PRIOR TO LOADING THE SYSTEM-7 PCM PROGRAM:

PERFORM CHECKOUT OF ALL PCM HARDWARE AND TAPE(S).

TO LOAD AND EXECUTE THE SYSTEM-7 PROGRAM, PROCEED AS FOLLOWS:

(1) RUN U-ZERO TAPE (LOAD UNIT ADDRESS = X'0000')

[U-ZERO, the tape to IPL the computer, is a small, blue punch tape kept right by the computer; put Address switches on 0000 (Addresses are control switches on front of computer; there are 4 Address switches, thus each Address switch is set on 0, as indicated by the four zeros in step (1), above)].

(2) LOAD IPL PROGRAM FROM DISK (LOAD UNIT ADDRESS = X'0002')

[IPL denotes "Initial Program Load". Leave the first 3 Address switches on zero, move the right hand Address switch to setting of 2].

*** IPOO A ENTER CONTROL STATEMENT

[The above is a statement that the computer sends back to you after you have done step (2)].

(3) CYCLE HOST ATTACH SWITCH TO (ENABLE AND IPL) AND THEN TO (ENABLE) WHERE IT MUST REMAIN FOR THE REMAINDER OF PROGRAM EXECUTION.

[The Host attach switch is another control switch on the front of the computer; switch it to "Off" (that's down), then up to "Enable and IPL" and back to center position, which is "Enable"; it must stay on "Enable" all the time you're transferring data from Sys.-7 to Sys.-370 - this is done in order to establish a linkage with the System-370.]

(4) SET DISK PROGRAM "DATA SET NAME" BY FOLLOWING R(REFER) STATEMENT:

[step (4) tells you to type an "R", that is, "Reference Statement", on the control typewriter. The statement to be typed, is as follows, below (be sure to leave a space between the "R" and the "J")]:

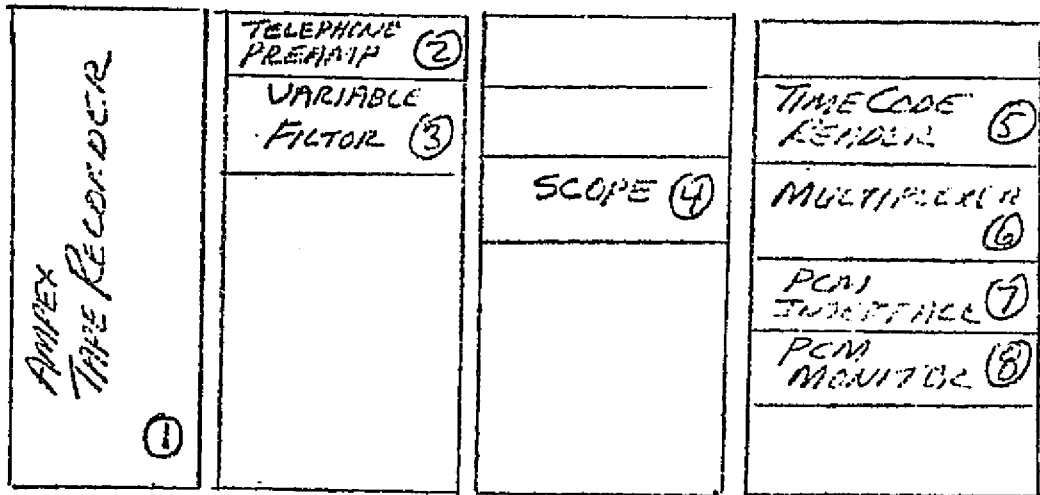
R JOBLIB,F2,,PCMUSER

(5) L(OAD) PCM PROGRAM INTO CORE BY FOLLOWING L(OAD) STATEMENT:

[after typing the statement of step (4)'s instruction, execute step (5) by typing the following statement, below. Leave a space between "L" and "P"].

L PCMO1B

THE SYSTEM-7 IS NOW PREPARED TO ACCEPT LINKUP WITH THE SYSTEM-370 AND WILL REMAIN IN A WAIT STATE UNTIL MFMR 1 PROGRAM IS EXECUTED BY THE SYSTEM-370.



BIT STRUCTURE ⑨

Telemetry Playback Console

- | | |
|--|---|
| <p>① LOAD & RUN</p> <p>② TURN ON</p> <p>③ TURN ON [SETTING @ H PASS 250
L PASS 2300]</p> <p>④ TURN ON [TIMING LEVEL MONITOR
SET 3.5 UP-P MAX
3.0 UP-P NORM
2.5 UP-P MIN]</p> <p>⑤ TURN ON [SET RQD TIMES
SYNG ERROR ENABLE COMES
ON SIGNAL TIMES</p> | <p>⑥ PWR ON 16-BIT [2]</p> <p>⑦ PWR ON</p> <p>⑧ PWR ON WORD 159</p> <p>⑨ PWR ON
BW = .1
Center Deviation Meter
* PRESS TO RESET</p> |
|--|---|

COMMENTS ON SYSTEM-7 PROGRAM

STMT	SOURCE STATEMENT	DOS ASM/7	(360A-TX-011) V1M2	12/10/74
2 *	PCMO10 PROGRAM SPECIFICATIGNS:			00000030
3 *	PURPOSE; INPUT (MFMR) OR (PMIS) DATA INTO A 648 WORD BUFFERS			00000040
4 *	(A OR B), DETERMINE TYPE (MFMR) OR (PMIS), CHECK FOR			00000050
5 *	PROPER SEQUENCE OF (TIME-WORD-3-FLAG) AND (FID) FORMS,			00000060
6 *	TRANSFER TOGGLED BUFFER AT (TIME-WORD-3) IF (VALID DATA)			00000070
7 *	FLAG IS PRESENT, AND SIGNAL (END-OF-FILE) WHEN			00000080
8 *	(VALID-DATA-FLAG) DROPS.			00000090
9 *				00000100
10 *				00000110
11 *	BUFFER FORMAT;			00000120
12 *				00000130
13 *	HEADER (8-WORDS)	DISP (0000)	CODE WORD (0000) DATA	00000140
14 *			(FFFF) EOF	00000150
15 *			(EEEE) EOJ	00000160
16 *			BLANK	00000170
17 *		{0002}	LOGID 2-CHARS (EBCDIC)	00000180
18 *		{0003}	LOGID 2-CHARS (EBCDIC)	00000190
19 *		{0004}	TIME-WORD1	00000200
20 *		{0005}	TIME-WORD2	00000210
21 *		{0006}	TIME-WORD3 (QUEUE XFR)	00000220
22 *		{0007}	BLANK	00000230
23 *				00000240
24 *	FRAME NUMBER (1)	{0008}	SYNC1	00000250
25 *		{0009}	SYNC2	00000260
26 *	DATA11 (30 WORDS)	{0010}	DATA	00000270
27 *			THRU	00000280
28 *		{0039}	DATA	00000290
29 *				00000300
30 *	FID1	{0040}	DID1 (FID CHK, SET TYPE)	00000310
31 *				00000320
32 *	DATA12 (127 WORDS)	{0041}	DATA	00000330
33 *			THRU	00000340
34 *		{0167}	DATA	00000350
35 *				00000360
36 *	FRAME NUMBER (2)	{0168}	THRU {0169} SYNC (TIME CHK)	00000370

ORIGINAL PAGE IS
OF POOR QUALITY

NOTES ON CONTROL TYPEWRITER PRINTOUT - MFMR DATA RUN

Explanation of Terms

LOG ID = name of the tape (4-digit word). The first digit must be either "M" or "P" in order for the computer to recognize data as being either MFMR or PMIS data.

OSC = running oscillator to de-bug tape.

PCM = pulse code modulation.

VDC = Test Id. number (name of file). The Test Id. is the "valid data" code, or word.

EOF = end of file.

EOJ = end of job.

Overflow

When overflow occurs, as it did during the processing of MFMR tape MO19 (indicated by arrow on "Example of Printout from Control Typewriter - MFMR Data Run" on the previous page), determination of where to re-start the job is made by: counting EOF's; and, by checking the time on the time code reader and the time code on the log. The tape is then backed up to the selected point, and the job is started again.

Although whole files are not lost prior to overflow (all files are lost afterward), it is possible to lose 25 data cycles, spread throughout the files, out of the job. There are 640 words per data cycle.

When data overflows: a bell rings; EOF messages cease to print out; and, the control typewriter skips lines where the messages would have been.

Valid-Data-Flag Drop

The twenty-second word of each PCM data cycle is the "valid data word" (VDC). The high-order bit of this word is the "Valid-Data Flag". The valid-data-flag is one (1) during each file and is zero (0) between files.

The System-7 program monitors the valid-data-flag and executes an end-of-file procedure each time the valid-data-flag drops, i.e., goes from 1 to 0. The MFMR 1 and PMIS 1 programs also monitor the value of the entire valid-data-word; in case the System-7 fails to execute an end-of-file procedure any time the VDC changes, the MFMR 1 and PMIS 1 programs will do so.

MFMR 1 PROGRAM CARD SETUP

The MFMR 1 program is executed by running the following setup on the System-370:

	17
	16
	15
	14
	13
	12
	11
99 99 99 "Disk Address Card" (optional)	10
// EXEC END30 (MFMR 1)	9
// UPST 10000011 (optional)	8
// EXTENT SYS001, DR2001, 1, 0, 03000, 00800	7
// DLBL FNAME, '11111111' , 76/001	6
// ASSIGN SYS001, X'335'	5
// PAUSE MOUNT DR2001 ON 335	4
// ASSIGN SYS032, X'201'	3
// ASSIGN SYS031, X'200'	2
// JOB MFMR1 COOPER, 4100, P, 14305, MFMR1	1

LOG NO. _____ JOB NAME MFMR 1 @/D FUND 14305 W.O. MFMR 1

REQUESTOR Cooper TEL 383 CC 4100 BEGIN _____

DATE _____ TIME _____ APPROX RUN TIME _____ END _____

TAPE DR.	TAPE NAME & DATE CREATED	W	TAPE LOC.	DISK	VOLSER NO.
280				335	DRZ001
281					
282					
283					

PUNCH _____ 2701 SEL. _____ REAL ALLOCATION _____

FORMS 1 2 4
 SPECIAL _____
 CARRIAGE TAPE _____

COMMENTS
System 7 Transfer
Run In Foreground 4

MFMR 1 PROGRAM CARD SETUP & PROGRAM OPTIONS

MFMR 1 Program Card Setup

1. Phase 1

The example of a "MFMR 1 Program Card Setup" given on the previous page actually includes three separate programs, MFMR 1, MFMR 2, and Job-Step Disk-Dump, all executed by the MFMR 1 program setup. When the three programs are thus used, MFMR 1, MFMR 2, and Job-Step Disk-Dump are the first, second, and third phases, respectively, of a single job.

By removing the MFMR 2 cards numbered 12 and 13, MFMR 1 can be run as a separate job.

2. Phase 2

MFMR 2 may also be run as a separate job.

3. Job-Step Disk-Dump

When MFMR 2 (or MFMR 1, if MFMR 2 was not included in the job setup) has processed all of the data on the disk, control is turned over to Job-Step Disk-Dump (cards #14 and #15). Job-Step Disk-Dump prints all of the data cycles that were dumped into the disk by MFMR 1.

This job step also computes the amount of run time for the entire program and prints this time on the SYSLOG and on the printer, thus must be included in all foreground MFMR and PMIS programs. Disk Dump dumps the disk only if it is enabled by following the // EXEC EMO3H card (#14) with the dump card (#15). If no dump is desired, follow the // EXEC EMO3H with the /* card (#16).

Optional Control Cards - MFMR 1 (First Phase)

1. Card No. 8, the UPSI card, is optional. It contains a string of eight binary digits.

The binary value of the seven low-order bits of this string is the number of data cycles which will be dumped onto the disk each time a new Test Id. is established, i.e., the number of data cycles dumped per file. Note: the last data cycle of each file (Test) is not under the control of the // UPSI card and is always placed (dumped) on the disk.

The high-order bit is a flag to determine whether or not the diagnostic is to be printed from MFMR 1 (Phase 1 of the example, "MFMR 1 Program Card Setup"). If the high-order UPSI bit is 1, the full printout is obtained; if the high-order bit is zero, or if there is no UPSI card, Phase 1 printout is suppressed.

MFMR 1 PROGRAM CARD SETUP & PROGRAM OPTIONS

Optional Control Cards - MFMR 1 (First Phase), cont'd

2. Card 10, "Disk Address" card, must be used with great caution. Its misuse can destroy all data on the disk, since it updates, i.e., changes the disk directory. On the card shown in the MFMR 1 program setup, each word has the value "99", which is the starting address. This initializes the disk and causes it to start loading data at the beginning of the disk file.

Format of Disk Address Card (when used in MFMR 1): 3I10.

- a. First word, HIGHON: the highest disk address that MFMR 1 or PMIS 1 has operated on up to a given instant;
- b. Second word, HIGHOFF: the highest disk address that MFMR 2 or PMIS 2 has operated on up to the same given instant;
- c. Third word, JOBEND: the highest disk address that the last MFMR 1 or PMIS 1 job has operated on up to the time it was terminated.

Note: the disk control is set up such that both MFMR 1 and MFMR 2 can operate simultaneously in different partitions of the computer. And, if MFMR 1 is in process of executing while MFMR 2 is also in the process of executing, then MFMR 2 has to know exactly where MFMR 1 is. Three variables are transmitted through the disk so that these two programs can communicate with one another; these variables are HIGHON, HIGHOFF, and JOBEND.

Optional Control Cards - MFMR 2 (Second Phase)

3. Cards numbered 12 and 13, the // EXEC EMO3E and the /* cards, respectively, are optional in the MFMR 1 program. Inclusion of these cards causes the MFMR 2 program to be executed in the MFMR 1 program job (see example of MFMR 1 program card setup).

When the MFMR 2 program has not been included in a MFMR 1 job and must be run at a later time, MFMR 2 is executed as a separate job (ref. "MFMR 2 Program - Usage as a Single-Phase Job").

If it becomes necessary to re-run MFMR 2 data that were run previously, the MFMR 2 program must be executed as a separate job (ref. "MFMR 2 Program - Usage as a Single-Phase Job").

MFMR 2 PROGRAM

When the EOJ instruction is issued at the System-7 terminal, the linkage between the System-370 and the System-7 is terminated, and program MFMR 1 (the first phase of the job) ends and turns control over to the second phase (MFMR 2 program).

MFMR 2 retrieves the raw data placed on disk DRZ001 by MFMR 1 and computes the engineering units; it then places these results on the disk, prints them out, and punches a card for each file (Test). These cards are referred to as "MFMR 2 Cards" (see example).

The MFMR 2 card will be used in the MFMR 3 program (see example of MFMR 3 program card setup).

Mode	Log Id	Valid Data Word (Test Id)	Encoded Time (IRIG B)	Disk Address	VDC
MFR	NU05	0000027	297816608 298341476	251050	MFMR2
000000000000000000	000	0000000000	00000000000000000000	000000000000	000
11111111111111111111	11111111111111111111	11111111111111111111	11111111111111111111	11111111111111111111	11111111111111111111
22222222222222222222	222	2222222222	2222222222222222	222222222222	2222222222
33333333333333333333	33333333333333333333	33333333333333333333	33333333333333333333	33333333333333333333	33333333333333333333
44444444444444444444	444	44444444444444444444	44444444444444444444	4444444444444444	4444444444444444
55555555555555555555	55555555555555555555	55555555555555555555	55555555555555555555	5555555555555555	5555555555555555
66666666666666666666	66666666666666666666	66666666666666666666	66666666666666666666	6666666666666666	6666666666666666
77777777777777777777	777	77777777777777777777	77777777777777777777	7777777777777777	7777777777777777
88888888888888888888	88888888888888888888	88888888888888888888	88888888888888888888	8888888888888888	8888888888888888
99999999999999999999	99999999999999999999	99999999999999999999	99999999999999999999	9999999999999999	9999999999999999

"MFMR 2 CARD" OUTPUT BY MFMR 2 PROGRAM

Note: the Log Id., above, is the name of the tape. The first digit must be either "M" or "P" in order for the computer to recognize data as being either MFMR or PMIS data. The Valid Data Word (or Valid Data Code, VDC) is the Test Id. number (name of file).

MFMR 2 PROGRAM

When MFMR 2 has processed all of the data on the disk, control is turned over to Job-Step Disk-Dump. This is the last job step of the three-phase job illustrated by the MFMR 1 Program Card Setup. Job-Step Disk-Dump prints all of the data cycles that were dumped into the disk by MFMR 1. Note: the last data cycle of each file (Test) is not under the control of the // UPSI card and is always placed (dumped) on the disk.

Job-Step Disk-Dump also computes the amount of run time for the entire program and prints this time on the SYSLOG and on the printer, thus must be included in all foreground MFMR and PMIS programs. Disk Dump dumps the disk only if it is enabled by following the // EXEC EMO3H card with the dump card. If no dump is desired, follow the // EXEC EMO3H with the /* card.

MFMR 2 PROGRAM - USAGE AS SINGLE-PHASE JOB

MFMR 2 Card Setup. Single-Phase Job.

The MFMR 2 program may or may not be run as the second phase of the three-phase MFMR 1 job as shown in the MFMR 1 program card setup; its inclusion is optional. However, if the MFMR 2 data are to be obtained at a later time, or if it should become necessary to re-run MFMR 2 data, the MFMR 2 program must be executed as a separate, single-phase job.

1. Run MFMR 2 as a separate, single-phase job to obtain MFMR 2 data not previously run (where the Test, or file, has been processed by MFMR 1, and MFMR 2 program was not included in the job setup) as follows:
 - a. with card #7, "Disk Address" card omitted, run the job shown in the "MFMR 2 Program Card Setup".
2. Run MFMR 2 as a separate, single-phase job to change existing MFMR 2 data by re-running it as follows:
 - a. run the job shown in the "MFMR 2 Program Card Setup"; and,
 - b. include card #7, "Disk Address" card, 2I10 format.

Disk Address Card

The disk address card is used to tell the program what values of HIGHOFF and JOBEND to use for this run. Unlike the Disk Address card used in MFMR 1, the 2I10 format card used in MFMR 2 overrides the disk directory instead of updating it.

Format (when used in MFMR 2 program): 2I10. Words: HIGHOFF, and, JOBEND, respectively.

- a. The first word, HIGHOFF, is -1+ the disk address of the first file to be recomputed. HIGHOFF is the highest address which MFMR 2 or PMIS 2 has operated on up to that time.
- b. The second word, JOBEND, is 149+ the disk address of the last file to be recomputed. JOBEND is the highest disk address MFMR 1 or PMIS 1 has operated on at the time the last job was ended.

Note: if MFMR 2 encounters PMIS data, such data are bypassed. Disk directory usage and the usage of HIGHON and HIGHOFF values proceed as if these data had been used.

MFMR 2 PROGRAM CARD SETUP

The MFMR 2 program is executed as a separate, single-phase job by running the following setup on the System-370:

		"Disk Address Card" - 2110 format	9
		1. <u>Is</u> included in MFMR 2 as single-phase job, data <u>re-run</u> .	8
		2. <u>Is not</u> included in MFMR 2 as single-phase job, <u>first</u> data <u>run</u> .	7
EXEC	EM03E		6
EXTENT	DR2001, DR2001, 1, 0, 02000, 00900		5
DE RL	ENGINE, *****		4
APPROX	*****		3
PAUSE	*****		2
*****	*****		1

LOG NO. _____ JOB NAME MFMR 2 @D FUND 14305 W.O. MFMR 2

REQUESTOR Cooper TEL 383 CC 4100 BEGIN _____

DATE _____ TIME _____ APPROX RUN TIME _____ END _____

TAPE DR.	TAPE NAME & DATE CREATED	W	TAPE LOC.	DISK	VOLSER NO.
280				335	DR2001
281					
282					
283					

PUNCH _____ 2701 SEL. _____ REAL ALLOCATION _____

FORMS 1 2 4
 SPECIAL _____
 CARRIAGE TAPE _____

COMMENTS

950 Rev. 8-74

MFMR 2 PROGRAM ~ SETUP FOR SEPARATE, SINGLE-PHASE JOB

page M2.4

ORIGINAL PAGE IS
 OF POOR QUALITY

SKYTMFMR PROGRAM

Before the loss program (MFMR 3) can be executed, it is necessary to run program SKYTMFMR with meteorological data taken on the same day as that of the MFMR data.

The input data cards for SKYTMFMR are of two types: (1) the header card; and (2) pressure, temperature, and dew point (PTD) cards.

The header card, followed by the PTD cards, must fit the following formats:

80 COLUMN PUNCH CARD FORMAT

1	2	3	4	5	6	7	8	9	10	11	12	13	14	15	16	17	18	19	20	21	22	23	24	25	26	27	28	29	30	31	32	33	34	35	36	37	38	39	40	41	42	43	44	45	46	47	48	49	50	51	52	53	54	55	56	57	58	59	60	61	62	63	64	65	66	67	68	69	70	71	72	73	74	75	76	77	78	79	80								
Header Card																																								04	FEB.	0200	MS	M040																																											
																																								DATE	TIME				LOG ID WORD																																										
PTD Cards																																								850.0	825.0	81.0	9.0	3.0	-7.0	-8.0	-99.0																																								
																																								PRESSURE (mb)	TEMPERATURE (°C)				DEW POINT (°C)																																										
																																								NOTE: comments may be made in these columns of the PTD card. For example, the Log Id. word, shown →																																															
																																								M040 M040 M040																																															

CARD FORMATS - HEADER CARD, PTD CARDS

1). SKYTMFMR Header Card

Card format: 39X,5A4

The Log Id. word in the header card must be the same as the Log Id. word on the first data tape for that date, i.e., for the first data tape to be associated with the particular meteorological data.

2). PTD Data Cards

Card format: 3F10.1.

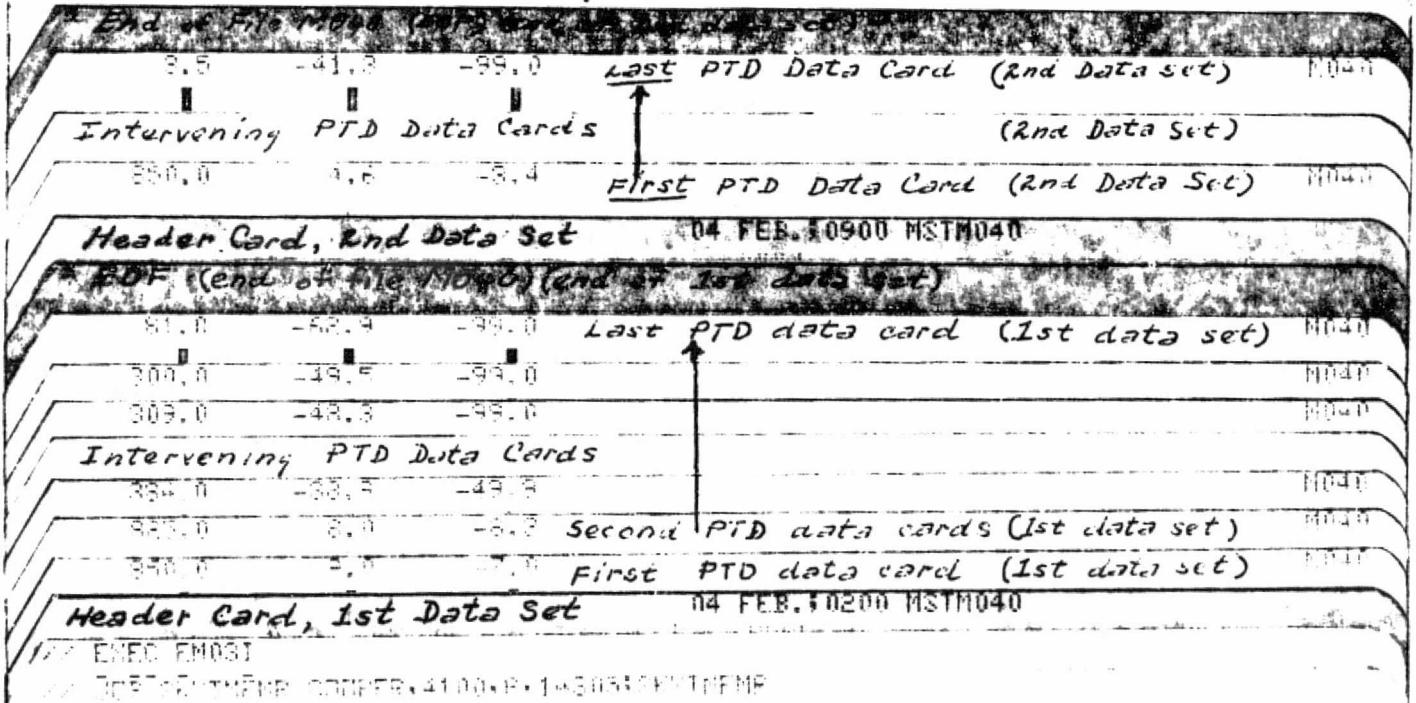
Wherever dew point data are missing, -99.0 should be punched in that field of the PTD data card(s). (See PTD cards in example of SKYTMFMR program card setup.)

SKYTMFMR PROGRAM CARD SETUP

Any number of these data sets may be stacked with one /* card separating data sets. Note that two consecutive /* cards terminates the program.

In order to run program SKYTMFMR, execute the following statements on the System-370:

- /* End of Job (EOJ)
- /* End of ALL Files in this Job (EOF)



LOG NO. _____ JOB NAME SKYTMFMR (P/D) FUND 14305 W.O. SKYTMFMR

REQUESTOR Cooper TEL 383 CC 4100 BEGIN _____

DATE _____ TIME _____ APPROX RUN TIME _____ END _____

TAPE DR.	TAPE NAME & DATE CREATED	W	TAPE LOC.	DISK	VOLSER NO.
280					
281					
282					
283					

PUNCH _____ 2701 SEL. _____ REAL ALLOCATION _____

FORMS 1 2 4
SPECIAL _____
CARRIAGE TAPE _____

COMMENTS

ORIGINAL PAGE IS
OF POOR QUALITY

MFMR 3

UNCORRECTED SKY BRIGHTNESS TEMPERATURE ANTENNA LOSS FACTOR - RADOME LOSS FACTOR

MFMR 3 is the program that computes the uncorrected sky brightness temperature, the antenna loss factors, and the radome loss factor.

UNCORRECTED SKY BRIGHTNESS TEMPERATURE, T'_B

The uncorrected sky brightness temperature is computed according to the formula:

$$T'_B = T_1 + \Delta T \frac{\bar{C}_A - \bar{C}_B}{\bar{C}_C - \bar{C}_B},$$

where:

T_1 and ΔT are the Y intercept and slope provided on the T_1 and ΔT cards;

\bar{C}_A is the average value of the counts when the radiometer is in the operate mode;

\bar{C}_B is the average of the base line counts; and,

\bar{C}_C is the average of the calibrate counts.

STANDARD DEVIATION OF THE UNCORRECTED SKY BRIGHTNESS TEMPERATURE, σ_{TB}

The standard deviation of the uncorrected sky brightness temperature is computed according to the formula:

$$\sigma_{TB} = \frac{|\Delta T|}{(\bar{C}_C - \bar{C}_B)^2} \sqrt{(\bar{C}_C - \bar{C}_B)^2 \sigma_A^2 + (\bar{C}_A - \bar{C}_C)^2 \sigma_B^2 + (\bar{C}_A - \bar{C}_B)^2 \sigma_C^2},$$

where:

σ_A = standard deviation of data counts;

σ_B = standard deviation of baseline counts; and,

σ_C = standard deviation of calibrate counts.

A standard deviation of zero in any of the data is an indicator of hardware trouble. Therefore, if σ_A , σ_B , or σ_C is zero, σ_T is flagged by changing its sign. A negative value of σ_T is thus an indicator of bad data; and, since this sign propagates through all subsequent calculations of antenna loss and radome loss, it automatically flags these calculations also.

MFMR 3

ANTENNA LOSS FACTOR - RADOME LOSS FACTOR

ANTENNA LOSS

Antenna loss is computed according to the formula:

$$L_A = \frac{T_S - T_A}{T'_B L_W - T_W (L_W - 1) - T_A} ,$$

where:

T_S is the sky temperature in °K;

T_A is the kinetic antenna temperature in °K;

T'_B is the uncorrected sky brightness temperature in °K;

L_W is the wave guide loss; and,

T_W is the wave guide temperature in °K.

STANDARD DEVIATION OF ANTENNA LOSS

The standard deviation of the antenna loss is computed according to the formula:

$$\sigma_{L_A} = \frac{L_A L_W \sigma_{T_B}}{T'_B L_W + T_W (1 - L_W) - T_A}$$

RADOME LOSS

The radome loss is computed according to the formula:

$$L_R = \frac{T_S - T_R}{T'_B L_A L_W - T_A (L_A - 1) - T_R - T_W (L_W - 1) L_A}$$

where T_R is the temperature of the radome °K (average of 5 radome thermistors).

STANDARD DEVIATION OF RADOME LOSS

The standard deviation of the radome loss is computed according to the formula:

$$\sigma_{L_R} = \frac{-L_R L_A \sigma_{L_A}}{T'_B L_A L_W - T_A (L_A - 1) - T_R}$$

MFMR 3 PROGRAM

Card Setup - "Radome Is Off"

Any number of data sets may be stacked behind the initial data control cards. The first data set of each job setup must use: the OPR, CAL, and BASE cards; the T1 and ΔT cards; and, the SKYTEMP cards. A /* card may be used to truncate succeeding data sets in any one of three places: after the OPR card; after the BASE card; or, after the ΔT card.

Data Cards

1. The first data card after the // EXEC EM03F is the "Radome Is Off" card (card #7).
2. Cards #8, #9, #10 are the MFMR 2 OPR, CAL, and BASE cards punched by the MFMR 2 program and used to tell MFMR 3 where to retrieve the engineering data. The format (given in less detail in the MFMR 2 writeup) and an example of each of the MFMR 2 cards is shown below:

Type	Log Id (A Format)	Valid Data Word (Test Id) (VDC)	Encoded Start Time (IRIG B)	Encoded Stop Time (IRIG B)	Disk Address of First Word in File	Program Name	VDC
BASE	M010	0000022A	169087268	169611596	300100	MFMR2	0000022A
CAL	M010	00000229	168349824	168874116	299950	MFMR2	00000229
OPR	M010	0000022E	171729480	172254336	300700	MFMR2	0000022E

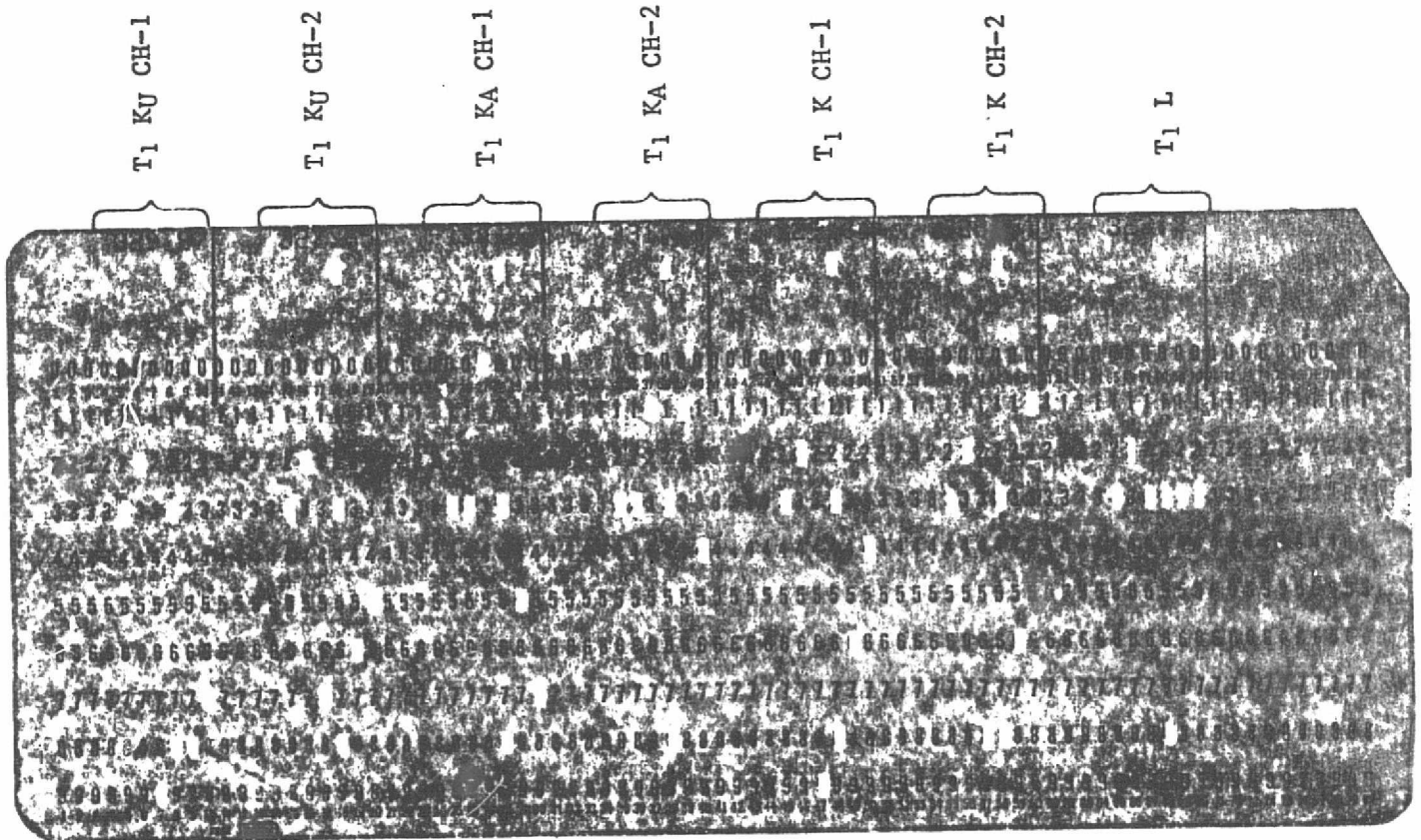
"MFMR 2 CARDS" OUTPUT BY MFMR 2 FOR INPUT TO MFMR 3 PROGRAM

MFMR 3 PROGRAM

Data Cards, "Radome Is Off", cont'd

3. Cards #11 and #12 are the T1 and ΔT cards required for the uncorrected sky brightness calculations.

Formats for these cards are as follows:



T1 CARD FOR INPUT TO MFMR 3 PROGRAM

MFMR 3 PROGRAM

Data Cards, "Radome Is Off", cont'd

3. continued

Format for the ΔT card is as follows:

ΔT KJ CH-1

ΔT KU CH-2

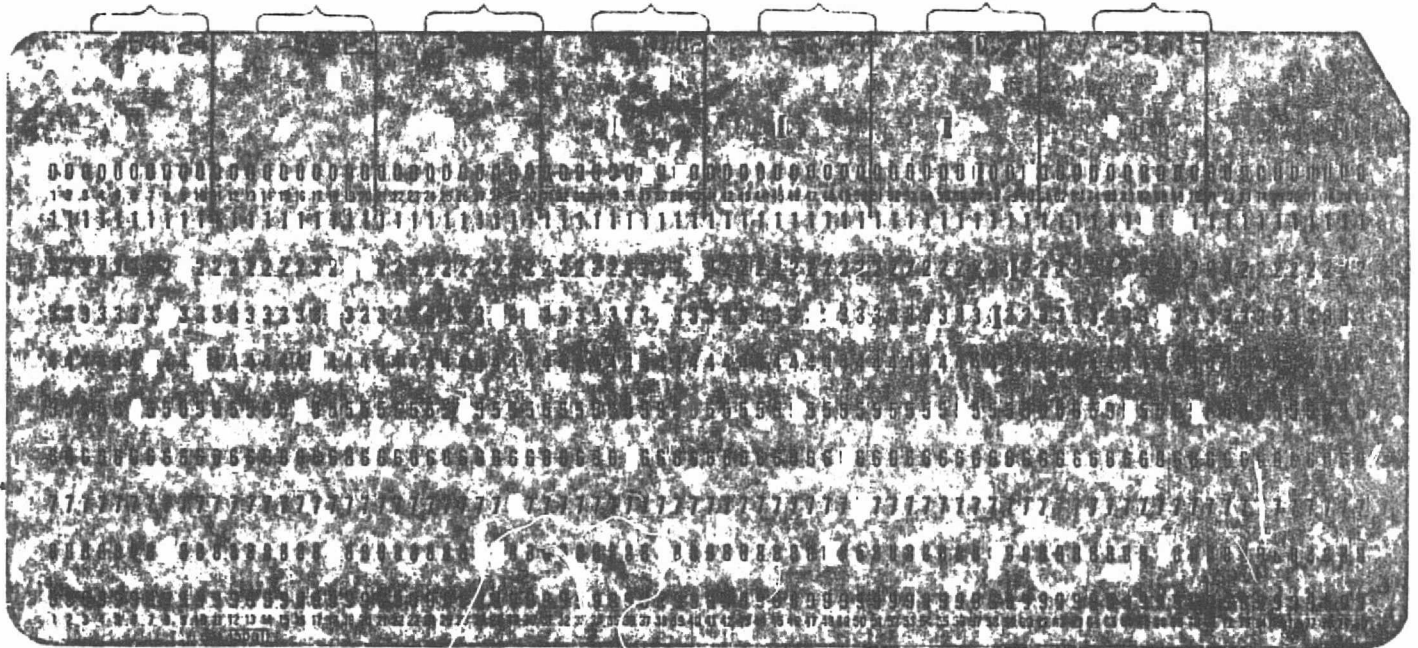
ΔT KA CH-1

ΔT KA CH-2

ΔT K CH-1

ΔT K CH-2

ΔT L



ΔT CARD FOR INPUT TO MFMR 3 PROGRAM

MFMR 3 PROGRAM - "RADOME IS ON" CARD SETUP

A MFMR 3 "Radome Is On" job is run by executing the following program on the System-370:

EOJ (end of Job.)
 EOF (end of All Files.)

```

    DPR      MO10  0000022F 17854252 176170272 300950  MFMR2  0000022F
RADOME IS ON MO04  0000025E 259600 0002E436 1st card of 2nd data set

    4.27 13 FEB. 0300 MSTMO10 14.1350E 08 1.000000E 00 4th SKYTEMP card
    16.13 13 FEB. 0300 MSTMO10 22.0500E 09 1.000000E 00 3rd SKYTEMP card
    11.34 13 FEB. 0300 MSTMO10 37.0000E 09 1.000000E 00 2nd SKYTEMP card
    6.48 13 FEB. 0300 MSTMO10 18.0000E 09 1.000000E 00 1st SKYTEMP card

    BASE     MO10  0000022A 169087268 169511596 300100  MFMR2  0000022A
    CAL      MO10  00000229 168349824 168874116 299950  MFMR2  00000229
    DPR      MO10  0000022E 171729480 172254336 300700  MFMR2  0000022E
RADOME IS ON MO04  0000025D 259450 0002D098 1st card of 1st data set

// EXEC PROG
// EXTENT SY001-DRZ001,1,0,03000,00900
// DIEL ENAME, '1111111'
// ASGN SY001, '335'
// PAUSE MOUNT DRZ001 ON 335
// JOB NAME: COOPER, 4100, P, 14305, MFMR3
    
```

LOG NO. _____ JOB NAME MFMR 3 D FUND 14305 W.O. MFMR 3
 REQUESTOR Wm. Cooper TEL 383 CC 4100 BEGIN _____
 DATE _____ TIME _____ APPROX RUN TIME _____ END _____

TAPE DR.	TAPE NAME & DATE CREATED	W	TAPE LOC.	DISK	VOLSER NO.
280				335	DRZ001
281					
282					
283					

PUNCH _____ 2701 SEL. _____ REAL ALLOCATION _____

FORMS 1 2 4 SPECIAL _____ CARRIAGE TAPE _____	COMMENTS _____
---	----------------

950 Rev. 8-74

ORIGINAL PAGE IS
OF POOR QUALITY

REFERENCES

- Blume, H-J. C. and C. T. Swift, "S-Band Radiometer Remote Sensing of Sea Surface Temperatures," Proc. 1972 URSI/USNC Conference, Williamsburg, Va., Dec. 12-15, 1972 (USNC-URSI, Nat'l. Acad. Sciences, 2101 Constitution Ave., N. W., Washington, D. C. 20418).
- Carver, K. R., "Remote Sensing Using Microwave Radiometry," Proc. 1973 IEEE Southeast-Con, Louisville, Ky., April 30 - May 2, 1973 (IEEE, 345 E. 47th St., New York, N. Y. 10017).
- Carver, K. R., Wm. Cooper and J. F. Paris, "Local Variations in Radiometric Sky Temperature Using Radiosonde Data," Proc. 1975 URSI/USNC Conference, Urbana, Ill., June 2-5, 1975.
- Fogarty, Wm. G., "Total Atmospheric Absorption at 22.2 GHz." IEEE Trans. Ant. and Prop., AP-23, May, 1975, pp. 441-444.
- Hach, J.-P., "A very Sensitive Airborne Microwave Radiometer Using Two Reference Temperatures," IEE Trans. Micro. Theory and Techniques, MTT-16, September, 1968, pp. 629-636.
- Hansen, R. C., Microwave Scanning Antennas, Vol. I, Academic Press (New York), 1964, pp. 24-46.
- Kerns, D. M., "Correction of Near-Field Antenna Measurements Made With an Arbitrary But Known Measuring Antenna," Electronics Letters, Vol. 6, No. 11, May 28, 1970.
- Kraus, J. D., Radio Astronomy, McGraw-Hill Book Co. (New York), 1966, p. 261.

PRECEDING PAGE BLANK NOT FILMED

REFERENCES (Continued)

- Kraus, J. D. and K. R. Carver, Electromagnetics, 2nd ed., McGraw-Hill Book Co. (New York), 1974, pp. 621-622.
- Mentzer, C. A., L. Peters, and R. C. Rudduck, IEEE Trans. Antennas and Prop., AP. 23, March, 1975, pp. 153-159.
- Paris, J. F., "A Program for Computing the Brightness Temperature of a Clear Atmosphere from Radiosonde Data," Tech. Rept. LEC/HASD No. 6490.21.068, Lockheed Electronics Co., Inc., Aerospace Systems Div., Houston, 1971.
- Paris, J. F., "Sky Brightness Temperature Error Analysis for Microwave Sensor Calibration," Job Order 75-415, Lockheed Electronics Co., Inc., Aerospace Systems Division, Houston, Feb., 1975.
- Sullivan, W. T., "Variations in Frequency and Intensity of 1.35 - centimeter H₂O Emission Profiles in Galactic HII Regions," Astrophys. J., vol. 116, 1971, pp. 321-332.
- Van Vleck, J. H. and V. H. Weisskopf, "On the Shape of Collision - Broadened Lines," Rev. Mod. Phys., vol. 17, 1945, pp. 227-236.
- Yu, J. S., R. C. Rudduck and L. Peters, IEEE Trans. Antennas and Prop., AP-14, March, 1966, pp. 138-149.